Wear of Total Ankle Replacements: An Explant Analysis

Shona Haston

This thesis is submitted for the degree of Doctor of Philosophy

Newcastle University

School of Engineering

March 2024

Abstract

Total ankle replacement (TAR) has increased in popularity in recent years; however, outcomes remain unsatisfactory, with revision rates at 10 years over twice that of hip and knee replacements. Currently, failure mechanisms of TARs are not well understood, and explant analysis studies are limited. This study aimed to characterise the wear-related damage modes and surface changes of explanted TARs in order to investigate the failure mechanisms of contemporary TARs. The influence of design features including bearing constraint on the identified damage was also analysed.

Twenty-eight explanted TARs which had been explanted for any reason were included. The cohort comprised 9 different designs of TAR, 3 of which were fixed bearing and 6 of which were mobile bearing. Explant analysis techniques including visual (microscopic and macroscopic) analysis, material characterisation, and surface profilometry were performed to identify damage modes present. Additionally, volumetric wear of the polyethylene component was quantified. All surfaces (articulating and non-articulating) of the TAR components were analysed.

A range of wear modes – including intended wear at the bearing as well as unintended wear of non-bearing surfaces and due to third body particles – were observed to have occurred *in vivo*. Damage to the articulating surfaces of the metallic components in the form of pitting, indicative of material loss, and talar sliding plane scratching, indicative of the presence of hard third body particles, was commonly seen in this cohort of explanted TARs. Evidence of porous coating loss was also frequently identified. Together, this suggests that particulate coating debris may contribute to TAR damage by acting as third body particles. Quantification of the volumetric wear loss at the polyethylene bearing surface revealed relatively low amounts of wear. Based on the findings from the present study, it is proposed that metal debris release may be an under-recognised failure mechanism of contemporary TARs.

List of Publications

Haston S, Langton D, Townshend D, Bhalekar R, Joyce T. Metal debris release is commonly seen from explanted total ankle replacements. Journal of the Mechanical Behaviour of Biomedical Materials. 2023;(144):105932. https://doi.org/10.1016/j.jmbbm.2023.105932.

List of Major Presentations

Haston S, Langton D, Townshend D, Bhalekar R, Joyce T. Metal Debris Release May Be Under-Recognised in Total Ankle Replacement. Presented at the British Orthopaedic Foot & Ankle Society (BOFAS) Annual Scientific Meeting, 2023.

Haston S, Langton D, Townshend D, Bhalekar R, Joyce T. Metal Release From Total Ankle Replacements: An Explant Analysis Study. Presented at the European Federation of National Associations of Orthopaedics and Traumatology (EFORT) Annual Congress, 2023.

Haston S, Langton D, Townshend D, Bhalekar R, Joyce T. Metal Damage Mechanisms of Total Ankle Replacements. Presented at the International Congress of the International Society for Technology in Arthroplasty (ISTA), 2023.

List of Major Awards

Klenerman Prize for Basic Science Paper. Metal Debris Release May Be Under-Recognised in Total Ankle Replacement. Presented at the British Orthopaedic Foot & Ankle Society Annual Scientific Meeting, 2023.

Dedication

I dedicate this thesis to my family who have always supported me in whatever I have chosen to pursue. To Dad, I hope I have made you proud.

Acknowledgements

Firstly, I would like to thank my supervisors Professor Tom Joyce, Dr Oana Bretcanu, and Dr David Langton for your continued guidance and encouragement which has made this thesis possible.

I wish to also acknowledge the support provided by others throughout my PhD. Mr Dave Townshend provided the samples analysed within this study. Dr Isabel Arce-Garcia assisted by performing some preliminary analysis via the ACMA service (www.ncl.ac.uk/acma). Matthew Nargol worked on the custom programmes which were used to generate the wear results. Thanks must also go to the rest of the ExplantLab team of Dr Rohan Bhalekar, Stephen Wells, and Shahrzad Shariatpanahi for their help throughout.

Finally, I extend my gratitude to my sponsors, ExplantLab and the European Regional Development Fund, for funding my PhD studies through the Intensive Industrial Innovation Programme.

Part of the work contained within this thesis has previously been published within the Journal of the Mechanical Behavior of Biomedical Materials as a first-author paper (included in Appendix A).

Table of Contents

List of Tables

List of Figures

List of Abbreviations

ALVAL	Aseptic lymphocyte-dominated vasculitis-associated lesions
AOANJRR	Australian Orthopaedic Association National Joint Replacement Registry
ARMD	Adverse reaction to metal debris
AS	Area score
BMI	Body mass index
CaP	Calcium phosphate
CMM	Coordinate measuring machine
Co	Cobalt
CoCr	Cobal-chromium
CPE	Conventional UHMWPE
DFS	Damage feature score
EDX	Energy dispersive X-ray spectroscopy
EHL	Elastohydrodynamic
EtO	Ethylene oxide
FDA	Food and Drug Administration
GVF	Gamma vacuum foil
HA	Hydroxyapatite
HD	Hydrodynamic
HXLPE	Highly cross-linked ultra-high molecular weight polyethylene
MC	Million cycles
MHRA	Medicines and Healthcare products Regulatory Agency
MoM	Metal-on-metal
MoP	Metal-on-polyethylene
NHS	National Health Service
NJR	The National Joint Registry for England, Wales, Northern Ireland, the Isle of Man and the States of Guernsey
NICE	England National Institute for Health and Clinical Excellence
OA	Osteoarthritis
OCD	Obsessive compulsive disorder
PE	Polyethylene
PMMA	Poly(methyl methacrylate)
S_a	Average surface roughness

S_{ku}	Kurtosis
S_p	Maximum peak height
S_q	Root mean square roughness
S_{sk}	Skewness
S_v	Maximum valley depth
S_z	Peak to valley height
SEM	Scanning electron microscopy
SS	Severity score
TAR	Total ankle replacement
TARVA	Total Ankle Replacement Versus Ankle Arthrodesis
THR	Total hip replacement
TKR	Total knee replacement
Ti	Titanium
TiN	Titanium nitride
UHMWPE	Ultra-high molecular weight polyethylene
XRF	X-ray fluorescence

Chapter 1. Introduction

In 1929, the MacAuslands wrote that *"under no circumstance is arthroplasty to be considered in the ankle-joint"*.[1] In the time since, attitudes have shifted considerably and total ankle replacement (TAR) is now considered to be a standard treatment option for end-stage arthritis of the ankle. However, outcomes following TAR remain sub-optimal, particularly in terms of failure rates. This thesis contains an investigation into the mechanisms of failure, with the current chapter serving as an introduction to this work.

The context of the present study will be set out by situating the topic that this thesis will cover within the area of ankle joint replacement research. Following this, the motivation for the study is given in terms of a problem statement to justify why this research is needed. The overall aim of the work is then described, and the scope for the study established. The significance of the study is explained by outlining the intended outcomes in terms of contributing to the field of research. Finally, an overview of the study is provided by outlining the structure of the thesis, in order to aid understanding of how this study will achieve the aim set out in this chapter.

1.1. Context of the Study

1.1.1. The issues to date

Contemporary total ankle replacement is a relatively recent joint replacement to be introduced.[2] The first ankle replacement was described in 1890 by Gluck, with little success.[3] Some years later, in the 1970s, first generation ankle replacements were implanted, although still with limited success, and the implant was again abandoned clinically for nearly a decade.[3, 4] Second generation implants were then introduced, followed by the currently-used third and fourth generation prostheses.

Outcomes following TAR have improved significantly over the last decade, however revision rates remain high in comparison to other lower limb total joint replacements.[5] The National Joint Registry for England, Wales, Northern Ireland, the Isle of Man and the States of Guernsey (NJR) 2023 report gives a 10-year revision rate of 9.05% for ankles, compared to 3.89% for hips and 3.93% for knees.[6] It is also noted that the actual number of TAR revisions performed is likely to be higher due to underreporting.[6]

TAR is performed as a surgical treatment for severe arthritis of the ankle. Osteoarthritis (OA) is by far the most common reason for ankle replacement surgery, with it being documented as an indication for 92% of surgeries by the NJR.[6] OA is a degenerative condition affecting about 1% of the adult population.[7] Rising obesity and injury incidence levels and the ageing population means that the prevalence of OA cases is expected to continue to increase globally.[8] In alignment with this, the number of TAR procedures performed has also risen, with the Australian Orthopaedic Association National Joint Replacement Registry (AOANJRR) reporting a 210% increase in TAR from 2014 to 2022.[9]

TAR is an alternative procedure to ankle fusion surgery, also known as ankle arthrodesis. Ankle fusion is considered the 'gold standard' of clinical surgical treatment for end-stage arthritis of the ankle.[4] However, with TARs offering comparatively better biomechanical function and with outcomes following TAR having improved since its introduction, TAR is becoming an increasingly popular alternative. The NJR shows a trend of increasing numbers of TARs being performed over the years it has been recording (since 2010), with the exception of 2020 and 2021 in which COVID-19 impacted the number of procedures being performed.[6] In 2019, the NJR reported 1008 primary TAR procedures; a 13% increase from the previous year.[6]

Revision surgery is necessary when a device fails. Throughout this thesis, failure of a joint replacement refers to a revision, defined as the exchange or removal of at least one of the components of the prosthesis, as per Henricson et al.[10] The most common reason for revision surgery following TAR according to the NJR is aseptic loosening, accounting for 24.1% of all revisions, followed by infection (14.9%), pain (10.8%) and lysis (10.7%).[6] Aseptic loosening commonly occurs as a result of a reaction to implant-generated wear particles wherein an immune response favouring bone resorption is induced, which results in the loosening of the prosthesis, leading to eventual failure meaning revision surgery is required.[11] Understanding the source of these particulates is therefore important in order to inform future designs with the intention of minimising implant wear.

The more a joint replacement is used (i.e., the more active the patient is), the greater the volume of generated wear debris. With joint replacements increasingly being performed in younger, more active patients, along with an increasingly obese and ageing population, it is generally accepted that the number of revision surgery cases will increase. However, revision surgeries are complex and expensive, making them undesirable. As well as adding an extra cost, revision

surgeries also come with increased risk and burden to patients. It is therefore important to aim to reduce implant failures, and therefore revision rates.

1.1.2. Situating explant analysis

Within the area of tribology research of TARs, studies may be broadly grouped together as being either simulator (i.e., *in vitro*) studies, or explant analysis (i.e., *ex vivo*) studies. Simulator studies aim to predict the tribological performance of the implant by replication of *in vivo* conditions using a joint simulator. All of the previously published TAR simulator studies have used modified knee joint simulators, meaning the motion being applied is inverted to that which the ankle prosthesis actually experiences in the body.[4] Explant analysis studies are those which analyse prostheses which have been removed from the body. Generally, these are prostheses which have been explanted from the body during revision surgery, meaning the device has failed, however in some cases well-functioning devices may be explanted from cadavers or when surgical intervention is required due to infection. The research contained within this thesis is concerned with the failure of TARs and therefore is limited to the explant analysis of devices retrieved during revision surgery. Since these explants have actually been used in the body, it can be argued that findings from explant analysis studies give the more clinically relevant insights into their tribological performance.

Explant analysis studies are situated within the broader research area of retrieval analysis, which provides important feedback on the performance of a joint replacement forming part of the post-market surveillance of these devices. As well as explant analysis, which in this thesis refers to analysis of the explanted prosthesis only, retrieval analysis also encompasses other areas of study. One such example is histological analysis, wherein periprosthetic tissue samples are studied for features such as implant-derived particles.

Explant analysis studies can provide valuable insights into how an implant actually performs *in vivo*, making it the truest test of a joint prosthesis. Despite their importance, however, the number of TAR explant analysis studies within the existing literature is limited, with fewer than ten currently published. Furthermore, these previous explant analysis studies have largely been focused on TARs which are no longer in use.

1.1.3. Research gaps

Medical device regulation states that there are four main classes of medical devices: Class I, Class IIa, Class IIb, and Class III (Figure 1.1). Medical devices are classified based on the device's intended purpose and inherent risks.[12]

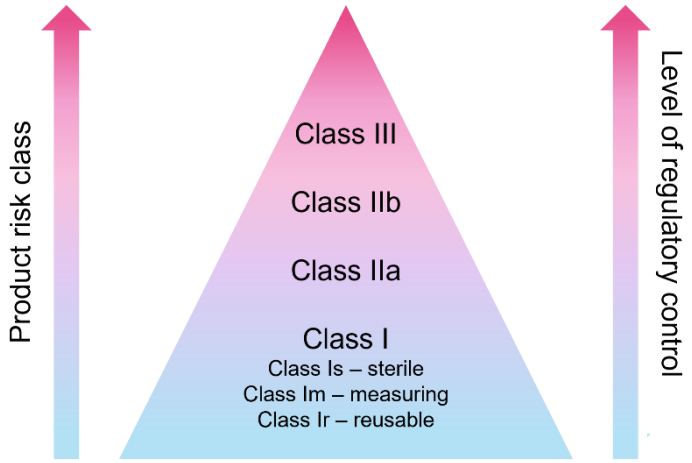

Figure 1.1. Diagram illustrating the classes of medical devices.

Total joint replacements of the hip, knee and shoulder were previously reclassified as Class III medical devices from Class IIb.[13] However, it is only more recently that all other joint replacement devices – including ankles – have followed suit.[13] This reclassification means that the level of regulatory control on these devices is increased; taking the form of stronger evidence required for clinical study, and expected proactive post-market surveillance, including follow-up clinical studies.[13] It is only within the last few years that an international standard for the wear testing of TARs (ISO 22622:2019)[14] has been introduced and no wear studies using this standard have been published to date.[4]

Contemporary TARs can be classified as one of two major designs, based on bearing constraint: fixed bearing or mobile bearing. A detailed look into the differences between the two in terms of design and performance is given within the following chapter. In recent years, fixed bearing TARs have overtaken mobile bearing TARs in popularity in the UK.[6] However, the literature comparing the two remains conflicting. Only one of the previously published TAR explant analysis studies included both fixed and mobile bearing designs in their analysis.[15] Therefore, more research into comparing the *in vivo* changes exhibited by fixed and mobile bearing TARs is required.

Aseptic loosening is the most commonly cited reason for revision of TARs.[6] Aseptic loosening refers to loosening of the implant due to surrounding bone degradation, without infection present. Often aseptic loosening occurs secondary to osteolysis. Osteolysis is characterised by an adverse inflammatory immune response to particulate debris, resulting in periprosthetic bone loss. What is not clear is the source of the particulate debris causing this loosening following TAR, whether they are originating from the PE component, metal components, or both. This should therefore be considered in future research.

In other metal-on-polyethylene (MoP) artificial joints, wear of the PE component is generally considered to be the primary factor limiting the lifespan of the device. In line with this, the limited number of previous TAR explant analysis studies have primarily focused on damage analysis of the polyethylene (PE) components. However, to date, no published studies have measured the volumetric wear from explanted TAR components.

Explant analysis of the metal components of retrieved TARs has not been widely performed. However, adverse reaction to metal debris (ARMD) is a known problem following metal-on-metal (MoM) hip replacement, and appreciable amounts of metal wear have also been reported from non-MoM hip replacements[16] and knee replacements,[17] as well as metal particles having been found in TAR cases.[18] Furthermore, it has been shown that a patient's propensity to develop an adverse inflammatory response to metal debris can be impacted by individual genetics, meaning relatively low blood cobalt (Co) levels can cause this adverse reaction in some patients.[19] Given that blood Co levels have been found to be significantly elevated 1 year post total knee replacement (TKR),[20] there is the possibility that this could also be the case for TARs. Despite this, cobalt-chromium (CoCr) alloy components are used in most total joint replacements. This evidence all suggests that there is a possibility that metal debris-related problems could exist following TAR. Further research into the tribological behaviour of metal components, including investigation of any potential differences in the performance of different metal alloy components, within TARs is therefore warranted.

1.2. Statement of the Problem

Since their introduction in the 1970s, TARs have seen development from the initial first-generation implants to the currently used third and fourth generation implants. Recently, longer term (over 10 years post implantation) survival data from national retrieval registries has

emerged. Revision rates for TARs are unsatisfactory in comparison to other lower limb total joint replacements, with over double the proportion of failures after 10 years.

To date, however, the limited number of published TAR explant analysis studies means that the failure mechanisms of TARs are not currently fully understood. In particular, there is a lack of explant analysis of TAR designs which are currently in use. In addition, a focus on the metallic components of failed prostheses is needed, in order to better determine potential factors contributing to high rates of implant failure.

1.2.1. Research question

To address the problem statement, the following question, which the research contained within this thesis aimed to answer, was posed: what wear-related damage and/or surface changes occur *in vivo* which may drive TAR failure?

1.3. Aim and Scope

In response to the problem statement and associated research question, set out in the previous section, the aim and scope of the present study was identified. The overall aim of the study is to investigate the damage modes and surface changes reflective of wear occurring *in vivo* for explanted TARs. The motivation behind this is to better understand the failure mechanisms of contemporary TARs. The research contained within this thesis therefore uses an explant analysis approach to describe the wear-related tribological patterns of various failed TARs. The main components of this explant analysis approach are visual analyses, profilometry, material characterisation, and form analysis, with the latter referring to volumetric wear and linear deviation.

The scope of the study is limited to TARs which have been revised and therefore can be considered to have failed. The scope of the study is also defined in terms of the analysis to be performed, with this being limited to explant analysis of explanted TARs. Therefore, other retrieval analysis approaches, such as histological analysis, are beyond the scope of this study. These boundaries allow the study to focus on the failure mechanisms of TARs from an engineering perspective.

1.3.1. Objectives

To address the aim described for the research in this thesis, the following objectives were identified:

i. Characterise the modes of damage present on explanted TAR components in terms of type, extent and severity.
ii. Evaluate the surface topography changes of explanted TAR components.
iii. Analyse the form changes of explanted TAR PE components.
iv. Correlate *in vivo* changes of explanted TAR components with implant characteristics.
v. Determine damage mechanisms likely to cause TAR failure.

1.4. Significance of the Study

The present study is significant in that it forms the largest explant analysis study of currently used TARs in the UK.

An intended outcome of this study is to advance knowledge regarding the clinical performance of contemporary TARs; specifically focusing on the identification of *in vivo* wear-related surface changes which may contribute to the high rates of failure of these devices. Relating to this, another intended outcome of the study is to quantify volumetric wear loss and linear deviation from explanted TAR PE components, thereby contributing to the understanding of wear performance of TARs, as well as enabling comparison to published wear volume results within the literature from simulator studies. Finally, the study also aims to contribute to the discourse concerning the comparison of fixed and mobile bearing TARs in terms of their wear performance and *in vivo* changes as described by the previous intended outcomes.

1.5. Overview

This thesis consists of five further chapters, following on from the current introductory chapter (Figure 1.2).

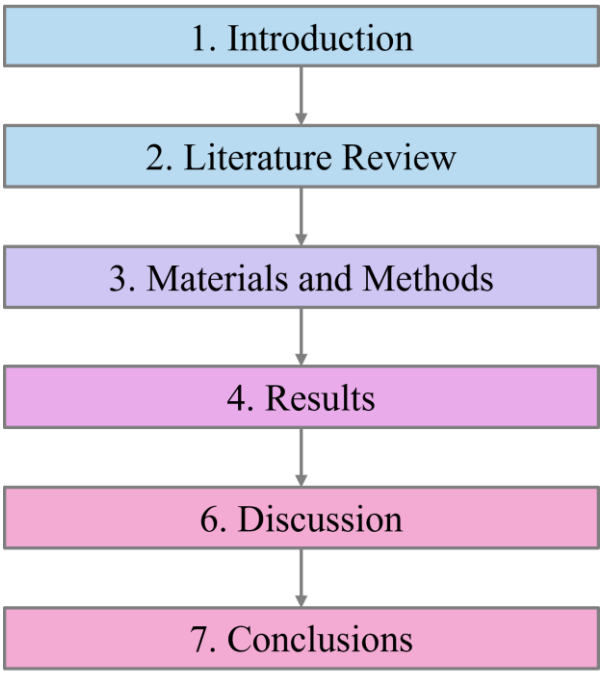

Figure 1.2. Overview of the thesis structure. The different colours correspond to introductory, methodology, results, and discussion chapters, respectively.

In Chapter 2, the present study is situated in relation to current research. An overview of contemporary TARs is given, including design principles, biomaterials used, biotribology of the devices and current theories on failure mechanisms. The existing relevant literature surrounding the topic of explant analysis of TARs is also critically evaluated. In this regard, different explant analysis techniques are explored, and previous retrieval studies are evaluated. Based on the identification of research gaps in the current literature, an argument is made for the need to investigate explanted TARs for indications of wear-related damage potentially causing failure.

Chapter 3 establishes the research methodology for this explant analysis study. Within this, the cohort of explanted TARs are described, along with corresponding clinical information where available. The methods which form the research design are then detailed; covering the techniques and instruments used to collect and analyse the data.

In Chapter 4, the original research results from the study of failed TARs are presented. This involves results from the initial identification of surface damage modes present and subsequent explant analysis techniques, as well as correlation of *in vivo* changes with implant characteristics.

Chapter 5 discusses the results of the study in the context of the existing literature. Key findings are expanded upon to inform the proposal of contemporary TAR failure mechanisms. Based on this, characteristics of TARs that may improve the wear performance are considered. The limitations of the research are also discussed.

Finally, Chapter 6 contains the conclusions of the study and reflects on the work contained within this thesis to suggest directions for further research.

Chapter 2. Literature Review

The literature regarding TARs is not as extensive as for other total joint replacements with a longer history of use. However, a background to the research topic, for the purpose of putting the present study into context, can be provided by the published literature. A critical review of the current literature is also carried out in order to set out the status of the existing work. This is synthesised so as to summarise the body of knowledge currently available on the failure mechanisms of total ankle replacements.

Firstly, background information is provided on the ankle joint and need for ankle replacement, as well as data relating to total ankle replacement implantations and failures. An overview of total ankle replacements is then given, including design, biomaterials, and biotribology. The various known mechanisms of total ankle replacement failure are described. Previously used explant analysis methods are then reviewed. Finally, the TAR retrieval studies published in the literature to date are evaluated.

2.1. The Ankle Joint

An aim of any total joint replacement is to replicate the capacity of the natural joint as closely as possible. It is therefore important to understand the role of the natural ankle joint, as well as the need for replacing the ankle and the alternatives.

2.1.1. Anatomy of the ankle joint

To describe anatomical locations, a set of terminology relating to the three anatomical planes (sagittal, coronal, and transverse) will be used throughout this thesis. Figure 2.1 illustrates this reference system.

The coronal plane creates medial and lateral sections, referring to closest and furthest from the midline of the body, respectively. The sagittal plane separates the body into posterior (back) anterior (front). Finally, the transverse plane separates the body into superior (top) and inferior (bottom).

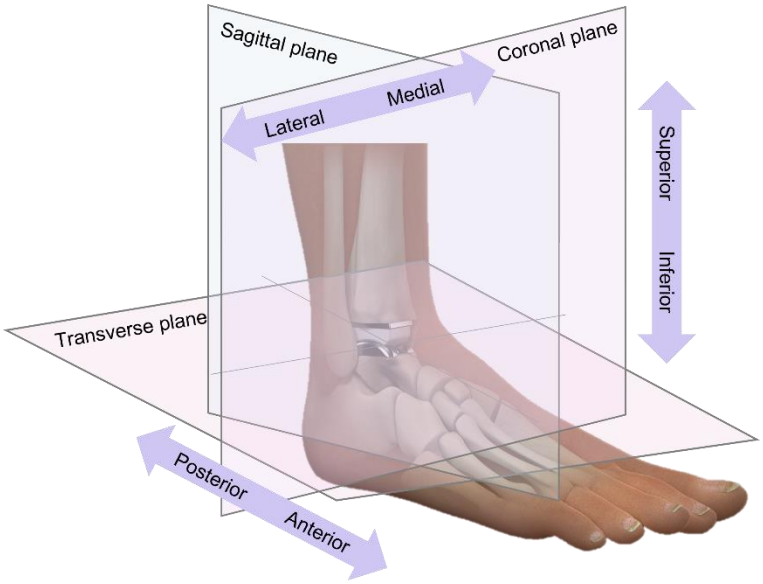

Figure 2.1. An illustration of the anatomical planes of the human body and respective terminology using a right sided ankle.

The ankle joint complex is comprised of three joints: the tibiotalar (talocrural), the subtalar (talocalcaneal), and the transverse tarsal (talocalcaneonavicular), as shown in Figure 2.2.[21]

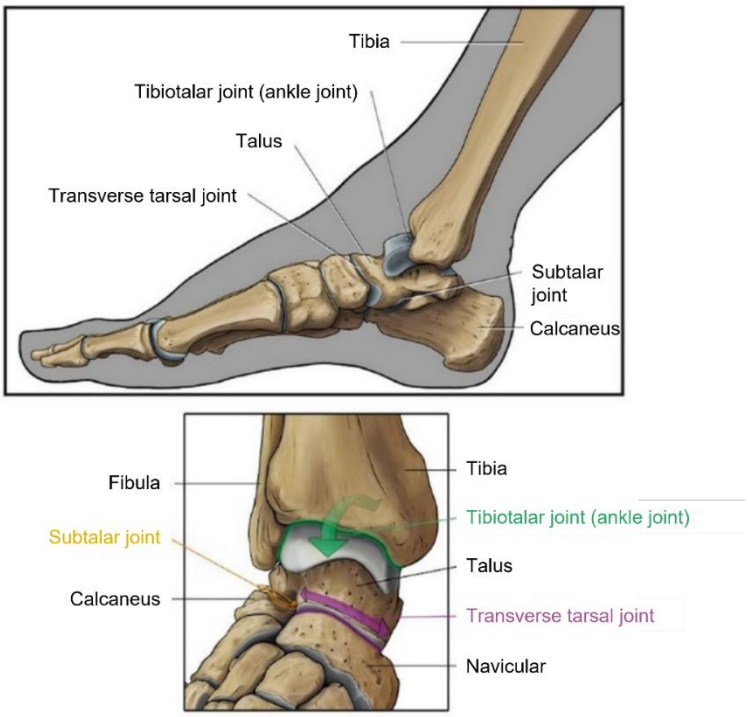

Figure 2.2. Anatomy of the ankle joint complex. Image adapted from TARVA trial.[22]

Historically, the ankle was generally considered to be a hinge joint, permitting the movements of dorsiflexion (i.e., flexing the foot) and plantarflexion (i.e., pointing the foot).[23] Multi-axial motion, however, due to internal and external rotation occurring during dorsiflexion and plantarflexion respectively, has been shown to occur at the ankle joint complex, suggesting that the initial hinge joint concept is an oversimplification.[21, 23]

The primary movements permitted at the ankle joint complex are plantarflexion and dorsiflexion occurring in the sagittal plane, abduction and adduction occurring in the transverse plane, and inversion and eversion occurring in the coronal plane, as illustrated by Figure 2.3.[21] Supination and pronation, three-dimensional movements corresponding to the position of the sole of the foot, are created by these motions in combination.[4] Plantarflexion, adduction and inversion together cause supination, defined as the sole of the foot facing medially (i.e., inwards); dorsiflexion, abduction and eversion together cause pronation, defined as the sole of the foot facing laterally (i.e., outwards).[4]

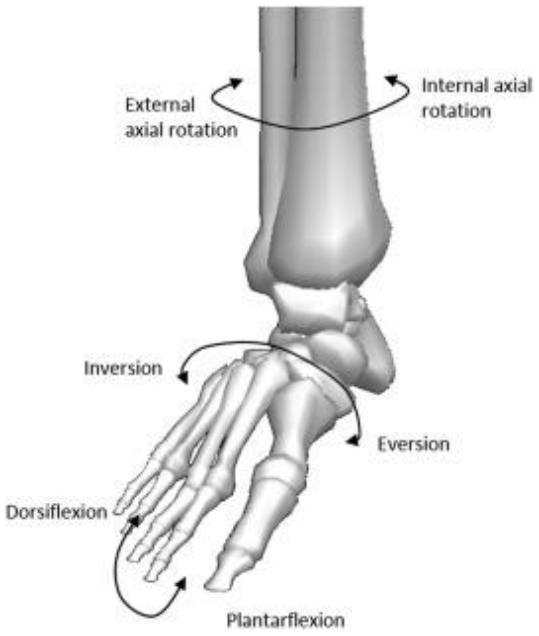

Figure 2.3. The motions of the ankle joint complex. Image from Brockett et al.[21]

The subtalar joint, along with the transverse tarsal joint, allows the inversion and eversion movement of the foot.[21] The distal ends of the tibia and fibula, along with the talus, form the tibiotalar joint, with the load bearing aspect comprising of the tibial-talar interface.[21] The tibiotalar joint is commonly referred to as the 'true' ankle joint,[23] and it is this articulation that

TAR – in which the ends of the tibia and talus bones are resurfaced – aims to treat. From here on, the term ankle joint will refer to the tibiotalar joint.

2.1.2. The need for ankle replacement

According to data from the 2023 annual report by the NJR, the vast majority of primary TARs are performed to treat OA, with it being reported as an indication for 92% of procedures.[6]

Ankle OA is a degenerative condition affecting approximately 1% of the adult population.[24] The disease significantly impacts quality of life, to the same degree as end-stage arthritis of the hip.[25]

Non-operative interventions such as weight loss or orthotics may be used in the first instance.[26, 27] Once the OA has progressed to be end-stage, however, surgery – either TAR or ankle arthrodesis – is the main treatment option.[27] An estimated at least 29,000 patients with symptomatic OA of the ankle each year are referred to specialist foot and ankle surgeons within the National Health Service (NHS), of which at least 3,000 undergo surgery (TAR or arthrodesis).[24] OA which meets the following two criteria is deemed to necessitate surgical intervention and therefore defined as being end-stage: radiological changes consistent with OA; unsuccessful treatment using non-operative methods for at least 6 months.[27]

Typically, those affected by OA of the ankle are younger than those affected by hip or knee OA. This may primarily be attributed to the fact that the majority of ankle OA is posttraumatic,[24] whereas primary OA is the most common form for hips and knees.[28] At the time of diagnosis, patients with posttraumatic ankle OA have been reported to be an average of 14 years younger, as well as experiencing a more rapid progression to end-stage OA, than those with OA of other joints.[29] The primary symptoms of ankle OA are severe joint pain and stiffness, due to the disease compromising the function of natural joints.[30, 31] In healthy joints, there is a layer of cartilage present which, together with the bone, absorbs shocks and permits smooth motion.[32, 33] In joints affected by OA, however, this articular cartilage is worn and/or damaged, meaning painful bone-on-bone contact ensues (Figure 2.4 and Figure 2.5).[34]

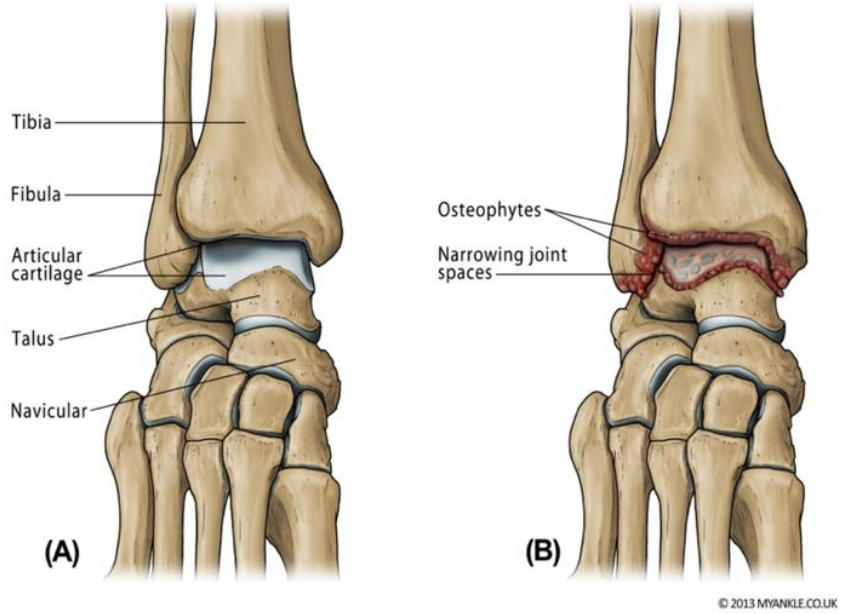

Figure 2.4. Comparison of healthy and osteoarthritic ankles. (A) a heathy ankle and (B) an ankle with OA. Image from TARVA Trial.[22]

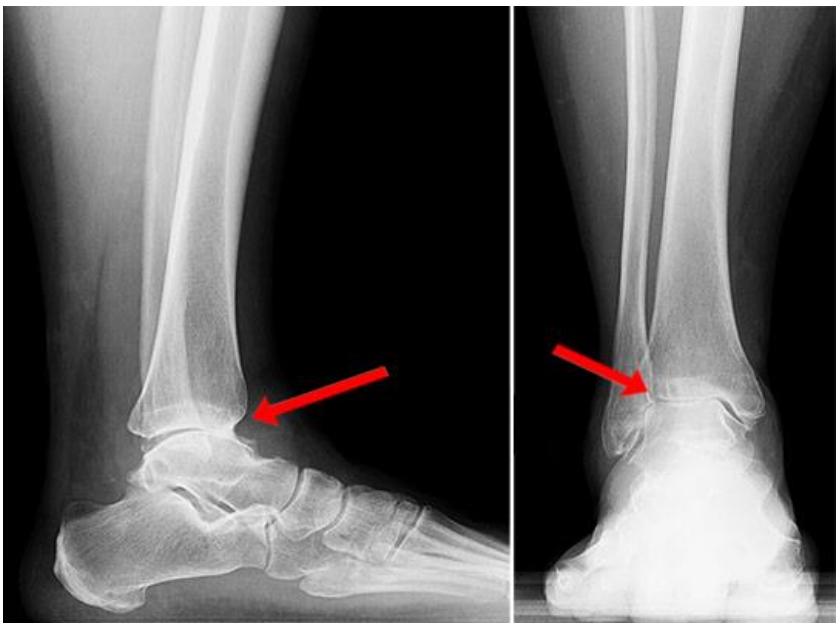

Figure 2.5. X-rays showing end-stage arthritis of the ankle with resulting bone-on-bone contact indicated by the red arrows. Image taken from HSS.[35]

Obesity, being a risk factor for OA, therefore also increases a patient's risk of requiring a joint replacement.[36] Based on body mass index (BMI) data, the NJR states that the average patient receiving a primary ankle replacement is classed as 'overweight'.[6] With an increasingly obese and ageing population, joint replacement surgeries are expected to continue to increase.[37]

2.1.3. Replacement versus arthrodesis

Ankle arthrodesis – also known as ankle fusion – is a surgical procedure which restricts motion at the affected joint.[22] The operation involves fusion of the ends of the two bones, following removal of remaining damaged cartilage, using either internal (e.g. screws) or external (e.g. plates) compression methods as fixation.[22, 38]

As with TAR, arthrodesis is predominantly performed to treat end-stage OA of the ankle. The procedures are very different however, with TAR aiming to restore motion by replacing the ankle joint, and arthrodesis aiming to restrict motion by fusing the bones (Figure 2.6).[27]

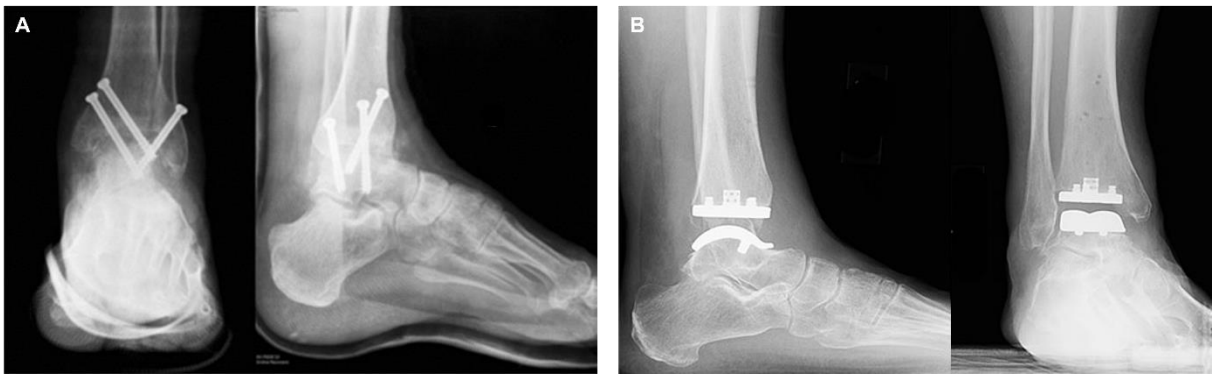

Figure 2.6. X-ray images of surgical treatments for ankle arthritis. (A) Ankle arthrodesis using screws as fixation. Image adapted from Cottino et al.[39] (B) Total ankle replacement. Image adapted from HSS.[35]

Each year, within the NHS, approximately 3,000 patients undergo either TAR or ankle arthrodesis to treat arthritis of the ankle.[22] There is, as of yet, no clear consensus in the literature as to a preference towards ankle replacement or arthrodesis for the surgical treatment of end-stage arthritis of the ankle. Rather, it is to a large extent down to the preference and experience of the individual surgeon. Some still consider arthrodesis to be the *"clinical gold standard"*[4], however the popularity of TAR procedures has been increasing in recent years.[6]

For both ankle replacement and arthrodesis, there are associated potential benefits and drawbacks. By removing motion at the ankle joint, pain too is aimed to be removed by arthrodesis.[40] However, reported complications for arthrodesis include abnormal gait mechanics and degeneration of adjacent joints.[41] On the other hand, whilst TAR has been

suggested to restore a more natural gait, it has also been suggested that a higher risk of further surgery is associated with it.[22]

There exists a learning curve for surgeons performing TAR, with a significant reduction in complications and increase in implant survival having been shown to occur as surgeon experience increases.[23] It follows therefore that at centres with long-term experiences of performing TAR, ankle replacement is generally the chosen procedure over arthrodesis, with the latter mostly being performed in instances where there are contraindications for TAR present.[23]

Initial results (at a 1-year follow-up) from the Total Ankle Replacement Versus Ankle Arthrodesis (TARVA) trial – the first randomised controlled trial comparing TAR and arthrodesis – were published in 2022.[27] Neither TAR nor ankle arthrodesis was shown to be superior in terms of clinical scores or risk of adverse events, however better outcomes were reported for a particular fixed bearing prosthesis (the INFINITY) at 1 year compared to ankle fusion.[22] These are only short-term results, however, and a longer follow-up is needed to compare the mid- and long-term performance of these interventions.

2.2. Total Ankle Replacement Trends

In comparison to other total joint replacements such as hips and knees, relatively low numbers of TARs are implanted; however, this number is increasing. The Norwegian Arthroplasty Register has data on ankle replacements dating back to 1994,[42] though in the UK specifically, longer term (> 10 years) data has recently started to be reported by the NJR.[6] As this follow-up data continues to emerge, more insights into the performance of the newest generation of TARs may be gained.

2.2.1. Implantation rates

There is a trend of increasing numbers of TAR procedures being performed year-on-year, with the exception of recent years in which operations were impacted by the COVID-19 pandemic.[43] Since starting recording ankle data, the NJR has recorded 8,788 primary ankle replacement procedures for the period of 1st January 2010 to 31st December 2022.[6] In 2019 – the last year before surgery numbers were affected by COVID-19 – 1008 primary TAR procedures were reported.[43] The average number of primary TARs performed per year for the five-year period

of 2015 to 2019 inclusive was 796; over a 50% increase on the average of 522 over the five-year period of 2010 to 2014.[43] The increase seen in TARs performed in recent years has largely been with fixed bearing designs.[43] This change may be linked with the introduction of the fixed bearing INFINITY prosthesis in 2014, the same year that the market leader at the time, the mobile bearing Mobility prosthesis, was voluntarily withdrawn.[43] The INFINITY prosthesis is now the most commonly implanted TAR in the UK – used in 64.5% of procedures in 2022 – as well as in Australia, New Zealand and Norway.[6, 9, 44, 45]

The percentage of primary ankle replacements performed by model of TAR over time, using data from the NJR, is plotted in Figure 2.7.

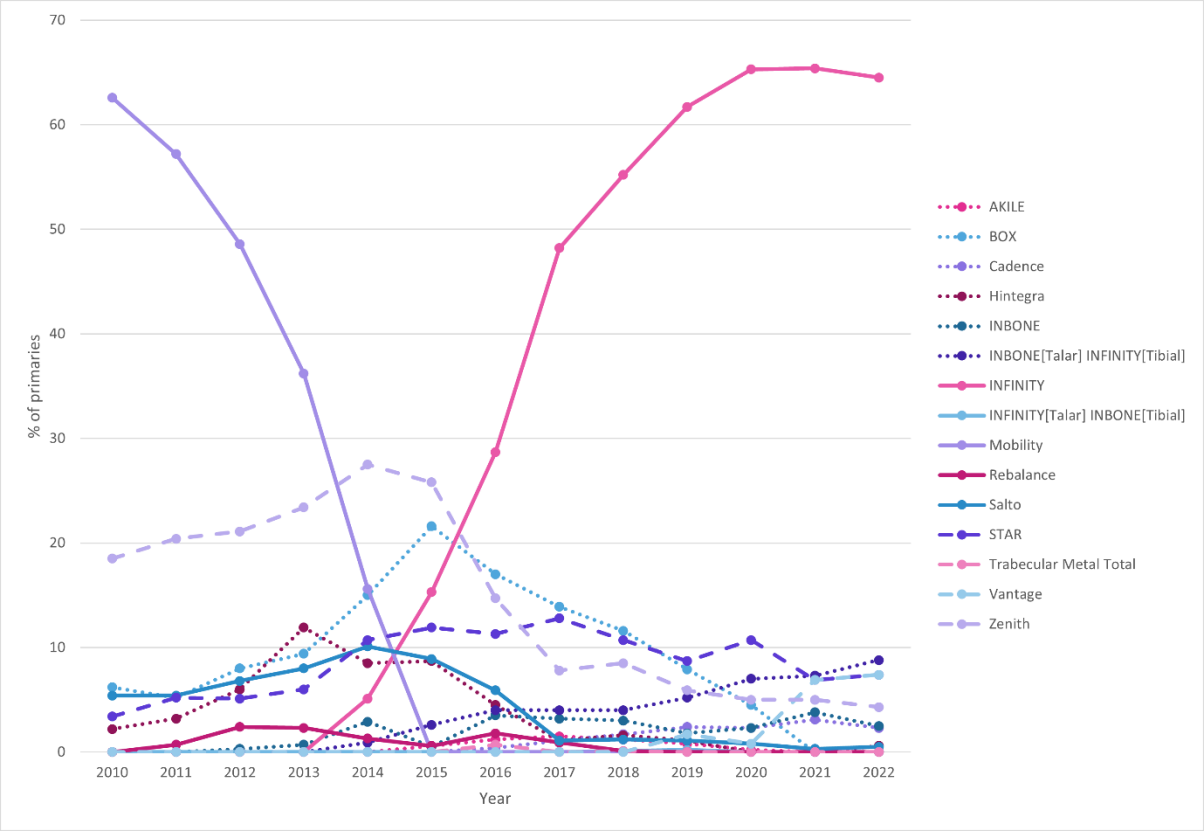

Figure 2.7. Plot of the percentage of primary ankle replacements by model over time using data from the NJR 2023 Annual Report.[6] Models with a total percentage of at least 0.1% are included.

2.2.2. Revision rates

The lack of consistency in defining the revision of TAR may account for why reported revision rates from TAR studies vary widely.[23] Following a literature search, Henricson et al. proposed

that a TAR revision should be defined as *"removal or exchange of one or more of the prosthetic components with the exception of incidental exchange of the polyethylene insert"*.[10] However, the NJR considers any procedure in which the implant is removed or exchanged to be a revision.[6] For the purposes of this work, the definition of a revision will be consistent with that currently used by the NJR (i.e., the removal or exchange of one or more components, including exchange of the PE insert only).

Long-term revision rates for TAR are considerably higher than for other lower limb total joint replacements (9.05% at 10 years, compared with 3.89% and 3.93% for hips and knees respectively according to NJR data) (Table 2.1).[6]

Data from the AOANJRR in 2023 reported a 7-year TAR revision rate of 7.7% for the period 2015 to 2022, and 12.9% for before 2015, therefore indicating that revision rates have generally improved over time.[9] Data from the Norweigan Arthroplasty Register also supports this finding that current designs had a better survival compared to earlier designs.[42] The NJR 7-year reported revision rate of 7.09% is similar to that reported by the AOANJRR for 2015 to 2022, however the NJR data covers the period of 2010 to 2022. Differences in the TARs used – for example the INFINITY prosthesis becoming the most commonly implanted later in Australia compared to the UK – may potentially contribute to variation in reported revision rates.

Whilst a criteria defining an acceptable revision rate following TAR does not currently exist, a benchmark revision rate of 22% at 10 years was proposed by van der Plaat et al. following a systematic review.[46] This is considerably higher than the England National Institute for Health and Clinical Excellence (NICE) guidance for hip replacements, which was updated in 2014 to recommend total hip replacement (THR) as a treatment for end-stage arthritis only when predicted revision rates were 5% or less at a follow-up of 10 years; replacing the previous benchmark 10-year revision rate of 10%.[47]

Primary joint replacement	**Time post-implantation (years)**							
	1	**3**	**5**	**7**	**10**	**12**	**15**	**19**
Hip	0.80	1.44	2.04	-	3.89	-	6.26	8.17
Knee	0.49	1.68	2.44	-	3.93	-	5.56	7.17
Ankle	0.77	3.14	5.47	7.09	9.05	9.58	-	-

Table 2.1. Selected revision rate data from the NJR 2023 Annual Report.[6]

2.2.3. Indications for failure

Failure, classed as revision of the implant, is typically the standard endpoint used in evaluating the success of TARs. Whilst this metric is useful for determining survivorship, defining failure in this way is a binary measure and does not account for other factors such as patient satisfaction and complications which do not lead to a revision. Additionally, the causes or aetiology of failure may not always be considered. It may not be clear therefore whether some failures are due to implant, surgical, or patient related factors.

Joint replacement revision surgeries come with further rehabilitation and hospitalisation, as well as an added risk of mortality, morbidity, and infection.[48] As well as this additional trauma for the patient, revision surgeries are also complex and expensive, contributing to the economic burden of the healthcare system.[48] With an increasingly obese and ageing population, the number of joint replacement surgeries – both primary and revision – being performed is expected to continue to increase.[37, 49-51]

Younger, more active patients tend to place greater demands on their joint replacements. Generally, the more a joint replacement is used (i.e., the more active the patient is), the greater the volume of generated wear debris. Tribologically, under boundary lubrication, this is due to a greater sliding distance for the bearing articulating surfaces to cover as, according to Archard's wear equation, volumetric wear is directly proportional to sliding distance.[31]

The literature contains three systematic reviews of TAR outcomes in terms of survivorship (or, inversely, failures). These reviews cover second and third generation TARs, but with the most recent of these systematic reviews having been published 10 years ago, in 2013, fourth generation devices are not included in these reviews. Despite having varying follow-ups, and number and generation of TARs included, all three reviews reported similar survivorship rates of between 89% and 90%, at follow-ups of 10 years (Zaidi et al.) and 5 years (Gougoulias et al. and Stengel et al.).[52-54] The largest TAR systematic review and meta-analysis to date was produced by Zaidi et al., which included 2942 second and third generation TARs from 56 studies.[54]

The literature also contains some studies evaluating risk factors for TAR failure.[55, 56] A systematic review of clinical complications following TAR by Curlewis et al. found an average complication rate of 3%, and an average mortality rate of 0.3%.[55] Reported risk factors from the study were revision procedures, diabetes, obesity, systemic co-morbidities, long duration

of anaesthetic, and preoperative blood transfusion.[55] In a separate study by Hermus et al. using data from the Dutch Arthroplasty Register, a higher risk of early revision following TAR was identified for patients with a higher BMI, a lower age, or who had undergone prior surgical treatment for obsessive compulsive disorder (OCD).[56] The study reported a survival rate of 95.3% at a median follow-up of 38 months.[56]

2.3. Total Ankle Replacements

Since their introduction in the 1970s, the design of TARs has evolved through four generations of designs (Figure 2.8). These generations can primarily be identified by the number of components that the implant has in combination with the fixation method.[57] The currently used designs are a mixture of third and fourth generation prostheses. Within this work, contemporary TARs are defined as these used third and fourth generation devices.

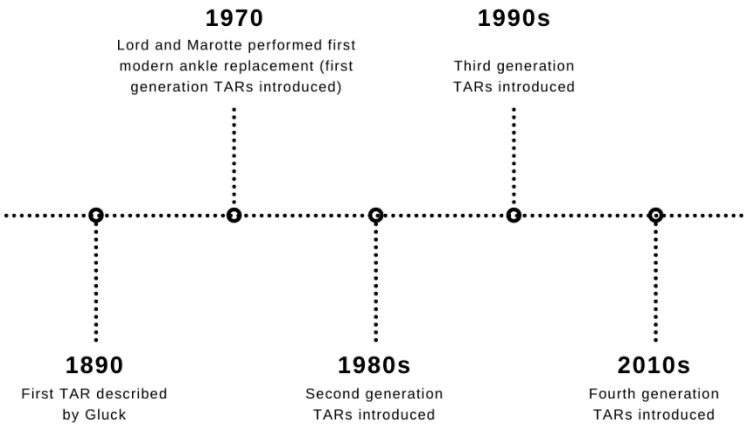

Figure 2.8. Timeline of the evolution of different generations of TAR.

2.3.1. Design principles

Contemporary TARs are comprised of three components: a metal (typically CoCr or titanium (Ti) alloy) tibial component, a metal (typically CoCr) talar component, and PE (typically UHMWPE) insert which sits in between the two metal components (Figure 2.9). The articulating surfaces of the talar component and PE insert make up the metal-on-polyethylene (MoP) bearing couple.

Contemporary TARs can be categorised as one of two main types depending on bearing constraint: fixed bearing and mobile bearing. The backside (i.e., non-bearing surface) of the PE insert may be attached to the inferior surface of the tibial component in the case of fixed bearing prostheses, or unconstrained in the case of mobile bearing prostheses.

Figure 2.9. Sagittal plane view of an explanted Mobility mobile bearing TAR. Top: metal tibial component. Middle: PE insert. Bottom: metal talar component.

For a TAR to function successfully, adequate fixation of the metal components to the bone is required. This is accomplished through one of two ways: the use of cement, or porous coatings. Cemented implants refers to the use of a bone cement for fixation, whereas uncemented components have a porous coating (typically Ti and/or hydroxyapatite (HA)) to promote osseointegration at the bone-implant interface. Contemporary designs typically utilise a porous coating rather than using cement for fixation as previous designs did.[58, 59] Whilst the NJR states that all of the TAR brands recorded by them are (CE marked as) uncemented implants, cement is used by surgeons in some instances (4.1% of primary procedures), for example where the bone stock is poor.[6]

As well as the presence of cement playing a role, the type of coating may also affect the outcomes of TAR. A study by Hintermann et al. of Hintegra prostheses used for revision TAR found that loosening was more common in components which were coated with a single HA layer compared those which were double-coated with Ti and HA (23% versus 5%).[60] Conversely, a design change of the AES prosthesis from a single HA coating to a double coating of Ti and HA resulted in an increased incidence of osteolysis, with Koivu et al. finding the risk of osteolysis to be over 3 times higher, as well as more severe, for devices with the Ti-HA double coating compared to the HA coating alone in a series of 130 AES TARs.[61] For AES

implants with Ti-HA coating, scanning electron microscopy (SEM) with energy dispersive X-ray spectroscopy (EDX) analysis by Koivu et al. revealed Ti and CoCr particles in periprosthetic tissue samples, with the amount of Ti high compared to that of the other metals present.[62] Although osteolysis following TAR is most commonly attributed to PE wear debris, studies have indicated that the inflammatory reaction may also be in response to necrotic autologous tissues or metal particles.[63] Therefore, the implant-derived Ti particles, reported previously with the AES prosthesis, may increase the risk of osteolysis occurring due to the associated inflammatory response to the particles, and therefore may in part explain the high prevalence of osteolysis following TAR which has been described.[61, 64]

Details of some of the currently available TAR models in the UK are given in Table 2.2. In addition to these, there are several other historical ankle replacements which are no longer in use, including Agility, AES, BOX, Buechel-Pappas, CCI, Mobility, and Rebalance, amongst others.[23]

Prosthesis	**Manufacturer**	**FDA approved**	**CE mark**	**Generation**	**Bearing constraint**
AKILE	I.CERAM	N/A	1995	Third	Mobile
Cadence	Integra Lifesciences	2015	2016	Third	Fixed
Hintegra	DTMedtech LLC	H2 2017; H3 2019	2000	Third	Fixed (H2)/ mobile (H3)
INBONE	Wright Medical Technology	2005	2011	Third	Fixed, modular system
INFINITY	Wright Medical Technology	2014	2014	Third	Fixed, modular system
INVISION	Wright Medical Technology	2018	2016	Fourth	Fixed
Salto/ Salto Talaris	Integra Lifesciences	2006 Salto Talaris	1997 (Salto);	Third	Mobile (Salto)/ fixed

Prosthesis	Manufacturer	FDA approved	CE mark	Generation	Bearing constraint
			2007 (Salto-Talaris)		(Salto Talaris)
STAR	Stryker Corporation	2009	Unknown	Third	Mobile
Trabecular Metal	Zimmer-Biomet	2012	2012	Third	Fixed
Vantage	Exactech	2016	2017	Third/ fourth	Mobile (non-USA)/ fixed (USA)
Zenith	Corin Group	N/A	2007	Third	Mobile

Table 2.2. Details of some of the currently available TAR models.[23]

2.3.2. Revision ankle replacements

Failure of TAR has traditionally meant conversion into arthrodesis.[23] However, as discussed in Section 2.1.3, ankle arthrodesis does have limitations such as limiting movement, and so revision TAR may instead be performed. The choice of procedure following TAR failure is largely dependent on the individual case in terms of both patient and surgeon.

Exchange of the PE insert, commonly due to fracture or wear of this component, is a frequently performed revision procedure, with the AOANJRR reporting that this type accounts for 48% of all revisions performed.[9] In cases where one or both of the metal components need to be revised, however, it is only recently that implants have been designed specifically for revision TAR, with the INVISION Total Ankle Revision System (Wright Medical) the first to be introduced.[65] Previously, the choice was between standard components or custom implants, the latter often being expensive and difficult to get.[23] Therefore, standard TAR components – often with bone cement added – were typically used for revision procedures.[23] The INBONE II prosthesis (Wright Medical) is one device which has been commonly employed for this purpose, and the components of which are utilised in the INVISION Total Ankle Revision System.[23]

The literature contains few studies reporting outcomes of revision TAR (i.e., replacement of a failed TAR by another). However, those that have been published indicate a high complication rate following revision TAR.[66-68] Lai et al. found that adverse events occurred more frequently following revision TAR compared to primary TAR procedures.[66] Similarly, an analysis of Swedish ankle registry revision cases by Kamrad et al. found a 55% 10-year survival rate; considerably lower than the 74% 10-year survival rate for primary procedures within the same registry.[67] A complication rate of 31% at an average follow-up of 9 months has also been reported by Williams et al. following replacement of failed Agility TARs with INBONE II TARs specifically.[68]

2.3.3. Fixed versus mobile bearing

Contemporary TARs can be classified as one of two types depending on the bearing constraint: fixed bearing and mobile bearing. In fixed bearing prostheses, the backside of the PE insert is fixed to the inferior surface of the tibial tray via a locking mechanism, making it a two-component device, whereas in mobile bearing devices, the PE insert is unconstrained, making it a three-component device. Figure 2.10 illustrates the differences in the tibial component inferior surfaces and PE insert backside surfaces (which are in contact with each other *in vivo*) of fixed and mobile bearing TARs.

Figure 2.10. Comparison of tibial component inferior surfaces and PE insert backside surfaces of explanted fixed and mobile bearing TARs. (A) Fixed bearing Salto Talaris. (B) Mobile bearing Salto.

Both fixed and mobile bearing TARs have their own perceived benefits. Mobile bearing devices were thought to increase tolerance to malpositioning during implantation.[69] On the

other hand, fixed bearing devices were considered to be associated with a reduced risk of dislocation of the PE insert.[70] In the US, the preferred choice of TAR has long been fixed bearing devices – this may be attributed to mobile bearing devices having been categorised as class III devices which undergo a more stringent regulatory pathway compared to fixed bearing devices which were able to go through the route of substantial equivalence (510(k))[71] – whereas mobile bearing devices were preferred in Europe until recent years.[26] In the UK, the increase seen in the number of TARs performed over the past decade has largely been with fixed bearing designs.[6] This change may be linked with the introduction of the fixed bearing INFINITY prosthesis in 2014; the same year that the market leader at the time, the mobile bearing Mobility prosthesis, was voluntarily withdrawn.[6] The INFINITY prosthesis is now the most commonly implanted TAR in the UK, used in 64.5% of procedures in 2022, as well as in Australia, New Zealand, and Norway.[6, 9, 44, 45]

The literature regarding whether fixed or mobile earing TAR designs are superior is limited and somewhat divided. Table 2.3 summarises the previously published studies which compare the outcomes of fixed and mobile bearing TARs. Three of these are classified as either a review, systematic review or meta-analysis, and one is an explant analysis study.

Five of the published studies were comparisons of a specific fixed bearing design with a specific mobile bearing design, with just three including multiple models of fixed and mobile bearing prostheses (including the explant analysis study by Currier et al. in which the mobile bearing group predominantly consisted of one specific TAR model (n = 35) with only one other mobile bearing TAR model (n = 1) also included. Currier et al. reported that fixed bearing prostheses were more prone to loosening than mobile bearing prostheses, with results showing that loosening was a more frequent occurrence in fixed bearing TARs (n = 18 (52.9%)) than in the mobile bearing TARs (n = 4 (11.1%)), and also after a shorter mean time *in vivo* (3.2 ± 2.1 years for fixed bearing versus 9.7 ± 4.5 years for mobile bearing).[15]

In contrast to this, other studies have reported superior revision rates for fixed bearing prostheses in comparison to mobile bearing prostheses.[72-74] A study by Assal et al. compared the fixed bearing Salto Talaris and mobile bearing Salto devices and found that the mobile bearing group had a three-times higher revision rate at 3 years post implantation.[72] Likewise, a systematic review by Roukis et al. of the Salto Talaris and Salto prostheses also reported a higher revision rate for the mobile bearing than fixed bearing model.[73] In terms of studies including different models of fixed and mobile bearing TARs, a meta-analysis by McKenna et

al. found that the survivorship of fixed bearing TARs (95.6%) was better than that of mobile bearing TARs (89.4%), however this difference did not reach statistical significance.[74]

However, other studies for which the primary outcome analysed was clinical performance found no significant differences between fixed and mobile bearing TARs.[75-78] A prospective randomised trial by Nunley et al. comparing the fixed bearing Salto Talaris and mobile bearing STAR prostheses at a minimum follow-up of 2 years reported a higher rate of reoperations for the mobile bearing device (n = 8 (19.5%)) than the fixed bearing device (n = 3 (7.0%)), however there were no significant differences in clinical improvement.[75]

Queen et al. compared the fixed bearing Salto Talaris with the mobile bearing STAR, and reported few significant differences in patient-reported outcomes, function and gait mechanics.[76] Gaudot et al. compared paired fixed bearing Salto Talaris and mobile bearing Salto TAR cases with a mean follow-up of approximately 2 years and found no significant differences in clinical performance.[77] A review by Valderrabano et al. also found no clear differences in the clinical outcomes of fixed and mobile bearing prostheses.[78]

Overall, these previously published studies which used revisions or reoperations as a primary outcome mostly agree that fixed bearing TARs have better outcomes than mobile bearing TARs. However, due to the majority of the comparative studies including one model of fixed and mobile bearing prostheses only, it is possible that conclusions given in favour of one bearing constraint or the other is actually related to specific TAR models instead. There is therefore scope for more research to be carried out into comparatively analysing fixed and mobile bearing prostheses of different designs. In particular, explant analysis studies including both fixed and mobile bearing prostheses are limited with only one meeting this criteria having been published to date.[15]

Study	TARs	Follow-up	Outcomes	Findings
Valderrabano (2012) (review)[78]	Fixed: Agility, TPR, TNK Mobile: BP, STAR, AES, Hintegra, Mobility, BOX			No clear differences
Nunley (2019)[75]	Fixed: Salto Talaris (n = 43) Mobile: STAR (n = 41)	Minimum 2 years (mean 4.5, range 2-6)	Reoperations (primary); lyst formation, tibial and talar subsidence (secondary)	Reoperations higher for mobile than fixed bearing, but no significant differences in clinical improvement
Assal (2021)[72]	Fixed: Salto Talaris (n = 131) Mobile: Salto (n = 171)	3 years	Time to revision (primary); reoperation frequency, cause, and type (secondary)	Revision rate 3x higher for mobile bearing at 3 years
Queen (2014)[76]	Fixed: Salto Talaris (n = 41) Mobile: STAR (n = 49)	2 years	Ankle kinetics and kinematics (primary); patient-reported and functional outcomes (secondary)	No significant differences
Gaudot (2014)[77]	Fixed: Salto Talaris (n = 33) Mobile: Salto (n = 33)	Fixed mean 24 months, mobile mean 23 months	AOFAS score and radiographs	No clear differences in clinical performance

Study	TARs	Follow-up	Outcomes	Findings
Roukis (2015) (systematic review)[73]	Fixed: Salto Talaris (5 studies, n = 212) Mobile: Salto (8 studies, n = 1209)	Weighted mean 55.2 months (Salto studies), 34.9 months (Salto Talaris studies)	Revisions	Revision more common in mobile (5.2%) than fixed bearing (2.6%)
McKenna (2020) (meta-analysis)[74]	Fixed: Salto Talaris, InBone Mobile: STAR, Hintegra, Mobility, Salto (total n = 1963)		Revisions	Survivorship better in fixed (95.6%) than mobile bearing (89.4%), p = 0.213
Currier (2019) (explant analysis)[15]	Fixed: 6 Agility, 14 InBone, 2 INFINITY, 11 Salto Talaris, 1 TM (n = 34) Mobile: 35 STAR, 1 BP (n = 36)	Median time *in vivo* 4.5 years (range 0.6-17.6)		Loosening more common in fixed (n = 18) than mobile (n = 14) and after a shorter duration (3.2 ± 2.1 years versus (9.7 ± 4.5 years)

Table 2.3. Summary of published studies comparing outcomes of fixed and mobile bearing TARs. Blank cells indicate that the information was unknown.

2.3.4. Biomaterials

Materials used in TARs need to have sufficient mechanical properties as well as being biocompatible in order to perform in a potentially corrosive environment and under demanding cyclic loads.[23] Biomaterials used in TARs will ideally have a similar stiffness (i.e., elastic modulus) to that of bone, have a high resistance to corrosion, and be bioactive in order to achieve osseointegration for fixation where necessary.[23]

The most common bearing combination used in contemporary TARs consists of a CoCr alloy talar component articulating against an ultra-high molecular weight polyethylene (UHMWPE) insert.[23] The tibial component, which the PE insert may or may not be fixed to depending on the bearing constraint, is typically CoCr or Ti alloy.

Table 2.4 gives the mechanical properties of different biomaterials commonly used in TARs, as well as for bone. The elastic modulus of Ti is closer to bone than that of CoCr, therefore theoretically reducing the effects of stress shielding, wherein bone density is reduced as a result of an implant removing the typical stress from the bone.

Material	**Ultimate tensile strength (MPa)**	**Yield strength (MPa)**	**Elastic modulus (GPa)**
Bone	90-140	-	10-40
CoCr	600-1795	170-750	200-230
Ti	960-970	850-900	110
UHMWPE	57	22	0.5

Table 2.4. Properties of different biomaterials used in TARs compared to bone.[23]

The metal talar component is usually manufactured from CoCr alloy via either cast or wrought forming (ASTM F75 or ASTM F1537, respectively), and the metal tibial component may be either CoCr alloy also or Ti alloy, again formed by either cast or wrought methods (ASTM F1108 or ASTM F136, respectively). Both F75 and F1537 CoCr alloys have previously been shown to have similar microstructures and microhardness.[79]

CoCr is used in most orthopaedic implants due to its desirable mechanical properties – such as strength – paired with biocompatibility.[23] CoCr is known to be a harder but less corrosion resistant material than Ti. It has also been previously demonstrated by Moharrami et al. that *in vivo* oxidation of Ti alloy can have a significant effect on its mechanical surface properties such that its hardness increases, whereas CoCr alloy was found to maintain at a constant hardness.[80]

Highly polished titanium nitride (TiN) ceramic coatings have been introduced with the aim of improving the wear performance of the metal component surfaces by increasing the hardness of the material.[23] The distinctive gold colour is given by the application of a thin film of TiN

onto the Ti (Ti6Al4V) base via physical vapour deposition (PVD).[23] These coatings may result in an increased resistance to damage from third body particles.[23] However, a high level of PE wear has been reported clinically with these thin TiN layers.[23] Experimentally, a higher surface roughness has been shown with TiN coatings in comparison to CoCr bearing surfaces; a factor which has been correlated with increased levels of PE wear.[23]

UHMWPE has long been used in joint replacements and remains the material of choice for TAR bearings due to its desirable properties of biocompatibility, strength and wear resistance.[81] Design features such as insert thickness and conformity can influence the level of stress transmitted, and in turn the performance of the UHMWPE.[23] In particular, the method of sterilisation can have a significant effect on the properties of the UHMWPE in the long-term.[23] Until about two decades ago, the standard sterilisation process for almost all UHMWPE components was gamma irradiation in air.[23] However, this method has been associated with oxidation of the UHMWPE which can often result in delamination and failure due to fatigue.[23] In all currently-used TARs, the UHMWPE insert is sterilised in an inert atmosphere instead to reduce the risk of oxidation occuring.[23]

Osteolysis due to PE wear debris has been frequently associated with failure of MoP implants.[23] The introduced of highly cross-linked UHMWPE (HXLPE) was made with the aim of reducing the amount of wear produced.[23] Most commonly, cross-linking is achieved through irradiation of the UHMWPE. This process produced free radicals, some of which create covalent bonds between chains (i.e., cross-links) by joining together.[82] As the dosage of gamma irradiation increases, so too does the degree of cross-linking.[23] With high degrees of cross-linking comes increased resistance to wear; however there is also an associated compromise in mechanical properties including reduced fatigue resistance and toughness.[23]

Simulator studies by Bischoff et al. and Schipper et al., each for 5 million cycles (MC), have both reported a significant reduction in wear rate for HXLPE compared to conventional UHMWPE inserts in TAR.[83, 84] Additionally, the study by Schipper et al. also demonstrated that significantly fewer wear particles were released by the HXLPE inserts.[84]

Implant fixation may be achieved by one of two methods: bone cement or osseointegration. The latter is promoted through the use of porous coatings on the non-articulating surfaces of the metallic components. Whilst cement has proven long-term success in hip and knee replacements, it has been identified as a source of failure in TARs.[23, 85] Currently, all the TAR brands recorded by the NJR are (CE marked as) uncemented implants. However, cement is still

used by surgeons in some instances (4.1% of primary procedures, with a further 2.3% being unconfirmed cases), for example where the bone stock is poor.[6] It should be noted that whilst the use of cement for fixation has largely stopped outside of the US, it remains that all Food and Drug Administration (FDA) approved TARs are indicated for cemented use only.[23]

Non-articulating surface coatings with a high porosity and roughness are utilised to promote fixation through osseointegration at the bone-implant interface.[23] Ti and HA are the most commonly used materials for these coatings, with plasma spraying a commonly used technique to create porous coatings onto the bulk material.

Ti theoretically has the advantage over CoCr alloy of having more similar mechanical properties to that of bone, therefore reducing the risk of stress shielding and subsequent osteolysis occuring.[23] By utilising a Ti coating with a graduation of porosity, this advantage can be further maximised through reducing the elastic modulus.[23]

For HA coatings, plasma spray is also the typical method of application. However, Bonit's technique, a method of electrochemical deposition, is an alternative that is also used.[23] There are proposed benefits of this alternative technique of applying HA. Thinner layers of coating are allowed by electrochemical deposition compared to plasma spraying (15 μm versus 50 μm). This decreased coating thickness may reduce the risk of delamination of the coating by decreasing the stresses acting at the HA-implant interface.[86] Additionally, a thinner HA layer also enables the porosity provided by the roughened surface beneath the coating – which is beneficial to promoting bony ingrowth – to be better preserved.[23]

Whilst experimentally, HA coating via both plasma spraying and electrochemical deposition has shown to improve bone-implant fixation, evidence from clinical studies is not so supportive.[60, 87] It has been suggested that HA coating may result in more periprosthetic bone cysts.[88] The AES prosthesis previously had a HA coating, however in 2004 it was replaced with the porous coating of Ti along with HA, a change with resulted in increased incidence of osteolysis.[61] In a series of 130 AES TARs, Koivu et al. found the risk of osteolysis to be over 3 times higher for implants with the Ti-HA coating compared to the HA coating.[61] Furthermore, the osteolysis cases observed were more severe after the design change.[61]

Whilst some contemporary TARs have single coatings of either Ti or HA, the most commonly utilised porous coating is a double coating of plasma sprayed Ti and HA. Some designs, for example Mobility and BOX, use sintered Ti beads on the non-articulating surfaces. Again, the aim of this coating is to promote osseointegration.

Finally, trabecular metal is an alternative fixation surface. Trabecular metal is a tantalum metal composite that is plasma sprayed onto the bulk material to form a porous structure, similar to that of cancellous bone. Currently, the Trabecular Metal TAR (Zimmer) is the only ankle prosthesis on the market to utilise this and its effectiveness is yet to be defined.[23]

2.3.5. Biotribology

Tribology may be defined as the study of *"interacting surfaces in relative motion and specifically refers to the friction, wear, and lubrication of the articulation"*.[26] The term biotribology refers to tribology in the context of biological systems.[89]

In the ankle, a synovial joint, two bony components slide relative to each other, allowing articulation of the joint.[31] This is enabled by the articulating surfaces of the bone being coated with articular cartilage (Figure 2.11).[31] In ankle joint replacements, the primary articulation is that of the MoP bearing, comprised of the bearing surfaces of the metal talar component and PE insert.

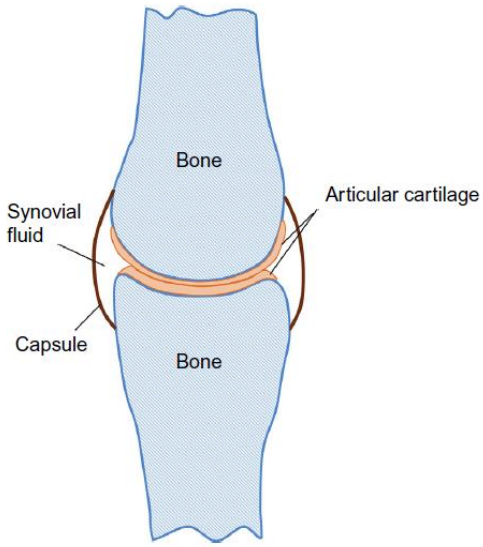

Figure 2.11. Schematic diagram of a synovial joint showing the key tribologically relevant features. Image from Hutchings.[31]

An estimated 13-17% of TAR failures are tribological-related (i.e., due to wear or breakage of the implant).[26] In addition, aseptic loosening, to which implant wear may be linked, is associated with a further approximately 19-38% of TAR failures.[26]

Wear can be defined as *"the removal of material from solid surfaces as a result of mechanical action"*, as per Rabinowicz.[90] The wear of a joint replacement is often used as an indication of its performance, with prostheses aiming to produce minimal amounts of wear.

Three laws of wear exist, which directly relate wear to load, sliding distance and hardness. Specifically, the laws state that wear volume is proportional to load and sliding distance, and inversely proportional to the hardness of the softer surface. These laws can be summed up by the Archard wear equation, where V is the volumetric wear, L is the normal load, S is the sliding distance, H is the hardness of the softer surface and K is the dimensionless wear coefficient:

$$V = \frac{KLS}{H}$$

Equation 1

The quantity K/H can be defined as the *specific wear rate*, denoted by the symbol k, and representing "*the volume of material removed by wear per unit distance slid per unit normal load on the contact*".[31] Hence, the Archard wear equation may also be expressed as:

$$V = kLS$$

Equation 2

From this, it can be seen that, under boundary lubrication, the volumetric wear is directly proportional to the sliding distance. This explains tribologically why the prostheses of more active patients will generally produce greater wear.

During the normal day-to-day use of a prosthesis, wear debris is inevitably generated from the bearing surfaces.[91] In initially well-fixed MoP prostheses, the majority of generated wear particles are expected to be accounted for by wear of the PE component, as a result of articulation against the harder metal component.[92]

Wear can also occur from contact between non-bearing surfaces due to micromotion, for example backside wear of PE inserts, as well as metal wear debris from damage of metallic components, cement particles in cemented implants, or from the porous coating of the non-articulating surfaces of metallic components in uncemented implants.[64, 92-94] Wear particles

from any of these sources may incite a foreign body reaction, osteolysis, which can limit the lifespan of the implant by causing aseptic loosening.[64]

The mechanisms of wear most commonly acting on TARs are adhesion, abrasion, and fatigue.[26] Adhesive (sliding) wear refers to material transfer between two surfaces in relative motion.[89] The Archard wear equation provides the theory of this.[31] Abrasive wear describes the removal of material due to hard particles, and is often categorised as either two-body or three-body abrasive wear accordingly.[89] Wear due to fatigue occurs as a result of cyclic stress.[89] There are also other possible wear mechanisms, for example corrosion; a process in which there is a dominating chemical reaction such as oxidative wear.[89] The different mechanisms may also occur concurrently or sequentially.[89] For example, wear particles generated due to adhesive wear may then cause abrasive wear by acting as third bodies.[89] Typically, the majority of the particulate wear debris generated in a normally functioning implant is accounted for by adhesion and abrasion, which often occur together.[26] The patient biomechanics, along with the geometry of the implant, can influence the high cyclic loads which implant materials experience, and which is associated with wear due to fatigue.[26]

Wear due to abrasion can present as damage such as scratching and burnishing, whereas cracking and delamination can indicate fatigue damage.[15, 89] Various factors can influence the severity of wear. These may be linked to the implant, for example manufacturing and sterilisation methods, the surgeon, for example alignment, and the patient, for example activity level.

There are limited published wear simulator studies for TAR, with less than ten full articles published to date.[26] This is largely due to the recent reclassification of TAR as a Class III device in Europe from a lower Class II device, and the associated higher requirements for *in vitro* testing prior to market approval. The international standard for TAR wear testing (ISO 22622:2019)[95] is a relatively recent introduction (compared to the equivalent ISO standard for hip replacements which has been in circulation for over two decades),[96] and to date no studies using this standard have been published.[26]

In synovial joints such as the ankle, synovial fluid – a natural lubricant – is retained in a capsule surrounding the joint.[31] There are three distinct lubrication regimes: boundary lubrication, fluid-film lubrication, and mixed lubrication (Figure 2.12). With boundary lubrication, there is significant contact between the asperities, which leads to high friction and wear.[89] For fluid-film lubrication, the two surfaces are completely separated, leading to low friction and minimal

wear.[89] Elastohydrodynamic (EHL) and hydrodynamic (HD) are both fluid-film lubrication regimes. The difference is that a high degree of geometric conformity is required between the two bearing surfaces for HD lubrication, whereas EHL occurs when there is a rolling motion with a low degree of conformity at the contact area. Mixed lubrication involves a mixture of the characteristics of the boundary and fluid-film regimes.[89] To minimise wear, the fluid-film lubrication is the ideal regime.[89] Typically, however, joint replacements consisting of hard-on-soft bearings, such as MoP, operate under boundary side of the mixed lubrication regime, with substantial contact between asperities.[31]

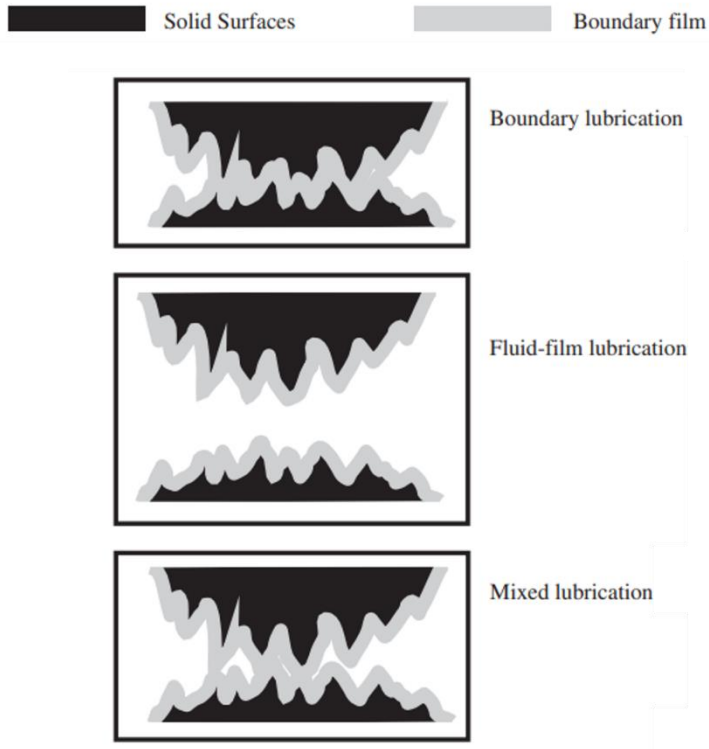

Figure 2.12. Schematic of the different lubrication regimes. Figure adapted from Jin et al.[89]

The Stribeck curve (Figure 2.13) correlates the friction coefficient with a dimensionless constant Sommerfeld number (z). The Sommerfeld number combines the variables of the lubricant viscosity (η), the bearing surfaces entraining velocity (u), and the load (W):

$$z = \frac{\eta u}{W}$$

Equation 3

In simple terms, friction can be considered as resistance to motion.[89] Low friction is desirable to decrease the likelihood of damage to the PE, with the subsequent release of wear particles.[97] However, very little research on friction of TARs has been conducted to date.[26]

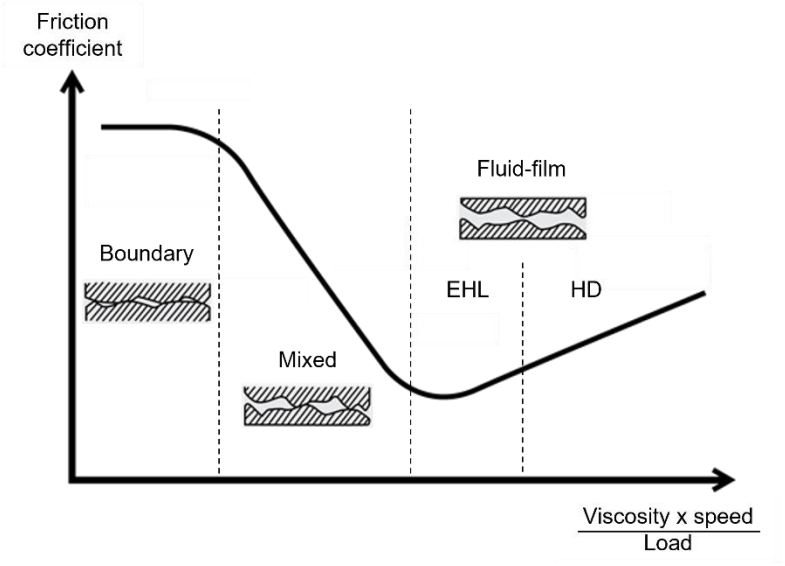

Figure 2.13. Stribeck curve with lubrication regimes. Image adapted from Ingram.[98] Notes: EHL, elastohydrodynamic; HD, hydrodynamic.

The lubrication regime is given by the λ ratio, a measure of the thickness of the lubricant film in relation to the composite roughness of the two bearing surfaces. Equation 4 defines this relationship, where h_{min} is the minimum film thickness and R_{a1} and R_{a2} are the roughness of the two surfaces.

$$\lambda = \frac{h_{min}}{[(R_{a1})^2 + (R_{a2})^2]^{1/2}}$$

Equation 4

A higher λ ratio indicates a greater separation between the bearing surfaces. $\lambda < 1$ corresponds to boundary lubrication, $1 < \lambda < 3$ to mixed lubrication, and $\lambda > 3$ to fluid-film lubrication. Since Equation 4 demonstrates that λ is inversely proportional to R_a, it therefore follows that in order to bring the bearing towards the ideal fluid-film lubrication regime, a low surface

roughness is desirable. Smooth surfaces are also required to optimise material properties and decrease the friction, as well as being correlated with reduced PE wear in TARs.[23]

2.4. Mechanisms of Total Ankle Replacement Failure

As the number of TARs being performed increases, inevitably so too does the number of failures. Various factors can contribute TAR failure, and these may act in isolation or in combination. Broadly, these causes can be grouped into three categories: patient factors, surgical factors, and implant factors. Examples of patient-related factors include obesity and activity level. Surgical-related factors include the learning curve of the surgeon and implant positioning. Implant-related factors include implant design and material choice.

Twelve main indications, which are not mutually exclusive, for revision following a primary ankle replacement are listed by the NJR.[6] In order of most to least reported, these were: aseptic loosening, infection, lysis, pain, malalignment, wear of polyethylene component, stiffness, other, soft tissue impingement, component migration/dissociation, implant fracture, and meniscal insert dislocation.[6] Aseptic loosening and lysis can be categorised as affecting either the tibial component only, the talar component only, or both; likewise with implant fracture with the additional option of affecting the PE component only.[6]

The various complications that can occur following TAR vary in severity. A classification system was proposed by Glazebrook et al. based on the likelihood of a given complication following TAR to cause failure (Table 2.5).[99] The proposed system classified complications as either low grade (very unlikely to cause failure), medium grade (leading to failure in < 50% of cases), or high grade (leading to failure in > 50% of cases).[99]

Low grade	Medium grade	High grade
Intra-operative bone fracture	Technical error	Deep infection
Wound healing problems	Subsidence	Aseptic loosening
	Postoperative bone fracture	Implant failure

Table 2.5. Classification system proposed by Glazebrook et al. for complications following TAR with grades corresponding to likelihood of causing failure.[99]

2.4.1. Patient factors

The extent to which patient-related factors contribute to the outcomes of TAR is unclear from the existing literature, although there are potential contraindications (currently undecided) for TAR including younger age (<50 years) and obesity of the patient.[23]

However, previous studies have investigated the influence of the patient-specific factors of age,[100] sex,[101] obesity,[102] diabetes,[103] and anxiety and depression[104] on outcomes following TAR, with no significantly increased complication rates reported for these patients. A set of factors relating to the patient to indicate that TAR should not be performed has therefore not yet been determined. However patient selection may impact the success of TAR. This decision will typically fall to the individual surgeon and patient in each case.

Lifestyle factors such as activity level are also likely to affect the performance of TAR, as more active patients will place higher demands on their prosthesis. This increased demand is often linked to younger patients who are generally more active.

Arthritis of the ankle, both posttraumatic and inflammatory, tends to occur in younger patients than that of degenerative hip or knee OA.[23] With younger patients, it may become necessary for a reoperation – either in the form of a revision of the implant or a conversion to arthrodesis – to be performed, due to the required implant lifespan likely being longer.[23]

The NJR reports that younger patients were more likely to need a revision, as well as a higher long-term (12-year) revision rate for females than males (10.17% versus 9.19% respectively, compared to 9.58% for all patients) (Figure 2.14).[6] Whilst patient sex is not thought to be a factor significantly influencing TAR survival,[23] a possible explanation may be offered by a reduced bone density which is typically associated with females,[105] and which has been associated with risk of periprosthetic fracture following TAR.[106]

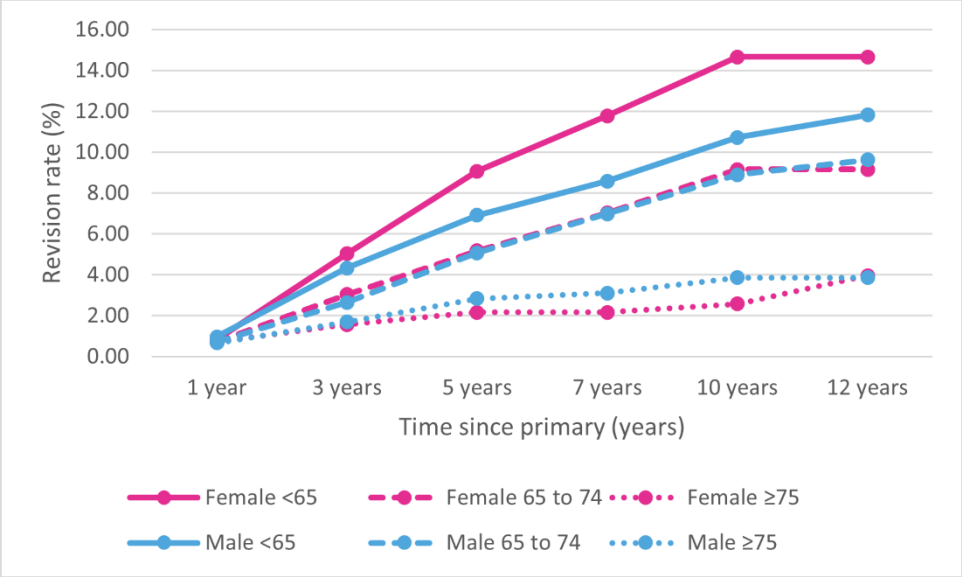

Figure 2.14. Plot of revision rates over time since primary implantation by patient sex and age using data from the NJR 2023 Annual Report.[6]

2.4.2. Surgical factors

Surgical factors refer to those related to the surgeon, that is the learning curve of the surgeon, and surgical technique, including implant positioning.

There is a learning curve associated with performing TAR procedures, meaning surgeon experience plays an important role in the success of TAR[23, 107] As the experience of the surgeon increases, a decrease in reoperations and complications is seen, reflecting the improvement in results and implant survivorship.[23]

In terms of surgical technique, the initial positioning of the implant can also play a role in the success of TARs. Component malpositioning or malalignment (Figure 2.15) is said to be the most common problem faced during TAR surgery.[23] Implant malpositioning resulting in a gap between the implant and the bone has been found, via finite element modelling, to result in a substantial increase in micromotion.[108] As excessive initial micromotion of the implant has been linked to aseptic loosening – the most commonly attributed reason for TAR failure – malpositioning is therefore a cause for concern.[108] Furthermore, malalignment can also elevate PE wear, leading to fracture of the PE insert.[23]

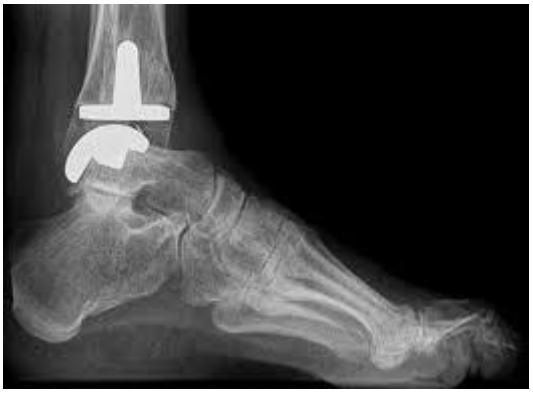

Figure 2.15. X-ray image of TAR showing talar component malalignment. Image from Thermann.[109]

Subsidence, defined as a change of ≥ 5° in the position of either the tibial or talar component, is another common problem following TAR; more frequently affecting the talar component (Figure 2.16).[110] It occurs as a consequence of the initial stabilisation of the component failing due to inadequate bony ingrowth or support of the component.[111] A correlation between talar component subsidence and periprosthetic osteolysis following TAR has also been reported by Kihara et al. [112]

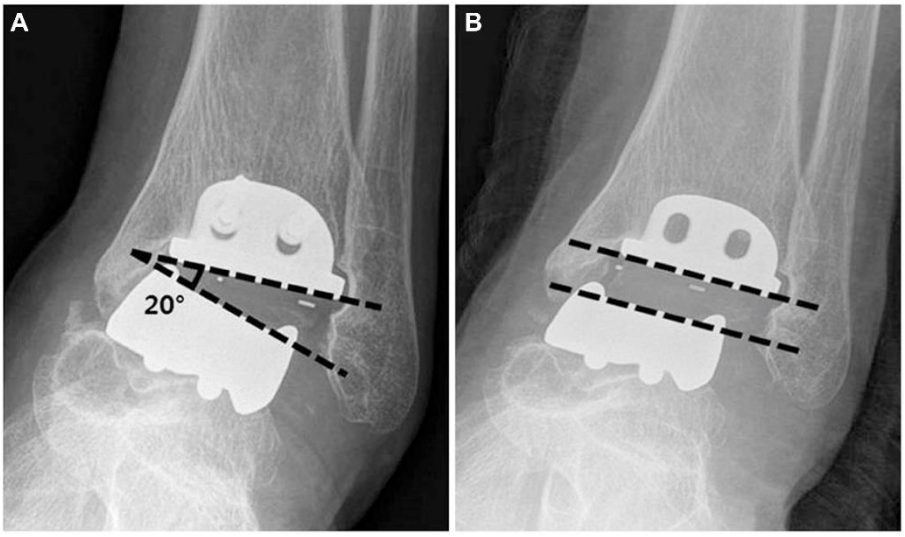

Figure 2.16. X-ray images post-TAR. (A) Talar subsidence, indicated by a change in angle ≥ 5°. (B) Corrected tibial-talar angle following revision. Image adapted from Kim et al.[113]

2.4.3. Device fixation and stress shielding

Four phases which make up the lifetime of a joint replacement (Figure 2.17) are defined by Karachalios.[114] Firstly, the early stable phase during which the initial implant fixation occurs. Then, the rest of the implant's lifespan consists of a potential early unstable phase, in which the implant fails due to surgical technique error, before a late unstable phase, where the implant fails due to the fixation being lost, or a late stable phase, where the implant fixation is maintained.[114]

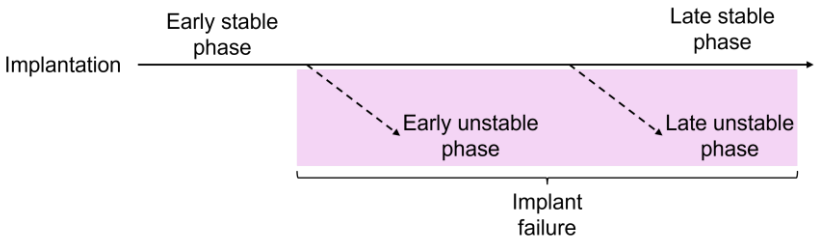

Figure 2.17. The four phases making up the lifetime of a total joint replacement. [114]

As the TARs currently in use in the UK are CE marked as uncemented implants, porous coatings are used to promote fixation via osseointegration. In addition, different TAR designs utilise a variety of different features for fixation, including long tibial stems, screws, and small bars (Figure 2.18). Each have proposed benefits and concerns (Table 2.6), meaning that there is not yet an optimised solution for fixation.[4]

Figure 2.18. Various fixation fixtures of explanted TAR metal components. Top row: tibial component fixation surfaces of (left to right) Salto Talaris, STAR, Zenith, and Cadence

prostheses. Bottom row: talar component fixation surfaces of (left to right) INFINITY, BOX, Salto Talaris, and Mobility prostheses.

Fixation fixture	Proposed benefits	Concerns
Tibial stems	Improved stability	Stress shielding
Screws	Early fixation	Implant loosening
Bars	Greater stress distributed to the bone	Increased contact stress due to decreased contact area

Table 2.6. Proposed benefits and concerns of different fixation features.[4]

Whilst porous coatings are commonly used in contemporary TARs, results from a study by Togher et al. suggested that TAR tibial components with a fully porous coated stem were associated with an increased risk of stress shielding compared to those with a smooth stem.[115] Stress shielding is a phenomenon which can cause bone resorption due to typical stresses being removed from the bone by the implant (because of the difference in mechanical properties of the two).[116] This can be described by Wolff's Law, which states that bone remodels (i.e., its density increases or decreases) in response to the stress placed on it.[117] Stress shielding may result in aseptic loosening, therefore increasing the risk of failure occurring.[116]

2.4.4. Polyethylene failure

Whilst cross-linking of UHMWPE to form HXLPE has been shown to reduce wear rates, which in turn may reduce the likelihood of failure due to PE wear debris, the irradiation sterilisation process (via electron beam or gamma irradiation) may also result in decreased mechanical properties which could lead to PE fracture or delamination.[15] Alternative sterilisation methods such as gas-plasma and ethylene oxide (EtO) have been used, however whilst these techniques do not result in the same risks of oxidation, they also do not result in the enhanced mechanical properties that come with cross-linking.[81]

A retrieval study by Currier et al. found that the oxidation rate for non-gamma (EtO or gas plasma) sterilised TAR PE inserts to be significantly lower than for gamma sterilised inserts.[15] A correlation between the oxidation measured and the presence of clinical fatigue features (i.e., delamination and/or cracking of the PE) was found.[15]

The process of irradiation involves the generation of free radicals which are introduced into the structure of the PE and either cross-link the PE (Figure 2.19) or react with available oxygen to initiate oxidation of the PE.[15] Oxidation has been shown to reduce the mechanical properties of PE to an extent such that fatigue or fracture of the component can occur, and thus is an undesirable outcome which may cause the implant to fail early.[15]

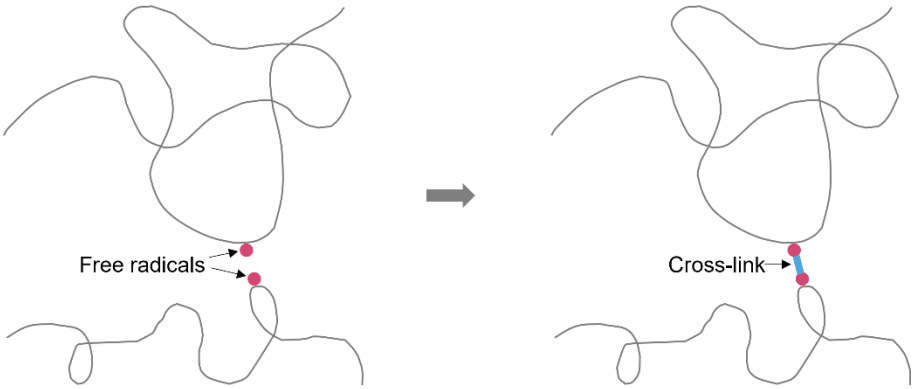

Figure 2.19. Cross-linking of PE by free radicals.

Oxidation can occur both pre- and post-implantation. Whilst barrier packaging to prevent oxygen from entering, along with sterilisation being performed in an inert environment (e.g., gamma vacuum foil (GVF) packaging of Mobility and nitrogen sterilisation under vacuum of STAR) has largely addressed oxidative degeneration pre-implantation, oxidation once the joint replacement has been implanted remains a concern.[2, 15, 23]

As well as oxidative degeneration potentially causing the PE insert to fracture, other factors may also contribute to failure via this mechanism. In March 2021, a safety alert issued by the FDA for the STAR prosthesis, the second most frequently implanted TAR in the UK in 2020, highlighted concerns over risk of the PE insert breaking. [118] As well as the thickness of the PE likely playing a role, with thinner (defined in this case as 6 mm or less) inserts reported to be more prone to fracture, younger patients aged less than 55 years (and so presumed to be leading a more active lifestyle), as well as those with OA were thought to be more susceptible to fracture of the UHMWPE component.[118]

2.4.5. Response to wear debris

In vivo, debris from TARs may be released from the metal or polymeric components, the porous coatings, or cement particles in those where it has been used; all of which have the potential to cause adverse responses.

This adverse response to wear debris, osteolysis, is an immune response resulting in periprosthetic bone resorption (Figure 2.20).[93] Aseptic loosening – the most common reason for TAR revision – may occur secondary to osteolysis.[91] Whilst osteolysis is most frequently attributed to PE particles, other particulate debris such as metal and HA may also cause this adverse inflammatory response.[61, 63]

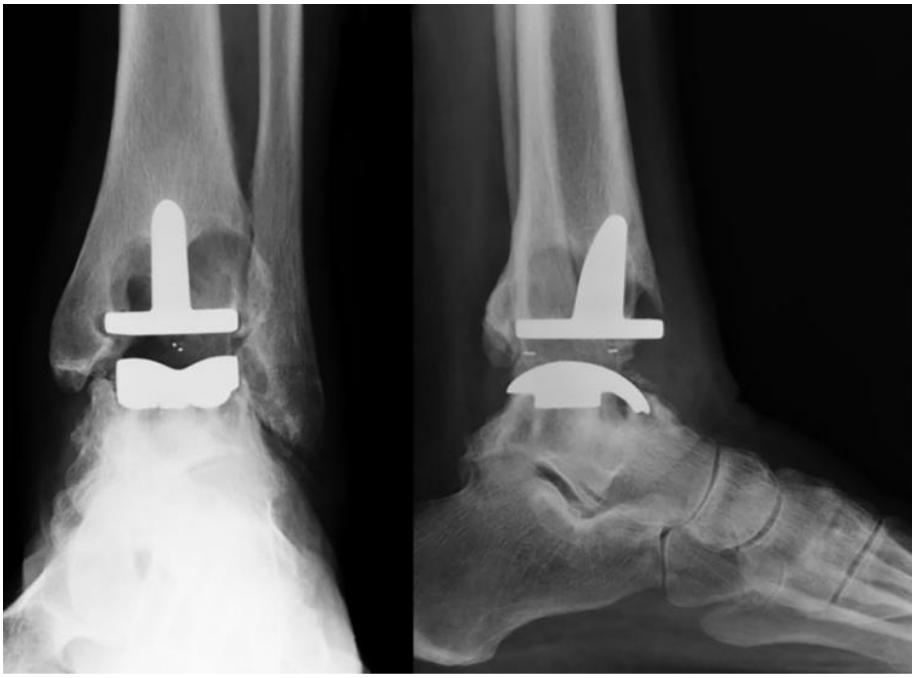

Figure 2.20. Severe osteolysis following TAR with periprosthetic bone resorption of the tibial component. Image taken from Ali et al.[119]

Micromotion (submillimetre movements between the implant and bone) is another possible source of osteolysis. Moreover, the subsequent periprosthetic bone resorption results in further micromotion, meaning a continuous cycle of stimulated osteolysis is generated.[63] By minimising the difference in the elastic modulus of the implant and bone, micromotion may be reduced.[63] Additionally, HA coatings may also decrease the risk of micromotion occurring.[63]

Whilst MoP prostheses produce considerably less metal wear debris than metal-on-metal (MoM) implants, for which adverse inflammatory responses to the generated metal particles is a known problem, it is not altogether eliminated. A THR study by Matharu et al. using NJR data found that 7.5% of the revision surgeries performed due to ARMD were for non-MoM hips.[16] Metal wear has also been reported in TKRs and TARs, with Schipper et al. having found metal implant-derived particles in 87% of 57 TAR osteolysis cases histologically analysed, and Kretzer et al. having reported about 12% of wear by weight from a TKR simulator test to be metallic.[17, 18] Furthermore, following TKR, blood cobalt (Co) levels have been found to be significantly elevated 1 year post surgery in comparison to measurements taken preoperatively.[20] These findings collectively demonstrate that metal debris may not be an insubstantial issue in MoP joint replacements.

Metal debris, in particular CoCr, is a known source of problems following joint replacement. The adverse effects of CoCr metal debris following MoM hip replacement are well documented in the literature.[120, 121] Additionally, adverse inflammatory responses following TAR have also been shown to be incited by Ti particles.[61]

ARMD is a general term[120] which encompasses more specific responses such as aseptic lymphocyte-dominated vasculitis-associated lesions (ALVAL), a concept first described by Willert et al.[122] ALVAL is a form of ARMD that presents as a hypersensitivity response and is associated with localised bone and tissue destruction.

It has been shown that individual genetics can impact a patient's susceptibility to having an inflammatory response to metal debris, meaning adverse reaction can be caused by relatively low blood Co concentrations in some patients.[19] Despite this, CoCr alloy components are used in most total joint replacements.[19]

A direct link between ALVAL infiltrate (i.e., CoCr sensitivity) and pain reported by patients with TKRs has also been shown.[123-125]

Unexplained pain is known to be common following TKR, affecting between 5-30% of patients.[126-128] Pain following TAR may also be a problem, with a reported up to two thirds of patients experiencing residual pain.[129] Whilst pain may be due to other causes such as malalignment of components or infection, in other cases the pain can be unexplained.[129] The NJR reports unexplained pain as an indication for TAR revision in 10.6% of cases.[6]

2.5. Explant Analysis Methods

Various established techniques for explant analysis have previously been used in published studies. Relevant methods include damage scoring, characterisation of surface profilometry, and wear measurement. Explant analysis can provide valuable information on the *in vivo* performance of a device.

2.5.1. Semi-quantitative damage scoring

The published literature on orthopaedic retrieval studies contains several different semi-quantitative damage scoring techniques. They are similar, however, in that they are derived from the seminal Hood scoring method.

In 1983, Hood et al. published a semi-quantitative method of assessing the damage of retrieved knee PE inserts, known now as Hood scoring.[130] In this method, the components were partitioned into sections for analysis (Figure 2.21), with each graded on a scale from 0 to 3, with 0 corresponding to no damage, 1 to 0% > 10%, 2 to 10% > 50%, and 3 to > 50% of the area covered by the respective damage mode. However, the grade given using Hood's scoring system also combined the severity of the damage, meaning a section with severe damage but covering a small amount of area could be given the same score as a section with moderate damage covering a larger area.

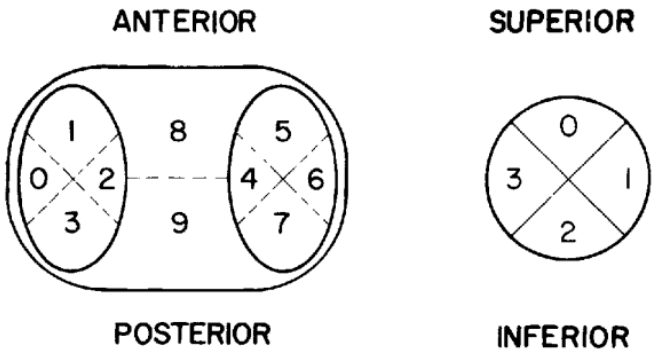

Figure 2.21. The partitioning of knee tibial insert and patellar components for the Hood scoring system. Image from Hood et al.[130]

Wasielewksi et al. built on Hood's method in their 1994 publication, which assigned separate scores for area and severity; the product of which gave an overall damage feature score (DFS).[131] The area score (AS) assigned was based on the Hood's original grading system of 0 to 3, and the severity score (SS) was also scored on a scale of 0 to 3, with 0 corresponding to no damage, 1 to mild damage (i.e., just visible), 2 to moderate damage, and 3 to severe damage (i.e., gross material loss). This method became known as the Hood/Wasielewksi method.

Following on from this, Brandt et al. published a modified version of this semi-quantitative scoring method in 2012, with the DFS again calculated from the product of the AS and SS.[132] In this method, however, the AS was graded on a scale from 0 to 10, with 0 corresponding to 0% of area covered by the respective damage feature, 1 to 0% > 10%, 2 to 10% > 20%, and so on until a score of 10 corresponding to 90% > 100% coverage. The SS was graded on a scale from 0 to 1, with 0 corresponding to no damage, 0.33 to mild damage (i.e., just visible), 0.66 to moderate damage, and 1 to severe damage.

More recently, in a 2020 paper by Ho et al., semi-quantitative damage scoring was applied to ankles. Ho et al. utilised a technique derived from Hood scoring to assess the damage of TAR PE inserts.[133] The PE inserts were analysed in quadrants (Figure 2.22), and scored each on a scale of 0 to 4, with 0 corresponding to 0% of the area covered by the respective damage feature, 1 to 0% > 25%, 2 to 25% to 50%, 3 to 50% > 75%, and 4 to 75% > 100%.

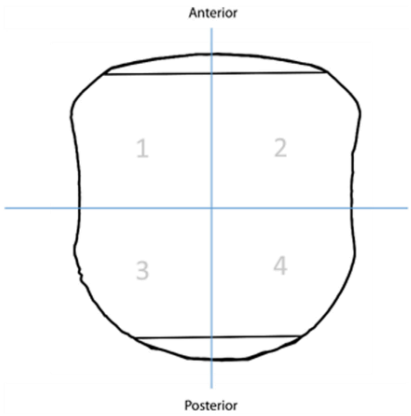

Figure 2.22. Quadrants for analysis of TAR PE inserts. Image from Ho et al.[133]

Table 2.7 summarises and compares the different semi-quantitative scoring methods described in this section. All four of the methods were originally applied to PE inserts from ether knee or ankle replacements.

Of the four methods described, two (Hood/Wasielewski and Brandt) incorporate both area covered and severity of the damage independently into the damage feature score. Both had four options for scoring the severity, however the method by Brandt et al. included substantially more options for scoring the area affected (11 versus 4). Brandt et al. compared their modified method to the Hood/Wasielewski method and found that a better representation of the PE surface damage appeared to be given by their modified method. The damage scoring method employed by Brandt et al. therefore may be the most appropriate to use in order to produce the most complete damage scores.

Method	**Damage feature score (DFS)**	**Area score (AS)**	**Severity score (SS)**
Hood[130]	DFS = AS	0-3 (0, <10%, 10-50%, >50%)	Incorporated into AS score
Hood/Wasielewski[131]	DFS = AS × SS	0-3 (0, <10%, 10-50%, >50%)	0-3 (0, 1, 2, 3)
Brandt[132]	DFS = AS × SS	0-10 (0, <10%, 10-20%, etc.)	0-1 (0, 0.33, 0.66, 1)
Ho[133]	DFS = AS	0-4 (0, <25%, 25-50%, 50-75%, >100%)	Not accounted for

Table 2.7. Summary of the different semi-quantitative scoring methods.

Seven modes of UHMWPE surface damage were identified by Hood: scratching, pitting, abrasion, burnishing, delamination, embedded debris (such as poly(methyl methacrylate) (PMMA)), and surface deformation.[130] Hood defined these damage modes as per the following descriptions. Scratching is a form of abrasive wear characterised by indented markings

typically observed in an anteroposterior direction in worn areas.[130] These typical characteristics of scratches are useful in differentiating those which have occurred *in vivo* with those which have been caused by component removal (i.e., surgical retrieval damage).[130] Pitting is described as small depressions in the articulating surface.[130] Abrasion refers to a mechanism of wear in which hard particles displace or remove material from a surface with a ploughing motion.[31] In these areas, the PE appears *"shredded or tufted"*.[130] Areas affected by burnishing appear highly polished with this damage corresponding to the mode of adhesive wear (which is related to sliding wear).[31, 130] Delamination is characterised by the removal of PE sheets.[130] Embedded debris can be recognised by the difference in colour and/or texture to that of the UHMWPE.[130] Initially, Hood limited this mode of damage to include PMMA debris only (i.e., particles from the PMMA bone cement), however other particles for example from the metallic components could also become embedded within the UHMWPE. This debris can cause third body wear. Finally, surface deformation describes a permanent (i.e., irreversible) change in the component surface.[130] It may also be referred to as plastic deformation. In contrast to the other damage modes defined, surface deformation does not necessarily correspond to wear as material is not removed.

2.5.2. Surface profilometry

Surface profilometry may be measured on lines (i.e., 2D), or areas (i.e., 3D). Areal profiles may provide additional, more relevant, information since real surfaces contact over areas rather than lines.[31]

The parameters traditionally used to describe the profile of a 2D surface (i.e., a line profile) such as average surface roughness, root mean square roughness, skewness, and kurtosis are typically denoted by R_a, R_q, R_{sk}, R_{ku} etc., respectively. For areal (3D) profiles, equivalent functions have been defined in the form of S_a, S_q, S_{sk}, S_{ku} etc.[31]

Whilst surface roughness measurement can be evaluated in both the microscale and nano- to atomic-scale, the former is sufficient for the majority of manufacturing and engineering surfaces.[134] Broadly, microscopic surface roughness measurement methods can be categorised as either contacting or non-contacting.[134] In retrieval analysis of orthopaedic implants, two common surface profilometry methods are using a mechanical stylus (contacting) and using an optical profilometer (non-contacting).

Mechanical stylus techniques involve taking at trace along a surface. There are potential disadvantages associated with mechanical styles techniques. Firstly, there is the possibility of damaging the surface if the load applied by the stylus cause the stresses to exceed the hardness of the material being analysed.[134] Secondly, the measured profile may be distorted to some degree due to the shape of the finite size of the stylus (Figure 2.23).[134]

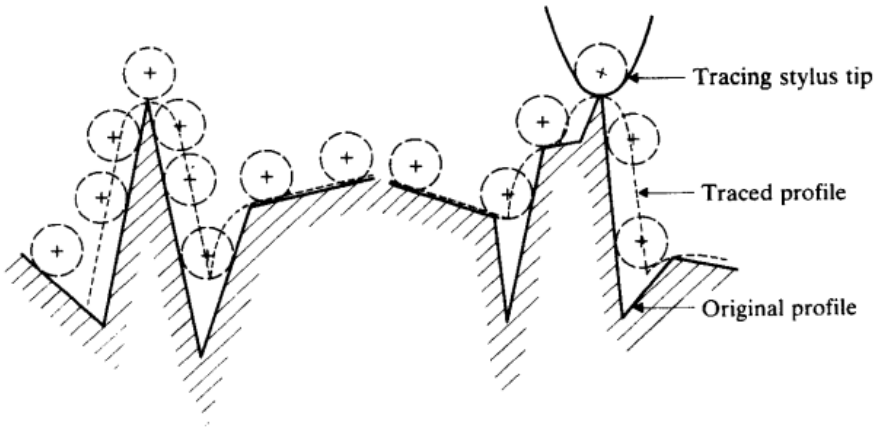

Figure 2.23. Exaggerated distorted measured surface profile using a contacting stylus. Image from Bhushan.[134]

Optical profilometers use scanning white light interferometry to measure and image surfaces.[135] As this is a non-contacting method, the surface being analysed is not damaged. Additionally, this technique provides more information by measuring 3D areal surfaces.

2.5.3. Wear measurement

With wear often being used as an indicator of the performance of a joint replacement, wear measurement is an important part of explant analysis.

Gravimetric testing is a standardised method of wear volume quantification.[136] It can be considered as the 'gold standard' for wear measurement and as such, is widely used as a benchmark within the analysis of joint replacements. This technique involves comparing the weight of the explanted (i.e., worn) component to that of an unused (i.e., unworn) one of the same design. The difference in mass can be converted to volume by knowing the density of the material of the component being examined using the following equation, where V is volume, m is mass, and ρ is density:

$$V = \frac{m}{\rho}$$

Equation 5

Whilst gravimetric measurement is useful for some applications, for example *in vitro* testing or validation of a new quantification methodology, it is not usually best suited to explant analysis due to the nature of requiring an unworn component matching the retrieved one, which generally is not practical. Additionally, the manufacturing tolerances on PE components can be relatively wide, meaning an unworn component may not precisely match a retrieved one.[137]

A coordinate measuring machine (CMM) methodology has previously been established for explanted hip and knee prostheses.[138-140] This volumetric wear analysis has been proved to be a reproducible method of producing results within a margin of accuracy that is clinically relevant.[139] The CMM technique uses a ruby probe to take scans of the geometry of the component surface being analysed and compares this to an ideal unworn surface. The volumetric wear loss that the retrieved component experienced *in vivo* can then be calculated, along with a geometrical wear map to illustrate the locations where wear occurred.

Whilst volumetric wear has been quantified for explanted hip and knee replacement components (specifically, hip heads, cups, trunnions, and tapers, and knee PE inserts), no similar technique has been established yet for use with explained ankle prostheses. To the best of the authors knowledge, no *ex vivo* wear rates for TARs have been reported in the existing literature. Instead, to date, TAR wear rates have come from a limited number of published *in vitro* simulator studies. Wear rates reported by these studies range from 1.2 ± 0.6 to 19.6 ± 12.8 mm^3/MC (i.e., approximately 1.2 to 19.6 mm^3/year, on the basis that 1 MC equates to approximately 1 year *in vivo*).[138] Table 2.8 summarises these previous TAR simulator studies and gives their reported wear rates. The wide range of wear rates reported may at least in part be accounted for by the varying simulator test conditions employed. As well as the models of TAR differing, it should be noted that the inputs, such as range of motion, load applied, lubricant used, and number of cycles tested, vary between studies. For example, Affatato et al. used a considerably lower peak axial load of 1.6 kN (approximately half the 5x body weight peak load used by the majority of the other studies).[26, 141] Additionally, the use of deionised water by Affatato et al. as a lubricant (rather than bovine serum) could affect the resulting wear rates due to being a poor representation of the *in vivo* lubrication.[26, 141] Taken together, these varying conditions means that direct comparisons between the reported results by these studies is not possible. Furthermore, the wear rates produced by these simulations may not accurately

represent the conditions experienced by TARs *in vivo*, and therefore there is a need for *ex-vivo* data to corroborate these.

Study	TAR design	Number of cycles (MC)	Wear rate (mm^3/MC)
Affatato et al. (2007)[141]	BOX	2	19.6 ± 12.8
Bell and Fisher* (2007)[142]	Buechel-Pappas	5	10.7 ± 11.8
	Mobility	5	3.3 ± 0.4
Bell and Fisher† (2007)[142]	Buechel-Pappas	5	16.4 ± 17.4
	Moblity	5	10.4 ± 14.7
Bischoff et al. (2014)[83]	Zimmer Trabecular Metal (CPE)	5	7.4 ± 1.3‡
	Zimmer Trabecular Metal (HXLPE)	5	1.9 ± 0.3‡
Smyth et al. (2017)[143]	Zenith	12	1.2 ± 0.6

*Table 2.8. Reported wear rates from published TAR simulator studies. Notes: MC, million cycles; CPE, conventional UHMWPE; *, without antero-posterior motion; †, with antero-posterior motion; ‡, mg/MC.*

Another previous study has measured the linear wear of retrieved TAR PE inserts. Affatato et al. used a CMM methodology to measure the linear penetration on the PE inserts of 3 retrieved BOX prostheses, as well as on 4 PE inserts of the same design following 2 MC on a joint simulator.[144] An average linear penetration of 0.058 mm was reported for both the retrieved inserts and those which had undergone simulator testing.[144]

2.6. Retrieval Studies

Outcomes following TAR are not as successful as other lower limb total joint replacements; a fact which can be in part attributed to the relatively poor understanding of their failure mechanisms. Retrieval studies are necessary to advance knowledge of the *in vivo* performance

of joint replacements. Explant analysis studies focus on analysis of the retrieved device, whereas histological studies look at the periprosthetic tissue. Both can provide useful insights regarding the implant-related reasons for failure. By understanding these reasons, TAR outcomes can be aimed to be improved by informing future design as well as clinical decisions.

2.6.1. Explant analysis studies

Explant analysis may be regarded as the truest method of researching how joint replacements perform because it analyses devices that have actually been used *in vivo*, covering the various 'normal' and adverse conditions that a prosthesis has experienced. It is a useful way of analysing the *in vivo* performance of a device as well as for validating results from *in vitro* studies, as done by Affatato et al.[144]

Despite its importance, however, retrieval analysis for TARs is limited, and the previous studies which have been carried out have primarily focused on analysis of the PE inserts, specifically surface damage mode analysis. These previous TAR explant analysis studies are summarised in Table 2.9.

Study	**TARs analysed**	**Explant analysis performed**
Vaupel* (2009)[145]	10 fixed bearing (Agility) – PE inserts, tibial and talar components	Damage mode analysis (PE bearing surface, tibial, and talar)
Greenwald* (2010)[146]	35 mobile bearing (STAR) – PE inserts	Damage mode analysis (PE insert bearing and backside surface)
Ho* (2021)[133]	14 fixed bearing (12 InBone, 2 INFINITY) – PE inserts	Damage mode analysis (PE insert bearing surface)
Currier* (2018)[15]	34 fixed bearing (6 Agility, 14 InBone, 2 INFINITY, 11 Salto Talaris, 1 TM), and 36 mobile bearing (35 STAR, 1 BP) – PE inserts focused	Wear and fatigue damage analysis (PE insert bearing surfaces); rated for fixation (metal components) and oxidation (PE insert)

Study	TARs analysed	Explant analysis performed
Cottrino† (2016)[64]	6 mobile bearing (AES) – PE inserts, tibial and talar components	Microstructural and tomographic analysis
Affatato‡ (2009)[144]	3 mobile bearing (BOX) – PE inserts	SEM, CMM, and micro-Raman spectroscopy (compared with simulator results)

*Table 2.9. Summary of previous TAR retrieval studies. Notes: *, US; †, France; ‡, Italy.*

From the previously published studies, burnishing, scratching, pitting, and abrasion were the most commonly identified damage features on the PE inserts.[15, 133, 145, 146] Fracture of the PE was also seen.[15, 146] Additionally, the findings from Vaupel et al. indicated that edge loading is experienced by the PE insert *in vivo*, resulting in PE wear due to greater contact stresses at the area of articulation.[145] Findings of non-uniform distribution of damage were also reported by Ho et al., with the PE inserts analysed exhibiting a greater concentration on the posterior aspects of the components, and resulting corresponding higher stresses in this area potentially contributing to the prosthesis failure.[133]

The analysis by Currier et al. comprises the largest published TAR explant analysis study to date, to the best of the author's knowledge. Within this study, retrieved PE inserts were analysed for four damage modes, with abrasion and burnishing used as indicators for wear, and cracking and delamination used to evaluate fatigue damage.[15] Loosening was found to be a more frequently experienced issue in fixed bearing devices compared to mobile bearing devices, and also after a shorter time *in vivo*.[15] A higher rate of oxidation was associated with PE inserts which had been gamma sterilised compared to those which were sterilised by other methods (gas plasma or EtO).[15] Furthermore, of the PE inserts analysed for oxidation via Fourier transform infrared spectroscopy (FTIR), 20% had fractured *in vivo*, of which all were gamma sterilised. A correlation between clinical fatigue damage of the PE inserts (indicated by delamination and/or cracking) and oxidation was also found.[15] It should be noted that the same implants analysed in a separate later study by Ho et al. were also part of this larger cohort of samples analysed by Currier et al.[15]

The AES implants included in the study by Cottrino et al. were designs with the double layer Ti-HA coating.[64] As has been previously described in other studies of AES implants, the issue

of coating particle release was identified.[64] These particles were thought to migrate in between the MoP bearing, accelerating wear of the device and therefore the potential for osteolysis to occur.[64]

To the best of the author's knowledge, none of the published explant analysis studies have included analysis of all four articulating surfaces of the TAR components (PE insert bearing and backside surfaces, tibial component inferior surface, and talar component bearing surface). In particular, limited research has been carried out on retrieved metal (tibial and talar) components, in terms of both their articulating and non-articulating surfaces, meaning there is scope for further analysis in this area.

2.6.2. Histological studies

Some histological studies in which the periprosthetic tissue surrounding TAR is analysed have also previously been published. A summary of the different types of particles identified in each is given in Table 2.10.

Study author	TARs analysed	Particles identified
Koivu (2009)[61]	130 AES	Ti, CoCr, Al, Mo
Dalat (2013)[147]	22 AES	PE, metal
van Wijngaarden (2015)[148]	1 AES, 6 Buechel-Pappas, 1 Salto, 13 CCI Evolution	PE, metal
Schipper (2017)[18]	48 Agility, 4 INBONE, 1 INBONE II, 2 Salto Talaris, 2 STAR	PE, metal
Stratton-Powell (2023)[149]	13 AES, 1 Rebalance, 1 Buechel-Pappas	UHMWPE, CaP, CoCr, CPTi, Ti, SS

Table 2.10. Summary of previous TAR histological studies. Notes: Ti, titanium; CoCr, cobalt-chromium; Al, aluminium; Mo, molybdenum; PE, polyethylene; CaP, calcium phosphate; CPTi, commercially pure titanium; SS, stainless steel.

Histological studies in the literature have primarily been of the Agility and AES prostheses, both of which are no longer in use. These previous studies have reported the presence of metal

particles, along with PE particles, in the periprosthetic tissue of between 60% and 90% of osteolytic samples.[18, 61, 147-149]

The histological studies by both Koivu et al. and Dalat et al. examined differences between the AES prosthesis before and after the porous coating changed from HA only to a Ti-HA double layer.[61, 147] Koivu et al. found that the incidence of osteolysis was 3 times higher for the Ti-HA coated implants.[61] Dalat et al. suggested that delamination of the Ti-HA coating may be induced due to fretting during the process of osseointegration.[147] It should be noted, however, that metal particles were also identified in the periprosthetic tissue of all of the HA coated group.[147]

All of the histological studies included in Table 2.10 were analysing TARs which had failed due to osteolysis. Whilst the phenomenon of osteolysis following TAR is not yet fully understood, the published studies agree that implant-derived wear particles – along with other factors – are likely to play a substantial role.[18, 147, 149] All studies identified both PE and metal (including CoCr and Ti) particles in the osteolytic samples, as well as other particles of CaP being commonly identified by Stratton-Powell et al.[149] These findings demonstrate that a complex environment exists around TARs, consisting of a range of implant-derived particulate debris which may all have the potential to cause an osteolytic response.

For well-functioning TARs, the size and concentration of PE wear particles found in the synovial fluid were found to be similar to those from TKRs.[150] However, the shape differed, with particles generated by TARs significantly rounder.[150] As both the morphology and amount of wear particles is known to affect the biological reaction incited by them, it may be that the response associated with TAR is not necessarily the same as that for other joint replacements, and as such, further ankle-specific research is warranted.

2.7. Summary

This review of the existing literature regarding the failure of TARs highlights the limited studies published, particularly explant analysis studies. This research gap may contribute to the lack of knowledge on the mechanisms of failures of TARs, which in turn may play a role in the unsatisfactory failure rates of TARs in comparison to other total joint replacements.

Aseptic loosening is known to be the most common reason for failure following TAR, however its causes are not fully understood. While the literature indicates that wear is believed to play

a key role, there are several types of implant-derived debris that could contribute to this type of failure, and the type(s) primarily responsible is unknown. This is in part due to the lack of quantification of wear from TARs to date. To the best of the author's knowledge, no previously published studies have measured the amount of volumetric wear produced by explanted TAR components.

For those explant analysis studies that have been published, there has been a focus on the PE component. Analysis of retrieved metal components – along with PE inserts – has the potential to provide further information on damage mechanisms of TARs.

One of the major themes that emerges from the literature is the discussion of fixed versus mobile bearing TARs, for which no conclusive answer has been determined as of yet. Through analysing the influence of design features including bearing constraint of different contemporary TARs, future design may be informed with the aim improve patient outcomes.

Chapter 3. Materials and Methods

The methods used to carry out the present research are described in this chapter. This covers an initial analysis to identify the damage modes present on the explanted components and also the ensuing explant analysis techniques informed by these findings and forming the main section of this work.

This chapter consists of several major sections. Firstly, the details of the explants included in this study are specified, along with corresponding clinical details where possible. The methods relating to the initial component surface damage mode analysis are then given. Next, the main explant analysis methods are detailed. Within this, several techniques are covered, which fall within the broader themes of semi-quantitative damage assessment, surface profilometry, material characterisation, and volumetric wear quantification. Finally, the statistical methods used for analysis of the data obtained from these methods described are outlined.

3.1. Explant Details

Twenty-eight explanted TARs were included in the present study. Here, TAR refers to the component explanted during revision surgery for each prosthesis. In the majority of cases within this study, this included retrieval of all three components (tibial component, talar component, and PE insert). However, in some instances, one or more of these components were not explanted. Specifically, this was the case for 6 of the explanted devices: 1 without PE insert, 1 without tibial component, 1 without talar component, and 3 without tibial and talar components.

Within TAR explant analysis studies, a common limitation is the lack of availability of explanted devices. This was also the case in the present study; whilst a range of TAR models were available, the numbers of each were limited somewhat. This may be attributed to the fact that in the UK, physical analysis of used medical devices such as joint replacements is not mandated.[151] Additionally, ethical approval, especially where patient data is concerned, can be a lengthy process. Therefore, explant analysis is not a routinely performed service and as such will not be considered for many TARs which are revised. Nevertheless, explant analysis can provide valuable insights and so has worthwhile benefits even considering the difficulties of obtaining explants for analysis.

3.1.1. Inclusion criteria

The explanted TARs included were revised for any reason (i.e., there was no exclusion criteria regarding the cause of failure). Likewise, there was no specific exclusion criteria limiting the model or bearing constraint of TARs. Also included were TARs where only one or two components were retrieved. The reasoning behind these criteria was to maximise the number of explants which could be analysed, and so which data could be collected from, thereby strengthening any conclusions found.

The study included contemporary TARs, defined here as third-generation or fourth-generation implants. While the majority of the TARs included are currently in use, this study was not limited to just those that were; hence the Mobility and BOX prostheses, which were voluntarily withdrawn in 2014 and 2020, respectively, were also included.[152] This was again so that the number of explants analysed could be maximised, given that these models made up over a third of the TARs available for this study. It was also reasoned that findings relating to these particular prostheses may not be implant specific, particularly given the similar design features to other TARs.

3.1.2. Explant preparation

Prior to the study commencing, ethical approval was obtained for the explant analysis from the County Durham and Tees Valley 2 Ethics Committee, IRAS 14119.

The explant details such as model and bearing constraint were catalogued, along with any available corresponding clinical details such as reason for revision. Patient-identifiable data such as name and date of birth were not recorded for use in this study in order to ensure patient anonymity. The explants were anonymised in the catalogue by assigning each explant a code in the format ANKXX.

The explant components were disinfected using a KEN IQ4 Medical Washer-Disinfector. All components (polymeric and metallic) underwent a cold wash cycle, and an additional thermal cycle was carried out for the metallic components. The thermal cycle was not carried out for the PE inserts due to the possibility of the high temperatures causing damage to the components. Prior to analysis, the component surfaces were also cleaned with acetone and lint-free cloth to ensure any remaining debris was removed.

All of the analysis techniques which were performed on the explants within this study were non-destructive.

3.1.3. Explant details

The cohort of 28 explanted TARs was comprised of 9 different models: INFINITY, Cadence, Salto Talaris, Salto, Mobility, STAR, Hintegra, BOX, and Zenith. To the best of the authors knowledge, all of these models except the Mobility and BOX are currently in use. Three of the prosthesis designs were fixed bearing, and 6 were mobile bearing. The details of these are given in Figure 3.1.

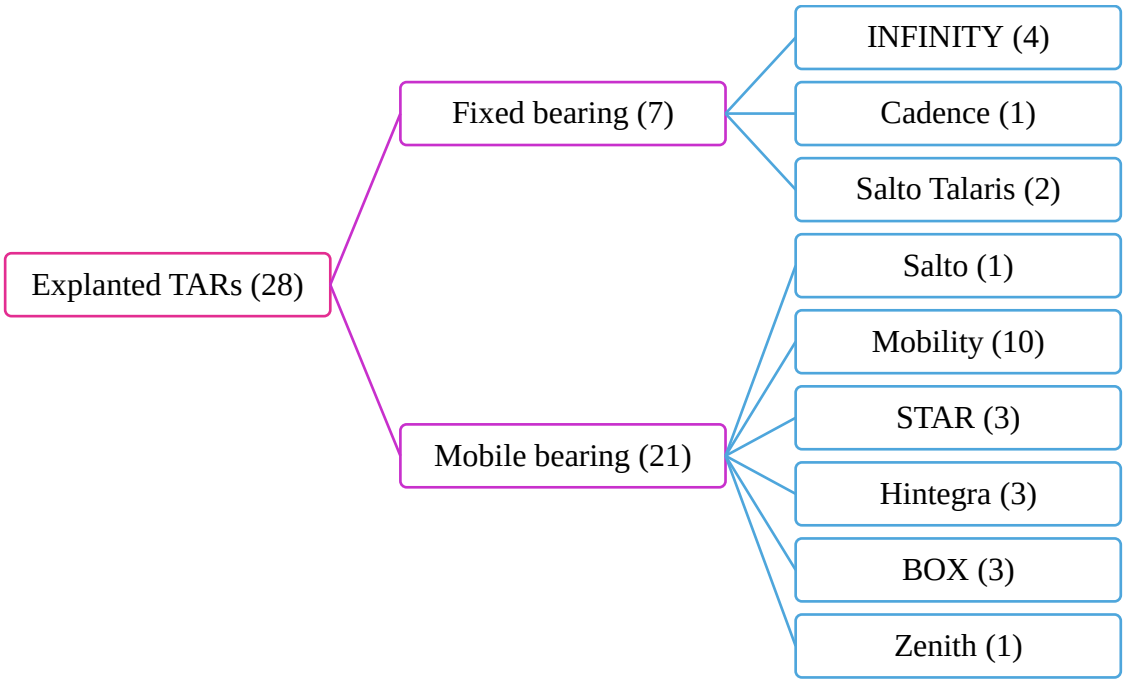

Figure 3.1. Numbers of the explanted TARs included.

From the 28 TARs included, 27 PE inserts, 24 tibial components and 24 talar components were present.

A comprehensive overview of the catalogued details is given in Table 3.1, including information on the explant as well as clinical details such as implantation side, implantation duration and patient sex where this was available.

Also included in Table 3.1 is the PE insert thickness. The value given by the manufacturer on the component was used where this was visible. For components where this value was either not present or not visible due to wear, the thickness of the PE insert was measured manually, taking the midpoint of the side of the component as the reference point. This was the case for ANK8, ANK9, ANK13, ANK16, ANK20, ANK22, ANK24, ANK25, ANK26 and ANK28.

Code	**Prosthesis**	**Components present**	**Insert thickness (mm)**	**Implantation side**	**Patient sex**	**Time *in vivo***
ANK1	Hintegra	No tibial or talar	6		Male	
ANK2	Salto Talaris	No talar	8		Male	
ANK3	Mobility		7	Right	Male	
ANK4	Mobility	No tibial	11	Left	Male	
ANK5	Mobility		5			
ANK6	Hintegra		7	Left	Male	
ANK7	Salto Talaris		8	Right		
ANK8	BOX		5			
ANK9	INFINITY		8		Male	4 years
ANK10	INFINITY		8	Left	Male	
ANK11	Salto		4	Right		
ANK12	Mobility		5	Right	Female	
ANK13	STAR		6			
ANK14	Mobility		5			
ANK15	Mobility		7			
ANK16	BOX		4	Left		
ANK17	STAR	No PE insert		Right		
ANK18	Mobility		5			
ANK19	Mobility		5			
ANK20	INFINITY		6		Female	
ANK21	Mobility	No tibial or talar	7			

Code	Prosthesis	Components present	Insert thickness (mm)	Implantation side	Patient sex	Time *in vivo*
ANK22	BOX		6		Male	
ANK23	Mobility		5		Male	Approx. 12 years
ANK24	STAR		6	Right	Male	
ANK25	Cadence		7	Left	Male	
ANK26	Zenith		5		Female	
ANK27	Hintegra		5	Left		
ANK28	INFINITY	No tibial or talar	6			

Table 3.1. Catalogue of TAR components included. A blank entry in the 'components present' column indicates that all three components were present. A blank entry in the 'implantation side', 'patient sex', or 'time in vivo' columns indicates that this information was unknown.

Figure 3.2 shows the component surfaces (tibial component articulating (inferior) and non-articulating surfaces, PE insert backside and bearing surfaces, and talar component bearing and non-articulating surfaces) of the different designs of TARs analysed. Enlarged versions of these images are also included as a supplementary (Appendix B).

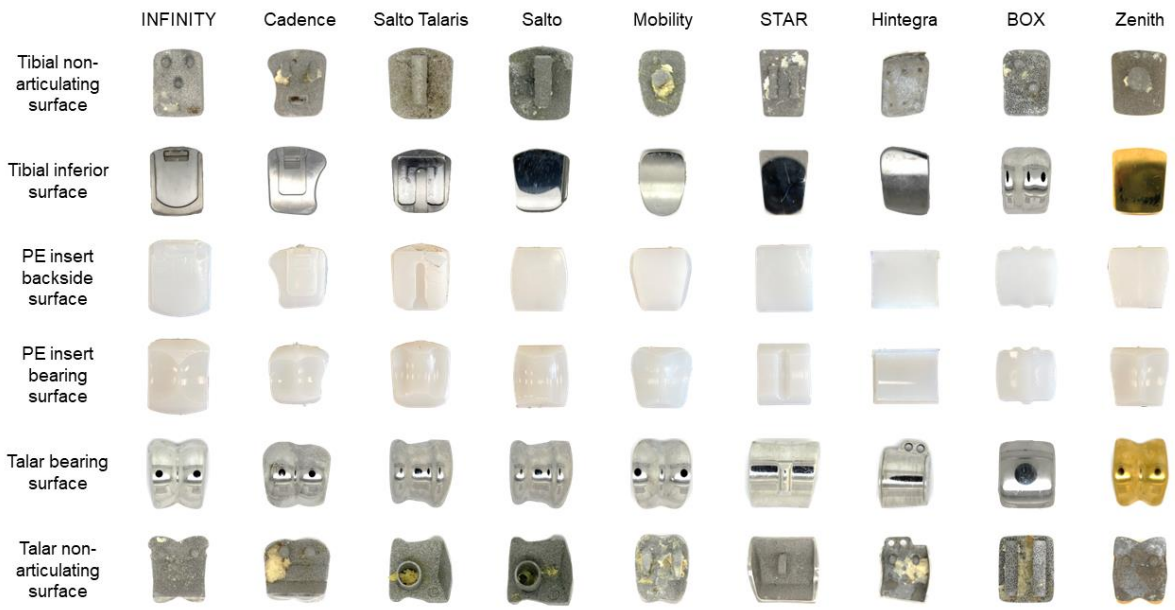

Figure 3.2. Macroscopic images of explanted components of the different TAR models.

According to available manufacturer information, 5 of the 24 tibial components were composed of Ti alloy (including 1 coated with a TiN ceramic layer), and the remining 19 were composed of CoCr alloy. Of the 24 talar components, just 1 was composed of Ti alloy (also with a TiN ceramic layer coating), and the other 23 were composed of CoCr alloy.

The majority of the metal components were manufactured from CoCr alloy (Co28Cr6Mo) as per ASTM 75, referring to forming by casting method, with Ti alloy (Ti6Al4V) formed by wrought method as per ASTM F136 also known to be used (Table 3.2). All of the talar component articulating surfaces have a polished finish, as well as all of the tibial component articulating surfaces except that of the INFINITY prostheses.

A variety of different porous coatings were utilised by the included explants: Ti only, HA only, double coated Ti and HA, and double coated HA and calcium phosphate (CaP). Two of the models (Mobility and BOX) had beaded non-articulating surfaces.

Prosthesis	Tibial component alloy	Talar component alloy	Non-articulating surfaces coating
INFINITY	Ti	CoCr	Ti plasma spray
Cadence	Ti ASTM F136	CoCr ASTM F75	Ti plasma spray
Salto Talaris	CoCr ASTM F75	CoCr ASTM F75	Ti plasma spray
Salto	CoCr ASTM F75	CoCr ASTM F75	Ti plasma spray
Mobility	CoCr	CoCr	Ti sintered beads (Porocoat; DePuy)
STAR	CoCr ASTM F75	CoCr ASTM F75	Double coated Ti plasma spray and HA
Hintegra	CoCr ASTM F75	CoCr ASTM F75	Double coated Ti plasma spray and HA
BOX	CoCr ASTM F75	CoCr ASTM F75	HA plasma sprayed beads
Zenith	Ti coated with TiN	Ti coated with TiN	Double coated Ti plasma spray and CaP (BONIT; DOT)

Table 3.2. Details of the total ankle replacement designs included. Notes: Ti, titanium; CoCr, cobalt-chromium; HA, hydroxyapatite; CaP, calcium phosphate.

Two of the TARs had been affixed using cement, with one BOX prosthesis having cement visible on the non-articulating surfaces of both the tibial and talar components, and one Mobility prosthesis having cement visible on the talar component, with the tibial component not having been received. The remaining 22 tibial and 23 talar components were uncemented, meaning fixation was achieved using bony ingrowth only.

In terms of the PE insert, this component was manufactured from UHMWPE, and all would have been sterilised in an inert environment. Table 3.3 gives additional properties, where the information was available, of the PE inserts of the different TAR models analysed in the present study. One of the included designs (Cadence) had a HXLPE insert, with the other designs all being conventional UHMWPE.

Prosthesis	Insert thickness	UHMWPE type	Manufacturing method	Sterilisation method
INFINITY				EtO
Cadence		Cross-linked GUR1020	Compression moulded	Cross-linked via gamma irradiation followed by annealing
Salto Talaris/ Salto	4-8 mm	Type B 4150HP resin	Moulded	Gamma irradiation under vacuum with double-peel package
Mobility		1050 powder	Machined from extruded bar	Gamma irradiation in nitrogen with gamma vacuum foil (GVF) barrier packaging
STAR	6-10 mm			Gamma irradiation in nitrogen-vacuum
Hintegra			Moulded	
BOX	5-8 mm	PUR 1020	Machined from pressed sheets	Gamma irradiation in nitrogen
Zenith	Minimum 5 mm	GUR 1050		

Table 3.3. PE insert properties of the different TAR inserts analysed. Blank cells indicate that the information could not be found.

3.1.4. Clinical details

Where possible, clinical details including implantation duration (calculated from implantation and explantation dates), implantation side, and reason for revision as indicated by the surgeon were recorded (Table 3.4). However, this data was not available for the majority of the included explants.

Patient sex	**Implantation duration**	**Implantation side**	**Reason for revision**
Male (11) Female (3) Unknown (14)	4 years (1) Approximately 12 years (1) Unknown (26)	Right (6) Left (6) Unknown (16)	Pain and cysts (tibial and talus) (1) Unknown (27)

Table 3.4. Clinical details corresponding to the retrieved TARs.

3.2. Surface Damage Mode Analysis

3.2.1. Articulating surfaces

An initial damage mode analysis was performed on the four articulating surfaces of the explanted TAR components: PE insert bearing surface, PE insert backside surface, tibial component inferior surface, and talar component bearing surface. This initial analysis was carried out in order to identify the damage modes present on these components. The results from this would then partly inform the future analyses to be performed.

The 28 PE insert bearing surfaces and backside surfaces, 24 tibial component inferior surfaces and 24 talar component bearing surfaces were visually inspected using light microscopy with 30x magnification as well as macroscopically for the following common damage modes: pitting, scratching, embedded debris, burnishing, abrasion, delamination, striations, and surface deformation.[145, 153] These damage modes are defined in Table 3.5. For this initial analysis, both the polymeric and metal surfaces were analysed for all damage modes; which damage modes were identified on each would then inform those included in the subsequent semi-quantitative damage assessment (section 3.3) of these surfaces.

Any other additional damage to the components such as that resulting from direct metal-on-metal contact or breaking of the PE insert was also recorded. Surgical retrieval damage – determined as deep grooves or markings not coinciding with areas of wear – was excluded.[130]

Damage mode	Description	Depiction
Machining marks	Indicative of unworn (i.e., as manufactured) surface	
Pitting	Small depressions, most likely due to 3rd body particles.[130, 133]	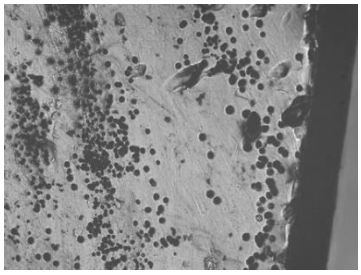
Scratching	Indented lines, typically found in worn areas.[130]	
Embedded debris	Third body particles embedded into the surface.[133]	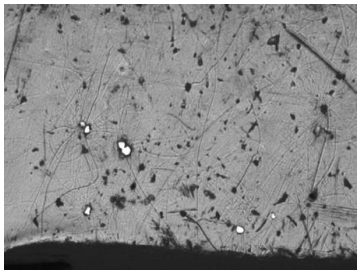
Striations	Oriented smooth peaks and valleys, typically observed on the PE bearing surface.[154]	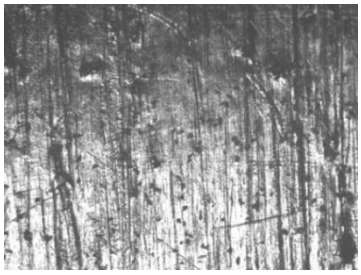
Burnishing	Characterised by a polished surface and	

Damage mode	Description	Depiction
	absence of machining marks.[130, 133]	
Abrasion	PE is tufted or shredded in appearance.[130]	
Delamination	Removal of large sheets of PE.[130]	
Surface deformation	Permanent (i.e., plastic) deformation of surface.[130]	

Table 3.5. Definitions of common damage modes along with microscopic depictions where relevant.

3.2.2. Non-articulating surfaces

The non-articulating surfaces of the 24 tibial and 24 talar components were macroscopically visually inspected for changes to their coatings. The different types of non-articulating surface coatings utilised by the tibial and talar components are given in Figure 3.3. Specifically, changes in terms of coating loss and/or changes in reflectivity were analysed.

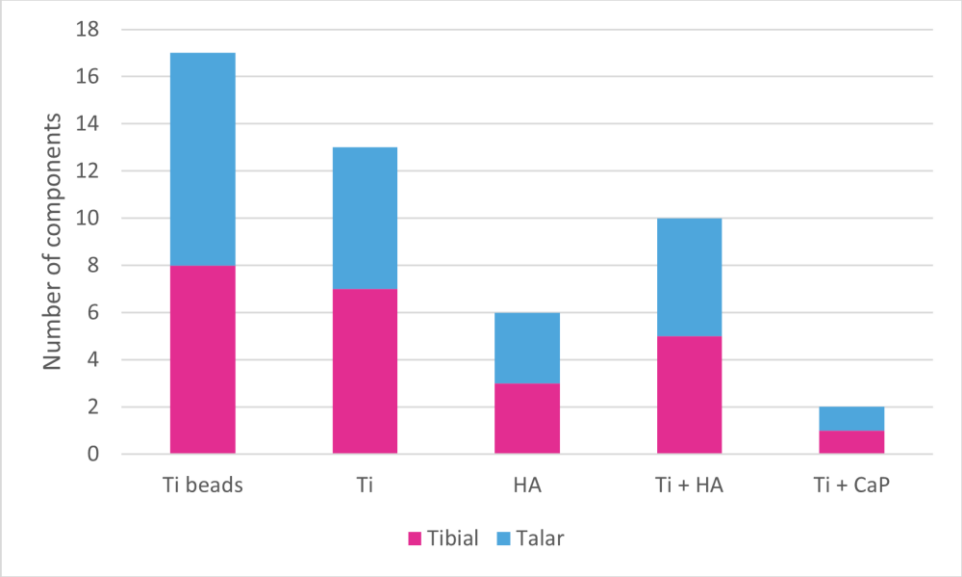

Figure 3.3. Number of tibial and talar components with different coating types.

3.3. Semi-Quantitative Damage Assessment

The results from the initial surface damage mode analysis in terms of the damage modes identified on each of the component articulating surfaces, polymeric and metallic, was then used to inform the following assessment of the surface damage using a semi-quantitative scoring method.

The component articulating surfaces were analysed using light microscopy with 30x magnification as well as macroscopically. Each surface was divided into quadrants. Since the implantation side was not known for the majority of the explanted prostheses, the quadrants were labelled as 1 to 4 rather than as anteromedial, anterolateral, posteromedial and posterolateral. However, the results were later analysed in terms of anterior and posterior aspects, as well as medial and lateral aspects where the implantation side was known.

The scoring method derived by Brandt et al. from the original Hood scoring system was followed for the semi-quantitative assessment of the component surfaces.[132] For each damage mode in each quadrant, a damage feature score (DFS) was calculated as the product of the area score (AS) and severity score (SS). The AS was graded on a scale of 0 to 10, giving 11 possibilities for the scoring which corresponded to the percentage of area covered by the respective damage mode (Table 3.6). The SS was graded on a scale of 0 to 1, giving 4 possibilities for the scoring which corresponded to the severity of the damage (i.e., how visible it was) (Table 3.7).

Area score (AS)	**% of area covered**
0	0
1	0 - 10
2	10 - 20
3	20 - 30
4	30 - 40
5	40 - 50
6	50 - 60
7	60 - 70
8	70 - 80

9	80 - 90
10	90 - 100

Table 3.6. Percentage of area covered by the respective damage mode and corresponding AS.

Severity score (SS)	**Severity of damage**
0	None
0.33	Mild
0.66	Moderate
1	Severe

Table 3.7. Severity of the respective damage mode and corresponding SS.

The component damage score (CDS) was given by the following equation:

$$\mathrm{CDS} = \sum_{j=1}^{4} \sum_{i=1}^{n} (\mathrm{AS} \times \mathrm{SS})$$

Equation 6

Where the DFS, given by (AS × SS) represents the score for each damage mode denoted by i, where i ranges from 1 to n, with n being the total number of damage modes. The overall CDS was then calculated as the sum of these scores for each quadrant, j.

Due to the nature of the SS being to 2 decimal places, the calculated CDS was also to 2 decimal places.

3.3.1. PE insert bearing damage scoring

For the assessment of the damage modes of the PE insert bearing surface, the component was divided into 4 quadrants (Figure 3.4). The anterior aspect was made up of quadrants 1 and 2, and the posterior aspect was made up of quadrants 3 and 4.

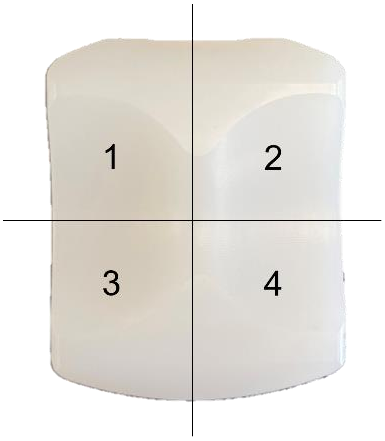

Figure 3.4. Quadrants (1-4) PE insert bearing surface divided into for semi-quantitative damage assessment.

The PE insert bearing surfaces were analysed for the following 7 damage features: pitting, scratching, embedded debris, burnishing, abrasion, delamination, and striations.

Taking into account the 7 damage features, the maximum CDS a PE insert bearing surface could get was therefore 280 (i.e., (10 x 1) x 7 x 4).

3.3.2. PE insert backside damage scoring

As for the bearing surface, the backside surface of the PE insert was divided into 4 quadrants for the assessment of the damage modes (Figure 3.5). Again, the anterior aspect was made up of quadrants 1 and 2, and the posterior aspect was made up of quadrants 3 and 4.

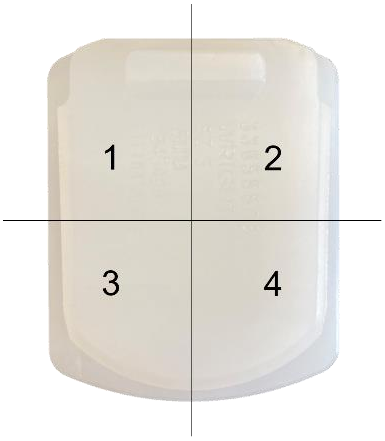

Figure 3.5. Quadrants (1-4) PE insert backside surface divided into for semi-quantitative damage assessment.

The PE insert backside surfaces were analysed for the following 7 damage features: pitting, scratching, embedded debris, burnishing, abrasion, delamination, and striations.

Taking into account the 7 damage features, the maximum CDS a PE insert backside surface could get was therefore 280 (i.e., (10 x 1) x 7 x 4).

3.3.3. Tibial component damage scoring

For the damage mode assessment of the tibial component inferior surfaces, the component was divided into 4 quadrants (Figure 3.6). Quadrants 1 and 2 made up the anterior aspect, while quadrants 3 and 4 made up of the posterior aspect.

Figure 3.6. Quadrants (1-4) tibial component inferior surface divided into for semi-quantitative damage assessment.

The tibial component inferior surfaces were analysed for the following 3 damage features: pitting, scratching, and abrasion.

Taking into account the 3 damage features, the maximum CDS a tibial component inferior surface could get was therefore 120 (i.e., (10 x 1) x 3 x 4).

3.3.4. Talar component damage scoring

The talar component bearing surface was also divided into 4 quadrants for the analysis of the damage modes (Figure 3.7). The anterior aspect comprised of quadrants 1 and 2, and the posterior aspect comprised of quadrants 3 and 4.

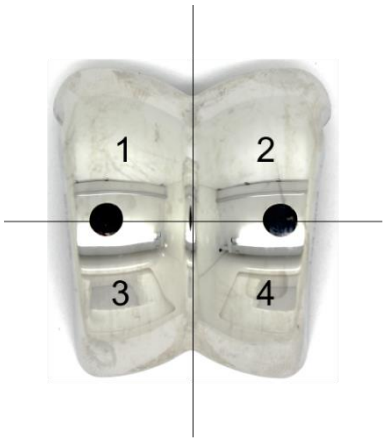

Figure 3.7. Quadrants (1-4) talar component bearing surface divided into for semi-quantitative damage assessment.

The talar component bearing surfaces were analysed for the following 3 damage features: pitting, scratching, and abrasion.

Taking into account the 3 damage features, the maximum CDS a talar component bearing surface could get was therefore 120 (i.e., (10 x 1) x 3 x 4).

3.4. Surface Profilometry

Surface profilometry was performed on the articulating surfaces of the metal components (i.e., the tibial component inferior surfaces and the talar component bearing surfaces). This was performed in order to investigate whether the roughness may affect bearing wear, and also to provide further analysis into the unexpectedly high prevalence of metallic pitting identified in terms of related changes to the surface profile. Therefore, this surface profilometry was limited to the articulating surfaces of the metal components only. A NewView 5000 non-contact 3D profilometer (Figure 3.8) with a vertical resolution of 0.1 nm was used to take the surface roughness measurements.[155] An objective lens of 10x magnification with a 2x zoom was used, giving a measurement surface area of 317 x 238 μm.

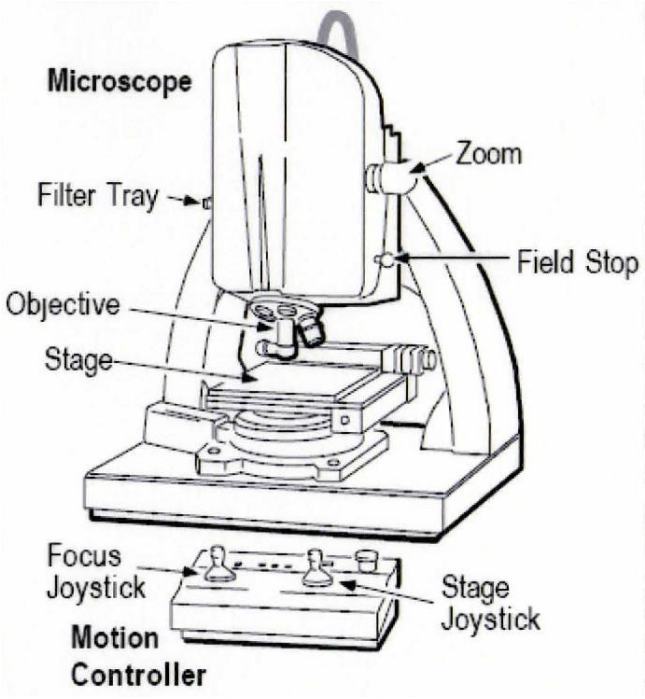

Figure 3.8. Diagram of NewView 5000 non-contact 3D surface profiler.[156]

The surface roughness parameters of average surface roughness (S_a), root mean square roughness (S_q), peak to valley height (S_z), maximum peak height (S_p), maximum valley depth (S_v), skewness (S_{sk}), and kurtosis (S_{ku}) and were measured. These parameters are defined in Table 3.8.

Parameter	**Definition**	**Depiction**
Mean surface roughness, S_a	Average deviation of the surface height from the mean	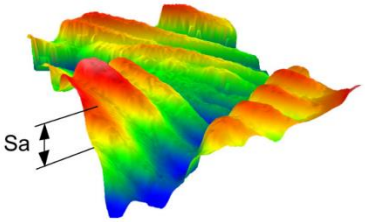
Root mean square roughness, S_q	Root mean square of the deviation of the surface height from the mean	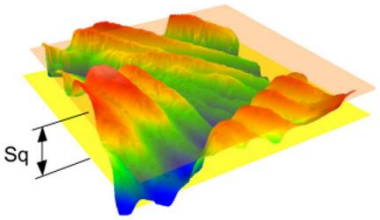

Parameter	Definition	Depiction
Peak to valley height, S_z	Height between the lowest and highest points of the areal surface	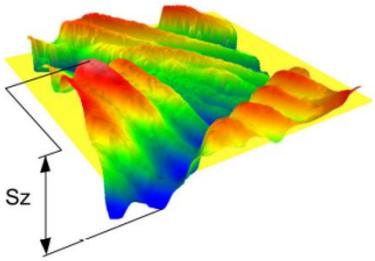
Maximum peak height, S_p	Height of the highest point of the areal surface	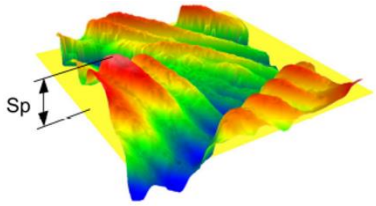
Maximum valley depth, S_v	Height of the lowest point of the areal surface	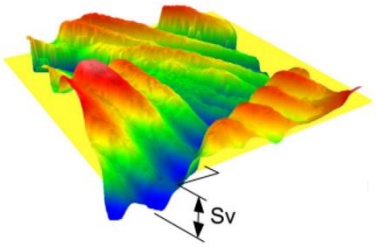
Skewness, S_{sk}	Gives an asymmetry measure by indicating the predominance of peaks ($S_{sk} > 0$) or valleys ($S_{sk} < 0$) making up the surface in terms of number or severity	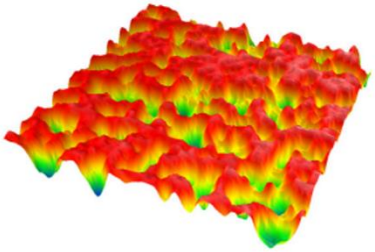
Kurtosis, S_{ku}	Indicates the presence of exceptionally high peaks or deep valleys ($S_{ku} > 3$) or lack thereof ($S_{ku} < 3$) comprising the surface	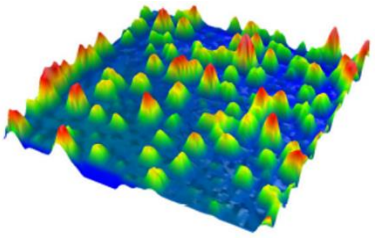

Table 3.8. Definitions of the surface roughness parameters measured. Images adapted from Zygo.[157]

3.4.1. Tibial component

Measurements were taken on both worn and unworn areas of the inferior surface. For the 13 tibial components on which pitting was identified prior via light microscopy these worn and unworn areas corresponded to pitted and unpitted areas, respectively. Five measurements were taken at each area, with the mean value used in subsequent analyses.

3.4.2. Talar component

As with the tibial components, measurements were taken on both worn and unworn areas of the bearing surface. For the 23 talar components on which pitting was identified previously, these worn and unworn areas corresponded to pitted and unpitted areas, respectively. Again, 5 measurements were taken at each area, with the mean of these used in following analyses.

3.5. Material Characterisation

Material characterisation analysis, in terms of determining the elemental composition, was performed on the metallic components as well as the identified embedded debris in PE inserts.

3.5.1. Elemental composition of metal components

An X-ray fluorescence (XRF) analyser (NITON XL3t GOLDD+, Thermo Fisher Scientific, Massachusetts, USA) was used to determine the percentage elemental composition of the metal tibial and talar components. Ten-second XRF scans were carried out. Each component was measured 3 times, and the resulting compositions for each identified element averaged.

3.5.2. Elemental composition of embedded debris

SEM-EDX analysis was performed on the embedded debris identified in the PE inserts. The purpose of this was to determine the composition of the embedded debris identified in 5 of the PE inserts (5 bearing surfaces and 4 backside surfaces).

The majority of the SEM-EDX analysis was performed using a TM3030 SEM/EDX (Hitachi High-Technologies Corporation, Tokyo, Japan) at 15 keV. The PE inserts were mounted onto a platform using double-sided carbon tape. The height of the platform was then adjusted so that the component surface was within the working distance of the SEM (approximately 1 mm) before being put inside the SEM for analysis. The remainder of the SEM-EDX analysis was performed by the Advanced Chemical and Materials Analysis (ACMA) service at Newcastle University.

3.6. PE Insert Form Analysis

The bearing surface volumetric wear loss and backside surface planicity of the PE inserts was quantified through CMM analysis. CMM analysis measures the changes in geometry of a surface. It therefore does not distinguish between wear (i.e., material removal) and/or deformation.[158] Throughout this thesis, the term 'wear' is used to describe any geometrical changes at the PE insert bearing surface, and the term 'planicity' is used to refer to changes to the backside geometry. Planicity may be defined as the difference between the minimum and maximum linear deviations, excluding those determined to be due to surgical retrieval damage.[158] This terminology follows that used in a previously published study by Bhalekar et al. in which CMM analysis was performed on the bearing and backside surfaces of PE components from knee replacements.[158]

Previously, CMMs have successfully been used to measure the wear volume loss from explanted MoP total hip[138, 139] and knee[140] replacements. However, to the best of the author's knowledge, to date no published studies have quantified the volumetric wear loss from TAR components. A similar methodology as previously described for hip and knee explants, consisting of CMM scanning using a custom MCOSMOS (Mitutoyo, Kanagawa, Japan) programme in combination with a custom Python (Python Software Foundation, Delaware, USA) programme, was used to measure the wear volumes from explanted TAR PE insert bearing surfaces. CMM analysis has also previously been established as a technique to quantify and map the backside planicity of PE inserts from knee prostheses. The same method was followed for this aspect of the present study.[158]

3.6.1. PE insert bearing surface volumetric wear validation

To validate the CMM methodology, the calculated wear volumes were compared against those given by gravimetric testing for various stages of wear.

Two previously unused INFINITY TAR PE (UHMWPE) inserts were used for the validation: one of size 5 and height 6 mm (Figure 3.9), and one of size 3 and height 6 mm (Figure 3.10). The same validation method was repeated on each of these PE inserts.

Figure 3.9. Pristine INFINITY PE insert (size 5, height 6mm) prior to starting validation.

Figure 3.10. Pristine INFINITY PE insert (size 3, height 6mm) prior to starting validation.

Material was removed from the PE insert bearing surface in increments to simulate *in vivo* wear. This was achieved using a drill driver (DeWalt, Maryland, US) with a sanding attachment. The component surface was then cleaned with acetone and lint-free cloth to ensure the removal of all debris prior to measurement. There were 4 wear stages, with material being removed from a new quadrant at each stage (Figure 3.11). Additionally, these measurements were also taken on the unworn component prior to any material being removed. At each wear stage, wear volume measurements were taken via both gravimetric testing and CMM scanning.

Figure 3.11. Quadrants the PE insert bearing surface was sectioned into.

Gravimetric testing is a standardised method of wear volume quantification.[136] The technique involves measuring the component mass before and after wear has occurred. The volume loss can then be calculated from the difference using the following equation, where V is volume, m is mass, and ρ is density:

$$V = \frac{m}{\rho}$$

Equation 7

Gravimetric measurements were taken using an analytical balance (Fisherbrand, Thermo Fisher Scientific, Massachusetts, USA) with a sensitivity of 0.1 mg. Following measurement, the measured gravimetric values were converted into volumes using Equation 5. For this conversion, a standard UHMWPE density of 0.945 g/cm³ was used.[159] Five gravimetric measurements were taken at each wear stage, and the mean wear volume calculated.

A STRATO-Apex 574 CMM (Mitutoyo, Kanagawa, Japan) with a 5 mm diameter ruby probe was used to take contour scans of the PE bearing surface to determine volumetric material loss. A calibration programme was run on the CMM each time it was turned on, prior to beginning scans. Figure 3.12 shows the setup of a PE insert during CMM scanning. The component was held by a clamp which was in turn secured in a jig. Plasticine was also used to ensure the jig did not move from the CMM platform.

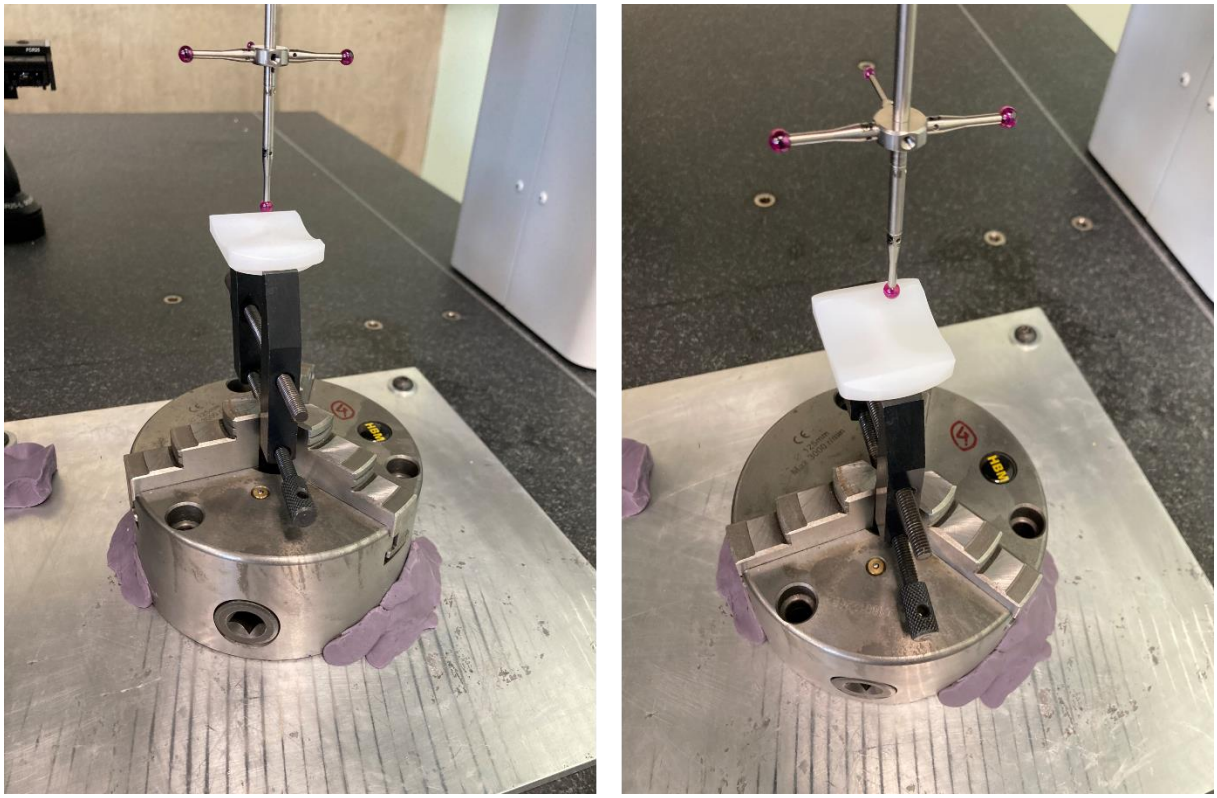

Figure 3.12. Setup of a pristine INFINITY PE inert during CMM scanning.

The protocol that was followed for the CMM scanning of the PE insert bearing surfaces is given in Appendix C. The parameters of point pitch (the distance between 2 points) and contour spacing (the distance between 2 traces) were input as 0.1 mm and 0.25 mm, respectively. Figure 3.13 defines these parameters. These parameter inputs comply with ISO 14242-2:2016 for THR wear measurement methods which states that the 'mesh spacing' (i.e., the point pitch and contour spacing) should be a minimum of 1 mm.[160] The 'manual position of datum' option was also selected, meaning the location of the component was given by manually positioning the probe directly above the centre of the component using the joystick on the motion controller.

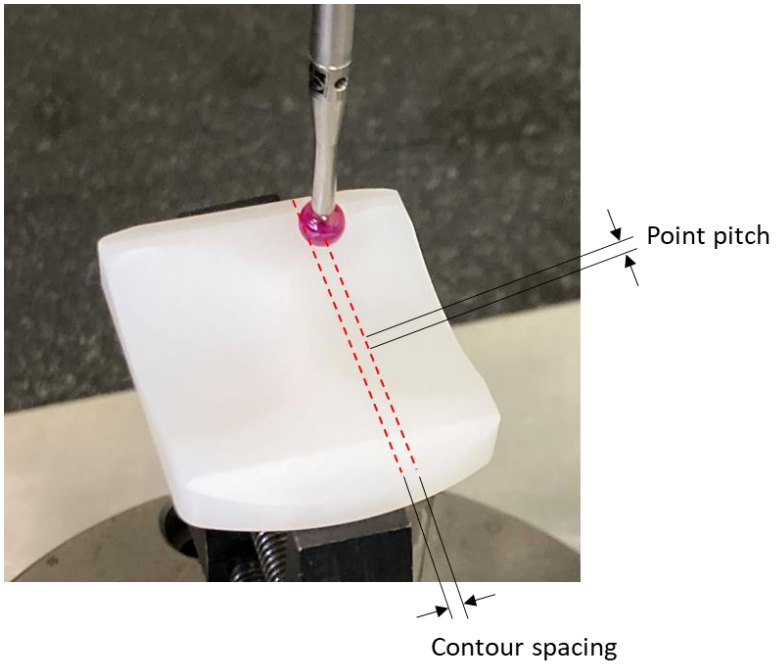

Figure 3.13. Schematic depicting the CMM programme inputs of point pitch and contour spacing.

The CMM uses a custom programme in MCOSMOS to scan the component surface and compare the geometry to an ideal unworn surface in order to calculate the volumetric material loss. The results from the scan are output in the format of an ASC file which can then be analysed in a custom Python programme to generate the value of the wear volume as well as producing a visual representation of the location and severity of the material loss in the form f a geometrical wear map. For each stage of wear, the absolute error (i.e., the difference between the wear volumes measured by the CMM and gravimetric testing) was calculated.

This method was adapted from a previously validated method for the PE components of knee replacements.[158] The CMM programme used an XY reference plane for the coordinate data of the PE insert bearing surface. This surface was established from measurement of the central areas of the backside surface of the component. Sequential linear contour traces were then taken on the component bearing surface, as depicted in Figure 3.13.

The 3D coordinate data obtained from the CMM scans were imported into a custom Python programme, and the data for each condyle interpolated onto a grid. For each condyle, a matrix of surface curvatures was then calculated. An established deep learning model was used to detect the bearing surface boundary, as needed for surface reconstruction. A similar model was also used to identify bearing surface wear regions. This worked by passing each condyle's

surface curvatures through a series of image filters, with the result being highlighted regions where the curvatures deviated from the original geometry of the surface, representative of the wear region boundaries. The volume under both the unworn and worn surfaces was calculated, and the volumetric wear value represented by the difference between the two. At each point on the bearing surface, linear wear was given by the difference in the Z-axis values for the worn surface and the approximated unworn surface. These linear wear values were then used to construct a visualisation of the depth and location of wear present on each condyle of the bearing surface in the form of a wear map.[158]

A limitation of this methodology to note is its reliance on unworn regions being present on the bearing surface. However, PE inserts with gross wear of the bearing surface were excluded for CMM bearing surface analysis, as noted in the following section. Additionally, this is the first time that this method of CMM analysis has been applied to TAR components, with the method being adapted from that which has previously been used for analysis of knee replacement components. An implication of this adaptation is that it is the TAR PE insert bearing surface is analysed in terms of two condyles, as this is the norm for the PE component of TKRs. This is also the case for the majority of the TAR models included, however the design of the Hintegra prosthesis differs in that there are no condyles as such, rather the bearing surface is one continuous curve. Whilst the method was considered to be appropriate to adapt for analysis of the ankle components, it is important to bear in mind this adaptation – along with other limitations such as the lack of relevant TAR-specific wear literature with which to compare results – when interpretating the data and to contextualise the results.

3.6.2. PE insert bearing surface volumetric wear measurement

The method for CMM analysis performed to determine the volumetric wear loss from the PE insert bearing surfaces follows that described for the validation in the previous section (3.6.1), with a STRATO-Apex 574 CMM with a 5 mm ruby stylus used to scan the surface geometries.

CMM analysis was achievable for the bearing surfaces of 18 of the 27 PE inserts included. Reasons for exclusion are given in Table 3.9.

Reason CMM analysis not achievable	Components excluded (n = 9)
Too worn	Mobility (2)
PE insert in pieces	Hintegra (1)
Crack on PE insert	Salto Talaris (1)
Damaged PE insert	Mobility (1)
Backside surface not flat*	BOX (3), Cadence (1)

*Table 3.9. Reasons for exclusion from TAR PE insert bearing surface CMM analysis. Notes: *, the geometries of the backside of these PE inserts made the CMM analysis unachievable due to the points taken on this surface by the probe. The backside surfaces of the BOX prostheses were concave, and the raised section of the Cadence backside surface prevented analysis.*

3.6.3. PE insert backside surface planicity measurement

The method used to analyse the geometries of the PE insert backside surfaces also used a STRATO-Apex 574 CMM with a 5 mm ruby stylus. The protocol for the backside CMM scans is given in Appendix D. The parameters of point pitch and contour spacing, as previously defined, were input as 0.1 mm and 0.5 mm, respectively. These again comply with the minimum mesh spacing defined in ISO 14242-2:2016.[160] For these backside surface CMM scans, custom MCOSMOS and Python programmes were used to compare the actual surface geometry to that of an ideal unworn surface. Results were then output in the form of a geometrical surface map indicating areas of material removed and areas of material added (i.e., deviations extending superiorly in an anatomical sense), as well as a planicity value which was calculated from the difference between the minimum and maximum linear deviations. A greater planicity is therefore indicative of greater deformation or wear of the surface.[161] In knees, it has previously been reported that an increased backside planicity of the PE component may be associated with increased rates of aseptic loosening.[161] Limited research has been carried out on the changes TAR PE insert backside surfaces undergo *in vivo*, therefore this analysis has the potential to provide further insights into this area.

The method of measuring planicity followed that previously used by Bhalekar et al. for the backside surfaces of knee PE components.[158] This method involves the CMM probe taking points to establish an 'XY plane' from which Z deviations were referenced, determined by the sequential linear contour traces performed. Spurious data points originating from scanned areas of deformation due to retrieval damage were removed by plotting the Z deviations following interpretation of the output cartesian coordinates using a bespoke programme. An XY plane where Z = 0 (i.e., no linear deviations) represented the ideal unworn surface from which

planicity was referenced. For this reason, only TARs with a flat PE insert backside surface were included in this analysis. For the TARs included in the present study, all mobile bearing designs had a PE insert with a backside surface intended to be flat with the exception of the BOX prosthesis. Therefore, this method of planicity analysis was suitable for the majority of the TARs within the present study. Overall, CMM analysis was achievable for the backside surfaces of 13 of the 27 PE inserts included. Reasons for exclusion are given in Table 3.10.

Reason CMM analysis not achievable	**Components excluded (n = 15)**
No PE insert	STAR (1)
Fixed bearing	INFINITY (4), Cadence (1), Salto Talaris (2)
Backside not flat*	BOX (3)
In pieces	Hintegra (1)
Part broken off	Mobility (3)

*Table 3.10. Reasons for exclusion from TAR PE insert backside surface CMM analysis. Notes: *, the backside surfaces of the BOX prostheses were concave, meaning analysis of the surface deviation was not possible.*

3.7. Statistical Methods

The statistical software programme Minitab (Minitab Inc., Pennsylvania State University, USA) was used to perform the statistical analyses.

To determine whether there was a statistically significant difference between proportions, a 2-proportion test was performed. A Ryan-Joiner test was performed to test the data for normality. For non-parametric data, a Mann-Whitney U test with a 95% confidence level was performed to determine whether statistical significance was reached. For parametric data, a 2 sample t-test was used instead. Reported p-values were adjusted for ties, and all p-values are given to 3 decimal places, with those less than 0.001 reported as $p<0.001$. Statistical significance was defined as $p<0.05$. For correlation analyses, Pearson correlation was used, with the r value interpreted with positive and negative values corresponding to the positive and negative correlations respectively, and using the following values as a guide: no correlation ($r = 0$); weak correlation ($0.25 < r < 0.5$); moderate correlation ($0.5 < r < 0.75$); strong correlation ($0.75 < r < 1$).

Chapter 4. Results

In this chapter, the original research results obtained during this explant analysis study – using the methods described in the previous chapter – are presented. These results are grouped into six main sections: surface damage mode analysis, semi-quantitative damage assessment, surface profilometry, material characterisation, PE insert form analysis, and correlation analyses. Firstly, the surface damage modes present are identified, followed by a semi-quantitative assessment of the component damage. The findings from the surface profilometry analysis of the metal components and the material characterisation in terms of both metal components and embedded debris are then given. Next, the results from the form analysis of the PE inserts, covering the validation and quantification of bearing volumetric wear as well as measurement of backside planicity is covered. Then, correlation analyses are presented to identify potential factors influencing damage of TARs. Finally, a summary of the damage mechanisms identified on each explanted TAR is provided.

4.1. Surface Damage Mode Analysis

An initial visual (macro- and microscopic) analysis of the explanted TAR component surfaces was performed in order to determine the damage features present. The articulating surfaces (PE insert bearing and backside surfaces, tibial component inferior surface, and talar component bearing surface) were analysed for common damage modes as described in the previous chapter (Section 3.2.1). The non-articulating surfaces of the tibial and talar components were also analysed for any visible changes to the porous coatings covering these surfaces. This analysis was performed in order to characterise coating changes and therefore was distinct from a bone ingrowth study. If bone coverage was identified which extended over the full surface, then no change to the porous coating would be assumed.

4.1.1. Articulating surfaces

The most commonly observed wear features from the microscopic damage mode analysis, across all surfaces, metallic and polymeric, were pitting and scratching (Figure 4.1). Burnishing was also frequently observed on the PE insert surfaces. Delamination and striations were identified on the bearing surfaces of PE inserts only, whereas surface deformation was

identified on the backside surfaces of PE inserts only. Embedded debris, abrasion, surface deformation, and delamination were the least frequently seen damage modes, with them being identified overall on 9, 8, 4, and 2 surfaces, respectively.

In particular, the high proportion of metallic components exhibiting pitting and scratching damage was unexpected given that this would not be typical for a well-functioning MoP bearing.[64]

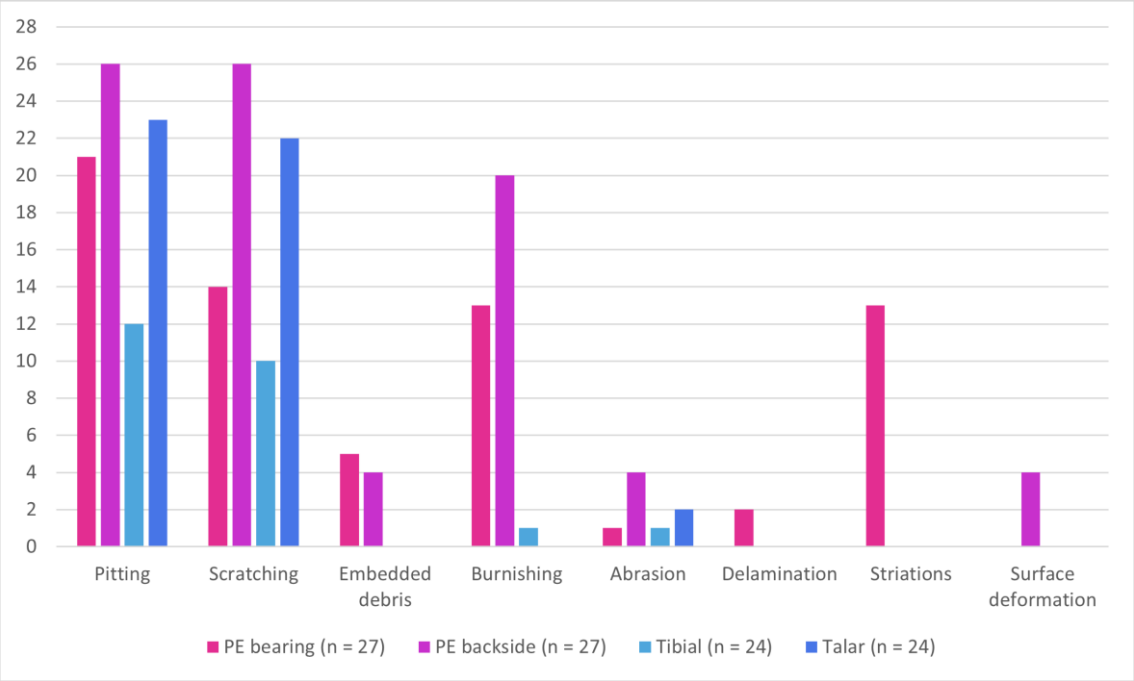

Figure 4.1. Number of each component articulating surfaces exhibiting the different damage modes.

The results were also stratified by bearing type to show the percentage of fixed and mobile bearing component surfaces showing each damage mode (Figure 4.2). From this visual representation, some differences can be seen. A higher proportion of mobile bearing than fixed bearing PE insert backside surfaces exhibited burnishing, and a higher proportion of mobile bearing than fixed bearing talar component bearing surfaces exhibited scratching. Conversely, burnishing and striations were both identified on a higher proportion of fixed bearing than mobile bearing PE insert bearing surfaces. However, none of these differences reached statistical significance (defined as $p < 0.05$) when using a 2 proportions test.

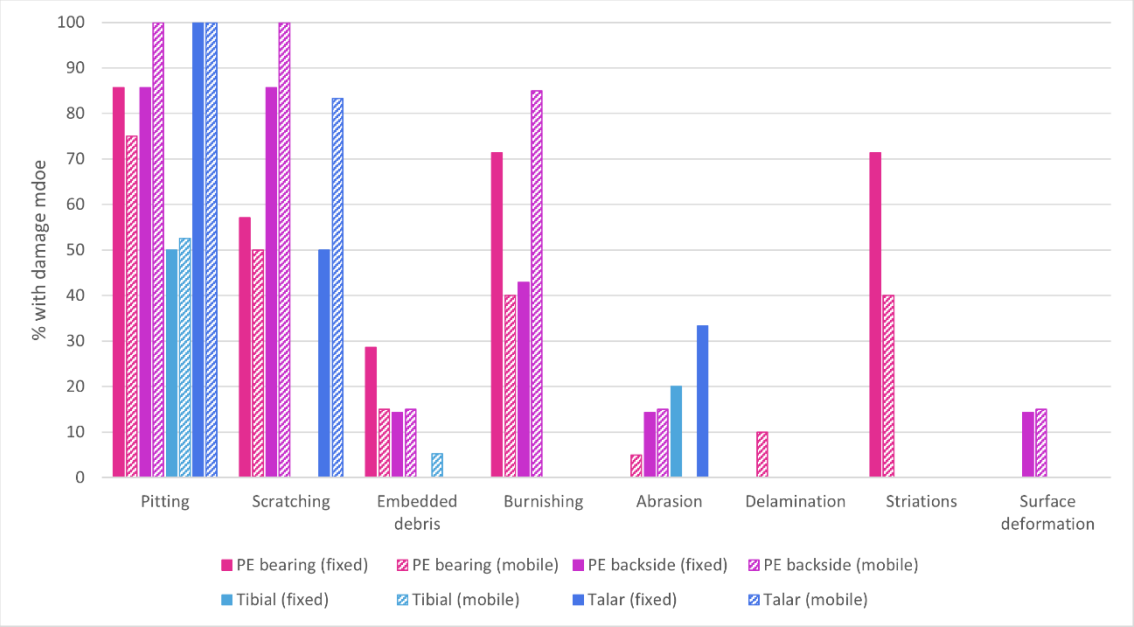

Figure 4.2. Percentage of fixed and mobile bearing components surfaces exhibiting each damage mode.

4.1.2. Non-articulating surfaces

Visual macro- and microscopic inspection of the non-articulating surfaces of the metal components revealed changes in terms of coating loss and/or changes in reflectivity in 20 (83%) of the 24 tibial components and 18 (75%) of the 24 talar components analysed (Figure 4.3).

The overall proportion of metal (tibial and talar) components with coating changes was 79%. In terms of the different types of coatings utilised on the non-articulating surfaces of the analysed metal tibial and talar components, those with Ti beads had the highest proportion with changes (coating loss/changes in reflectivity), and those with a double coating of Ti-CaP the lowest. Figure 4.4 shows the percentage of each different coating type which exhibited changes, with this ranging from 50% to 94%.

Figure 4.3. Changes in the coating of a STAR tibial component non-articulating surface.

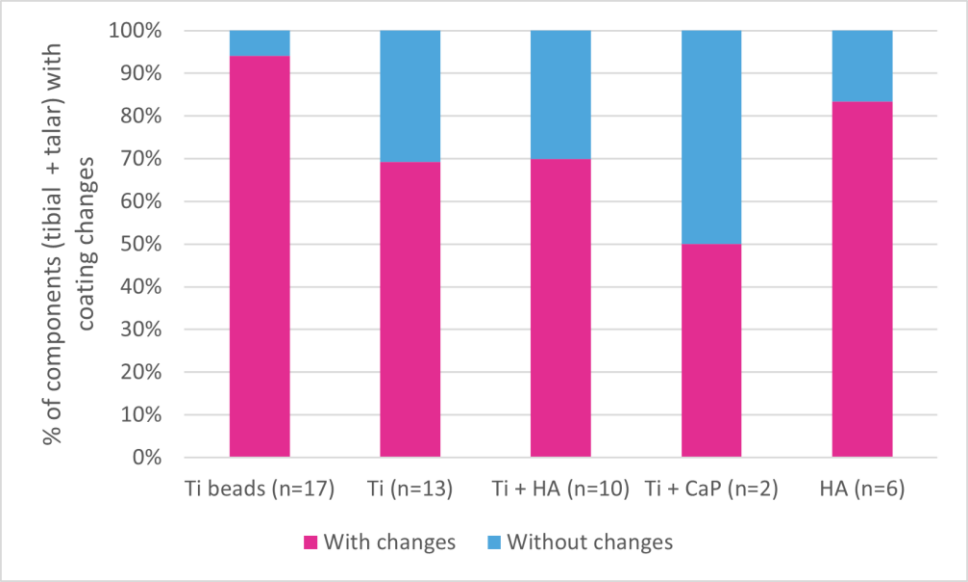

Figure 4.4. Number of metal (tibial and talar) component non-articulating surfaces with each coating type exhibiting changes.

Changes to the coating in terms of coating loss and/or changes in reflectivity was observed on the non-articulating surfaces of at least one of the metal components of all of the TARs which had tibial pitting and on all except two of those which had talar pitting and/or talar sliding plane scratching. In these two cases, the tibial component of one was not present and so the porous coating was not able to be analysed, and the other exhibited evidence of direct MoM contact occurring, along with a severely damaged PE insert (having broken into two pieces). These findings therefore suggest that loss of coating may be a primary cause of the metal component damage observed by acting as third body debris (i.e., causing damage through the mechanism of third body wear) at the articulations.

Two of the TARs had been fixed using cement, with one BOX prosthesis having cement visible on the non-articulating surfaces of both the tibial and talar components, and one Mobility having cement visible on the talar component, with the tibial component not received (Figure 4.5). The remaining 23 tibial and 22 talar components were uncemented, meaning fixation was achieved using bony ingrowth only. Here it should be noted that the Mobility prosthesis is intended to be an uncemented device,[162] as are all of the currently implanted TARs for use in the UK.

Figure 4.5. Explanted cemented Mobility talar component.

4.1.3. Talar sliding plane scratching

Scratching on the sliding plane (i.e., linear scratches in the direction of the antero-posterior movement allowed at the ankle during the motions of plantarflexion and dorsiflexion), as shown in Figure 4.6, was observed macroscopically on 19 (79%) of the 24 metal talar components analysed.

Figure 4.6. Macroscopic image showing severe scratching on the sliding plane of an explanted mobile bearing Hintegra talar component bearing surface. This form of damage was clearly visible to the naked eye.

Table 4.1 breaks down these results by model of TAR. Three (60%) of the 5 fixed bearing talar components exhibited the macroscopic sliding plane scratching, compared to 16 (84%) of the 19 mobile bearing talar components. The sliding plane scratching indicates the presence of hard third body particles, as this kind of damage would not be expected to be seen during normal articulation of the metal talar component and PE insert bearing surface.

Talar component	**N**	**N with sliding plane scratching (%)**
INFINITY	3	3 (100%)
Cadence	1	0 (0%)
Salto Talaris	1	0 (0%)
Salto	1	1 (100%)
Mobility	9	9 (100%)
STAR	3	1 (33%)
Hintegra	2	2 (100%)
BOX	3	2 (67%)
Zenith	1	1 (100%)

Table 4.1. Number of each model of TAR with talar component sliding plane scratching.

4.1.4. Metallic pitting and abrasive changes

Light microscopy revealed the presence of pitting on the majority of the metal component articulating surfaces. Pitting was identified on the articulating surfaces of 13 (54%) of the 24 tibial components and on 23 (96%) of the 24 talar components (Figure 4.7A and Figure 4.7B, respectively). Pitting was defined as small indentations, indicative of material loss, most likely to have occurred *in vivo*. The pits had dimensions of approximately 90 µm (length) x 40 µm (width) x 3 µm (depth). The pitted tibial components were all manufactured from CoCr alloy, with 63% exhibiting this pitting. None of the Ti alloy tibial components exhibited pitting, however abrasive changes were identified on one (Figure 4.7C).

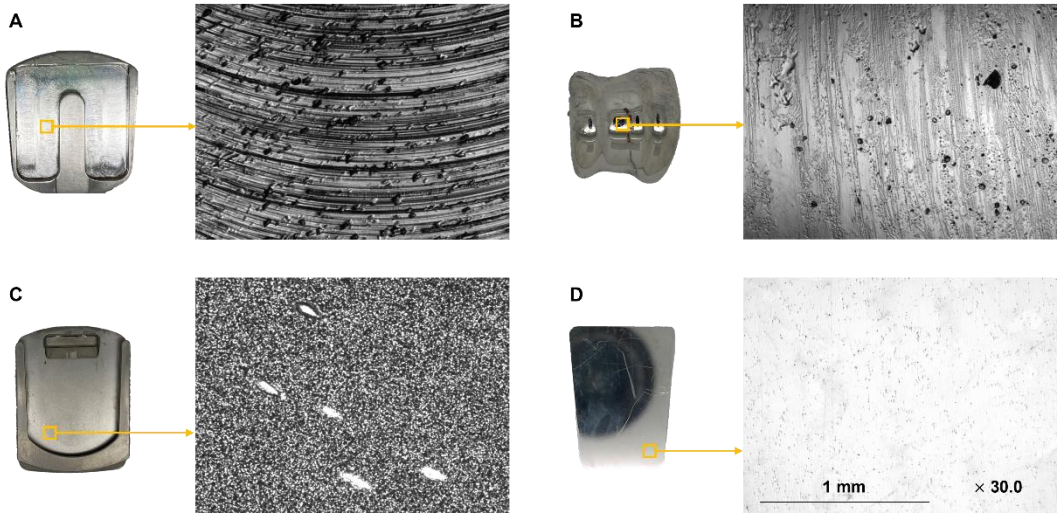

Figure 4.7. Microscopic images of pitting and abrasive changes. (A) pitting on a CoCr alloy tibial component. (B) pitting on a CoCr alloy talar component. (C) abrasive changes on a Ti alloy tibial component. (D) as manufactured surface of a CoCr alloy tibial component. (A) Salto Talaris. (B) Salto Talaris. (C) INFINITY. (D) STAR.

The results broken down by TAR model are given in Table 4.2. Fifty per cent of fixed and 56% of mobile bearing tibial components exhibited pitting. One hundred per cent of fixed and 95% of mobile bearing talar components exhibited pitting. The size of the pits was visually similar for the different models of TARs analysed. Additionally, the small numbers of most of the different models included means that it is difficult to make conclusions on any specific model. However, the semi-quantitative damage scoring assessment (section 4.2) incorporated both severity (i.e., visibility of the damage) and the area covered (i.e., the amount of damage). There

were some differences seen between the average pitting damage score for fixed and mobile bearing metallic components. For tibial components, the pitting damage scores were greater on average for fixed bearing compared to mobile bearing components, while the opposite was true for talar components. In both of these cases, the difference seen in the scores was primarily accounted for by the average area scores, rather than the average severity scores for pitting.

	Tibial components		**Talar components**	
Prosthesis	**N (total n = 24)**	**N with pitting (total n = 13)**	**N (total n = 24)**	**N with pitting (total n = 23)**
INFINITY	3	1	3	3
Cadence	1	0	1	1
Salto Talaris	2	2	1	1
Salto	1	1	1	1
Mobility	8	4	9	9
STAR	3	3	3	3
Hintegra	2	1	2	2
BOX	3	1	3	2
Zenith	1	0	1	1

Table 4.2. Number of tibial and talar components with pitting.

4.1.5. Embedded debris

Embedded debris was identified via light microscopy in the PE inserts of 5 TARs (19%), 4 of which had embedded debris on both the bearing and backside surfaces, and 1 of which had embedded debris on the bearing surface only (Figure 4.8).

The shiny silver appearance of the embedded debris indicated that it was likely to be metallic; SEM-EDX analysis was subsequently carried out in order to confirm this (Section 4.4.2).

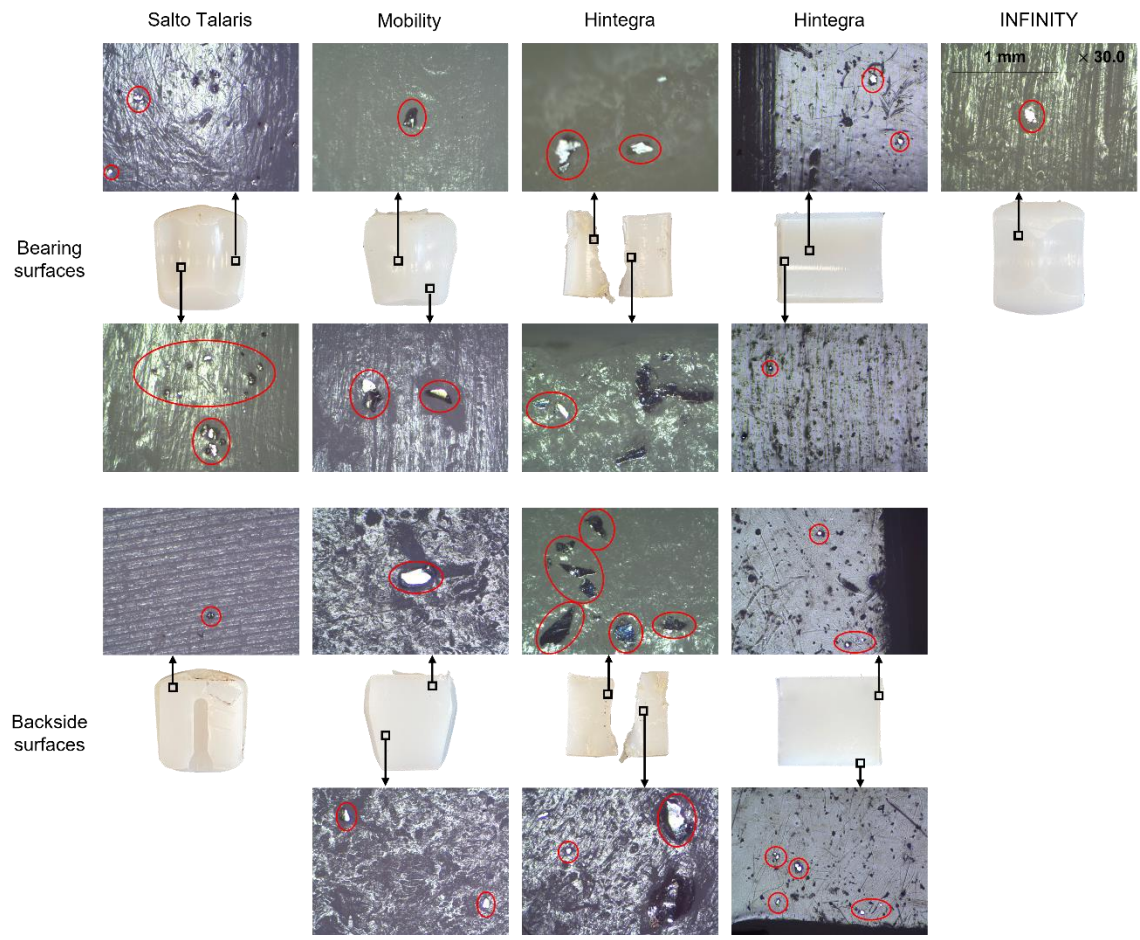

Figure 4.8. Microscopic images of embedded debris (indicated by red ellipses) on PE insert bearing and backside surfaces.

4.1.6. Special cases

Macroscopic analysis of the PE inserts revealed severe damage in 6 of the 27 components (1 insert had broken in half, 1 had a crack in the bearing surface, and 4 had part broken off) (Figure 4.9). However, it was not conclusively known whether this identified damage of these components occurred *in vivo* or during surgical retrieval of the device.

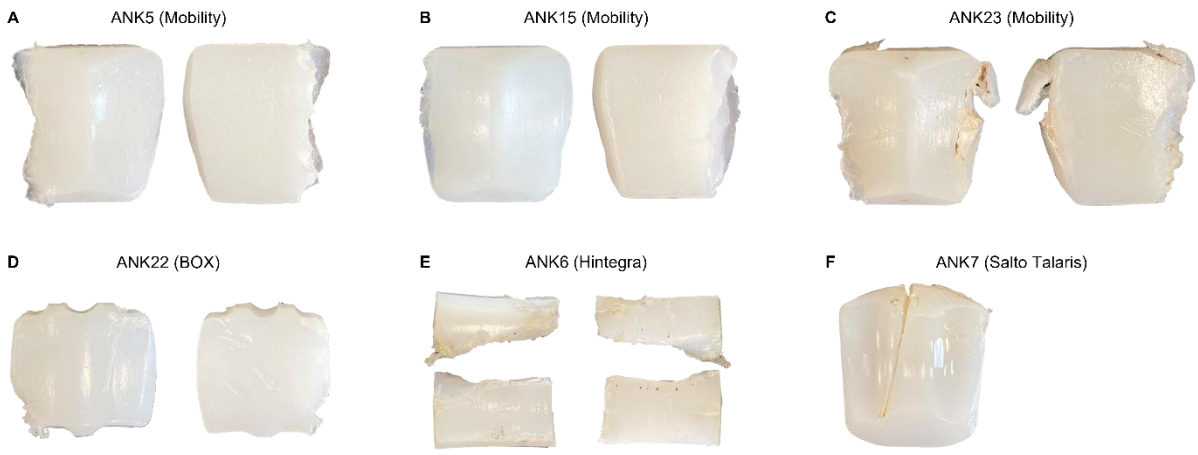

Figure 4.9. Macroscopic images of the severely damaged PE inserts. (A-D) with part broken off. (E) broken into two pieces (F) with a crack in the bearing surface.

Four other PE inserts exhibited surface deformation (i.e., permanent changes due to plastic deformation) of the backside surface upon macroscopic inspection of the components. Table 4.3 states the affected quadrants for each of these PE insert backside surfaces where surface deformation was identified. Due to the implantation side being unknown for all four of these prostheses, the quadrants affected could not be described in terms of medial and lateral aspects. Surface deformation was more commonly seen on the anterior aspect (i.e., quadrants 1 and 2) than posterior aspect (i.e., quadrants 3 and 4) of these PE insert backsides, based on this small sample size of components.

PE insert	**Implantation side**	**Quadrants affected**
ANK1 (Hintegra)	Unknown	1, 2, 3, 4
ANK2 (Salto Talaris)	Unknown	1, 2
ANK23 (Mobility)	Unknown	1, 3
ANK26 (Zenith)	Unknown	2

Table 4.3. PE insert backside surface quadrants affected by surface deformation. Quadrants 1 and 2 correspond to the anterior aspect, and quadrants 3 and 4 corresponding to the posterior aspect.

Evidence of direct MoM contact occurring between the metal tibial and talar components was identified in four of the TARs (Table 4.4). Of these four devices, all were mobile bearing devices, though one did not have a PE insert present. Unsurprisingly, the corresponding PE inserts for the other three devices all had signs of severe damage, with the PE insert either being broken into two pieces (in one case) or have part broken off (in two cases).

Prosthesis	**Bearing constraint**	**Notes**
ANK6 (Hintegra)	Mobile	PE insert broken into two pieces
ANK17 (STAR)	Mobile	No PE insert present
ANK22 (BOX)	Mobile	PE insert with part broken off
ANK23 (Mobility)	Mobile	PE insert with part broken off Approx. 12 years implantation time

Table 4.4. TARs with damage identified indicative of direct metal-on-metal contact having occurred.

In the case of the Hintegra prosthesis (ANK6), the PE insert was broken into two pieces upon receipt. Whilst it was not explicitly known whether this damage occurred during surgical retrieval of the device or *in vivo*, the damage observed on the metal components suggests that the PE insert fractured *in vivo*, leading to direct MoM contact between the tibial and talar components, as shown by Figure 4.10.

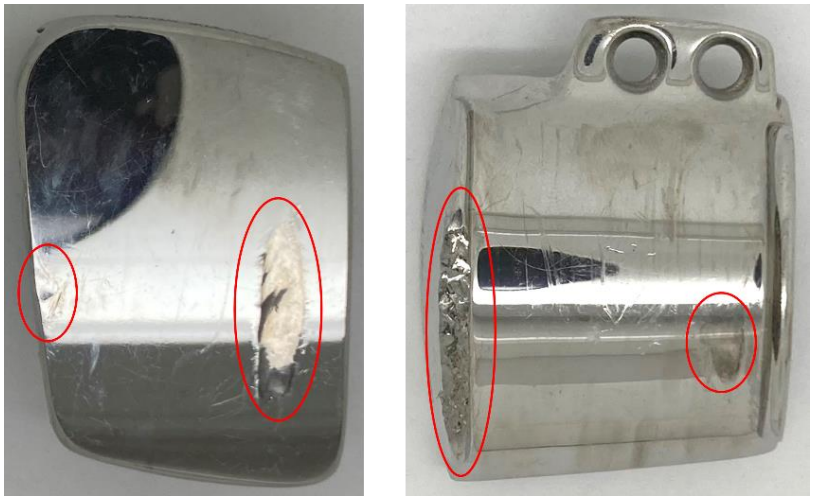

Figure 4.10. Macroscopic images of Hintegra tibial and talar components (ANK6). The corresponding PE insert was broken into two pieces. Red ellipses indicate areas of material removal most likely due to direct metal-on-metal contact occurring as a result of fracture of the PE insert.

The PE insert of the STAR prosthesis (ANK17) was not received with the explanted device, and therefore it is not known whether the component was damaged. The damage identified on the tibial and talar components, however, is indicative of direct contact between the two metal components occurring (Figure 4.11).

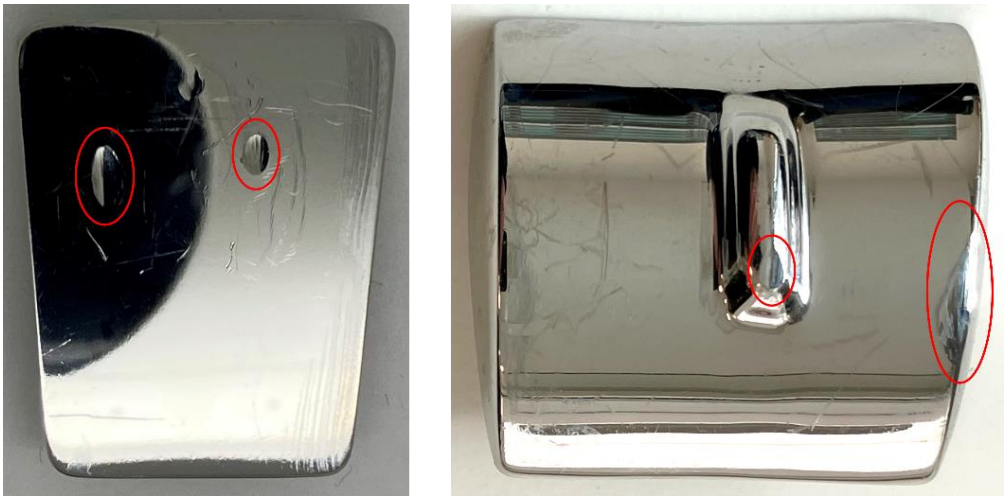

Figure 4.11. Macroscopic images of STAR tibial and talar components (ANK17). The corresponding PE insert was not received with this explanted TAR. Red ellipses indicate areas of material removal most likely due to direct metal-on-metal contact occurring.

The BOX prosthesis (ANK22) had a PE insert which was severely damaged in that part of the component was broken off. Damage to the tibial and talar components was identified which could be due to direct MoM contact occurring between these two components (Figure 4.12).

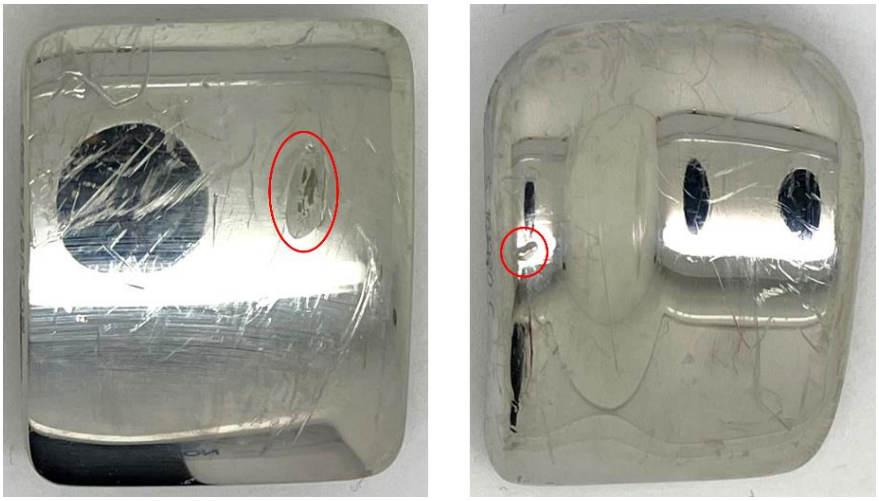

Figure 4.12. Macroscopic images of BOX tibial and talar components (ANK22). The corresponding PE insert had part broken off. Red ellipses indicate areas of material removal most likely due to direct metal-on-metal contact occurring.

Lastly, the Mobility prosthesis (ANK23) also had a severely damaged PE insert in that part of it was broken off. Damage was identified on the metal tibial and talar component surfaces which was indicative of direct MoM contact between the two components having occurred *in vivo* (Figure 4.13).

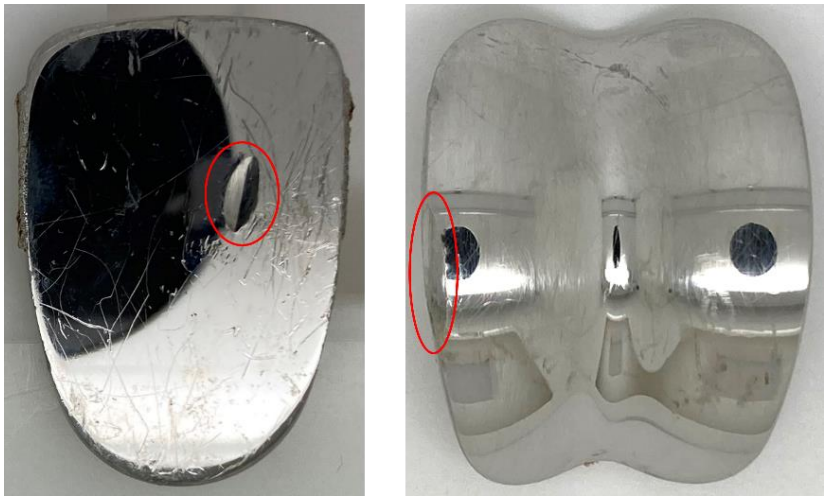

Figure 4.13. Macroscopic images of Mobility tibial and talar components (ANK23). The corresponding PE insert had part broken off. Red ellipses indicate areas of material removal most likely due to direct metal-on-metal contact occurring.

4.2. Semi-Quantitative Damage Assessment

Here the results of the semi-quantitative damage assessment of the articulating surfaces of the components are given in terms of component damage scores (CDS) (a sum of the damage feature scores (DFS) for each damage feature and for quadrant, where the DFS is the product of the area score (AS) and severity score (SS) for that particular damage feature).

4.2.1. Damage feature scores

The average DFS per quadrant for each of the damage features analysed for the different component surfaces are given in Table 4.5. Across these, scratching on the talar components had the highest average quadrant DFS, followed by burnishing on the PE insert backside surfaces, pitting on the PE insert bearing surfaces, and scratching on the PE insert backside surfaces.

	PE bearing	PE backside	Tibial	Talar
Pitting	3.53	3.30	1.38	2.50
Scratching	1.72	3.46	1.85	5.04
Abrasion	0.17	0.45	0.55	0.12
Embedded debris	0.27	0.14	-	-
Burnishing	3.13	4.54	-	-
Delamination	0.06	0.00	-	-
Striations	2.24	0.00	-	-

Table 4.5. DFS per quadrant for each damage feature on each component surface. Maximum for each individual DFS is 10.

For the PE insert bearing surfaces, the average DFS for the whole surface (i.e., the sum of the DFS from each of the four quadrants) was greatest for pitting, followed by burnishing, scratching, and striations (Figure 4.14).

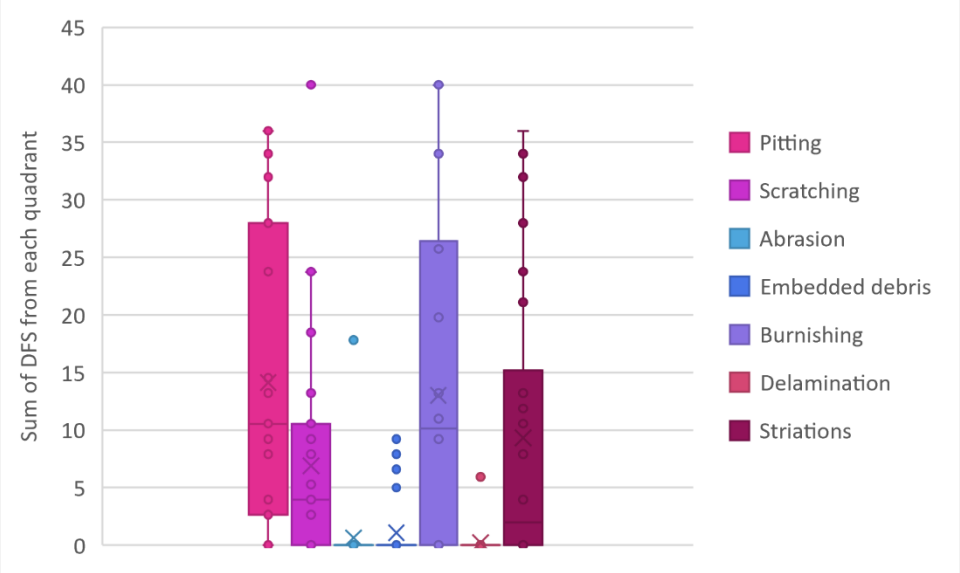

Figure 4.14. Box and whisker plot of the sum (from each quadrant) of different DFS for PE insert bearing surfaces.

For the PE insert backside surfaces, the average DFS summed from the four quadrants was highest for burnishing, followed by scratching and pitting (Figure 4.15).

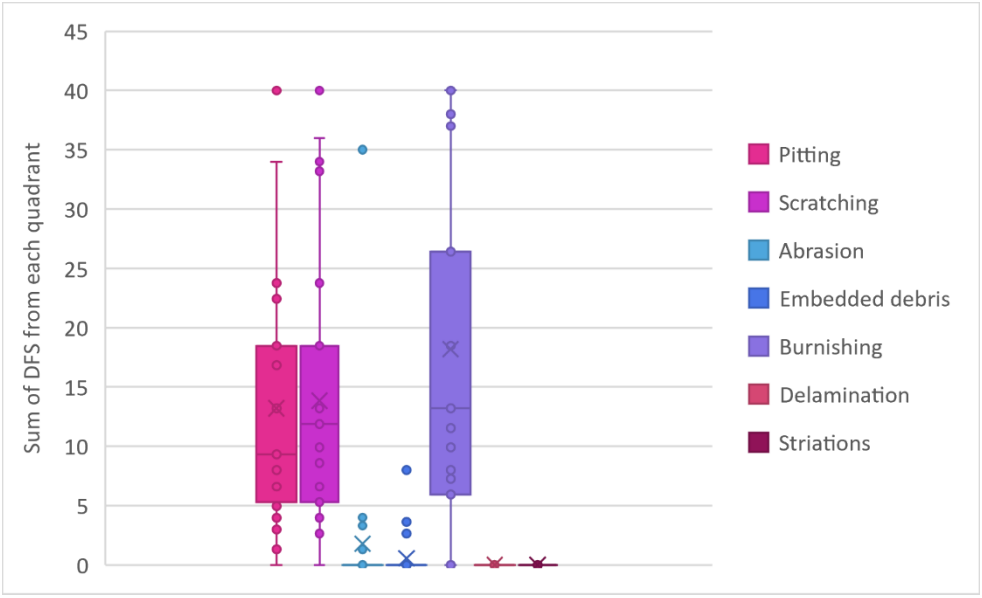

Figure 4.15. Box and whisker plot of the sum (from each quadrant) of different DFS for PE insert backside surfaces.

For the tibial component inferior surfaces, the average DFS summed across the four quadrants was greatest for scratching, followed by pitting (Figure 4.16).

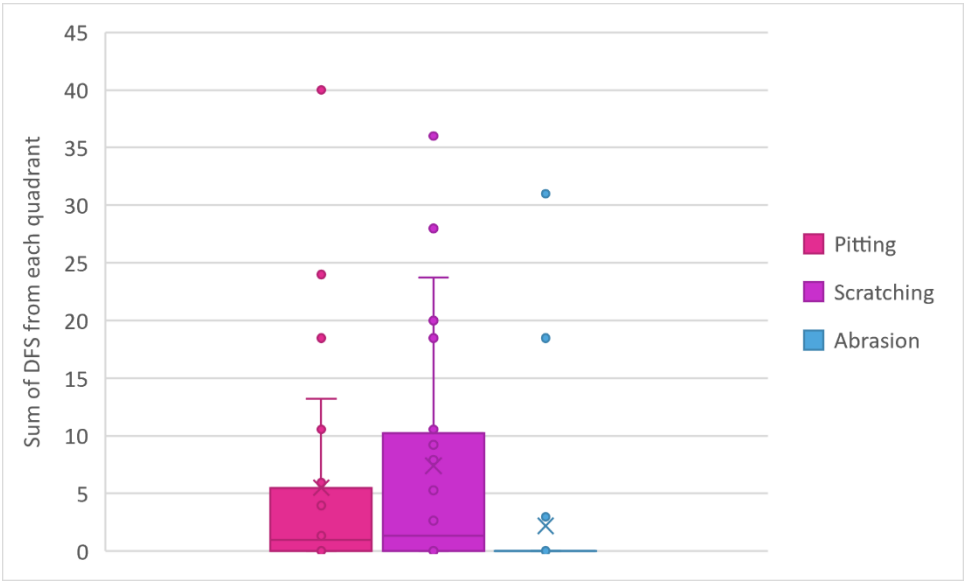

Figure 4.16. Box and whisker plot of the sum (from each quadrant) of different DFS for tibial component inferior surfaces.

Similarly, for the talar component bearing surfaces, the average DFS summed across the four quadrants was again greatest for scratching, followed by pitting (Figure 4.17).

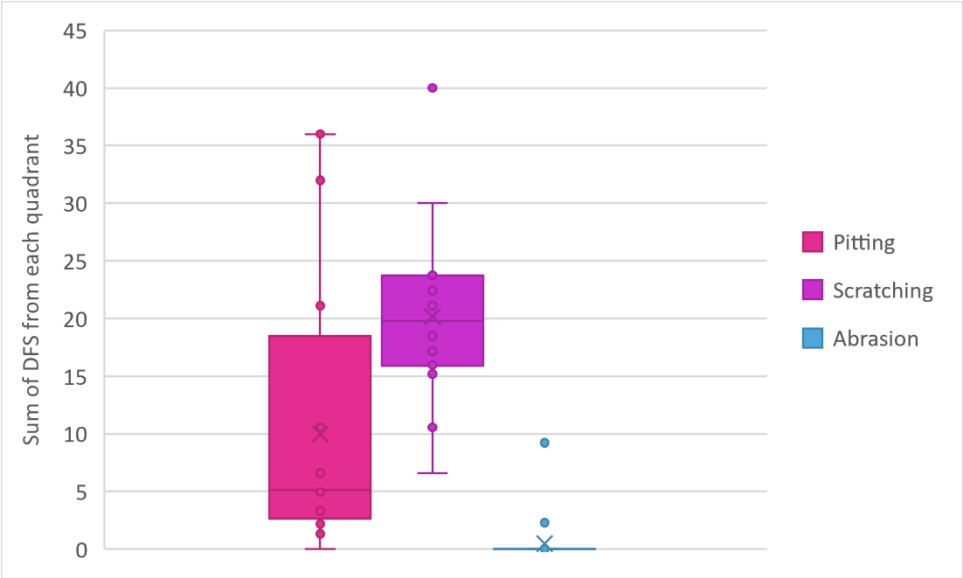

Figure 4.17. Box and whisker plot of the sum (from each quadrant) of different DFS for talar component bearing surfaces.

4.2.2. Component damage scores

The average CDS for each of the analysed surfaces (PE insert bearing surface, PE insert backside surface, tibial component inferior surface, and talar component bearing surface) are given in Table 4.6.

Component surface	**CDS**
PE bearing (n = 27)	44.46 ± 33.92 (max. 280)
PE backside (n = 27)	47.55 ± 29.23 (max. 280)
Tibial (n = 24)	15.09 ± 15.46 (max. 120)
Talar (n = 24)	30.63 ± 15.37 (max. 120)

Table 4.6. Average (mean ± SD) CDS for the different component surfaces analysed.

There was no significant difference ($p = 0.775$) found between the average CDS of the backside surfaces of the PE inserts and the bearing surfaces of the PE inserts (Figure 4.18).

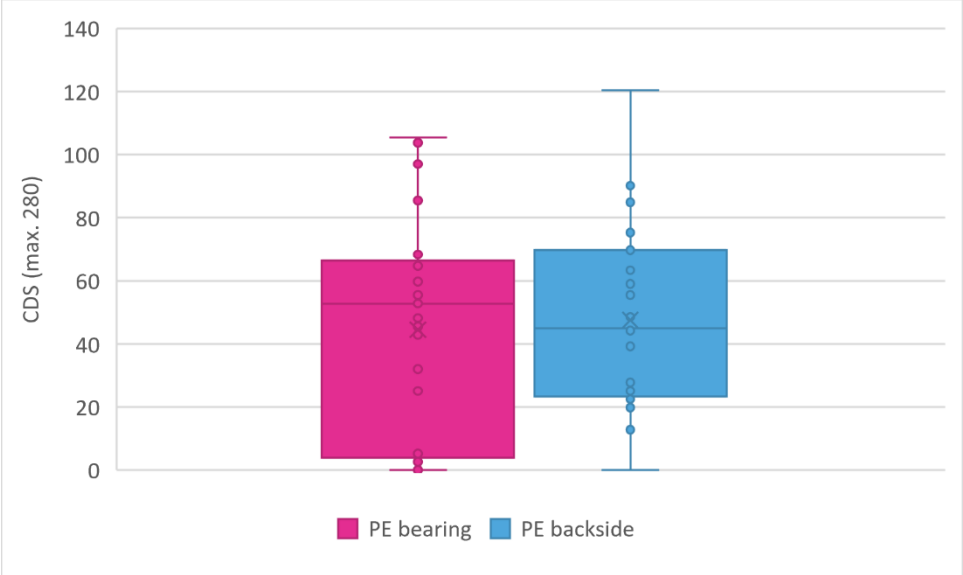

Figure 4.18. Box and whisker plot comparing the distribution of CDS for PE insert bearing surfaces and PE insert backside surfaces. The maximum CDS for each surface was 280.

When comparing the articulating surfaces of the tibial components and talar components, both of which had the same damage modes analysed and so the same maximum possible CDS, the CDS was significantly higher on average for the talar component bearing surfaces compared to the tibial component inferior surfaces ($p = 0.001$), as illustrated by Figure 4.19.

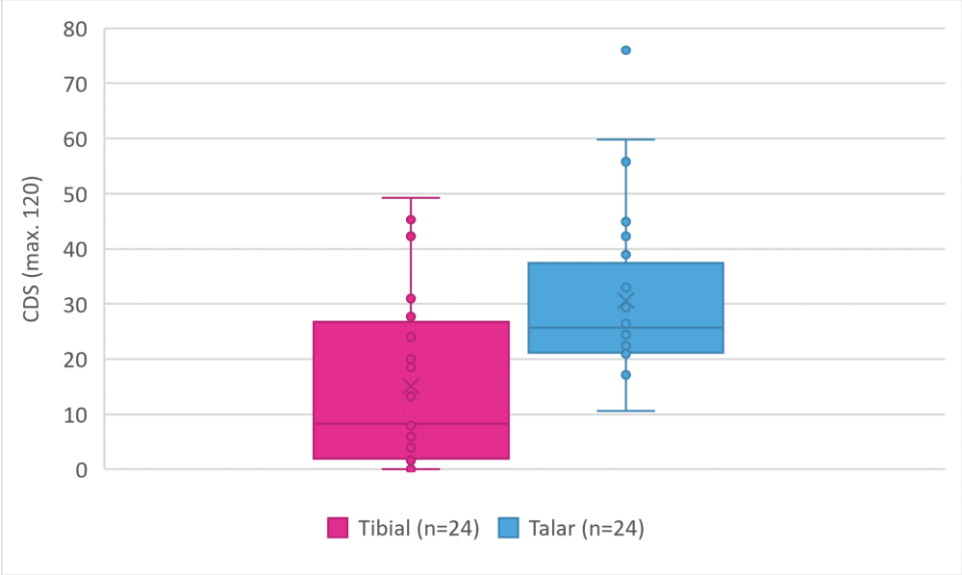

Figure 4.19. Box and whisker plot comparing the distribution of CDS for tibial component inferior surfaces and talar component bearing surfaces. The maximum CDS for each surface was 120.

The relationship between the PE insert backside surface CDS and tibial component inferior surface CDS of the TARs is plotted in Figure 4.20. No correlation between the two variables was found (Pearson correlation, r = -0.004).

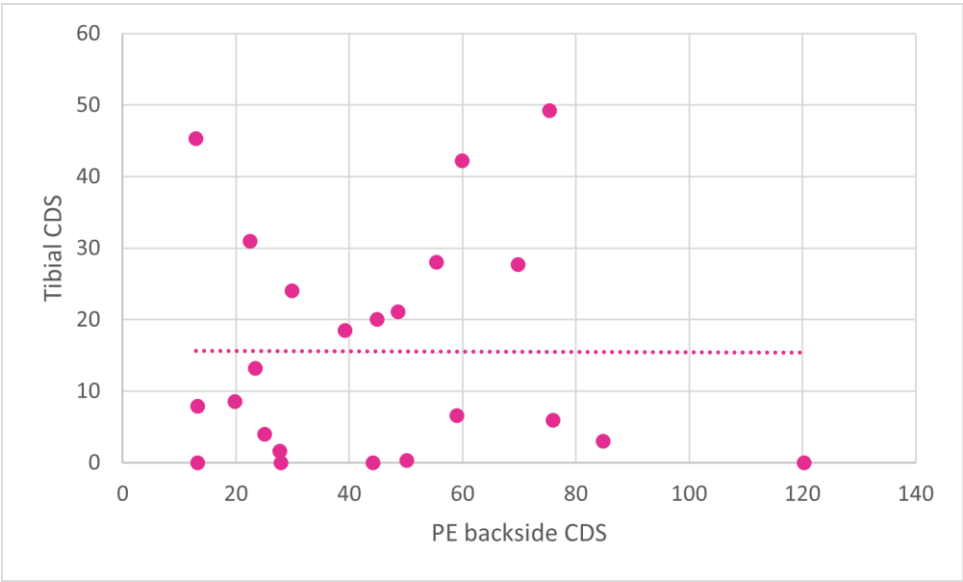

Figure 4.20. Scatter plot with linear trendline correlating PE insert backside surface CDS with tibial component inferior surface CDS.

Figure 4.21 plots the relationship between the PE insert bearing surface CDS and talar component bearing surface CDS of the TARs. No correlation was found between the two variables (Pearson correlation, r = 0.057).

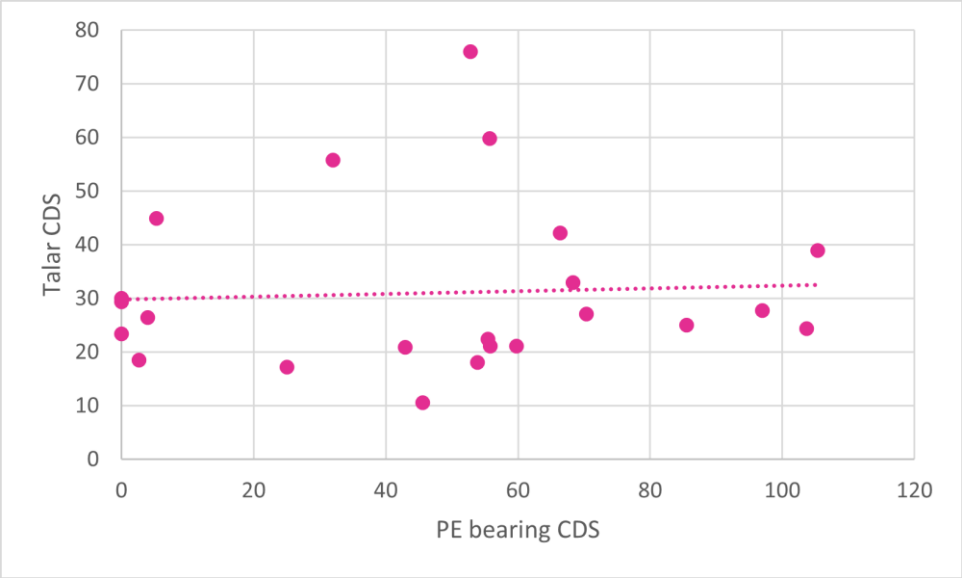

Figure 4.21. Scatter plot with linear trendline correlating PE insert bearing surface CDS with talar component bearing surface CDS.

The relationship between the PE insert bearing surface CDS and PE insert backside surface CDS of the TARs is plotted in Figure 4.22. No correlation between the two variables was found (Pearson correlation, r = 0.018).

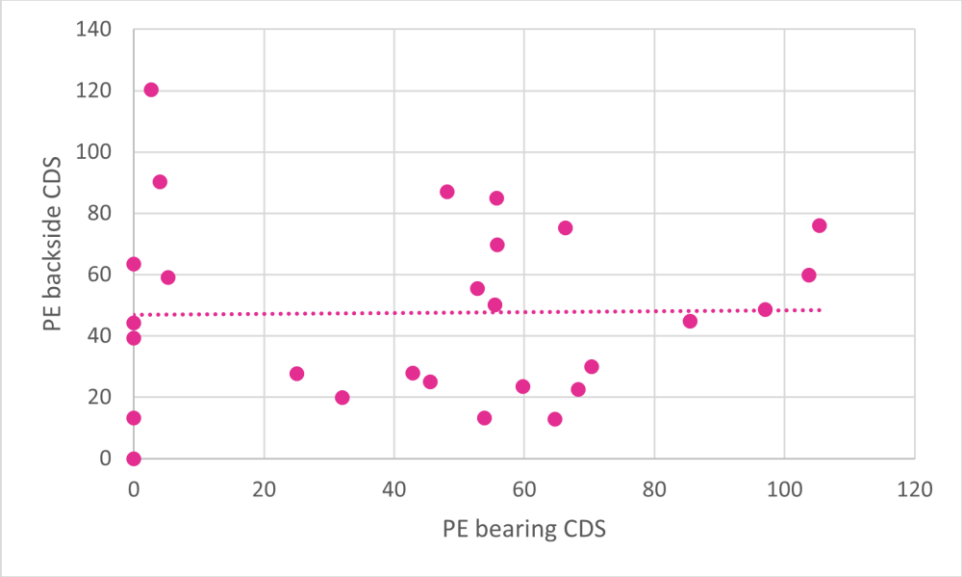

Figure 4.22. Scatter plot with linear trendline correlating PE insert bearing surface CDS with PE insert backside surface CDS.

Figure 4.23 plots the relationship between the tibial component inferior surface CDS and talar component bearing surface CDS of the TARs. A weak positive correlation was found between the two variables (Pearson correlation, r = 0.238).

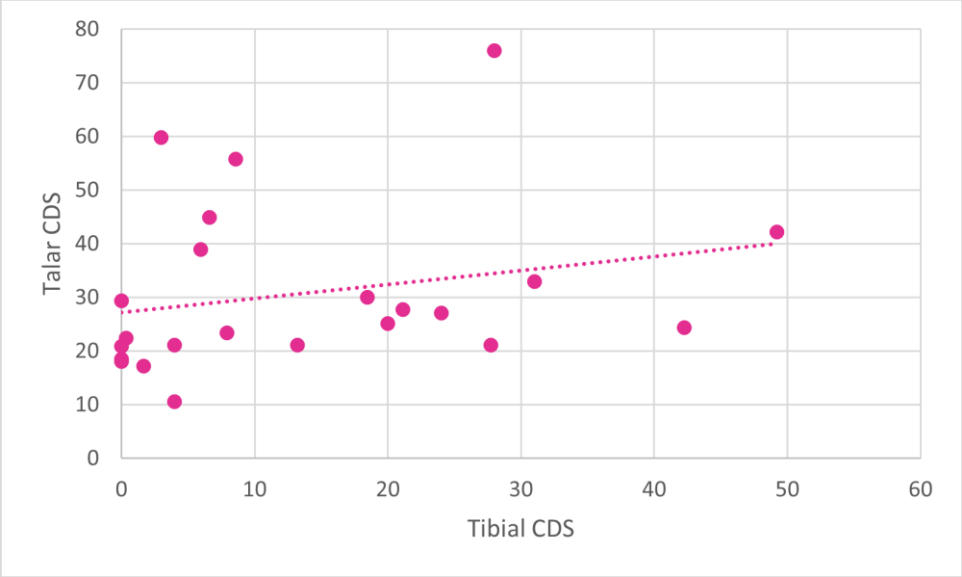

Figure 4.23. Scatter plot with linear trendline correlating tibial component inferior surface CDS with talar component bearing surface CDS.

4.2.3. Distribution of component damage

Table 4.7 gives the CDS for the anterior and posterior aspects (i.e., the sum of the DFS from quadrants 1 and 2 or quadrants 3 and 4, respectively) of each component surface. No clear pattern emerged in terms of damage being greater on either the anterior or the posterior aspects.

Surface	Anterior	Posterior	P-value
PE bearing	22.28 ± 17.02	22.17 ± 16.92	0.958
PE backside	23.39 ± 15.31	24.16 ± 14.26	0.897
Tibial	7.61 ± 7.45	7.48 ± 8.22	0.885
Talar	15.94 ± 7.31	14.68 ± 8.48	0.509

Table 4.7. CDS of each component surface for medial and lateral aspects. The anterior aspect CDS is the sum of the DFS from quadrants 1 and 2, and the posterior aspect CDS is the sum of the DFS from quadrants 3 and 4.

There average CDS was similar for the anterior aspects and posterior aspect of the bearing surfaces of the PE inserts (Figure 4.24), with no significant difference ($p = 0.958$).

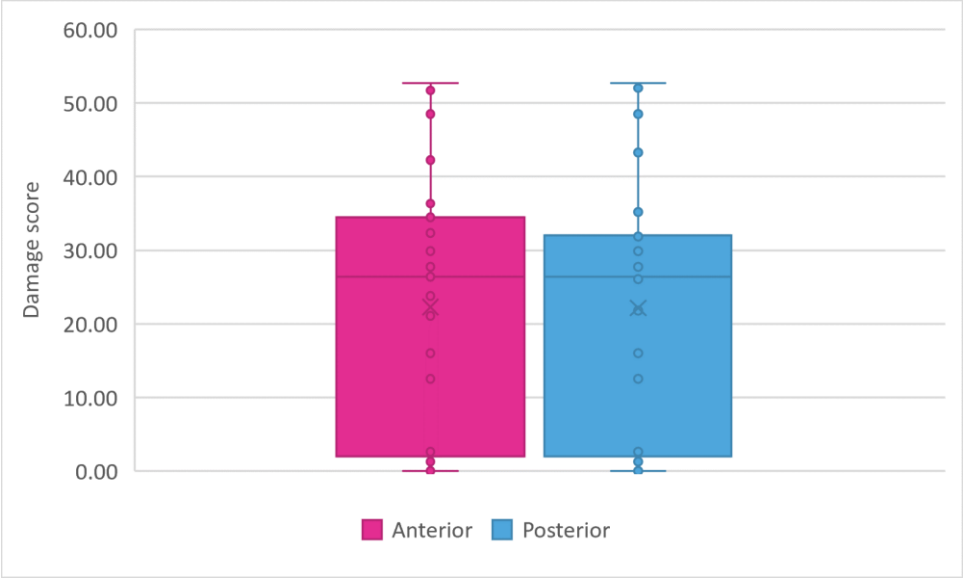

Figure 4.24. Box and whisker plot of damage scores for anterior and posterior aspects of PE insert bearing surfaces. Anterior damage score given by the sum of DFS from quadrants 1 and 2, and posterior damage score given by sum of DFS from quadrants 3 and 4.

The average CDS was also similar for the posterior aspects and anterior aspects of the backside surfaces of the PE inserts (Figure 4.25), with no significant difference ($p = 0.897$).

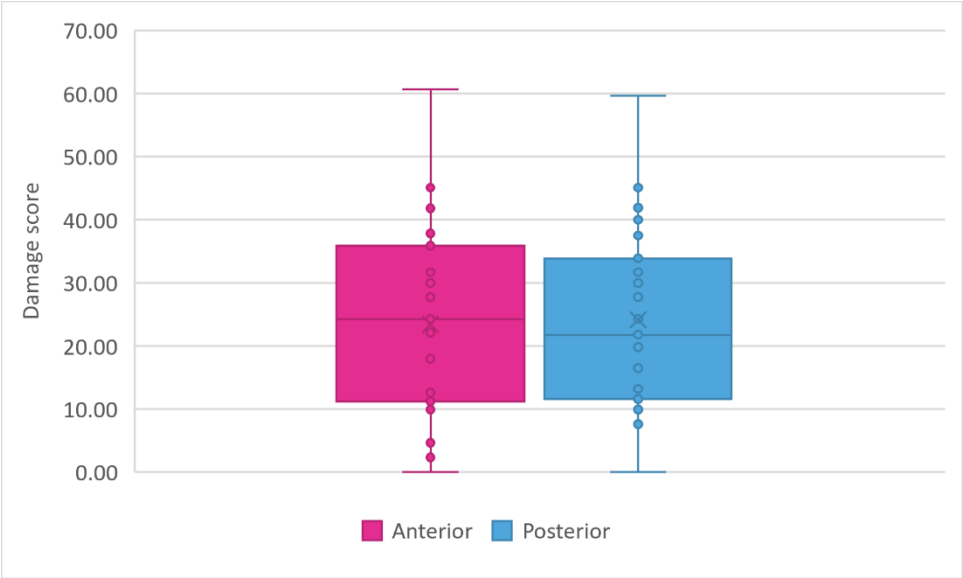

Figure 4.25. Box and whisker plot of damage scores for anterior and posterior aspects of PE insert backside surfaces. Anterior damage score given by the sum of DFS from quadrants 1 and 2, and posterior damage score given by sum of DFS from quadrants 3 and 4.

For the inferior surfaces of the tibial components, the average CDS was again similar for the anterior aspects and posterior aspects (Figure 4.26), with no significant difference ($p = 0.885$).

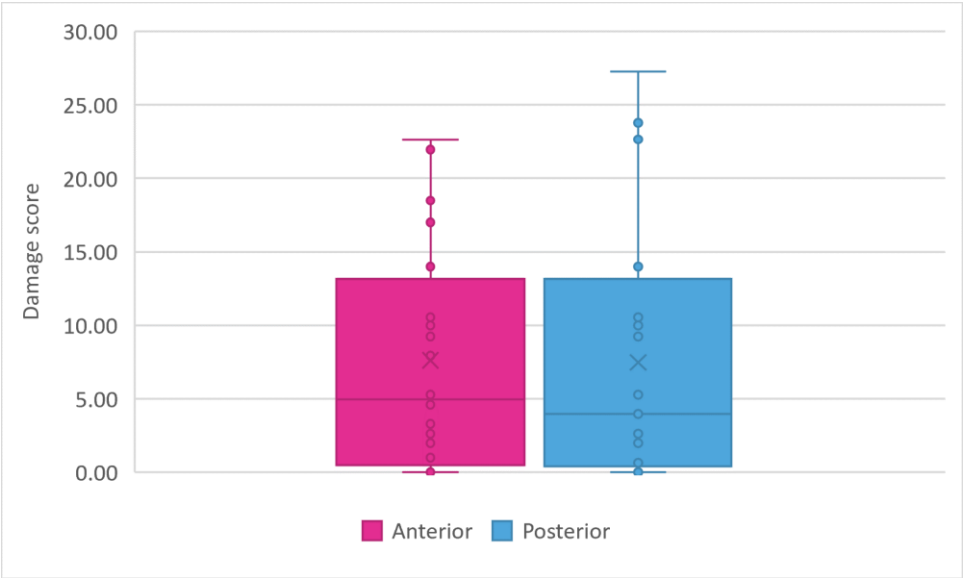

Figure 4.26. Box and whisker plot of damage scores for anterior and posterior aspects of tibial component inferior surfaces. Anterior damage score given by the sum of DFS from quadrants 1 and 2, and posterior damage score given by sum of DFS from quadrants 3 and 4.

There was also no significant difference ($p = 0.509$) between the average CDS for anterior aspects and posterior aspects of the bearing surfaces of the talar components (Figure 4.27).

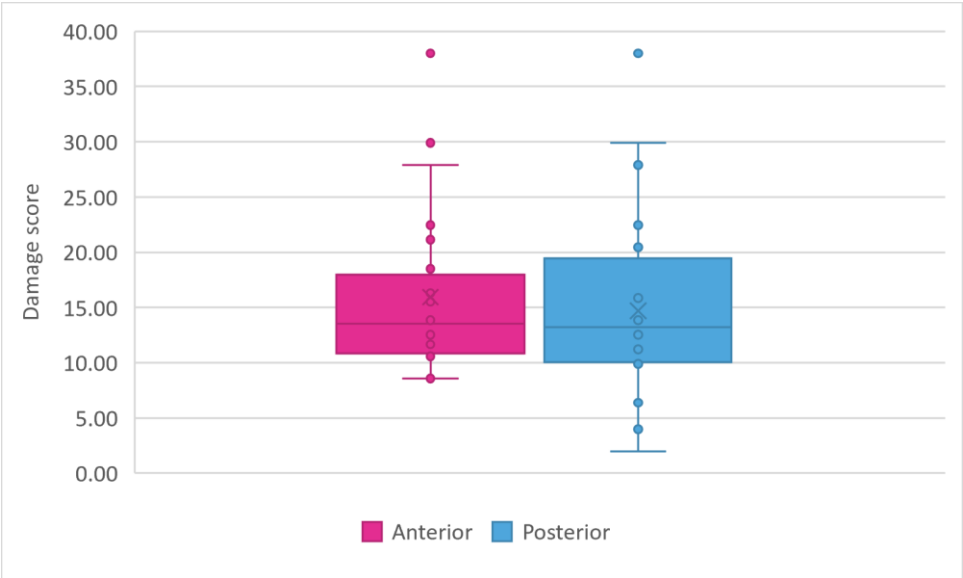

Figure 4.27. Box and whisker plot of damage scores for anterior and posterior aspects of talar component bearing surfaces. Anterior damage score given by the sum of DFS from quadrants 1 and 2, and posterior damage score given by sum of DFS from quadrants 3 and 4.

For the components where implantation side was known (11 PE inserts, 10 tibial components, and 11 talar components), the average CDS for the medial and lateral aspects, along with their corresponding p-values, are compared in Table 4.8. As with the anterior and posterior aspects, no clear pattern was seen in terms of damage being greater on either the medial or the lateral aspects.

Surface	Medial	Lateral	P-value
PE bearing	11.49 ± 8.14	11.25 ± 7.71	0.895
PE backside	12.99 ± 6.05	13.43 ± 5.02	0.948
Tibial	4.72 ± 4.34	4.90 ± 4.45	1.000
Talar	7.79 ± 4.32	7.75 ± 4.29	0.931

Table 4.8. CDS of each component surface (where the implantation side was known) for medial and lateral aspects. The medial and lateral CDS are the sum of the DFS from quadrants 1 and 3 or quadrants 2 and 4, depending on the implantation side.

For the bearing surfaces of the PE inserts, the average CDS was similar on the medial aspects and lateral aspects (Figure 4.28), with no significant difference (p = 0.895).

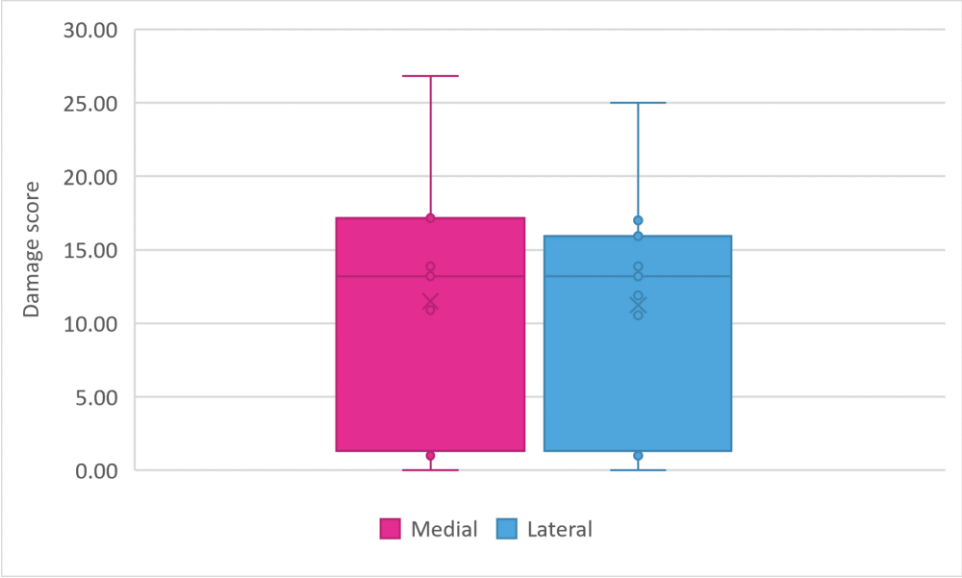

Figure 4.28. Box and whisker plot showing damage scores for medial and lateral aspects of PE insert bearing surfaces.

For the backside surfaces of the PE inserts, the average CDS was similar on the lateral aspects and the medial aspects (Figure 4.29), with no significant difference (p = 0.948).

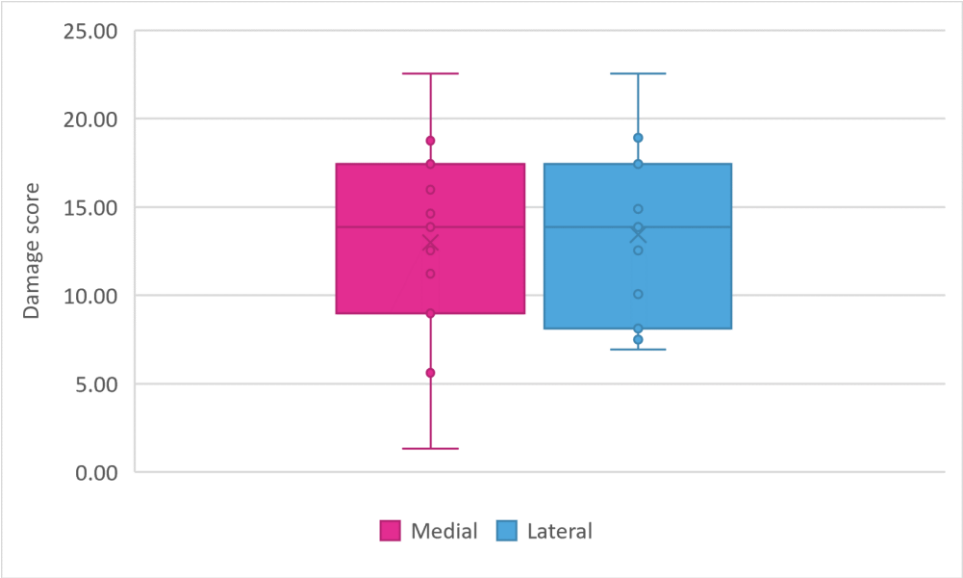

Figure 4.29. Box and whisker plot showing damage scores for medial and lateral aspects of PE insert backside surfaces.

For the inferior surfaces of the tibial components, the CDS was also similar on the lateral aspects and the medial aspects (Figure 4.30), with no significant difference (p = 1.000).

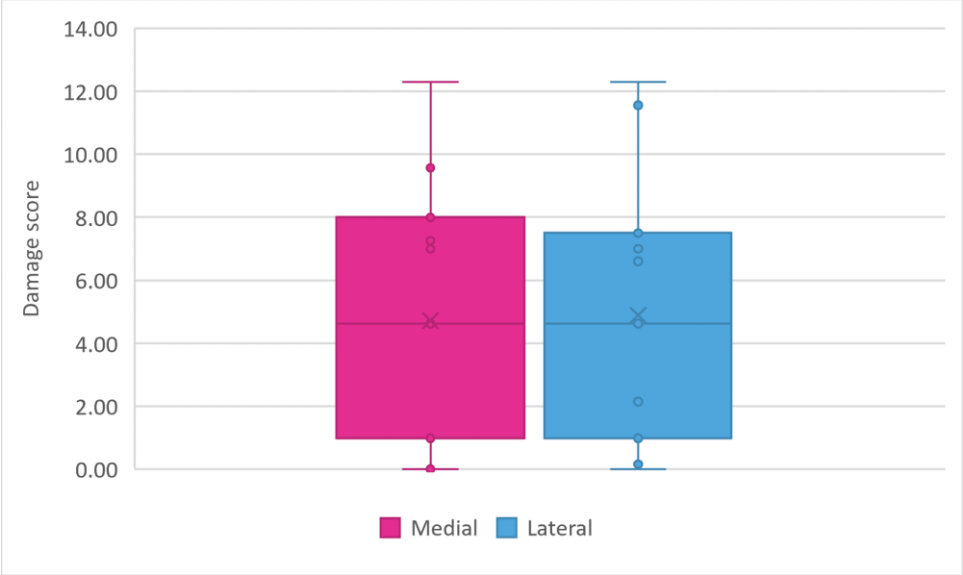

Figure 4.30. Box and whisker plot showing damage scores for medial and lateral aspects of tibial component inferior surfaces.

For the bearing surfaces of the talar components, the CDS was again similar on average on the medial aspects and the lateral aspects (Figure 4.31), with no significant difference ($p = 0.931$).

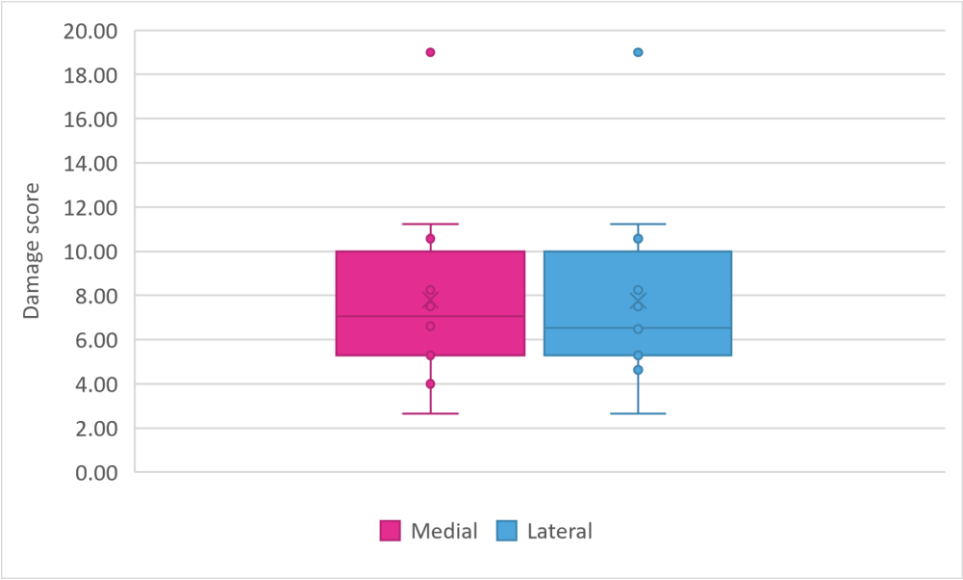

Figure 4.31. Box and whisker plot showing damage scores for medial and lateral aspects of talar component bearing surfaces.

4.2.4. Influence of bearing constraint

The differences between the average CDS for fixed and mobile bearing prostheses are given for each component surface in Table 4.9. A notable difference was seen in the CDS on PE insert backside surfaces, with this being significantly higher on those from mobile bearing prostheses compared to those from fixed bearing prostheses.

Surface	Fixed	Mobile	P-value
PE bearing	49.38 ± 24.32	42.73 ± 37.09	0.677
PE backside	18.79 ± 10.65	57.62 ± 26.78	0.002
Tibial	17.38 ± 18.93	14.33 ± 14.69	0.973
Talar	21.92 ± 8.58	32.92 ± 16.10	0.135

Table 4.9. Average (mean ± SD) CDS of each component surface for fixed and mobile bearing TARs.

For the bearing surfaces of the PE inserts, the CDS was higher on average on those from fixed bearing TARs compared to mobile bearing TARs (Figure 4.32). However, this difference did not reach statistical significance (0.677).

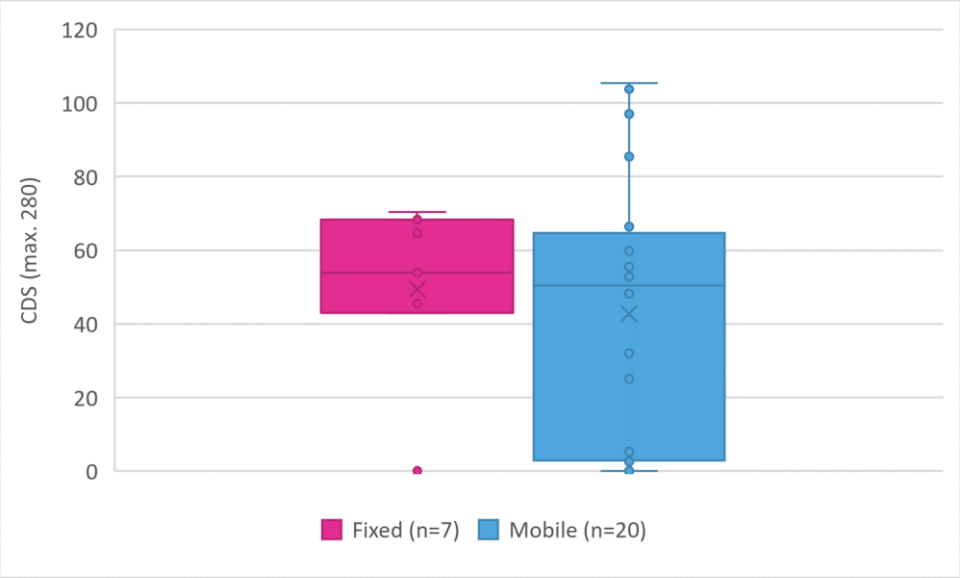

Figure 4.32. Box and whisker plot showing the distribution of CDS for PE insert bearing surfaces from fixed bearing and mobile bearing TARs.

For the backside surfaces of the PE inserts, the CDS was significantly higher ($p = 0.002$) on average on those from mobile bearing TARs compared to those from fixed bearing TARs (Figure 4.33).

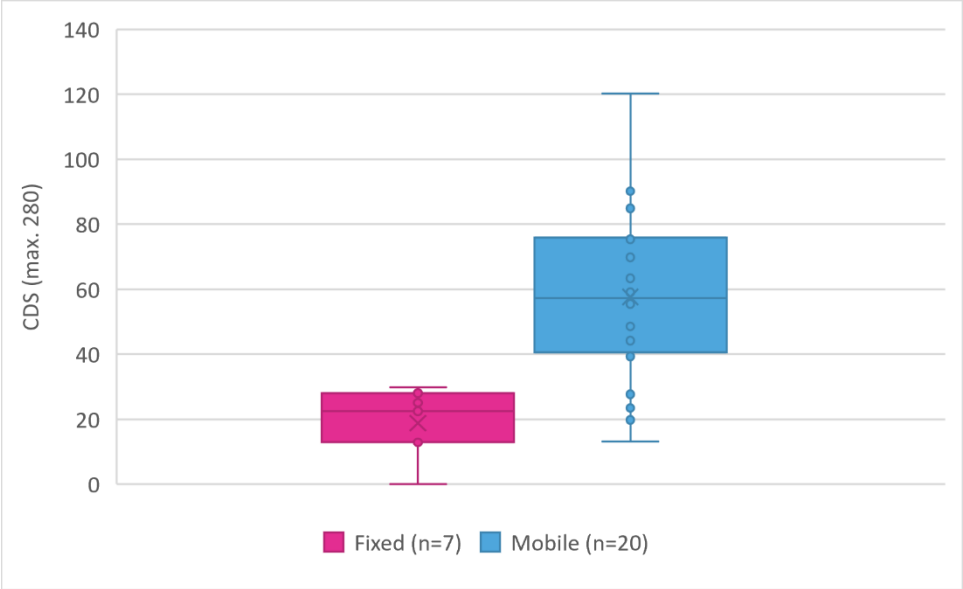

Figure 4.33. Box and whisker plot showing the distribution of CDS for PE insert backside surfaces from fixed bearing and mobile bearing TARs.

For the inferior surfaces of the tibial components, the CDS was higher on average on those from fixed bearing TARs compared to those from mobile TARs (Figure 4.34). However, this difference was not statistically significant ($p = 0.973$)

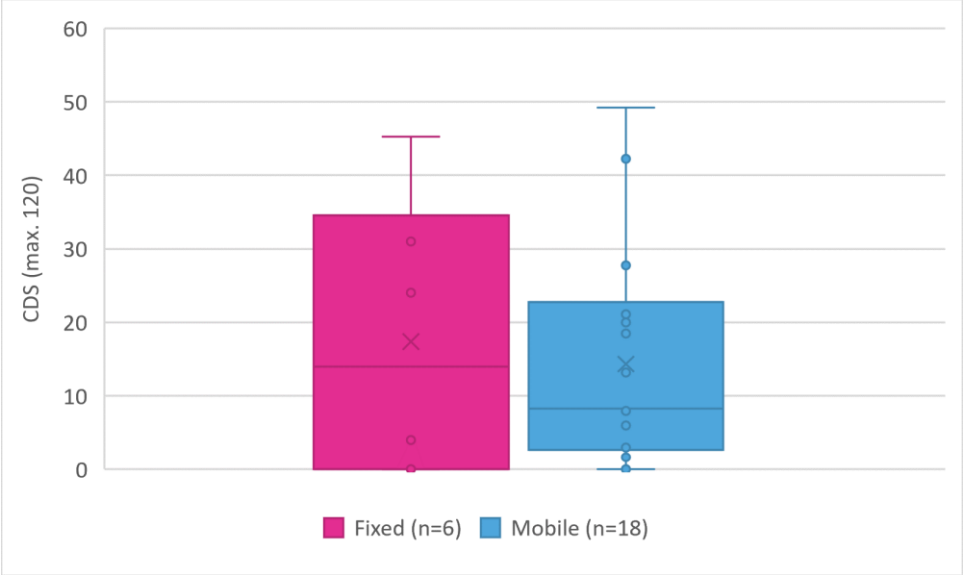

Figure 4.34. Box and whisker plot showing the distribution of CDS for tibial component inferior surfaces from fixed bearing and mobile bearing TARs.

For the bearing surfaces of the talar components, the CDS was higher on average on those from mobile bearing TARs compared to those from fixed bearing TARs (Figure 4.35). However, this difference also did not reach statistical significance ($p = 0.135$).

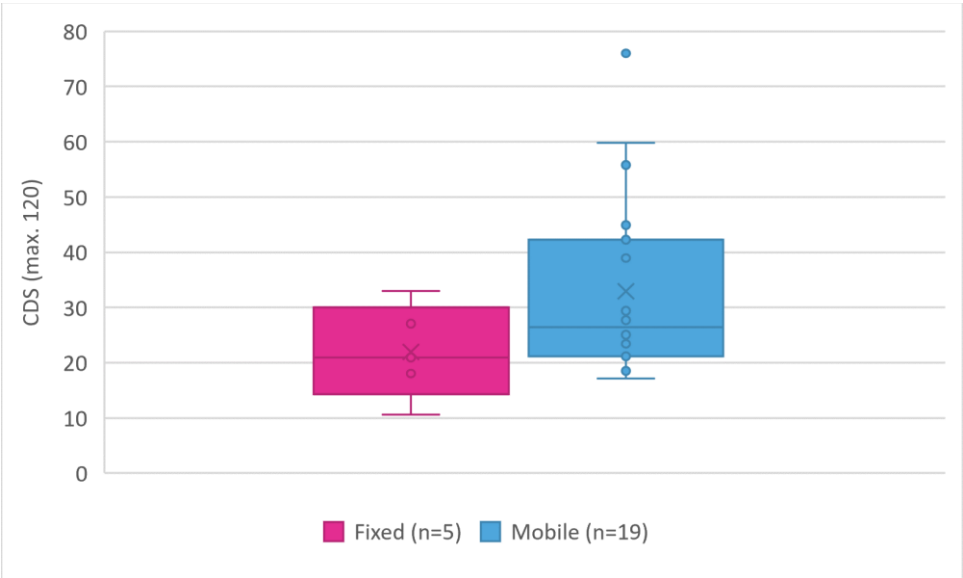

Figure 4.35. Box and whisker plot showing the distribution of CDS for talar component bearing surfaces from fixed bearing and mobile bearing TARs.

4.2.5. Influence of tibial component alloy

The average CDS for tibial component inferior surfaces and PE insert backside surfaces corresponding to different alloy tibial components (CoCr or Ti) are given in Table 4.10. For the purpose of this analysis only, the tibial component which had a TiN coating (n = 1) was excluded. Both the tibial component inferior surfaces and the PE insert backside surfaces had a higher CDS on average on those corresponding to CoCr alloy compared to Ti alloy tibial components, with the difference seen in the PE insert backside surface CDS being statistically significant.

Surface	**CoCr**	**Ti**	**P-value**
Tibial	16.17 ± 15.74	13.75 ± 16.13	0.598
PE backside	50.95 ± 24.41	18.72 ± 12.31	0.021

Table 4.10. Average (mean ± SD) CDS for tibial component inferior surfaces and PE insert backside surfaces corresponding to CoCr alloy and Ti alloy tibial components. The tibial component with a TiN coating (n = 1) was excluded from this analysis.

The CoCr alloy tibial components had a higher CDS on average compared to Ti alloy tibial components (Figure 4.36), though this difference did not reach statistical significance (p = 0.598).

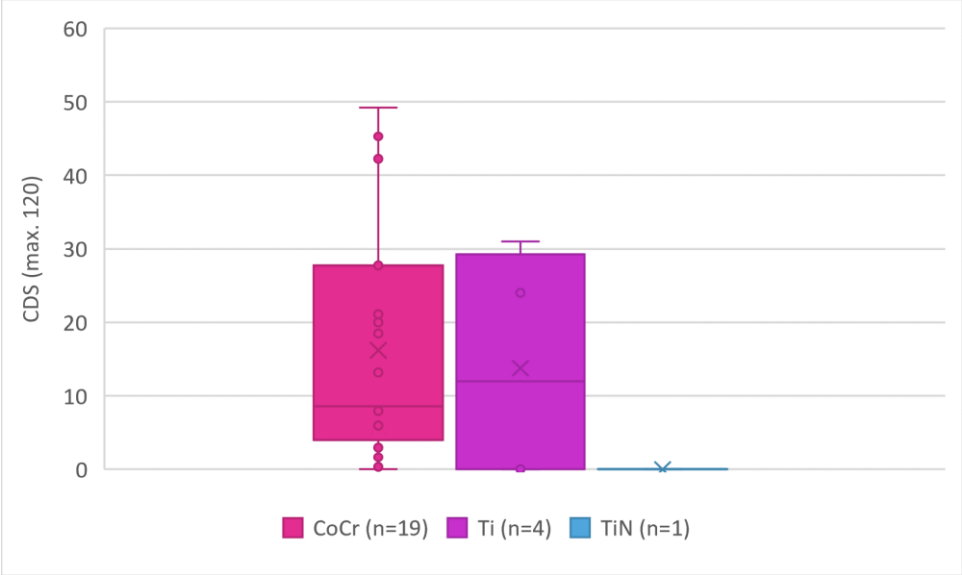

Figure 4.36. Box and whisker plot showing the distribution of CDS for tibial component inferior surfaces from tibial components manufactured from CoCr alloy, Ti alloy, and with a TiN coating.

The backside surfaces of the PE inserts corresponding to CoCr alloy tibial components also had a higher CDS on average compared to those corresponding to Ti alloy tibial components (Figure 4.37), with this difference reaching statistical significance ($p = 0.021$).

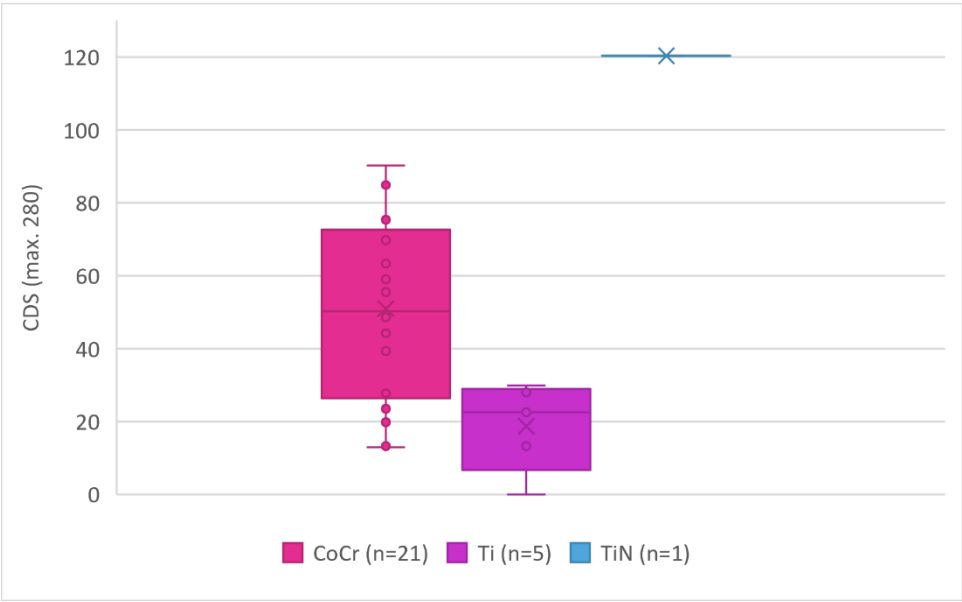

Figure 4.37. Box and whisker plot showing the distribution of CDS for PE insert backside surfaces corresponding to tibial components manufactured from CoCr alloy, Ti alloy, and with a TiN coating.

4.3. Surface Profilometry

Non-contacting 3D profilometry was performed on the 'unworn' and worn areas of the articulating surfaces of the metal tibial and talar components. For those which exhibited pitting, measurements were taken on both unpitted and pitted areas in order to compare the topography. As defined in the previous chapter (Section 3.4), the following parameters were measured: S_a, S_q, S_z, S_p, S_v, S_{sk}, and S_{ku}.

4.3.1. Tibial component

Representative surface topography images showing the oblique plots and intensity maps for both unworn and worn (pitted) areas of a tibial component articulating surface are shown in Figure 4.38. For each component area analysed, 5 measurements were taken, all of which were included in the statistical analyses.

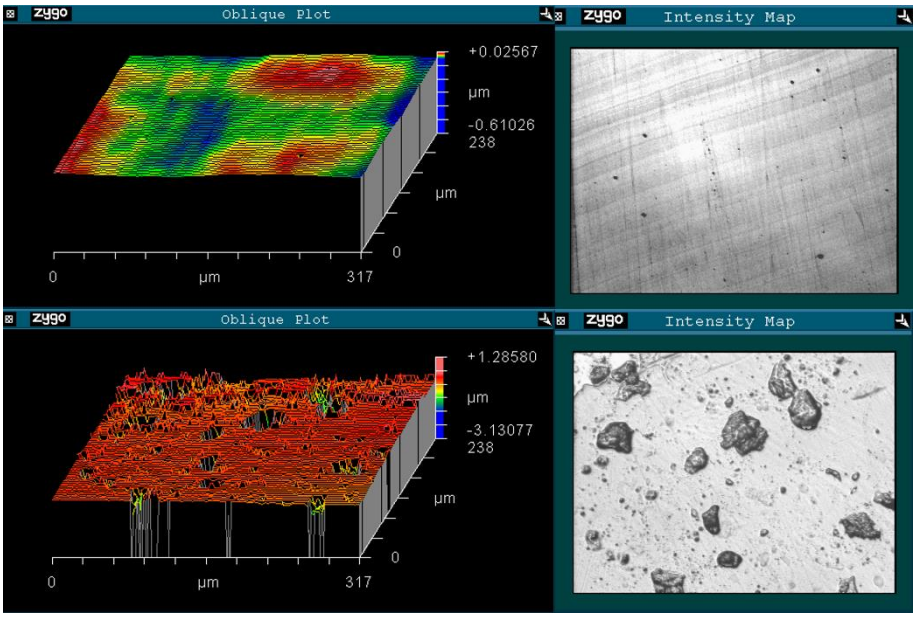

Figure 4.38. Surface profilometry images of unpitted and pitted areas of a Mobility tibial component inferior surface.

The results of the measured surface roughness parameters of the 'unworn' areas (i.e., areas without identified damage) of the different tibial component articulating surfaces are given in Table 4.11. For the parameter of S_a specifically, the various measured values from unworn

areas of the different TAR models are plotted in Figure 4.39. The fixed bearing designs (INFINITY, Cadence, and Salto Talaris) recorded significantly higher measured S_a values on these unworn areas of tibial component articulating surfaces than the mobile bearing designs (Salto, Mobility, STAR, Hintegra, BOX, and Zenith) (0.253 ± 0.116 µm versus 0.016 ± 0.009 µm, respectively) ($p < 0.001$) (Figure 4.40).

Tibial component	**S_a (µm)**	**S_q (µm)**	**S_z (µm)**	**S_p (µm)**	**S_v (µm)**	**S_{sk}**	**S_{ku}**
INFINITY (n = 3)	0.360 ± 0.015	0.456 ± 0.016	3.668 ± - 0.201	1.881 ± 0.152	-1.787 ± 0.098	0.135 ± 0.148	3.206 ± 0.119
Cadence (n = 1)	0.161 ± 0.004	0.204 ± 0.004	2.401 ± 0.160	0.903 ± 0.117	-1.498 ± 0.138	-0.483 ± 0.078	3.781 ± 0.138
Salto Talaris (n = 2)	0.140 ± 0.067	0.175 ± 0.083	1.552 ± 0.617	0.766 ± 0.245	-0.786 ± 0.387	-0.385 ± 0.065	3.180 ± 0.030
Salto (n = 1)	0.023 ± 0.000	0.032 ± 0.000	0.759 ± 0.019	0.400 ± 0.003	-0.359 ± 0.017	1.678 ± 0.034	10.996 ± 0.366
Mobility (n = 10)	0.009 ± 0.004	0.013 ± 0.005	0.551 ± 0.122	0.204 ± 0.118	-0.349 ± 0.138	-1.328 ± 4.131	202.078 ± 319.827
STAR (n = 3)	0.017 ± 0.006	0.021 ± 0.008	0.669 ± 0.115	0.357 ± 0.090	-0.312 ± 0.082	0.399 ± 0.818	26.959 ± 31.140
Hintegra (n = 2)	0.017 ± 0.007	0.032 ± 0.014	0.942 ± 0.129	0.523 ± 0.184	-0.385 ± 0.117	5.086 ± 1.362	75.902 ± 46.016
BOX (n = 3)	0.025 ± 0.007	0.037 ± 0.012	0.825 ± 0.107	0.399 ± 0.085	-0.425 ± 0.088	-0.449 ± 0.964	15.394 ± 8.517
Zenith (n = 1)	0.032 ± 0.001	0.058 ± 0.002	2.543 ± 1.115	1.022 ± 0.102	-1.521 ± 1.214	1.801 ± 2.500	103.470 ± 107.604

Table 4.11. Measured surface roughness parameter values for unworn areas of tibial components. Values given as mean ± SD. Notes: S_a, average surface roughness; S_q, root mean square roughness; S_z, peak to valley height; S_p, maximum peak height; S_v, maximum valley depth; S_{sk}, skewness; S_{ku}, kurtosis.

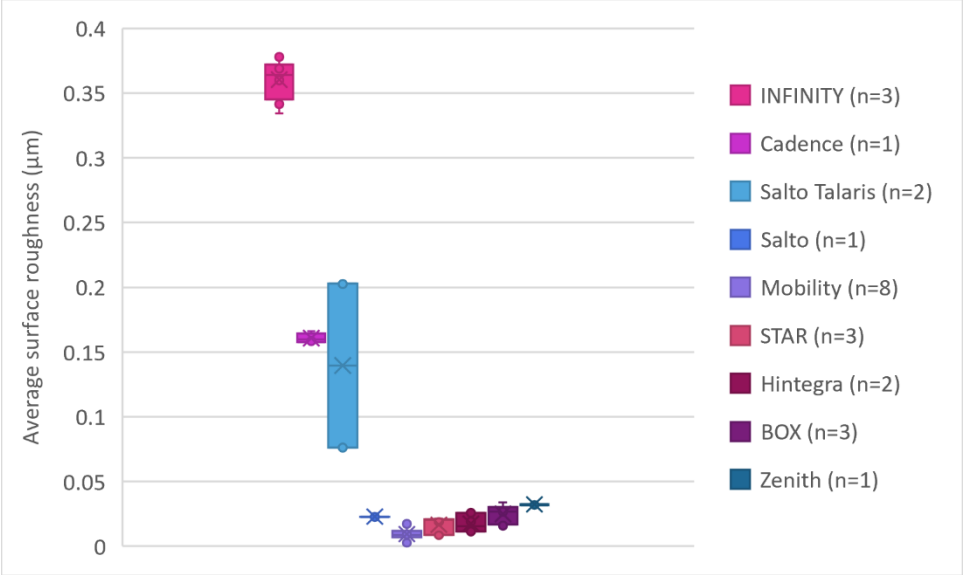

Figure 4.39. Box and whisker plot of the measured average surface roughness (S_a) values from unworn areas of the articulating surfaces of different tibial components.

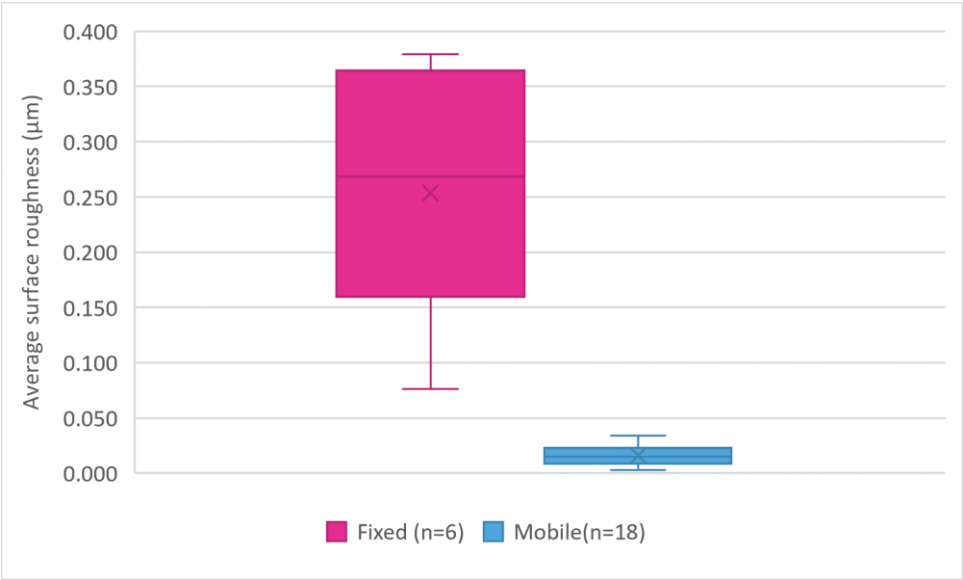

Figure 4.40. Box and whisker plot of the measured average surface roughness (Sa) values from unworn areas of the articulating surfaces of fixed and mobile bearing tibial components.

There were significant differences between the measured S_a values from unworn areas of tibial component articulating surfaces of different alloys (Figure 4.41). The average surface roughness of Ti alloy tibial components (INFINITY and Cadence) (0.310 ± 0.090 µm) was significantly higher than that of CoCr alloy tibial components (Salto Talaris, Salto, Mobility,

STAR, Hintegra, and BOX) (0.028 ± 0.044 µm) ($p < 0.001$). The average surface roughness of the Ti alloy tibial components was also significantly higher than that of the tibial components coated with TiN (Zenith) (0.032 ± 0.001 µm) ($p = 0.001$). Finally, the average surface roughness of the TiN coated tibial components was significantly higher than that of the CoCr alloy tibial components ($p = 0.004$). It should be noted that both Ti alloy tibial components were of fixed bearing constraint.

The INFINITY prosthesis in particular had a visibly rougher surface finish of the tibial component inferior surface compared to the those of the other TAR models analysed. This is evident throughout the surface profilometry results presented within this section. Whilst manufacturing information regarding surface finishing treatment is not readily accessible, typically mobile bearing tibial components will have a highly polished articulating surface finish, while those of fixed bearing constraint may not. This is because the mobile bearing tibial components are needed to be smooth to act as an articulating surface, whereas this is not a requirement for fixed bearing tibial components.

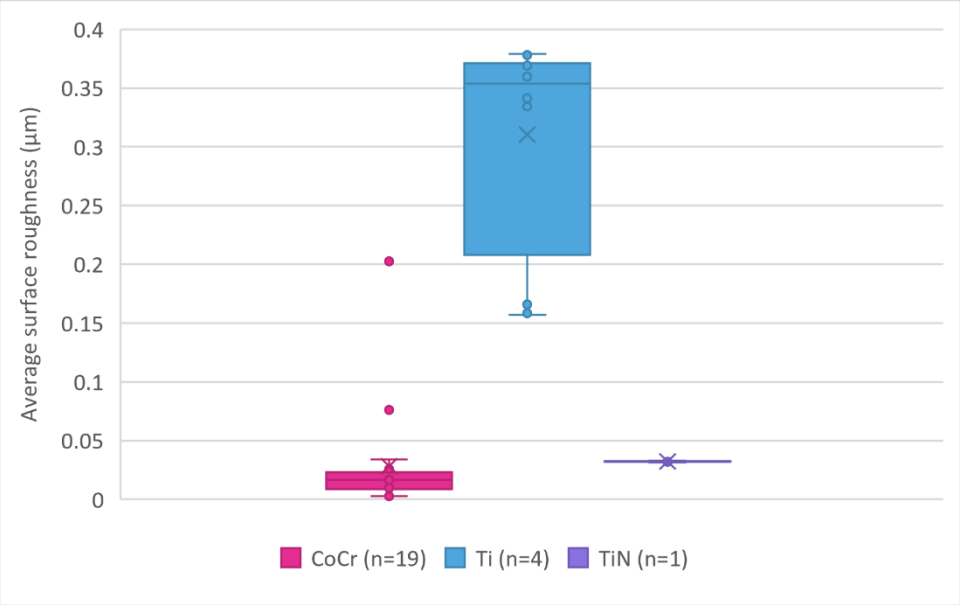

Figure 4.41. Box and whisker plot of the measured average surface roughness (Sa) values from unworn areas of the articulating surfaces of tibial components, separated by alloy.

For the articulating surfaces of the tibial components on which pitting was identified specifically, the measured average surface roughness (S_a) and maximum valley depth (S_v)

values were both statistically significantly higher ($p < 0.05$) for pitted areas than unpitted areas (Table 4.12).

Tibial component	**N with pitting**	**Unpitted S_a (µm)**	**Pitted S_a (µm)**	**P-value**	**Unpitted S_v (µm)**	**Pitted S_v (µm)**	**P-value**
Salto Talaris	2	0.140 ± 0.067	0.248 ± 0.031	< 0.001	-0.786 ± 0.387	-5.399 ± 0.403	< 0.001
Salto	1	0.023 ± 0.000	0.059 ± 0.001	0.012	-0.359 ± 0.017	-2.262 ± 0.010	< 0.001
Mobility	4	0.011 ± 0.004	0.058 ± 0.016	< 0.001	-0.423 ± 0.133	-3.068 ± 1.222	< 0.001
STAR	3	0.017 ± 0.006	0.083 ± 0.054	< 0.001	-0.312 ± 0.082	-2.677 ± 0.286	< 0.001
Hintegra	1	0.011 ± 0.000	0.028 ± 0.000	0.012	-0.473 ± 0.037	-2.384 ± 0.020	< 0.001
BOX	1	0.032 ± 0.001	0.072 ± 0.002	< 0.001	-0.538 ± 0.030	-2.938 ± 0.010	< 0.001

Table 4.12. Average surface roughness (S_a) and maximum valley depth (S_v) values for different tibial component articulating surfaces with pitting. Values given as mean ± SD.

The tibial component articulating surfaces measured average surface roughness (S_a) values were higher on worn areas than unworn areas on all models of TAR (Table 4.13). These differences were statistically significant ($p < 0.05$) for all models except Zenith.

Tibial component	**Unworn S_a (µm)**	**Worn S_a (µm)**	**P-value**
INFINITY (n = 3)	0.360 ± 0.015	0.479 ± 0.114	< 0.001
Cadence (n = 1)	0.161 ± 0.004	0.249 ± 0.002	< 0.001
Salto Talaris (n = 2)	0.140 ± 0.067	0.248 ± 0.031	< 0.001
Salto (n = 1)	0.023 ± 0.000	0.059 ± 0.001	0.012
Mobility (n = 10)	0.009 ± 0.004	0.039 ± 0.022	< 0.001
STAR (n = 3)	0.017 ± 0.006	0.083 ± 0.054	< 0.001

Hintegra (n = 2)	0.017 ± 0.007	0.053 ± 0.027	< 0.001
BOX (n = 3)	0.025 ± 0.007	0.063 ± 0.013	< 0.001
Zenith (n = 1)	0.032 ± 0.001	0.036 ± 0.007	0.296

Table 4.13. Average surface roughness (S_a) values for unworn and worn areas of different tibial component articulating surfaces. Values given as mean ± SD.

The measured root mean square roughness (S_q) values for the tibial component articulating surfaces were also higher in worn areas compared to unworn areas for all of the TAR models (Table 4.14). Again, these differences were statistically significant ($p < 0.05$) for all models except Zenith.

Tibial component	**Unworn S_q (µm)**	**Worn S_q (µm)**	**P-value**
INFINITY (n = 3)	0.456 ± 0.016	0.725 ± 0.321	< 0.001
Cadence (n = 1)	0.204 ± 0.004	0.315 ± 0.003	0.012
Salto Talaris (n = 2)	0.175 ± 0.083	0.381 ± 0.040	< 0.001
Salto (n = 1)	0.032 ± 0.000	0.128 ± 0.001	< 0.001
Mobility (n = 10)	0.013 ± 0.005	0.103 ± 0.097	< 0.001
STAR (n = 3)	0.021 ± 0.008	0.136 ± 0.049	< 0.001
Hintegra (n = 2)	0.032 ± 0.014	0.120 ± 0.006	< 0.001
BOX (n = 3)	0.037 ± 0.012	0.148 ± 0.049	< 0.001
Zenith (n = 1)	0.058 ± 0.002	0.062 ± 0.010	0.452

Table 4.14. Root mean square roughness (S_q) values for unworn and worn areas of different tibial component articulating surfaces. Values given as mean ± SD.

The measured peak to valley height (S_z) values were higher for worn areas than unworn areas of the tibial component articulating surfaces for all models of TAR except Zenith, for which the opposite was true (Table 4.15). These differences were statistically significant ($p < 0.05$) for all models except INFINITY.

Tibial component	Unworn S_z (µm)	Worn S_z (µm)	P-value
INFINITY (n = 3)	3.668 ± 0.201	5.313 ± 2.370	0.089
Cadence (n = 1)	2.401 ± 0.160	2.934 ± 0.320	0.012
Salto Talaris (n = 2)	1.552 ± 0.617	6.711 ± 0.564	< 0.001
Salto (n = 1)	0.759 ± 0.019	3.035 ± 0.092	0.012
Mobility (n = 10)	0.551 ± 0.122	3.471 ± 3.782	< 0.001
STAR (n = 3)	0.669 ± 0.115	3.669 ± 0.320	< 0.001
Hintegra (n = 2)	0.942 ± 0.129	2.368 ± 0.734	< 0.001
BOX (n = 3)	0.825 ± 0.107	3.572 ± 1.624	< 0.001
Zenith (n = 1)	2.543 ± 1.115	1.871 ± 0.140	0.037

Table 4.15. Peak to valley height (S_z) values for unworn and worn areas of different tibial component articulating surfaces. Values given as mean ± SD.

The measured maximum peak height (S_p) was once again higher on worn than unworn areas of tibial component articulating surfaces for all TAR models except Zenith, which had a greater unworn S_p (Table 4.16). These differences were statistically significant ($p < 0.05$) for all models except INFINITY.

Tibial component	Unworn S_p (µm)	Worn S_p (µm)	P-value
INFINITY (n = 3)	1.881 ± 0.152	1.912 ± 0.313	0.678
Cadence (n = 1)	0.903 ± 0.117	1.224 ± 0.104	0.003
Salto Talaris (n = 2)	0.766 ± 0.245	1.312 ± 0.203	< 0.001
Salto (n = 1)	0.400 ± 0.003	0.773 ± 0.083	0.012
Mobility (n = 10)	0.204 ± 0.118	1.343 ± 3.065	< 0.001
STAR (n = 3)	0.357 ± 0.090	0.992 ± 0.224	< 0.001
Hintegra (n = 2)	0.523 ± 0.184	0.744 ± 0.170	0.014
BOX (n = 3)	0.399 ± 0.085	1.378 ± 1.075	< 0.001
Zenith (n = 1)	1.022 ± 0.102	0.633 ± 0.121	0.012

Table 4.16. Maximum peak height (S_p) values for unworn and worn areas of different tibial component articulating surfaces. Values given as mean ± SD.

For all TAR models except Zenith the maximum valley depth (S_v) was greater on worn areas than unworn areas (Table 4.17). The differences observed were statistically significant ($p < 0.05$) in the cases of 6 of the designs, and not in the other 3.

Tibial component	**Unworn S_v (µm)**	**Worn S_v (µm)**	**P-value**
INFINITY (n = 3)	-1.787 ± 0.098	-3.399 ± 2.084	0.081
Cadence (n = 1)	-1.498 ± 0.138	-1.710 ± 0.238	0.144
Salto Talaris (n = 2)	-0.786 ± 0.387	-5.399 ± 0.403	< 0.001
Salto (n = 1)	-0.359 ± 0.017	-2.262 ± 0.010	< 0.001
Mobility (n = 10)	-0.349 ± 0.138	-2.129 ± 1.340	< 0.001
STAR (n = 3)	-0.312 ± 0.082	-2.677 ± 0.286	< 0.001
Hintegra (n = 2)	-0.385 ± 0.117	-1.623 ± 0.803	< 0.001
BOX (n = 3)	-0.425 ± 0.088	-2.195 ± 0.564	< 0.001
Zenith (n = 1)	-1.521 ± 1.214	-1.238 ± 0.027	0.144

Table 4.17. Maximum valley depth (S_v) values for unworn and worn areas of different tibial component articulating surfaces. Values given as mean ± SD.

The measured skewness was more negative (indicative of a predominance of valleys, in terms of more severe valleys or a great number of valleys, rather than peaks) on the worn areas than unworn areas of the tibial component articulating surfaces for all TAR models except Zenith (Table 4.18). The differences were also statistically significant ($p < 0.05$) for all models except Zenith.

Tibial component	Unworn S_{sk}	Worn S_{sk}	P-value
INFINITY (n = 3)	0.135 ± 0.148	-1.266 ± 1.636	0.009
Cadence (n = 1)	-0.483 ± 0.078	-0.691 ± -0.024	0.005
Salto Talaris (n = 2)	-0.385 ± 0.065	-4.112 ± 1.066	< 0.001
Salto (n = 1)	1.678 ± 0.034	-7.966 ± 0.157	0.012
Mobility (n = 10)	-1.328 ± 4.131	-5.384 ± 7.306	< 0.001
STAR (n = 3)	0.399 ± 0.818	-4.403 ± 2.011	< 0.001
Hintegra (n = 2)	5.086 ± 1.362	-5.933 ± 6.865	< 0.001
BOX (n = 3)	-0.449 ± 0.964	-4.604 ± 2.403	< 0.001
Zenith (n = 1)	1.801 ± 2.500	-1.877 ± 1.802	0.060

Table 4.18. Skewness (S_{sk}) values for unworn and worn areas of different tibial component articulating surfaces. Values given as mean ± SD.

The measured kurtosis (S_{ku}) of the tibial component articulating surfaces was higher on worn areas than unworn areas for all TAR models except Cadence and Zenith (Table 4.19). The differences were statistically significant ($p < 0.05$) in 5 cases, and not for the other 4 models.

Tibial component	Unworn S_{ku}	Worn S_{ku}	P-value
INFINITY (n = 3)	3.206 ± 0.119	7.815 ± 7.095	0.678
Cadence (n = 1)	3.781 ± 0.138	3.682 ± 0.059	0.201
Salto Talaris (n = 2)	3.180 ± 0.030	45.422 ± 22.771	< 0.001
Salto (n = 1)	10.996 ± 0.366	99.817 ± 3.063	0.012
Mobility (n = 10)	202.078 ± 319.827	225.993 ± 596.463	0.266
STAR (n = 3)	26.959 ± 31.140	91.595 ± 70.302	0.001
Hintegra (n = 2)	75.902 ± 46.016	87.998 ± 85.491	1.000
BOX (n = 3)	15.394 ± 8.517	51.880 ± 23.017	< 0.001
Zenith (n = 1)	103.470 ± 107.604	31.012 ± 10.826	0.012

Table 4.19. Kurtosis (S_{ku}) values for unworn and worn areas of different tibial component articulating surfaces. Values given as mean ± SD.

The differences between the measured surface roughness parameters on fixed and mobile bearing TARs for both unworn and worn areas of the tibial component articulating surfaces are given in Table 4.20.

The parameters of S_a, S_q, S_z, S_p, and S_v measured on unworn areas were all significantly ($p < 0.05$) higher on fixed bearing than mobile bearing tibial components. The S_{sk} was also more negative on fixed bearing than mobile bearing components, however this difference did not reach statistical significance ($p = 0.088$). Conversely, the S_{ku} was significantly ($p < 0.05$) higher on mobile bearing than fixed bearing tibial components.

For worn areas, the measured S_a, S_q, S_z, S_p, and S_v were again all significantly ($p < 0.05$) higher on fixed bearing than mobile bearing tibial components. The S_{ku} was also again significantly ($p < 0.05$) higher on mobile bearing than fixed bearing components. The difference in S_{sk}, on the other hand, was reversed compared to what it was for unworn areas, with significantly ($p < 0.05$) more negative values measured on worn areas of mobile bearing than fixed bearing tibial components.

	Unworn fixed (n = 6)	**Unworn mobile (n = 18)**	**P-value**	**Worn fixed (n = 6)**	**Worn mobile (n = 18)**	**P-value**
S_a (µm)	0.253 ± 0.116	0.016 ± 0.009	< 0.001	0.364 ± 0.143	0.053 ± 0.032	< 0.001
S_q (µm)	0.321 ± 0.146	0.024 ± 0.015	< 0.001	0.542 ± 0.292	0.117 ± 0.073	< 0.001
S_z (µm)	2.751 ± 1.045	0.782 ± 0.521	< 0.001	5.382 ± 2.114	3.285 ± 2.649	< 0.001
S_p (µm)	1.346 ± 0.574	0.354 ± 0.226	< 0.001	1.597 ± 0.406	1.152 ± 2.093	< 0.001
S_v (µm)	-1.405 ± 0.512	-0.425 ± 0.389	< 0.001	-3.784 ± 1.968	-2.133 ± 1.020	< 0.001
S_{sk}	-0.141 ± 0.305	0.160 ± 3.503	0.088	-2.119 ± 1.934	-5.100 ± 5.579	< 0.001
S_{ku}	3.293 ± 0.243	111.664 ± 229.965	< 0.001	19.662 ± 23.036	141.400 ± 404.464	0.006

Table 4.20. Comparison of the measured surface roughness parameters for unworn and worn areas of fixed and mobile bearing tibial component articulating surfaces. Values given as mean ± SD.

The differences between both unpitted and pitted the S_a and S_v values for fixed and mobile bearing tibial component articulating surfaces on which pitting was identified are given in Table 4.21. The average measured values for unpitted S_a, pitted S_a, unpitted S_v, and pitted S_v were all greater on fixed bearing than mobile bearing tibial components, with all of these differences being statistically significant ($p < 0.05$).

Tibial component	Fixed (n= 6)	Mobile (n = 18)	P-value
N with pitting	2	10	-
Unpitted S_a (µm)	0.140 ± 0.067	0.016 ± 0.008	< 0.001
Pitted S_a (µm)	0.248 ± 0.031	0.064 ± 0.035	< 0.001
Unpitted S_v (µm)	-0.786 ± 0.387	-0.400 ± 0.119	0.002
Pitted S_v (µm)	-5.399 ± 0.403	-2.789 ± 0.828	< 0.001

Table 4.21. Average surface roughness (S_a) and maximum valley depth (S_v) values for fixed and mobile bearing tibial component articulating surfaces with pitting. Values given as mean ± SD.

The variation in measured S_a and S_v values on both unworn and worn areas of tibial component articulating surfaces for different component alloys are given in Figure 4.42 and Figure 4.43, respectively.

For both unworn and worn areas, Ti alloy components had the highest S_a (0.310 ± 0.090 µm and 0.422 ± 0.141 µm, respectively) compared to CoCr alloy components (0.028 ± 0.044 µm and 0.074 ± 0.068 µm, respectively) and TiN coated components (0.032 ± 0.000 µm and 0.035 ± 0.007 µm, respectively) (mean ± SD).

The Ti alloy components also had the greatest average S_v for both unworn and worn areas (-1.714 ± 0.166 µm and -2.977 ± 1.943 µm, respectively) compared to CoCr alloy components (-0.406 ± 0.210 µm and -2.524 ± 1.393 µm, respectively) and TiN coated components (-1.521 ± 1.215 and -1.238 ± 0.027 µm, respectively) (mean ± SD).

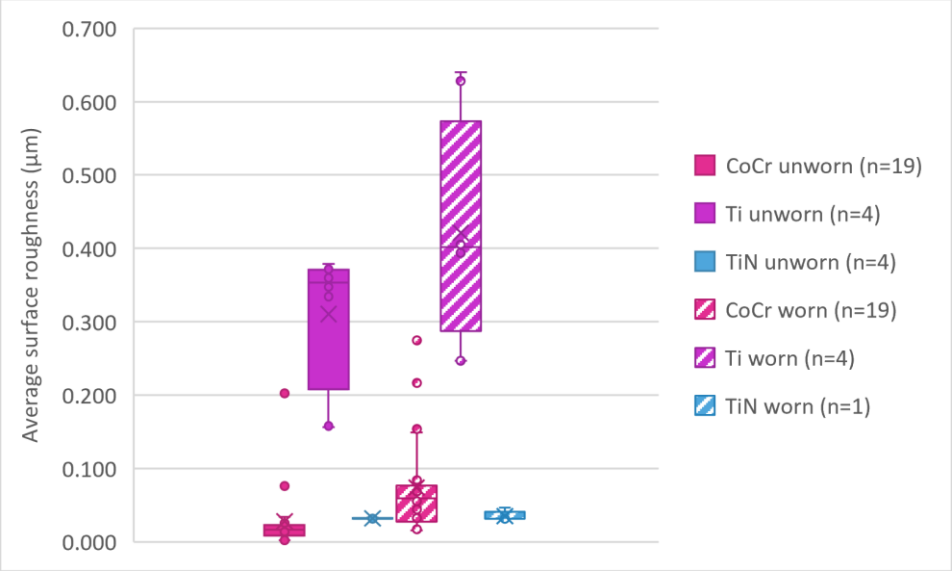

Figure 4.42. Box and whisker plot of unworn and worn average surface roughness (S_a) values of the articulating surfaces of different alloy tibial components.

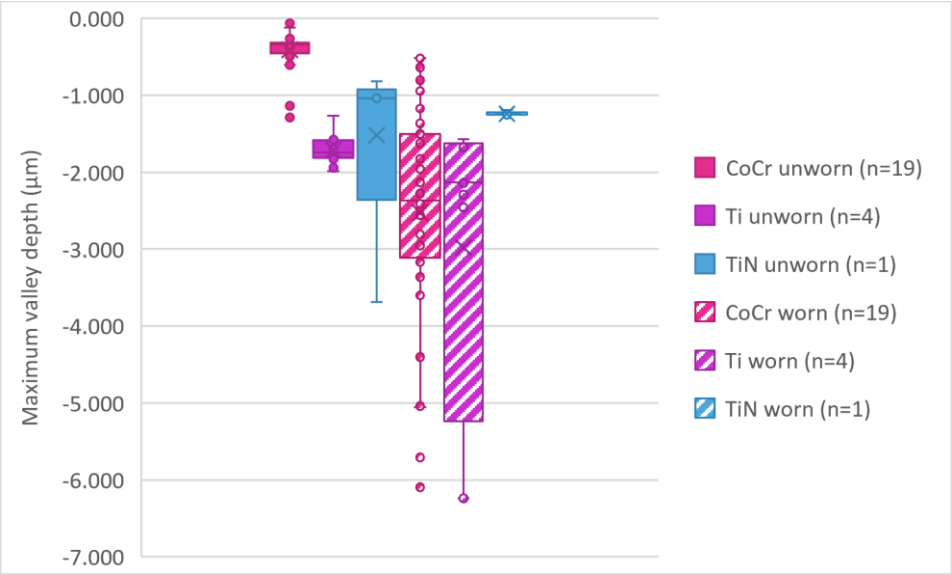

Figure 4.43. Box and whisker plot of unworn and worn maximum valley depth (S_v) values of the articulating surfaces of different alloy tibial components.

4.3.2. Talar component

Representative surface topography images showing the oblique plots and intensity maps for both unworn and worn (pitted) areas of a talar component articulating surface are shown in Figure 4.44. As with the tibial component, 5 measurements were taken for each analysed area of the component, all of which were included in subsequent statistical analyses.

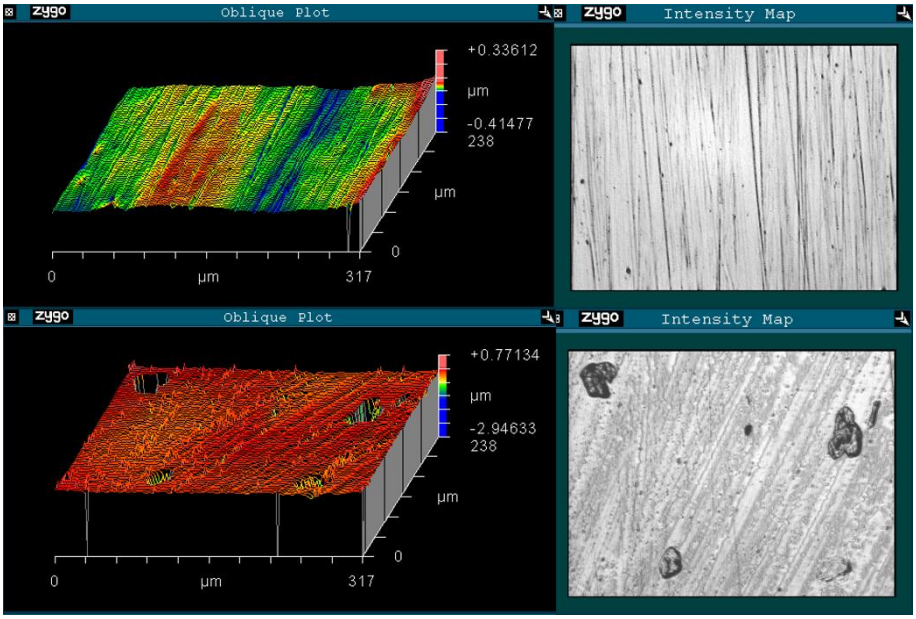

Figure 4.44. Surface profilometry images of unpitted and pitted areas of a Mobility talar component bearing surface.

The average values of the surface roughness parameters measured on 'unworn' areas (i.e., areas without identified damage) of the different talar component articulating surfaces are given in Table 4.22. For the parameter of S_a specifically, the various measured values from unworn areas of the different TAR models are plotted in Figure 4.45.

The talar components corresponding to mobile bearing TARs (Salto, Mobility, STAR, Hintegra, BOX, and Zenith) recorded significantly higher S_a values than those corresponding to fixed bearing TARs (INFINITY, Cadence, and Salto Talaris) (0.057 ± 0.031 µm versus 0.029 ± 0.025 µm, respectively (mean ± SD)) ($p < 0.001$) (Figure 4.46).

Talar component	**S_a (µm)**	**S_q (µm)**	**S_z (µm)**	**S_p (µm)**	**S_v (µm)**	**S_{sk}**	**S_{ku}**
INFINITY (n = 3)	0.020 ± 0.007	0.026 ± 0.009	0.581 ± 0.101	0.220 ± 0.082	-0.362 ± 0.036	-0.431 ± 0.921	20.173 ± 22.964
Cadence (n = 1)	0.009 ± 0.000	0.012 ± 0.000	0.606 ± 0.006	0.270 ± 0.006	-0.336 ± 0.011	-2.570 ± 0.395	67.999 ± 5.024
Salto Talaris (n = 1)	0.076 ± 0.001	0.101 ± 0.002	1.608 ± 0.040	0.461 ± 0.036	-1.146 ± 0.024	-0.366 ± 0.051	5.892 ± 0.561
Salto (n = 1)	0.078 ± 0.002	0.107 ± 0.002	1.360 ± 0.062	0.685 ± 0.064	-0.676 ± 0.027	-0.492 ± 0.120	5.804 ± 0.248
Mobility (n = 9)	0.034 ± 0.013	0.047 ± 0.022	0.690 ± 0.273	0.285 ± 0.165	-0.406 ± 0.218	-0.088 ± 1.032	11.746 ± 13.069
STAR (n = 3)	0.065 ± 0.023	0.082 ± 0.028	0.805 ± 0.113	0.419 ± 0.051	-0.386 ± 0.105	-0.074 ± 0.383	3.328 ± 0.524
Hintegra (n = 2)	0.113 ± 0.031	0.142 ± 0.042	0.918 ± 0.354	0.491 ± 0.175	-0.427 ± 0.179	-0.004 ± 0.358	3.203 ± 0.449
BOX (n = 3)	0.077 ± 0.014	0.099 ± 0.017	0.866 ± 0.190	0.393 ± 0.109	-0.474 ± 0.110	0.016 ± 0.381	3.525 ± 0.968
Zenith (n = 1)	0.045 ± 0.000	0.079 ± 0.000	2.530 ± 0.282	0.993 ± 0.139	-1.537 ± 0.186	0.302 ± 0.491	24.269 ± 2.460

Table 4.22. Measured surface roughness parameter values for unworn areas of tibial components. Values given as mean ± SD. Notes: S_a, average surface roughness; S_q, root mean square roughness; S_z, peak to valley height; S_p, maximum peak height; S_v, maximum valley depth; S_{sk}, skewness; S_{ku}, kurtosis.

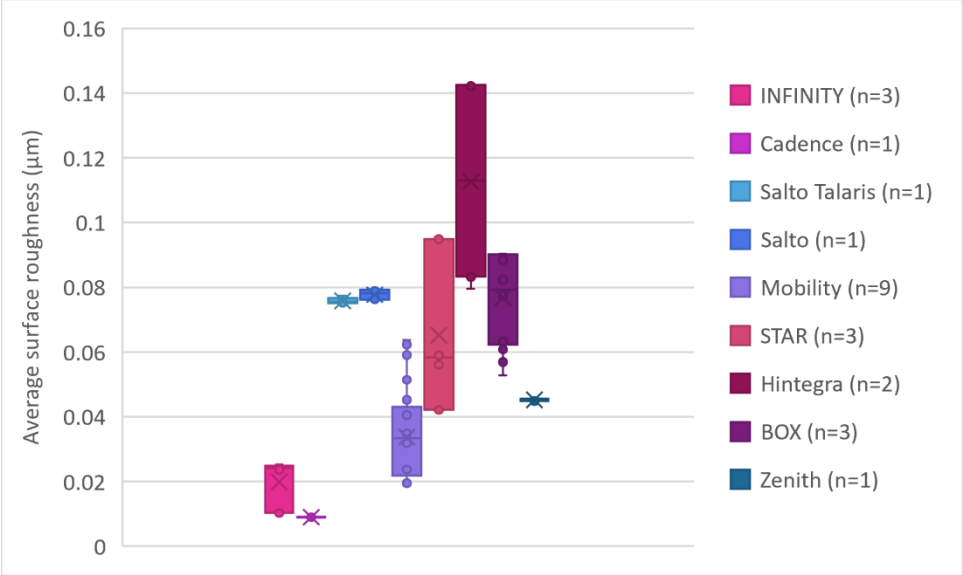

Figure 4.45. Box and whisker plot of the measured average surface roughness (S_a) values from unworn areas of the articulating surfaces of different talar components.

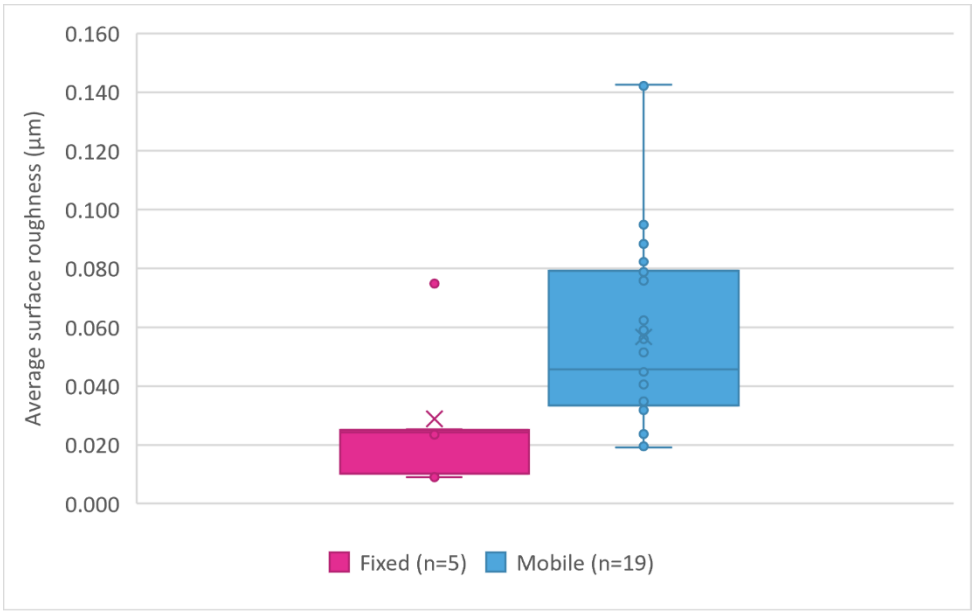

Figure 4.46. Box and whisker plot of the measured average surface roughness (S_a) values from unworn areas of the articulating surfaces of talar components from fixed and mobile TARs.

There was no significant difference between the measured S_a values from unworn areas of talar component articulating surfaces of different alloys (Figure 4.47). The average surface roughness of CoCr alloy talar components (all TAR models except Zenith) (0.051 ± 0.033 µm) was higher than that of talar components coated with TiN (Zenith) (0.045 ± 0.000 µm),

however this difference did not reach statistical significance ($p = 0.885$), and the number of components composed of CoCr alloy (n = 23) vastly exceeded those coated with TiN (n = 1).

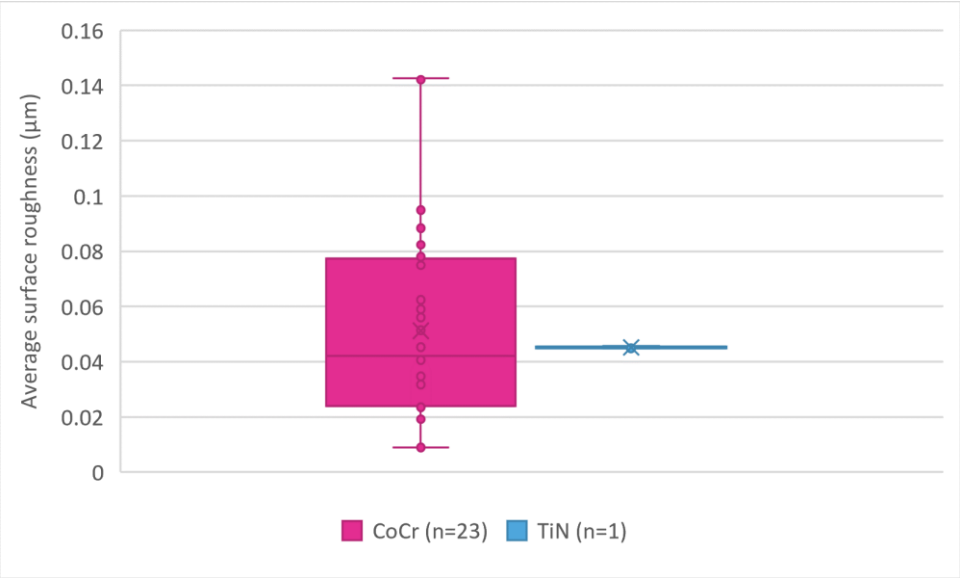

Figure 4.47. Box and whisker plot of the measured average surface roughness (S_a) values from unworn areas of the articulating surfaces of talar components, separated by alloy.

As with the tibial components, for the articulating surfaces of talar components on which pitting was identified, the measured average surface roughness (S_a) and maximum valley depth (S_v) values were significantly ($p < 0.05$) higher on pitted areas compared to unpitted areas for all designs of TAR analysed (Table 4.23).

Talar component	N with pitting	Unpitted S_a (µm)	Pitted S_a (µm)	P-value	Unpitted S_v (µm)	Pitted S_v (µm)	P-value
INFINITY	3	0.020 ± 0.007	0.106 ± 0.058	< 0.001	-0.362 ± 0.036	-2.822 ± 0.593	< 0.001
Cadence	1	0.009 ± 0.000	0.074 ± 0.008	0.012	-0.336 ± 0.011	-2.850 ± 0.040	0.012
Salto Talaris	1	0.076 ± 0.001	0.379 ± 0.006	0.012	-1.146 ± 0.024	-4.123 ± 0.382	0.012
Salto	1	0.077 ± 0002	0.167 ± 0.001	0.012	-0.683 ± 0.027	-2.509 ± 0.419	0.012
Mobility	9	0.034 ± 0.013	0.085 ± 0.023	< 0.001	-0.406 ± 0.218	-2.262 ± 0.784	< 0.001
STAR	3	0.065 ± 0.023	0.152 ± 0.015	< 0.001	-0.386 ± 0.105	-2.654 ± 0.288	< 0.001
Hintegra	2	0.113 ± 0.031	0.162 ± 0.060	0.036	-0.427 ± 0.179	-2.239 ± 0.522	< 0.001
BOX	2	0.086 ± 0.006	0.282 ± 0.026	< 0.001	-0.509 ± 0.120	-4.201 ± 0.775	< 0.001
Zenith	1	0.045 ± 0.000	0.080 ± 0.001	0.012	-1.537 ± 0.186	-2.441 ± 0.234	0.012

Table 4.23. Average surface roughness (S_a) and maximum valley depth (S_v) values from unpitted and pitted areas of different talar component articulating surfaces with pitting. Values given as mean ± SD.

The average surface roughness (S_a) values measured were higher on worn areas than unworn areas on all models of talar component articulating surfaces (Table 4.24). These differences were statistically significant ($p<0.05$) for all models except Hintegra.

Talar component	Unworn S_a (µm)	Worn S_a (µm)	P-value
INFINITY (n = 3)	0.020 ± 0.007	0.106 ± 0.058	< 0.001
Cadence (n = 1)	0.009 ± 0.000	0.074 ± 0.008	< 0.001
Salto Talaris (n = 1)	0.076 ± 0.001	0.379 ± 0.006	0.012
Salto (n = 1)	0.078 ± 0.002	0.167 ± 0.001	0.012
Mobility (n = 9)	0.034 ± 0.013	0.085 ± 0.023	<0.001
STAR (n = 3)	0.065 ± 0.023	0.152 ± 0.015	<0.001
Hintegra (n = 2)	0.113 ± 0.031	0.162 ± 0.060	0.064
BOX (n = 3)	0.077 ± 0.014	0.232 ± 0.075	<0.001
Zenith (n = 1)	0.045 ± 0.000	0.080 ± 0.001	< 0.001

Table 4.24. Average surface roughness (S_a) values for unworn and worn areas of different talar component articulating surfaces. Values given as mean ± SD.

The root mean square roughness (S_q) was also greater on worn than unworn areas for all models of talar component articulating surfaces (Table 4.25). This difference was statistically significant ($p < 0.05$) for all models except Hintegra.

Talar component	Unworn S_q (µm)	Worn S_q (µm)	P-value
INFINITY (n = 3)	0.026 ± 0.009	0.189 ± 0.051	< 0.001
Cadence (n = 1)	0.012 ± 0.000	0.119 ± 0.003	< 0.001
Salto Talaris (n = 1)	0.101 ± 0.002	0.488 ± 0.009	< 0.001
Salto (n = 1)	0.107 ± 0.002	0.239 ± 0.002	< 0.001
Mobility (n = 9)	0.047 ± 0.022	0.164 ± 0.046	< 0.001
STAR (n = 3)	0.082 ± 0.028	0.220 ± 0.035	< 0.001
Hintegra (n = 2)	0.142 ± 0.042	0.225 ± 0.057	0.064
BOX (n = 3)	0.099 ± 0.017	0.399 ± 0.151	< 0.001
Zenith (n = 1)	0.079 ± 0.000	0.114 ± 0.001	< 0.001

Table 4.25. Root mean square roughness (S_q) values for unworn and worn areas of different talar component articulating surfaces. Values given as mean ± SD.

The peak to valley height (S_z) was significantly ($p < 0.05$) higher on worn areas compared to unworn areas of all models of talar component articulating surfaces (Table 4.26).

Talar component	Unworn S_z (µm)	Worn S_z (µm)	P-value
INFINITY (n = 3)	0.581 ± 0.101	3.343 ± 0.547	< 0.001
Cadence (n = 1)	0.606 ± 0.006	3.245 ± 0.087	0.012
Salto Talaris (n = 1)	1.608 ± 0.040	5.143 ± 0.381	0.012
Salto (n = 1)	1.360 ± 0.062	3.078 ± 0.436	0.012
Mobility (n = 9)	0.690 ± 0.273	3.109 ± 0.917	< 0.001
STAR (n = 3)	0.805 ± 0.113	3.688 ± 0.759	< 0.001
Hintegra (n = 2)	0.918 ± 0.354	3.572 ± 0.071	< 0.001
BOX (n = 3)	0.866 ± 0.190	5.464 ± 2.040	< 0.001
Zenith (n = 1)	2.530 ± 0.282	3.112 ± 0.250	0.011

Table 4.26. Peak to valley height (S_z) values for unworn and worn areas of different talar component articulating surfaces. Values given as mean ± SD.

The measured maximum peak height (S_p) was greater on worn than unworn areas of the talar component articulating surfaces for all models of TAR except Salto and Zenith (Table 4.27). These differences were statistically significant ($p < 0.05$) for all models except Salto.

Talar component	Unworn S_p (µm)	Worn S_p (µm)	P-value
INFINITY (n = 3)	0.220 ± 0.082	0.521 ± 0.184	< 0.001
Cadence (n = 1)	0.270 ± 0.006	0.398 ± 0.095	0.040
Salto Talaris (n = 1)	0.461 ± 0.036	1.020 ± 0.011	< 0.001
Salto (n = 1)	0.685 ± 0.064	0.619 ± 0.049	0.109
Mobility (n = 9)	0.285 ± 0.165	0.847 ± 0.530	< 0.001
STAR (n = 3)	0.419 ± 0.051	1.034 ± 0.546	< 0.001
Hintegra (n = 2)	0.491 ± 0.175	1.334 ± 0.475	< 0.001
BOX (n = 3)	0.393 ± 0.109	2.008 ± 1.269	< 0.001
Zenith (n = 1)	0.993 ± 0.139	0.671 ± 0.032	0.012

Table 4.27. Maximum peak height (S_p) values for unworn and worn areas of different talar component articulating surfaces. Values given as mean ± SD.

The measured maximum valley depth (S_v) was significantly ($p < 0.05$) greater for worn areas compared to unworn areas of all models of talar component articulating surfaces (Table 4.28).

Talar component	**Unworn S_v (µm)**	**Worn S_v (µm)**	**P-value**
INFINITY (n = 3)	-0.362 ± 0.036	-2.822 ± 0.593	< 0.001
Cadence (n = 1)	-0.336 ± 0.011	-2.850 ± 0.040	< 0.001
Salto Talaris (n = 1)	-1.146 ± 0.024	-4.123 ± 0.382	0.012
Salto (n = 1)	-0.676 ± 0.027	-2.459 ± 0.419	0.012
Mobility (n = 9)	-0.406 ± 0.218	-2.262 ± 0.784	< 0.001
STAR (n = 3)	-0.386 ± 0.105	-2.654 ± 0.288	< 0.001
Hintegra (n = 2)	-0.427 ± 0.179	-2.239 ± 0.475	< 0.001
BOX (n = 3)	-0.474 ± 0.110	-3.456 ± 1.255	< 0.001
Zenith (n = 1)	-1.537 ± 0.186	-2.441 ± 0.234	0.012

Table 4.28. Maximum valley depth (S_v) values for unworn and worn areas of different talar component articulating surfaces. Values given as mean ± SD.

The skewness was more negative – indicating a greater number and/or severity of valleys rather than peaks – on worn areas than unworn areas for all models of talar component articulating surfaces (Table 4.29). These differences were statistically significant ($p < 0.05$) for all TAR models except Hintegra.

Talar component	Unworn S_{sk}	Worn S_{sk}	P-value
INFINITY (n = 3)	-0.431 ± 0.921	-6.047 ± 3.412	< 0.001
Cadence (n = 1)	-2.570 ± 0.395	-6.391 ± 0.758	< 0.001
Salto Talaris (n = 1)	-0.366 ± 0.051	-1.190 ± 0.020	0.012
Salto (n = 1)	-0.492 ± 0.120	-2.561 ± 0.543	0.012
Mobility (n = 9)	-0.088 ± 1.032	-5.007 ± 2.560	< 0.001
STAR (n = 3)	-0.074 ± 0.383	-2.183 ± 0.741	< 0.001
Hintegra (n = 2)	-0.004 ± 0.358	-1.337 ± 1.937	1.000
BOX (n = 3)	0.016 ± 0.381	-2.771 ± 0.848	< 0.001
Zenith (n = 1)	0.302 ± 0.491	-0.913 ± 0.425	0.012

Table 4.29. Skewness (S_{sk}) values for unworn and worn areas of different tibial component articulating surfaces. Values given as mean ± SD.

The measured kurtosis (S_{ku}) of the talar component articulating surfaces was higher on worn areas than unworn areas for all TAR models except Salto Talaris (Table 4.30). The differences were statistically significant ($p < 0.05$) for all models except Salto Talaris and Zenith.

Talar component	Unworn S_{ku}	Worn S_{ku}	P-value
INFINITY (n = 3)	20.173 ± 22.964	71.158 ± 43.453	< 0.001
Cadence (n = 1)	67.999 ± 5.024	111.996 ± 16.646	0.005
Salto Talaris (n = 1)	5.892 ± 0.561	5.811 ± 0.224	0.676
Salto (n = 1)	5.804 ± 0.248	15.540 ± 7.650	0.012
Mobility (n = 9)	11.746 ± 13.069	55.892 ± 45.394	< 0.001
STAR (n = 3)	3.328 ± 0.524	16.160 ± 7.021	< 0.001
Hintegra (n = 2)	3.203 ± 0.449	21.090 ± 15.289	< 0.001
BOX (n = 3)	3.525 ± 0.968	19.215 ± 9.233	< 0.001
Zenith (n = 1)	24.269 ± 2.460	25.618 ± 7.337	0.403

Table 4.30. Kurtosis (S_{ku}) values for unworn and worn areas of different tibial component articulating surfaces. Values given as mean ± SD.

Table 4.31 gives a comparison of the measured surface roughness parameters of both unworn and worn areas for talar component articulating surfaces corresponding to fixed and mobile bearing TARs.

For unworn areas, talar components from mobile bearing prostheses had a higher S_a, S_q, S_z, and S_p compared to those from fixed bearing prostheses, with all of these differences except for S_z reaching statistical significance ($p < 0.05$). On the other hand, components corresponding to fixed bearing prostheses had a higher S_v and S_{ku}, as well as a more negative S_{sk}, compared to those from mobile bearing prostheses, with these differences being statistically significant ($p < 0.05$) in the cases of S_{ku} and S_{sk}, but not for S_v.

For worn areas, talar components from fixed bearing prostheses had a higher S_a, S_q, S_z, S_v, and S_{ku}, as well as a more negative S_{sk}, compared to those from mobile bearing prostheses. These differences were statistically significant ($p < 0.05$) in the cases of S_v, S_{ku}, and S_{sk}. Components corresponding to mobile bearing prostheses had a significantly ($p < 0.05$) higher S_p compared to those from fixed bearing prostheses.

	Unworn fixed (n = 5)	Unworn mobile (n = 19)	P-value	Worn fixed (n = 5)	Worn mobile (n = 19)	P-value
S_a (µm)	0.029 ± 0.025	0.057 ± 0.031	< 0.001	0.154 ± 0.124	0.131 ± 0.067	0.434
S_q (µm)	0.038 ± 0.033	0.075 ± 0.039	< 0.001	0.235 ± 0.138	0.218 ± 0.110	0.719
S_z (µm)	0.791 ± 0.424	0.892 ± 0.483	0.116	3.684 ± 0.870	3.620 ± 1.345	0.647
S_p (µm)	0.278 ± 0.115	0.403 ± 0.222	0.013	0.596 ± 0.265	1.090 ± 0.792	< 0.001
S_v (µm)	-0.513 ± 0.324	-0.489 ± 0.310	0.235	-3.088 ± 0.714	-2.530 ± 0.868	0.001
S_{sk}	-0.846 ± 1.138	-0.061 ± 0.764	0.004	-5.144 ± 3.313	-3.478 ± 2.446	0.040
S_{ku}	26.882 ± 28.000	8.566 ± 10.501	0.004	66.256 ± 48.576	36.447 ± 36.883	< 0.001

Table 4.31. Comparison of the measured surface roughness parameters for unworn and worn areas of talar component articulating surfaces corresponding to fixed and mobile bearing TARs.

Table 4.32 shows the differences between talar component articulating surfaces corresponding to fixed and mobile bearing TARs in terms of the measured S_a and S_v values for both unpitted and pitted areas. Talar components corresponding to fixed bearing prostheses had higher pitted S_a values as well as both unpitted and pitted S_v values compared to those from mobile bearing prostheses. However, only the difference between the pitted S_v values reached statistical significance ($p < 0.05$). The unpitted S_a values, on the other hand, were significantly ($p < 0.05$) higher on talar components corresponding to mobile bearing TARs compared to those from fixed bearing prostheses.

Talar component	Fixed (n = 5)	Mobile (n = 19)	P-value
N with pitting	5	18	-
Unpitted S_a (µm)	0.029 ± 0.025	0.057 ± 0.032	< 0.001
Pitted S_a (µm)	0.154 ± 0.124	0.131 ± 0.069	0.436
Unpitted S_v (µm)	-0.513 ± 0.324	-0.494 ± 0.318	0.246
Pitted S_v (µm)	-3.088 ± 0.714	-2.561 ± 0.882	0.001

Table 4.32. Average surface roughness (S_a) and maximum valley depth (S_v) values for talar component articulating surfaces with pitting corresponding to fixed and mobile bearing TARs. Values given as mean ± SD.

The variation in measured S_a and S_v values on both unworn and worn areas of talar component articulating surfaces for the different component alloys are given in Figure 4.48 and Figure 4.49, respectively.

For both unworn and worn areas, CoCr alloy components had the higher S_a (0.051 ± 0.033 µm and 0.138 ± 0.083 µm, respectively) compared to TiN coated components (0.045 ± 0.000 µm and 0.080 ± 0.001 µm, respectively) (mean ± SD).

The CoCr alloy components also had the higher S_v for worn areas (-2.655 ± 0.883 µm) compared to the TiN coated components (-2.441 ± 0.234 µm) (mean ± SD). However, for unworn areas, CoCr components had a lower S_v (CoCr -0.449 ± 0.225 µm) compared to TiN coated components (-1.537 ± 0.186 µm) (mean ± SD).

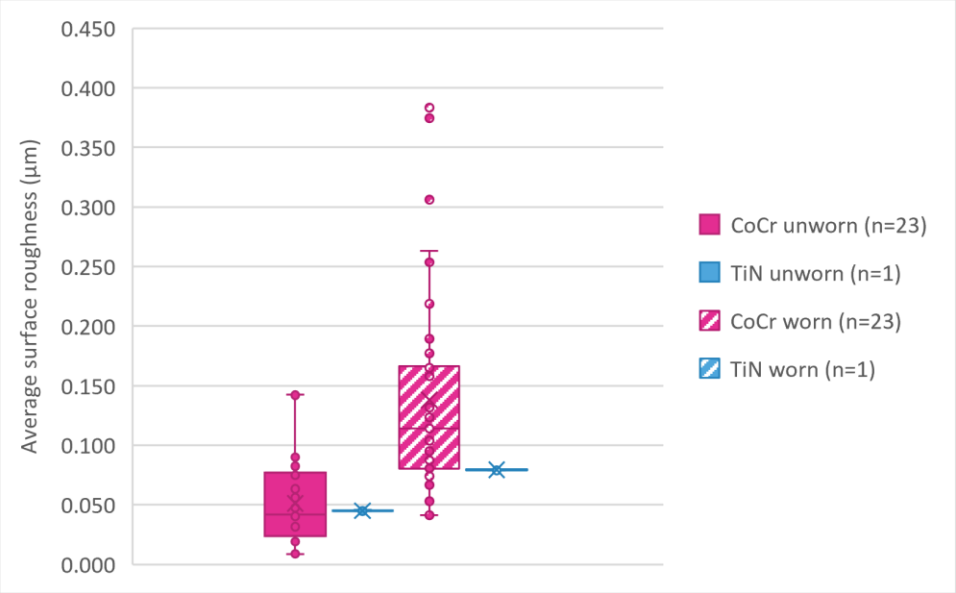

Figure 4.48. Box and whisker plot of unworn and worn average surface roughness (S_a) values of the articulating surfaces of different alloy talar components.

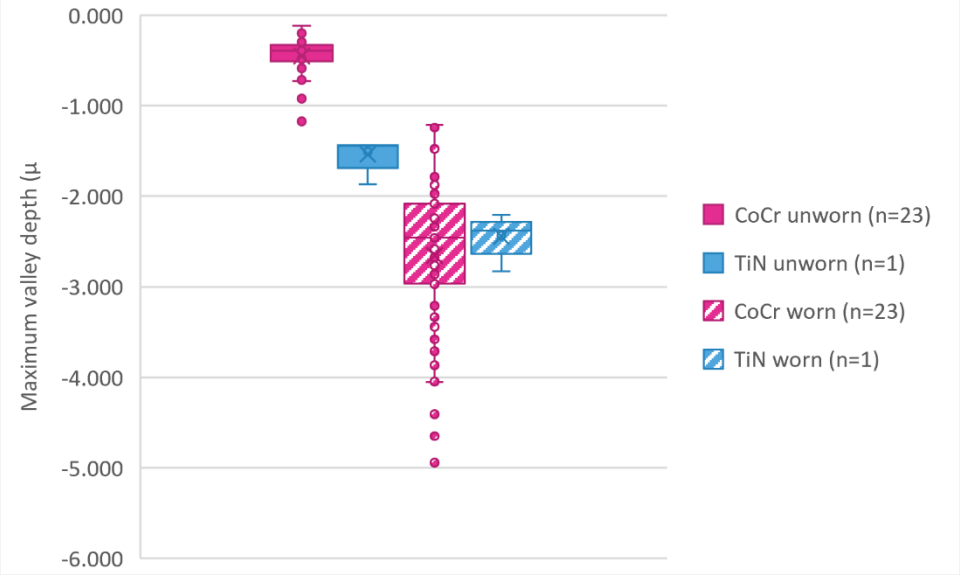

Figure 4.49. Box and whisker plot of unworn and worn maximum valley depth (S_v) values of the articulating surfaces of different alloy talar components.

4.4. Material Characterisation

Elemental composition analysis was performed to characterise the alloys used for the metal components as well as to determine the materials comprising the embedded debris identified.

4.4.1. Elemental composition of metal components

The results of the XRF elemental composition analysis for the metal tibial and talar components are given in Table 4.33 and Table 4.34, respectively. The results are given in terms of mean percentage compositions for the main elements present (i.e., excluding trace elements). The component alloys (i.e., CoCr or Ti) identified by the XRF elemental composition analysis match those stated by the manufacturer, as provided in the previous Chapter (Section 3.1.3).

A small amount of Ti was unexpectedly identified in the CoCr alloy tibial and talar components of the BOX prosthesis as well as the CoCr alloy talar component of the Mobility prosthesis. The Ti was identified in all of the BOX tibial and talar components analysed. Since BOX is the only prosthesis included to not have a coating on the non-articulating surfaces containing Ti, it was presumed to be part of the component composition. Ti was identified in 1 of the Mobility talar components analysed, suggesting that metal debris may have been released from the Ti coating and embedded into the talar component in this case.

	% elemental composition (mean ± SD)							
Tibial component	**Co**	**Cr**	**Mo**	**Mn**	**Fe**	**Ti**	**Al**	**V**
INFINITY (n = 3)			0.01 ± 0.00		0.21 ± 0.01	89.91 ± 0.08	5.69 ± 0.02	4.18 ± 0.06
Cadence (n = 1)					0.19	89.95		4.19
Salto Talaris (n = 2)	63.00 ± 0.45	29.89 ± 0.13	6.19 ± 0.06	0.48 ± 0.03	0.39 ± 0.19			
Salto (n = 1)	63.35	29.67	6.11	0.47	0.31			
Mobility (n = 7)	63.99 ± 0.10	29.02 ± 0.03	6.02 ± 0.02	0.34 ± 0.01	0.50 ± 0.06			
STAR (n = 3)	61.79 ± 0.04	31.05 ± 0.06	6.08 ± 0.03	0.62 ± 0.06	0.39 ± 0.05			
Hintegra (n = 1)	63.16	29.96	6.01	0.43	0.39			
BOX (n = 3)	64.79 ± 0.10	29.06 ± 0.06	5.19 ± 0.05	0.61 ± 0.01	0.16 ± 0.01	0.10 ± 0.04		
Zenith (n = 1)			0.01		0.09	90.69	5.74	3.46

Table 4.33. Tibial component XRF elemental composition showing the main elements present : cobalt (Co), chromium (Cr), molybdenum (Mo), manganese (Mn), iron (Fe), titanium (Ti), aluminium (Al), vanadium (V). Blank cells indicate that the element was not present.

	% elemental composition (mean ± SD)							
Talar component	**Co**	**Cr**	**Mo**	**Mn**	**Fe**	**Ti**	**Al**	**V**
INFINITY (n = 3)	64.80 ± 0.21	28.47 ± 0.05	5.47 ± 0.08	0.84 ± 0.03	0.29 ± 0.23			
Cadence (n = 1)	64.84	28.60	5.40	0.85	0.25			
Salto Talaris (n = 1)	62.23	29.70	6.18	0.46	0.34			
Salto (n = 1)	63.22	29.73	6.22	0.42	0.34			
Mobility (n = 8)	63.93 ± 0.15	29.05 ± 0.07	6.04 ± 0.05	0.36 ± 0.04	0.47 ± 0.11	0.02 ± 0.04		
STAR (n = 3)	61.74 ± 0.19	30.78 ± 0.32	6.33 ± 0.11	0.63 ± 0.04	0.41 ± 0.10			
Hintegra (n = 2)	63.54 ± 0.16	29.57 ± 0.02	6.02 ± 0.11	0.39 ± 0.01	0.42 ± 0.06			
BOX (n = 3)	64.54 ± 0.18	28.96 ± 0.07	5.33 ± 0.10	0.70 ± 0.07	0.19 ± 0.03	0.14 ± 0.03		
Zenith (n = 1)					0.08	90.67	5.72	3.52

Table 4.34. Talar component XRF elemental composition showing the main elements present : cobalt (Co), chromium (Cr), molybdenum (Mo), manganese (Mn), iron (Fe), titanium (Ti), aluminium (Al), vanadium (V). Blank cells indicate that the element was not present.

4.4.2. Elemental composition of embedded debris

SEM-EDX analysis confirmed that the embedded debris identified on the 5 PE inserts (4 backside surfaces and 5 bearing surfaces) was metallic (Table 4.35). Specifically, the presence of Ti (Figure 4.50) or Co and Cr (Figure 4.51) was confirmed for the embedded debris of each surface.

All of the elements identified within the PE insert embedded debris (Ti, Co, Cr, Mo) are likely to have originated from the implant. The coatings of non-articulating surfaces for all of the devices which had embedded debris identified in the PE inserts contained Ti, and all the corresponding tibial and talar components were manufactured from CoCr(Mo) alloy, with the exception of the Ti alloy INFINITY tibial component (which was not in contact with the PE insert bearing surface on which Ti debris was identified in this case). It is therefore likely that the Ti embedded debris identified in these PE inserts originated from the porous coatings of these prostheses.

PE insert	**Bearing surface embedded debris**	**Backside surface embedded debris**
Salto Talaris (ANK2)	Ti, Co, Cr	Ti
Mobility (ANK3)	Co, Cr	Co, Cr, Mo
Hintegra – in pieces (ANK6)	Co, Cr, Mo	Co, Cr
Hintegra (ANK27)	Ti	Ti
INFINITY (ANK10)	Ti	-

Table 4.35. The elements identified in the embedded debris of the PE inserts.

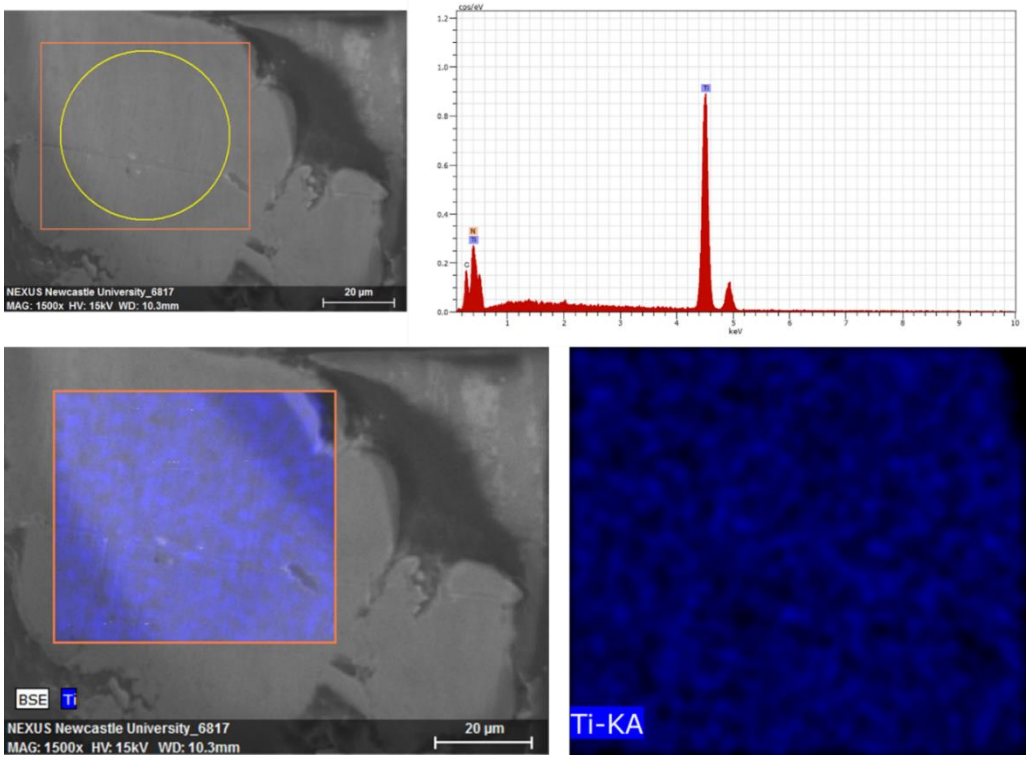

Figure 4.50. SEM-EDX analysis of INFINITY (ANK10) TAR PE insert backside surface embedded debris.

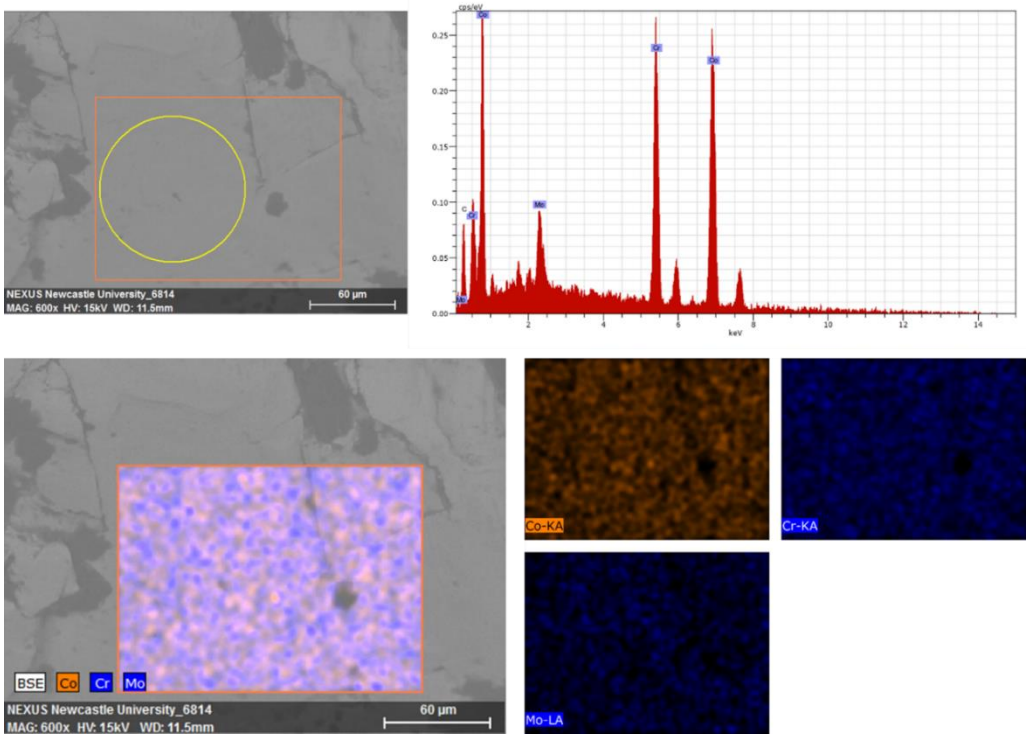

Figure 4.51. SEM-EDX analysis of Hintegra (ANK6) TAR PE insert bearing surface embedded debris.

4.5. PE Insert Form Analysis

The quantification of volumetric wear from the PE insert bearing surfaces of the explanted TARs was performed using a CMM. In order to validate this method, the calculated wear volumes were compared to those obtained via gravimetric measurement. Additionally, the geometries of the PE insert backside surfaces were analysed in terms of planicity, also using a CMM.

4.5.1. Validation of PE insert bearing wear measurement

The validation process for the CMM wear volume measurement technique involved manual removal of material from the two previously unused PE insert bearing surfaces (one INFINITY size 5 and one INFINITY size 3). The stages of simulated wear as a result of incremental removal of material from the bearing surfaces of the two pristine PE inserts, along with wear maps produced by CMM analysis, are shown by Figure 4.52 and Figure 4.53 (validation round 1) and Figure 4.55 and Figure 4.54 (validation round 2), respectively.

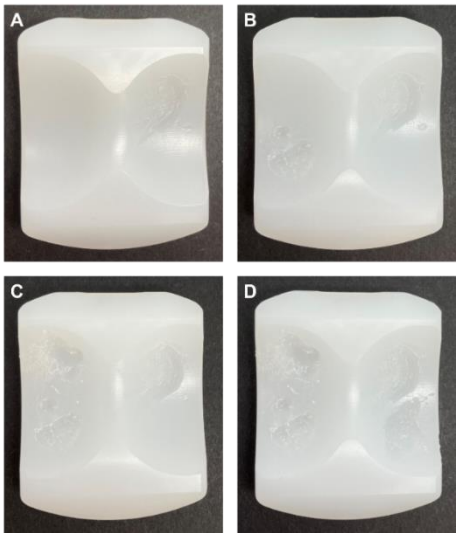

Figure 4.52. Stages of increasing wear of the size 5 PE insert bearing surface. Material was manually removed from a new quadrant at each wear stage (A-D).

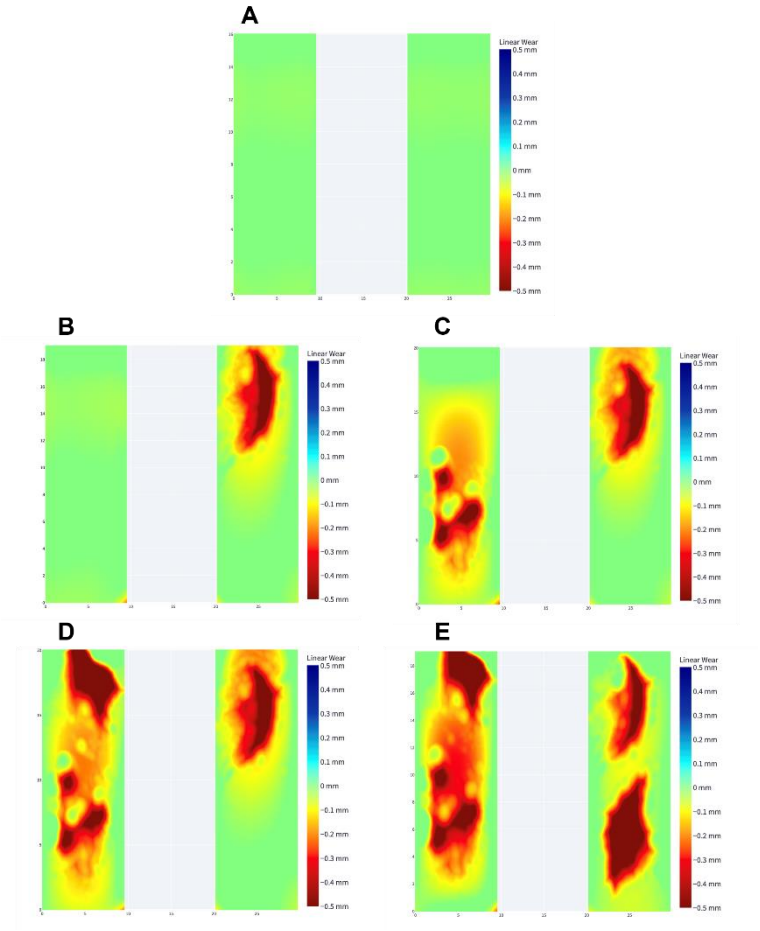

Figure 4.53. Linear wear maps (scale -0.5 mm to 0.5 mm) from CMM analysis of the size 5 PE insert bearing surface. (A) unworn. (B-D) wear stages 1-4.

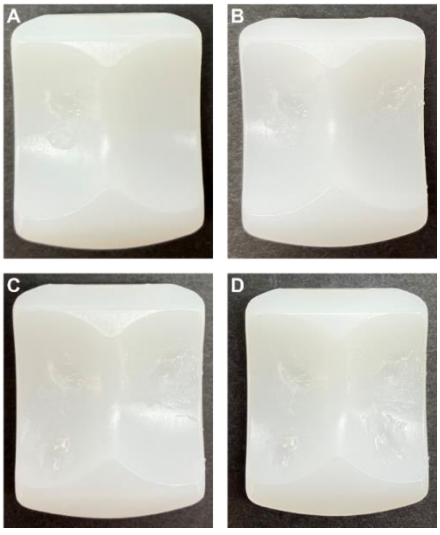

Figure 4.54. Stages of increasing wear of the size 3 PE insert bearing surface. Material was manually removed from a new quadrant at each wear stage (A-D).

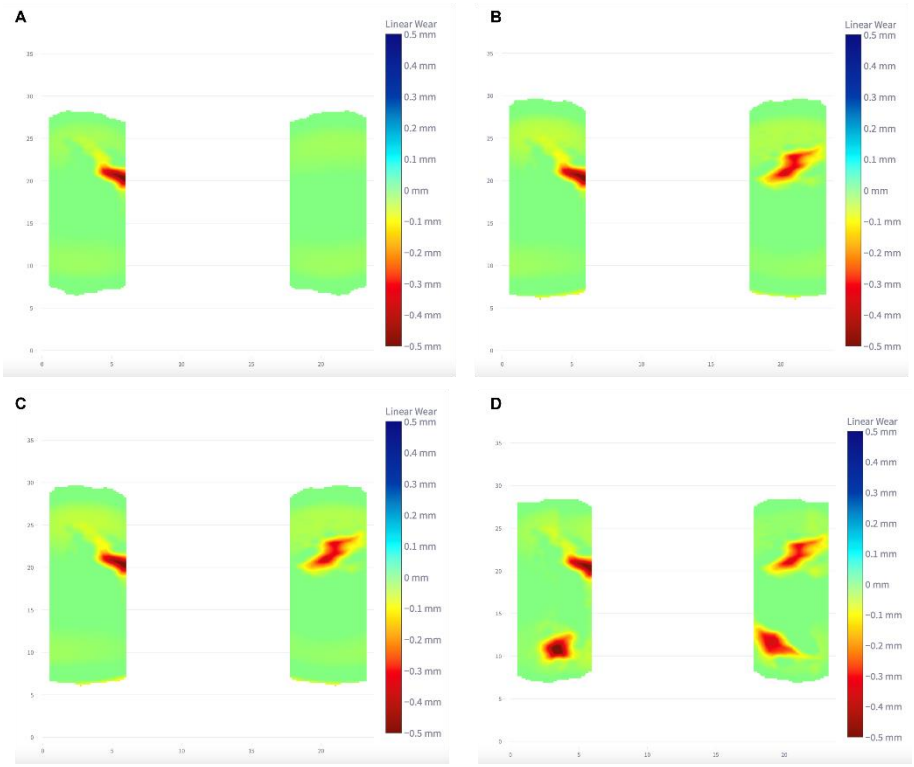

Figure 4.55. Linear wear maps (scale -0.5 mm to 0.5 mm) from CMM analysis of the size 3 PE insert bearing surface. (A-D) wear stages 1-4.

The CMM and gravimetrically calculated wear volumes for each stage of wear with the first of the PE inserts (size 5) are given in Table 4.36, along with the absolute errors (i.e., the difference between the value obtained from the CMM analysis and that obtained from gravimetric measurement). The corresponding percentage errors (calculated by dividing the absolute error by the gravimetrically calculated wear volume (i.e., the 'true' value)) increased with each wear stage: 7.33% for wear stage 1, 9.82% for wear stage 2, 40.49% for wear stage 3, and 49.09% for wear stage 4. A steep increase in the absolute errors was seen after the second wear stage, which could be due to the way the material was removed meaning the CMM probe could not properly trace these worn areas. A plot illustrating the differences between the wear volumes given by gravimetric analysis and CMM analysis for this PE insert bearing surface is given by Figure 4.56.

Wear stage	Gravimetric wear volume (mm^3)	CMM wear volume (mm^3)	Absolute error (mm^3)
Unworn	-	1.33	1.33
Worn 1	17.60	16.31	1.29
Worn 2	32.06	35.20	3.15
Worn 3	86.96	51.75	35.21
Worn 4	120.73	61.47	59.26

Table 4.36. Results from validation of CMM PE insert bearing surface wear volume quantification compared against gravimetric testing, using an INFINITY size 5 PE insert.

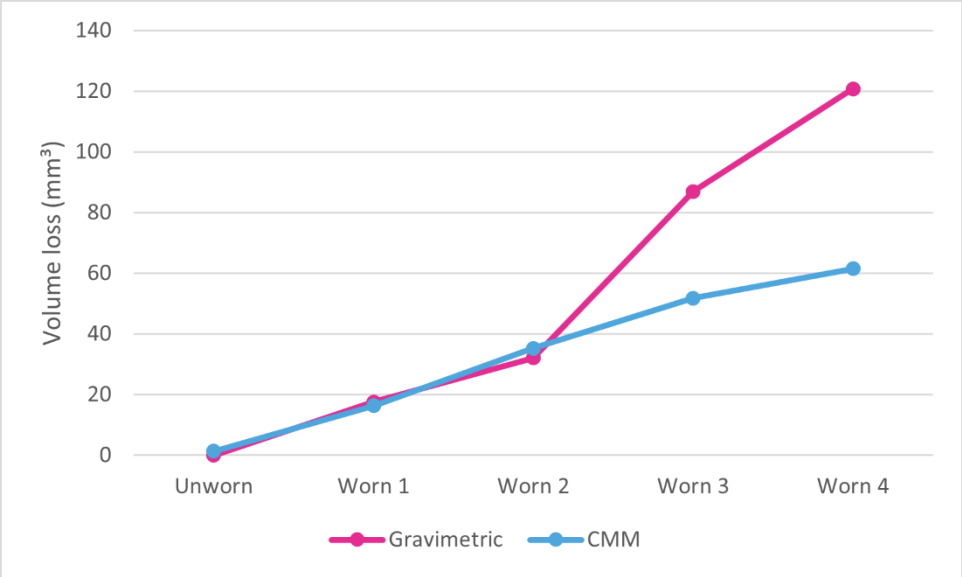

Figure 4.56. Plot of the volumetric wear loss calculated by gravimetric measurement and CMM analysis for the size 5 PE insert bearing surface.

The wear volumes calculated from CMM analysis and gravimetric measurement, along with the absolute error, for the second of the PE inserts (size 3) is given in Table 4.37.

The difference in the wear volumes given by gravimetric analysis and CMM analysis for this second PE insert bearing surface is shown by Figure 4.57. As with the first round of validation, the corresponding percentage errors again increased with the wear stages: 35.57%, 43.10%, 55.35%, and 56.14%. These larger percentage errors however reflect the smaller amount of volumetric wear being measured in this second validation round. Although the difference was

not as extreme as that seen in the previous round of validation, the gravimetrically and CMM measured wear volumes did diverge as the wear stages increased again.

Wear stage	Gravimetric wear volume (mm^3)	CMM wear volume (mm^3)	Absolute error (mm^3)
Worn 1	4.62	2.98	1.65
Worn 2	10.19	5.80	4.39
Worn 3	16.21	7.24	8.97
Worn 4	19.63	8.56	11.08

Table 4.37. Results from validation of CMM PE insert bearing surface wear volume quantification compared against gravimetric testing, using an INFINITY size 3 PE insert.

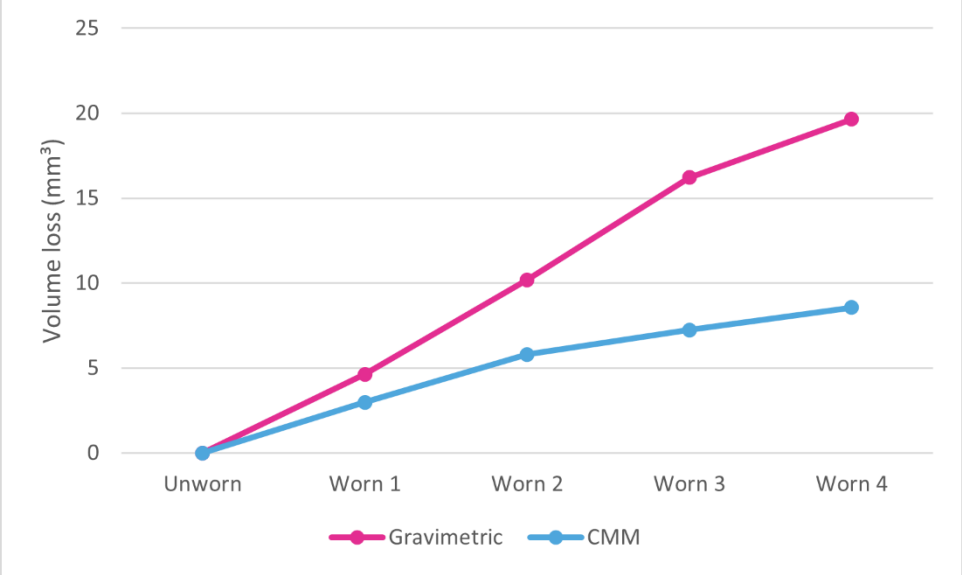

Figure 4.57. Plot of the volumetric wear loss calculated by gravimetric measurement and CMM analysis for the size 3 PE insert bearing surface.

4.5.2. PE insert bearing surface volumetric wear measurement

Of the 27 explanted PE inserts that were available for analysis, CMM analysis of the bearing surfaces was achievable for 18. Table 4.38 gives the measured wear volumes for these PE insert bearing surfaces in terms of volumetric material loss from the left and right condyles and the total, along with details of the implants.

The implantation duration was only known for 1 TAR (ANK2); a fixed bearing Salto Talaris device. The total wear volume for the PE insert bearing surface of this prosthesis was measured as 4.29 mm^3 (1.65 mm^3 from the left condyle and 2.64 mm^3 from the right condyle, with implantation side unknown). Based on a known implantation duration of 48 months (i.e., 4 years), the total volumetric wear rate for this PE insert bearing surface was calculated as 1.07 mm^3/year (0.41 mm^3/year from one condyle and 0.66 mm^3/year from the other).

As well as determining the volumetric wear loss from the component surfaces, the CMM analysis also produced a visual representation of the wear in the form of geometrical wear maps. These wear maps show the linear wear across the analysed surface, from which the severity of the wear at different areas can be identified. The PE insert bearing surfaces on which CMM analysis was performed included 7 different designs of TARs, 2 of which were fixed bearing and 5 of which were mobile bearing. The wear maps for each of the designs are given in the following figures: INFINITY (Figure 4.58), Salto Talaris/Salto (Figure 4.59), Mobility (Figure 4.60), STAR (Figure 4.61), Hintegra (Figure 4.62), and Zenith (Figure 4.63).

Code	Prosthesis	Bearing	Side	Time *in vivo*	Left volume (mm^3)	Right volume (mm^3)	Total volume (mm^3)
ANK1	Hintegra	Mobile			1.22	1.08	2.30
ANK2	Salto Talaris	Fixed		4 years	1.65	2.64	4.29
ANK3	Mobility	Mobile	Right		0.93	0.09	1.02
ANK4	Mobility	Mobile	Left		0.14	0.39	0.53
ANK9	INFINITY	Fixed			0.74	3.59	4.33
ANK10	INFINITY	Fixed	Left		1.52	1.69	3.21
ANK11	Salto	Mobile	Right		2.76	4.22	6.98
ANK12	Mobility	Mobile	Right		0.65	0.21	0.86
ANK13	STAR	Mobile			0.29	0.32	0.61
ANK14	Mobility	Mobile			0.91	0.26	1.17
ANK15	Mobility	Mobile			0.16	0.24	0.40
ANK18	Mobility	Mobile			0.27	0.52	0.79
ANK19	Mobility	Mobile			0.03	0.05	0.08
ANK20	INFINITY	Fixed			0.16	0.40	0.56
ANK24	STAR	Mobile	Right		0.23	0.11	0.34
ANK26	Zenith	Mobile			0.49	0.33	0.82
ANK27	Hintegra	Mobile	Left		0.25	1.29	1.54
ANK28	INFINITY	Fixed			0.26	0.29	0.55

Table 4.38. Measured PE insert bearing surface obtained via CMM analysis. A blank cell in the 'side' or 'time in vivo' column indicates that the implantation side or implantation duration was unknown, respectively.

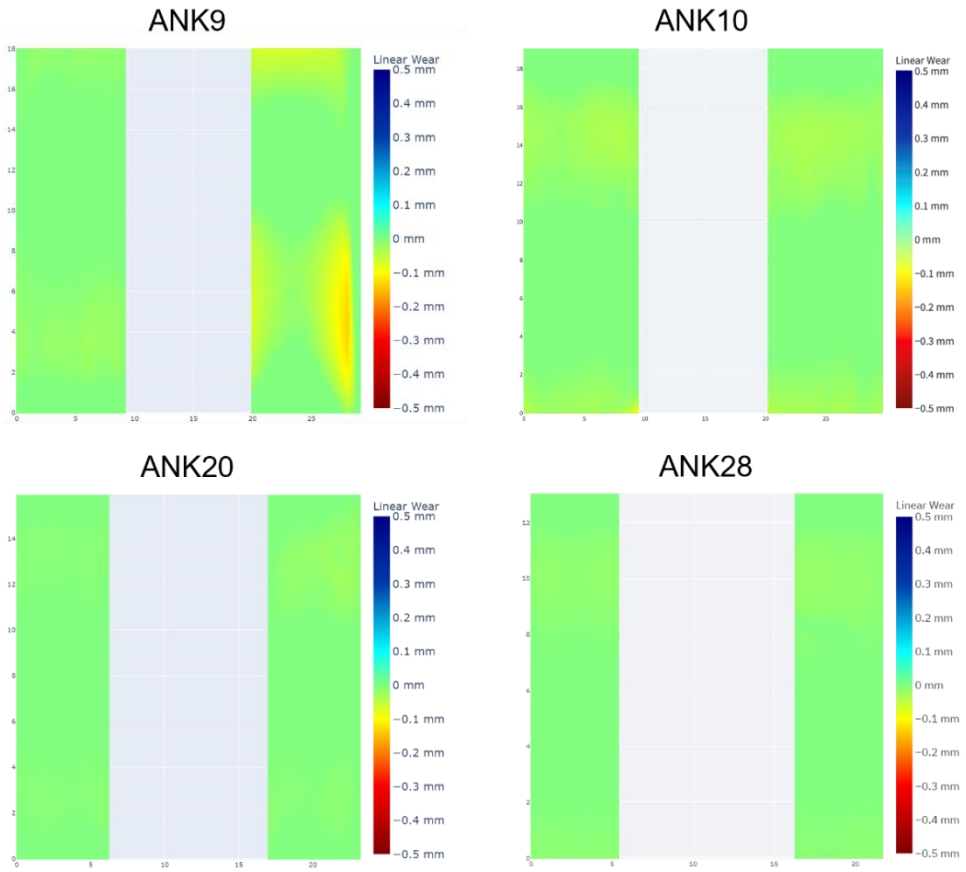

Figure 4.58. Linear wear maps (scale -0.5 mm to 0.5 mm) from CMM analysis of the fixed bearing INFINITY TAR PE insert bearing surfaces. Red indicates material removed and blue indicates material added.

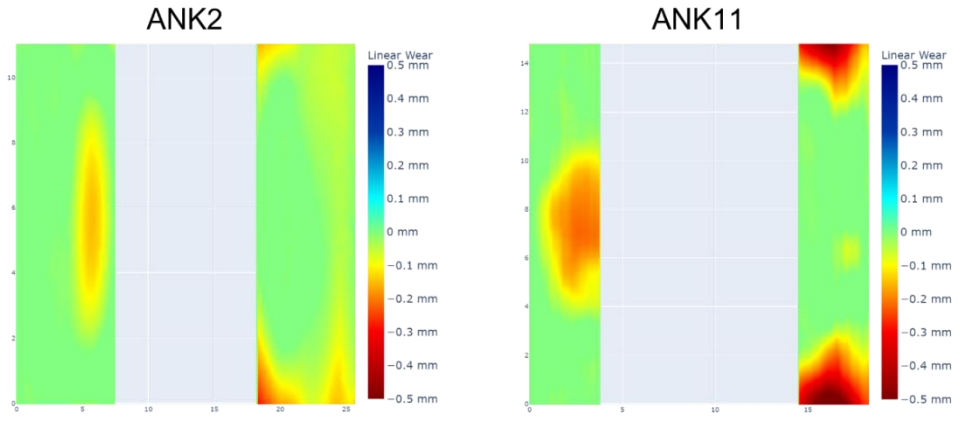

Figure 4.59. Linear wear maps (scale -0.5 mm to 0.5 mm) from CMM analysis of the fixed bearing Salto Talaris (ANK2) and mobile bearing Salto (ANK11) TAR PE insert bearing surfaces. Red indicates material removed and blue indicates material added.

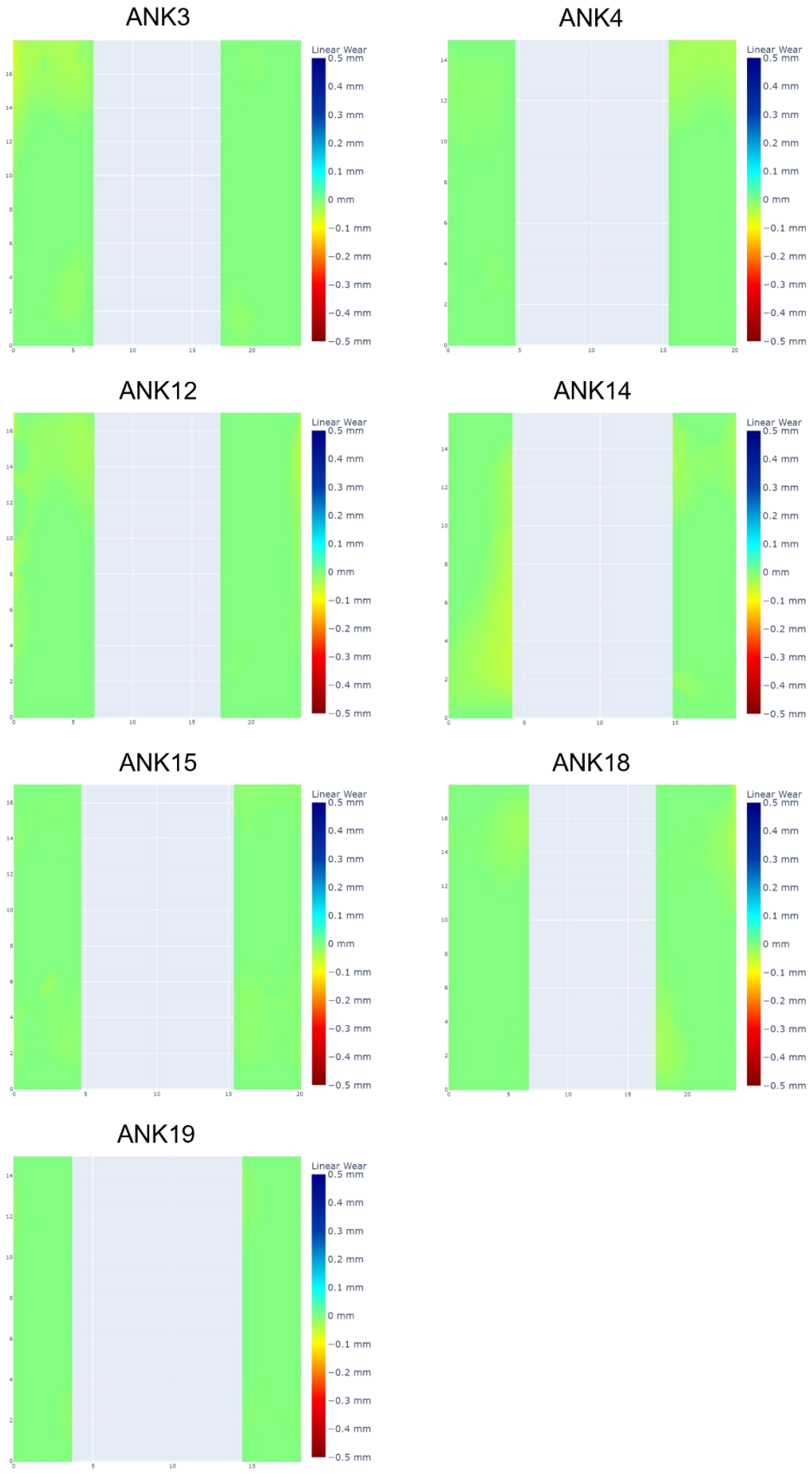

Figure 4.60. Linear wear maps (scale -0.5 mm to 0.5 mm) from CMM analysis of the mobile bearing Mobility TAR PE insert bearing surfaces. Red indicates material removed and blue indicates material added.

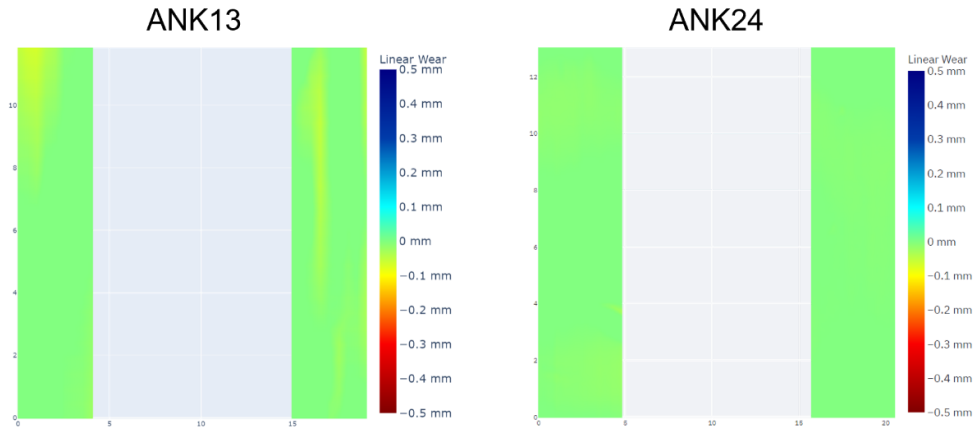

Figure 4.61. Linear wear maps (scale -0.5 mm to 0.5 mm) from CMM analysis of the mobile bearing STAR TAR PE insert bearing surfaces. Red indicates material removed and blue indicates material added.

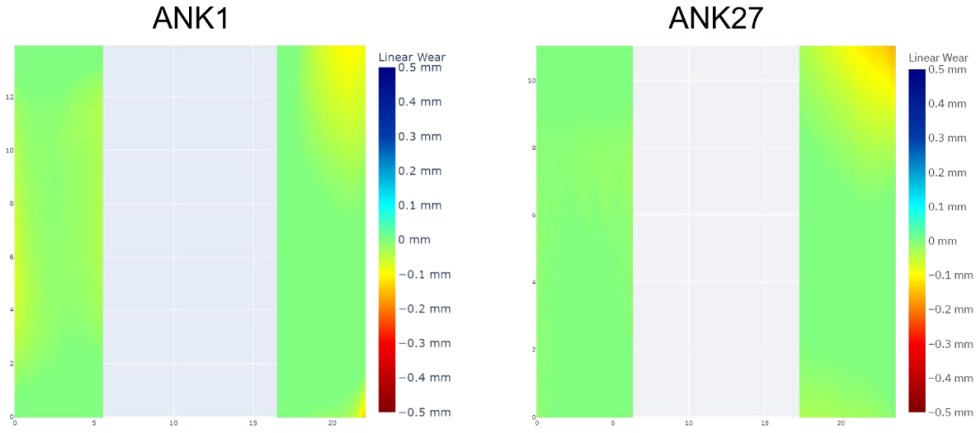

Figure 4.62. Linear wear maps (scale -0.5 mm to 0.5 mm) from CMM analysis of the mobile bearing Hintegra TAR PE insert bearing surfaces. Red indicates material removed and blue indicates material added.

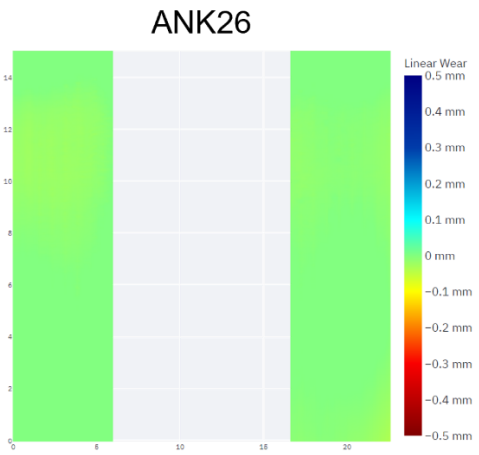

Figure 4.63. Linear wear map (scale -0.5 mm to 0.5 mm) from CMM analysis of the mobile bearing Zenith TAR PE insert bearing surface. Red indicates material removed and blue indicates material added.

For the 18 PE insert bearing surfaces for which CMM analysis was achievable, the total volume of material loss (i.e., the sum of the wear volumes from the medial and lateral condyles) ranged from 0.08 mm^3 to 6.98 mm^3. The average total wear across all the component bearing surfaces analysed was 1.69 mm^3 ± 1.86 mm^3 (mean ± SD).

Figure 4.64 shows the variation in measured total wear volumes from the PE insert bearing surfaces of different TARs designs. The highest wear volumes were recorded by the Salto and Salto Talaris prostheses; however, it should be noted that wear rates (i.e., the average volume of wear loss per year) could not be calculated due to implantation durations being unknown.

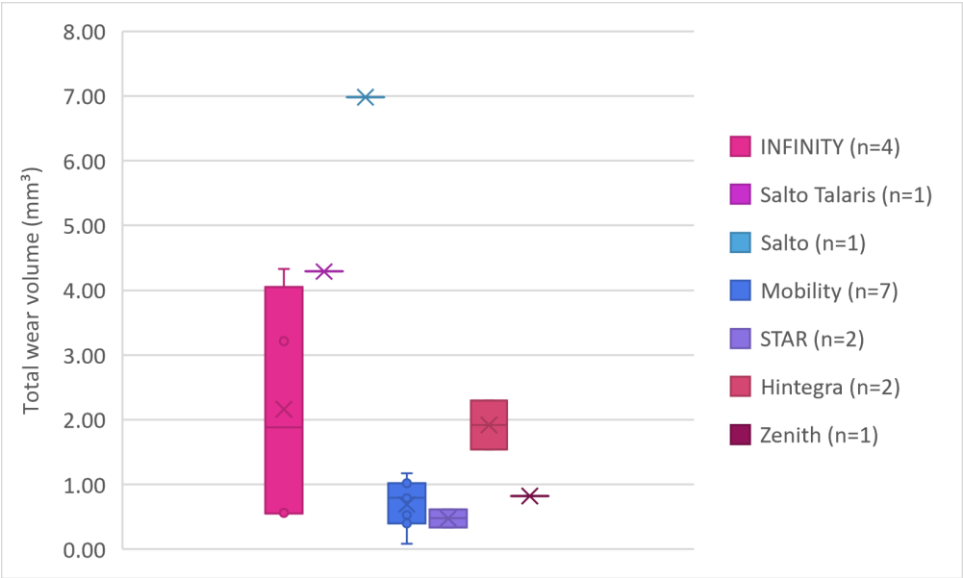

Figure 4.64. Box and whisker plot of the PE insert bearing surface total wear volumes measured from each of the TAR designs.

The variation in the measured wear volumes from the fixed and mobile bearing PE insert bearing surfaces is shown in Figure 4.65. The average total wear volume from the fixed bearing prostheses was higher than that for the mobile bearing prosthesis (2.59 mm^3 ± 1.91 mm^3 versus 1.34 mm^3 ± 1.79 mm^3 (mean ± SD)), though this difference was not statistically significant ($p = 0.533$). Again, it is also important to note that these values are reported in terms of wear volumes rather than wear rates due to implantation durations being unknown.

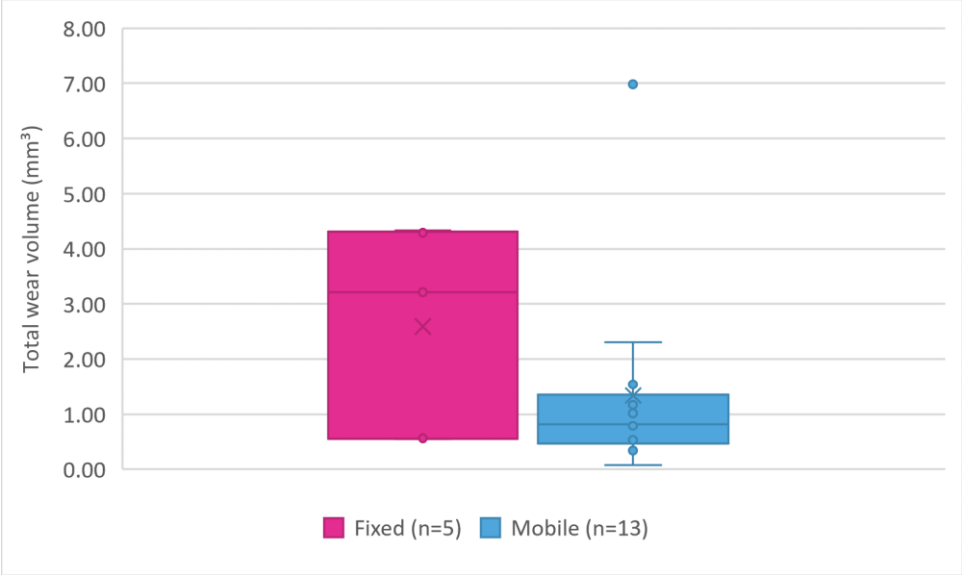

Figure 4.65. Box and whisker plot of the PE insert bearing surface total wear volumes measured from fixed and mobile bearing TARs.

The implantation side was known for 7 of the prostheses on which CMM analysis was performed, 1 of which was a fixed bearing design and 6 of which were mobile bearing designs. The measured wear volumes for the lateral and medial aspects of these PE insert bearing surfaces are given in Table 4.39. Also given is the asymmetry ratio, which represents the ratio between the higher and lower of the wear volumes of the two aspects. The lateral aspect had greater wear than the medial aspect for all except one of the PE insert bearing surfaces for which implantation side was known, and the average wear volume for the lateral aspects was higher than for the medial aspects (1.13 mm^3 ± 0.88 mm^3 versus 0.93 mm^3 ± 1.54 mm^3 (mean ± SD)), however this difference did not reach statistical significance ($p = 0.160$). The calculated asymmetry ratios ranged from 1.11 to 10.33, with an average of 3.73 ± 3.20 (mean ± SD), meaning that on average, across these 7 components, one side of the bearing surface generated over 3 times more volumetric wear than the other side.

Prosthesis	Implantation side	Lateral volume (mm^3)	Medial volume (mm^3)	Asymmetry ratio*
ANK10 (INFINITY)	Left	1.69	1.52	1.11 (lat > med)
ANK11 (Salto)	Right	2.76	4.22	1.53 (med > lat)
ANK3 (Mobility)	Right	0.93	0.09	10.33 (lat > med)
ANK4 (Mobility)	Left	0.39	0.14	2.79 (lat > med)
ANK12 (Mobility)	Right	0.65	0.21	3.10 (lat > med)
ANK24 (STAR)	Right	0.23	0.11	2.09 (lat > med)
ANK27 (Hintegra)	Left	1.29	0.25	5.16 (lat > med)

*Table 4.39. Lateral and medial aspect TAR wear volume results from CMM scanning of the PE insert bearing surfaces for those which implantation side was known. Notes: *, asymmetry ratio calculated as higher/lower.*

4.5.3. PE insert backside surface planicity measurement

CMM analysis of the backside surfaces was achievable for 13 of the explanted PE inserts. The measured planicities for the backside surfaces of these PE inserts are given in Table 4.40. The implantation duration was not known for any of the PE inserts for which CMM analysis of the backside surfaces was achievable.

Geometrical surface maps providing a visual representation of the deformation were also produced along with calculated planicity values. The linear deformation across the analysed surface is shown by these wear maps. The PE inserts on which CMM analysis was performed on the backside surfaces included 5 mobile bearing designs of TAR, the mapped geometries of which are given in the following figures: Salto (Figure 4.66), Mobility (Figure 4.67), STAR (Figure 4.68), Hintegra (Figure 4.69), and Zenith (Figure 4.70).

Code	Prosthesis	Planicity (µm)
ANK1	Hintegra	916.2
ANK3	Mobility	90.8
ANK4	Mobility	47.2
ANK11	Salto	81.8
ANK12	Mobility	197.8
ANK13	STAR	180.9
ANK14	Mobility	73.5
ANK18	Mobility	220.8
ANK19	Mobility	111.1
ANK21	Mobility	126.9
ANK24	STAR	113.3
ANK26	Zenith	196.5
ANK27	Hintegra	87.8

Table 4.40. Measured planicity of PE insert backside surfaces obtained via CMM analysis. All are mobile bearing designs.

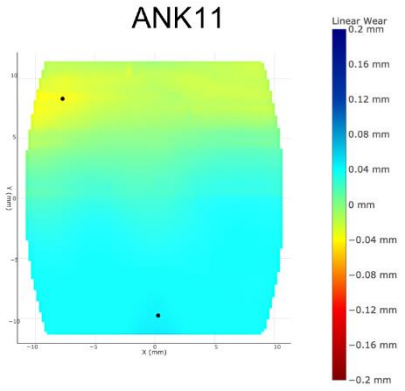

Figure 4.66. Backside geometry (scale -0.2 mm to 0.2 mm) from CMM analysis of the Salto PE insert backside surface. Red indicates material removed and blue indicates material added (i.e., deviations extending superiorly in an anatomical sense).

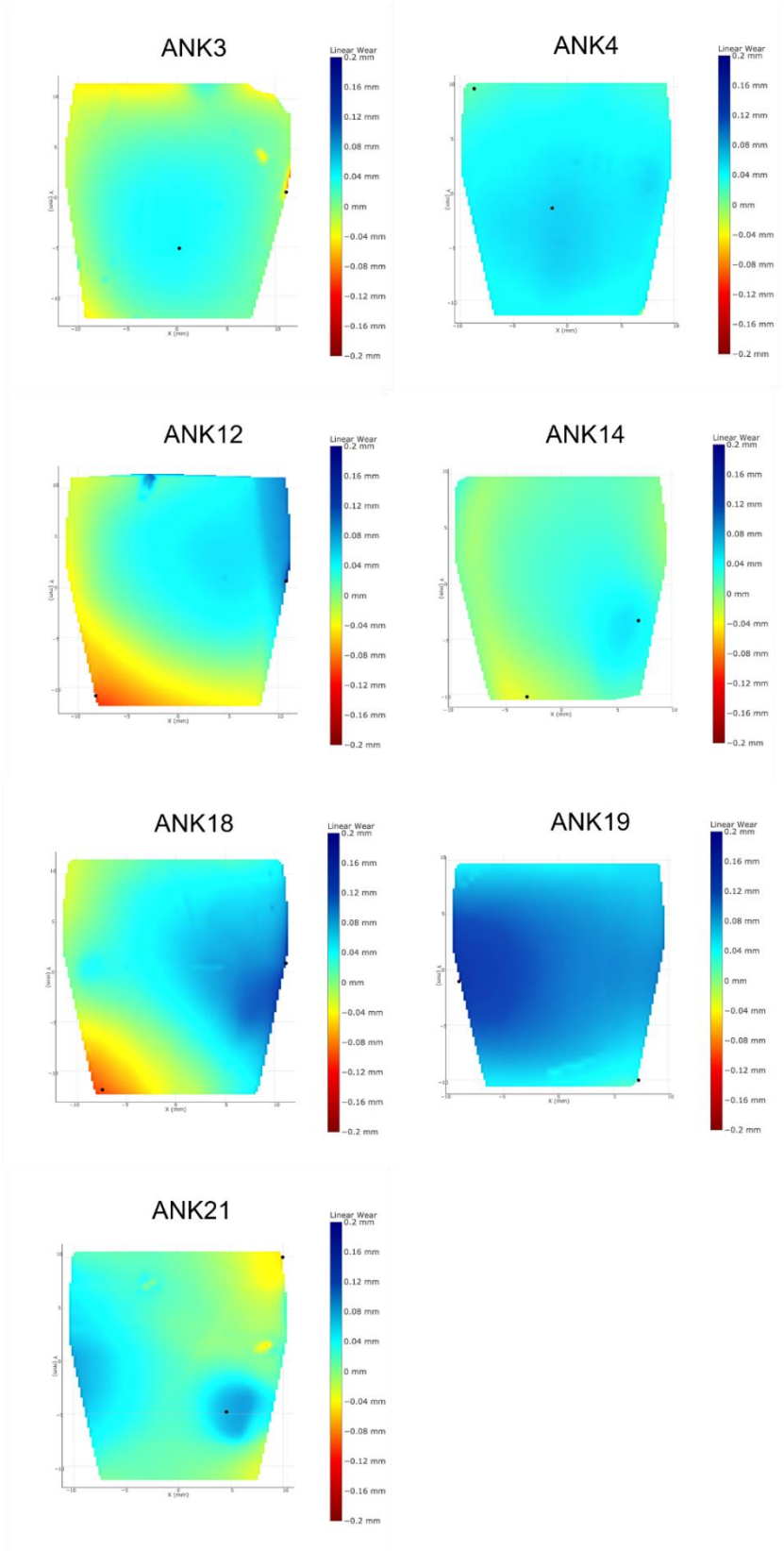

Figure 4.67. Backside geometries (scale -0.2 mm to 0.2 mm) from CMM analysis of the Mobility PE insert backside surfaces. Red indicates material removed and blue indicates material added (i.e., deviations extending superiorly in an anatomical sense).

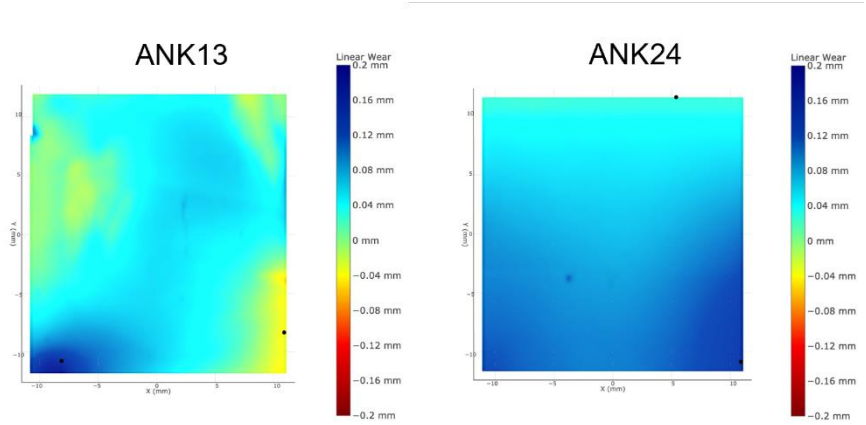

Figure 4.68. Backside geometries (scale -0.2 mm to 0.2 mm) from CMM analysis of the STAR PE insert backside surfaces. Red indicates material removed and blue indicates material added (i.e., deviations extending superiorly in an anatomical sense).

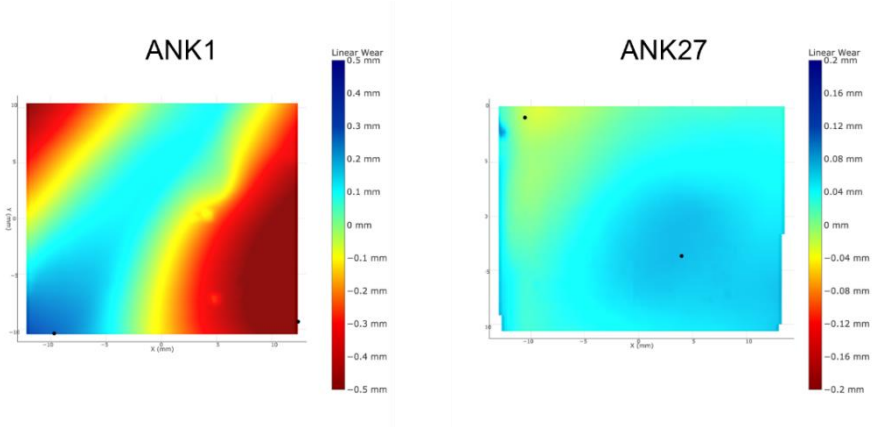

Figure 4.69. Backside geometries (scale -0.2 mm to 0.2 mm) from CMM analysis of the Hintegra PE insert backside surfaces. Red indicates material removed and blue indicates material added (i.e., deviations extending superiorly in an anatomical sense).

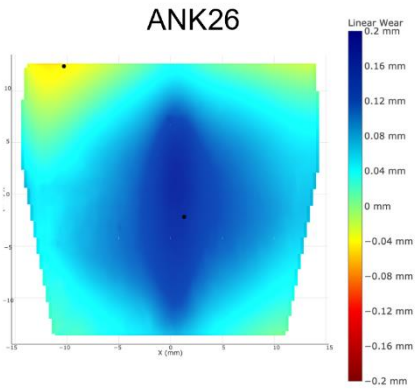

Figure 4.70. Backside geometry (scale -0.2 mm to 0.2 mm) from CMM analysis of the Zenith PE insert backside surface. Red indicates material removed and blue indicates material added (i.e., deviations extending superiorly in an anatomical sense).

The measured planicity of the backside surfaces of the PE inserts ranged from 47.2 to 916.2 µm (average 188.0 ± 225.6 µm). It should be noted that two of the PE insert backside surfaces for which CMM analysis was performed were identified as exhibiting surface deformation of the backside surface upon visual analysis as previously described in this chapter (section 4.1.6): ANK1 (Hintegra) and ANK26 (Zenith). Both recorded high planicity values of 916.2 µm and 196.5 µm, respectively. The former value in particular was substantially higher than any of the other measured planicites. It therefore follows that the Hintegra PE inserts recorded the highest backside planicities on average (Figure 4.71).

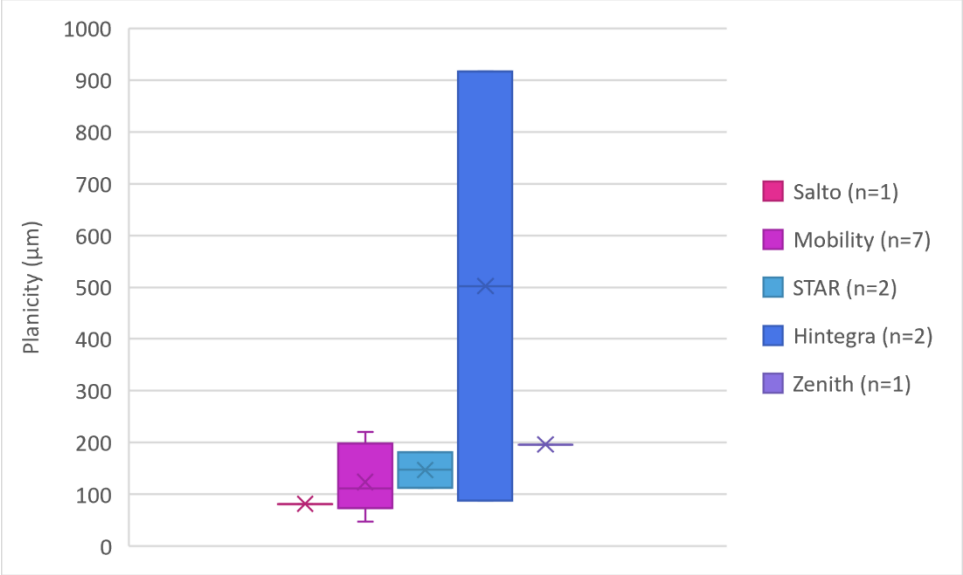

Figure 4.71. Box and whisker plot showing the variation in backside planicities for different TAR designs.

No correlation between the backside surface planicity and the bearing surface wear volume was found (r = 0.083, Pearson correlation) (Figure 4.72).

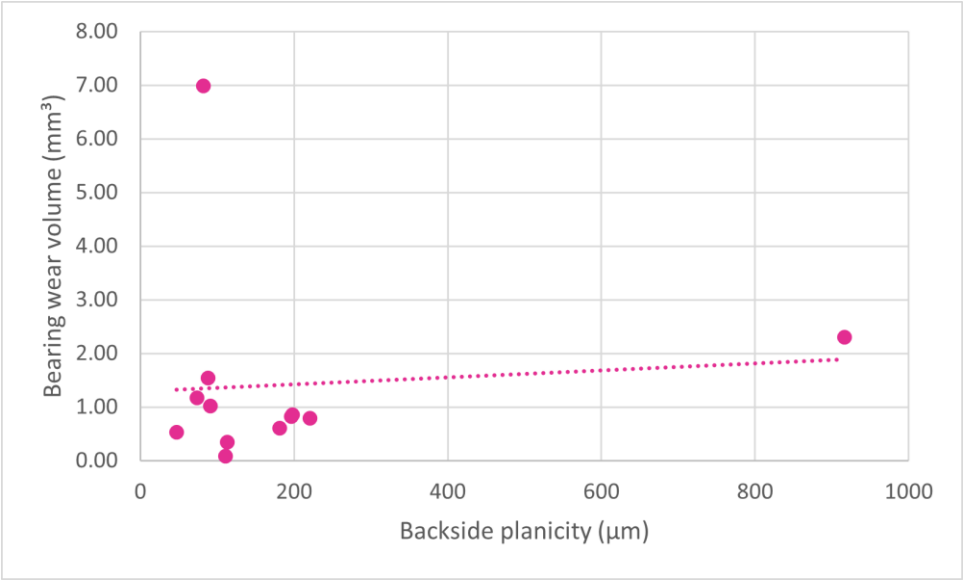

Figure 4.72. Scatter plot with linear trend line correlating backside planicity and bearing wear volume of PE inserts.

4.6. Correlation Analyses

In this section, selected results previously reported in this chapter are correlated in order to identify potential relationships between TAR characteristics and component damage. In this way, potential factors (patient or implant related) influencing the damage experienced by TARs may be identified.

4.6.1. Patient factors

In terms of patient factors, most of the clinical data was unknown for this cohort of explanted TARs, therefore limiting the analysis that could be performed. However, patient sex was known for 14 of the analysed TARs; 11 corresponded to male patients and 3 corresponded to female patients. The total wear volumes (i.e., the sum of medial and lateral aspects) are given in Table 4.41 for these devices.

Male (n = 11)		**Female (n = 3)**	
Prosthesis	**Bearing wear (mm^3)**	**Prosthesis**	**Bearing wear (mm^3)**
ANK1	2.30	ANK12	0.86
ANK2	4.29	ANK20	0.56
ANK3	1.02	ANK26	0.82
ANK4	0.53		
ANK6	-		
ANK9	4.33		
ANK10	3.21		
ANK22	-		
ANK23	-		
ANK24	0.34		
ANK25	-		

*Table 4.41. Bearing surface wear volumes of the PE inserts from TARs for which the corresponding patient sex was known. Notes: *, average given in terms of mean ± SD.*

The average wear volume measured from the bearing surface of the PE inserts from TARs corresponding to male patients was higher than that for female patients (2.29 ± 1.71 mm^3 versus

0.75 ± 0.16 mm³), however this difference did not reach statistical significance (p = 0.362) (Figure 4.73).

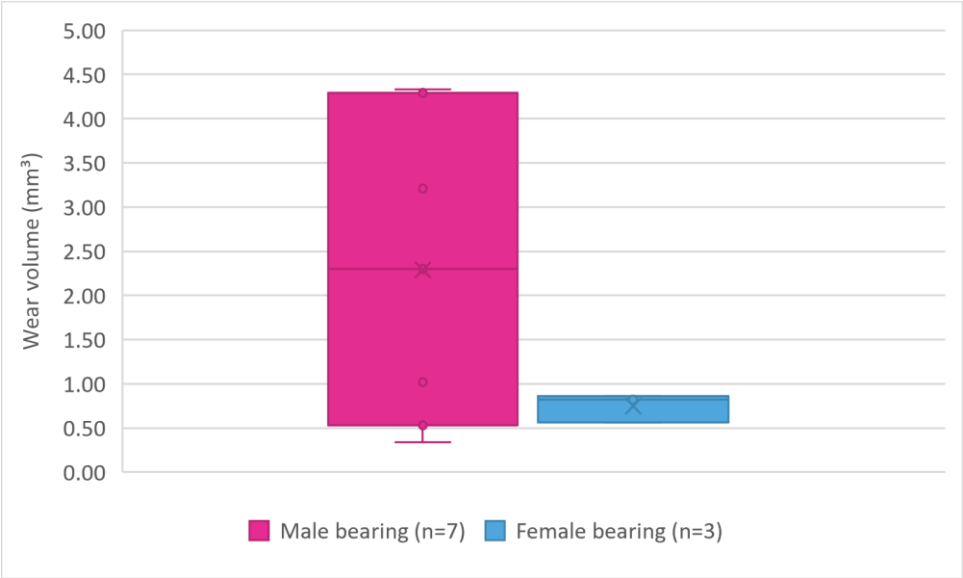

Figure 4.73. Box and whisker plot showing variation in total wear volumes measured from the bearing surfaces of PE inserts corresponding to TARs from male and female patients.

The CDS, as reported in section 4.2. of this chapter, were also analysed in terms of potential influence of patient sex. Table 4.42 gives the average CDS of the different component surfaces analysed during the semi-quantitative damage scoring for those with a known corresponding patient sex (14 PE inserts, 12 tibial components, and 12 talar components). The CDS for PE insert bearing surfaces (Figure 4.74), PE insert backside surfaces (Figure 4.75), and tibial component inferior surfaces (Figure 4.76) was higher on average for those which corresponded to male patients compared to female patients. The CDS for talar component bearing surfaces (Figure 4.77), on the other hand, was higher on average for those which corresponded to female patients compared to male patients. However, none of these differences reached statistical significance.

Surface	Male	Female	P-value
PE bearing	65.50 ± 27.18	19.40 ± 23.21	0.062
PE backside	48.13 ± 25.91	46.84 ± 36.07	0.755
Tibial	21.36 ± 17.55	5.02 ± 5.74	0.063
Talar	26.66 ± 8.44	31.80 ± 15.99	0.460

Table 4.42. Average (mean ± SD) CDS of the different component surfaces analysed for male and female patients.

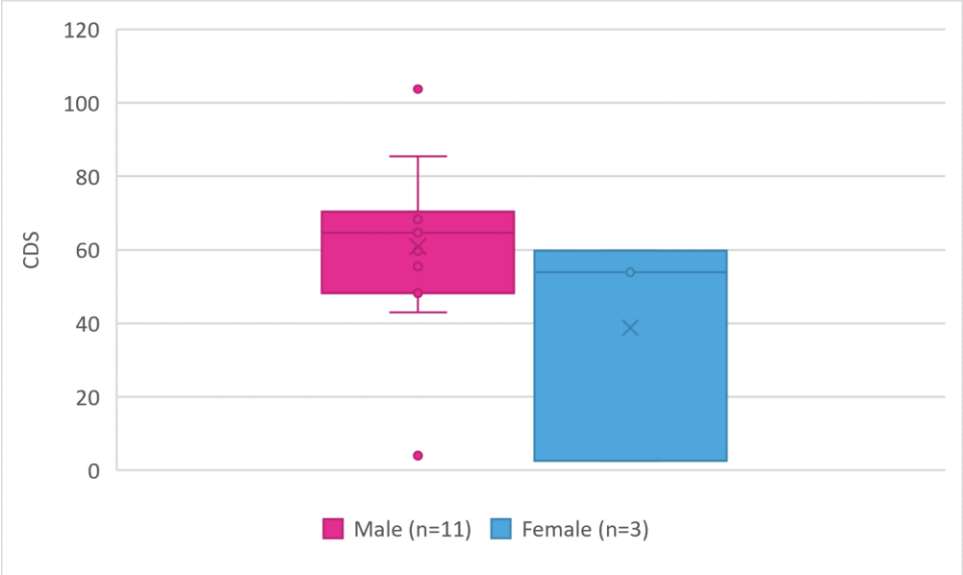

Figure 4.74. Box and whisker plot showing the distribution of CDS for PE insert bearing surfaces corresponding to male and female patients.

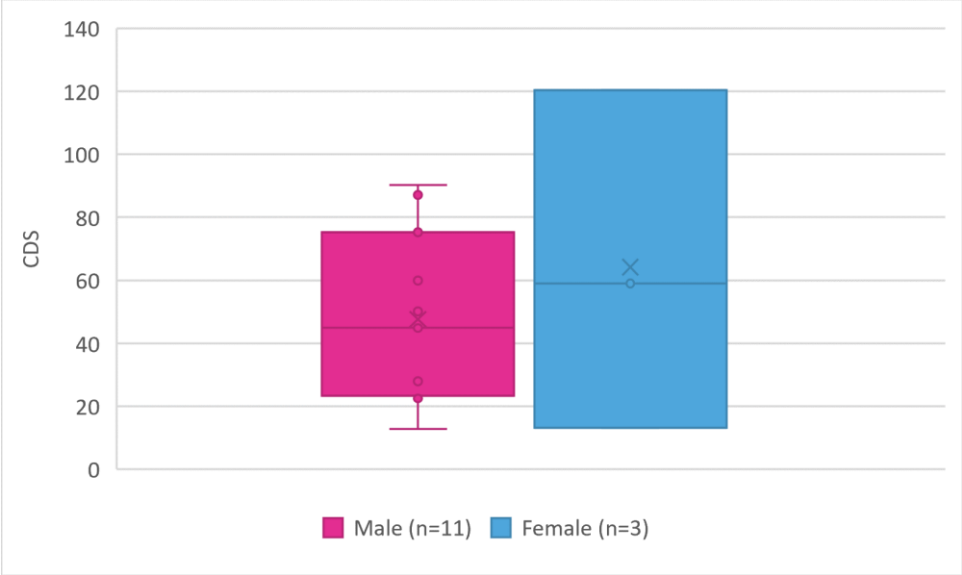

Figure 4.75. Box and whisker plot showing the distribution of CDS for PE insert backside surfaces corresponding to male and female patients.

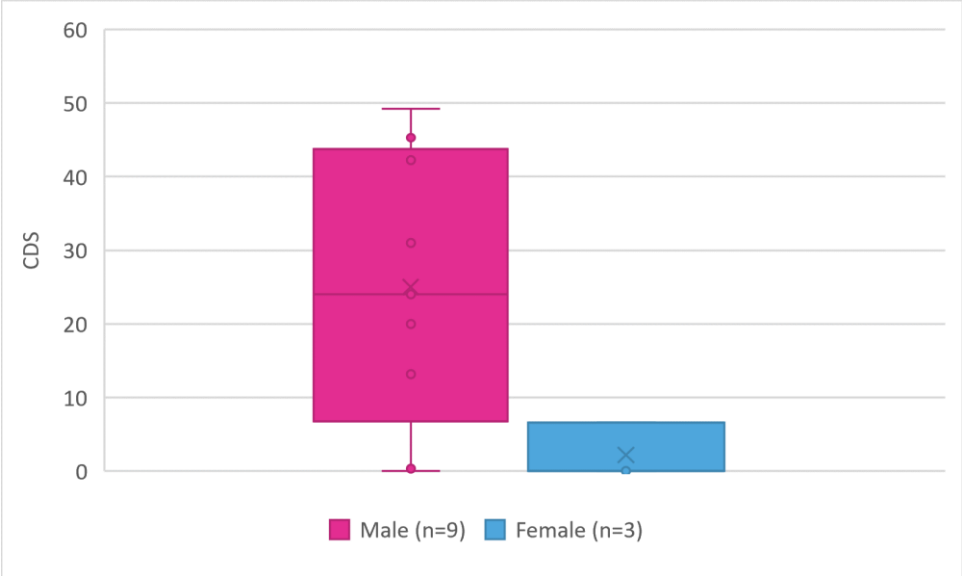

Figure 4.76. Box and whisker plot showing the distribution of CDS for tibial component inferior surfaces corresponding to male and female patients.

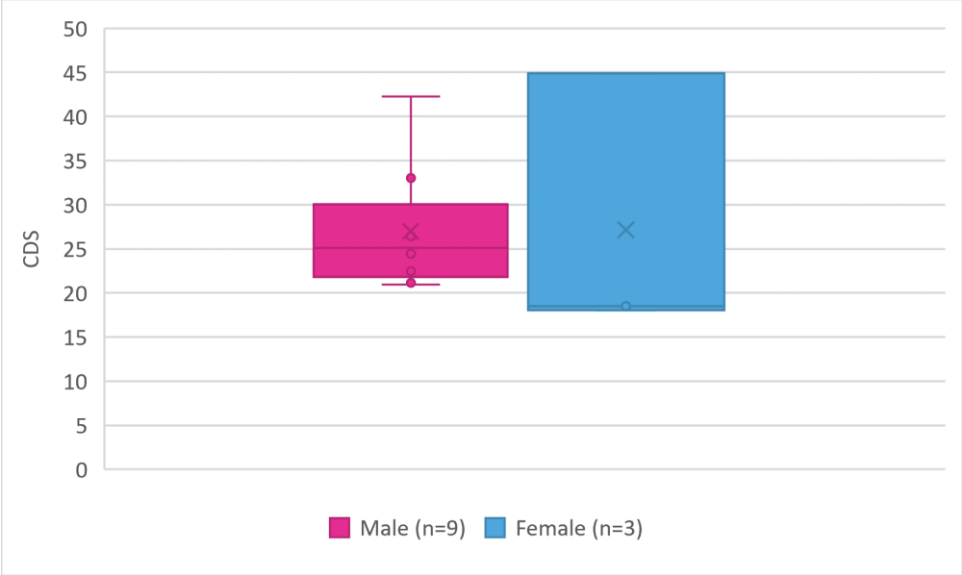

Figure 4.77. Box and whisker plot showing the distribution of CDS for talar component bearing surfaces corresponding to male and female patients.

4.6.2. Implant factors

Factors relating to the design of the implant were also correlated with results from different damage analyses of the explanted TARs. Namely, the implant factors of PE insert cross-linking, tibial component alloy, the surface roughness of the tibial and talar components, and the thickness of the PE insert were correlated with damage to the PE insert in terms of wear and CDS. These correlation analyses were including components only where both variables being analysed were known.

Only one of the PE inserts within the cohort of explanted TARs was manufactured from HXLPE (Cadence), with the others all being manufactured from conventional UHMWPE. CMM analysis was not achievable for the HXLPE insert meaning wear volume and planicity for this component could not be quantified.

A comparison of the CDS for both the bearing and backside surfaces of the conventional UHMWPE inserts and the HXLPE insert are shown by Figure 4.78 and Figure 4.79, respectively. For the PE insert bearing surfaces, the CDS for the HXLPE component (42.90) was similar to the average of that for the conventional UHMWPE components (44.52 ± 34.59). For the PE insert backside surfaces, the CDS for the HXLPE component (27.96) was at the lower end of the interquartile range of that for the conventional UHMWPE components (average 48.30 ± 29.54).

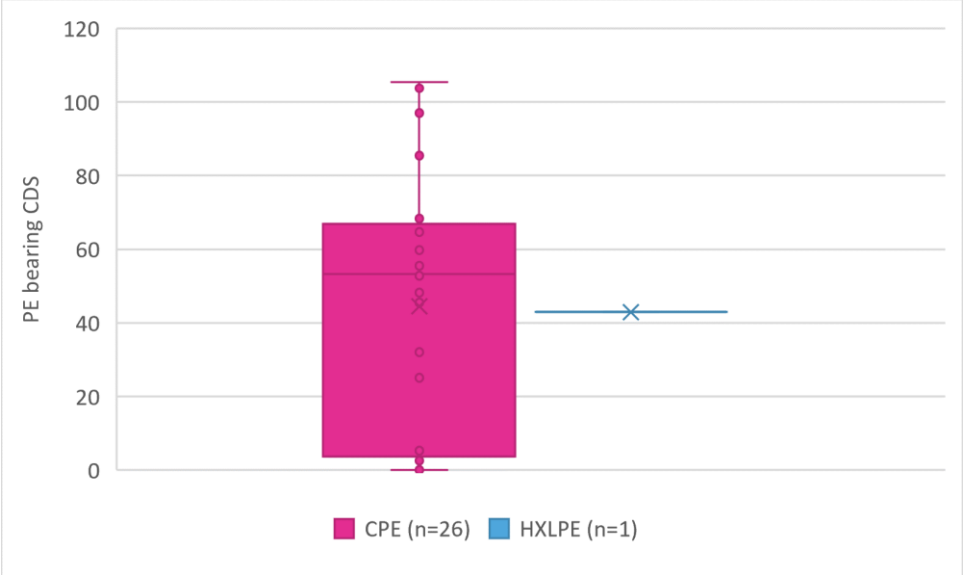

Figure 4.78. Box and whisker plot of PE bearing surface CDS for conventional UHMWPE (CPE) inserts and highly cross-linked UHMWPE (HXLPE) inserts.

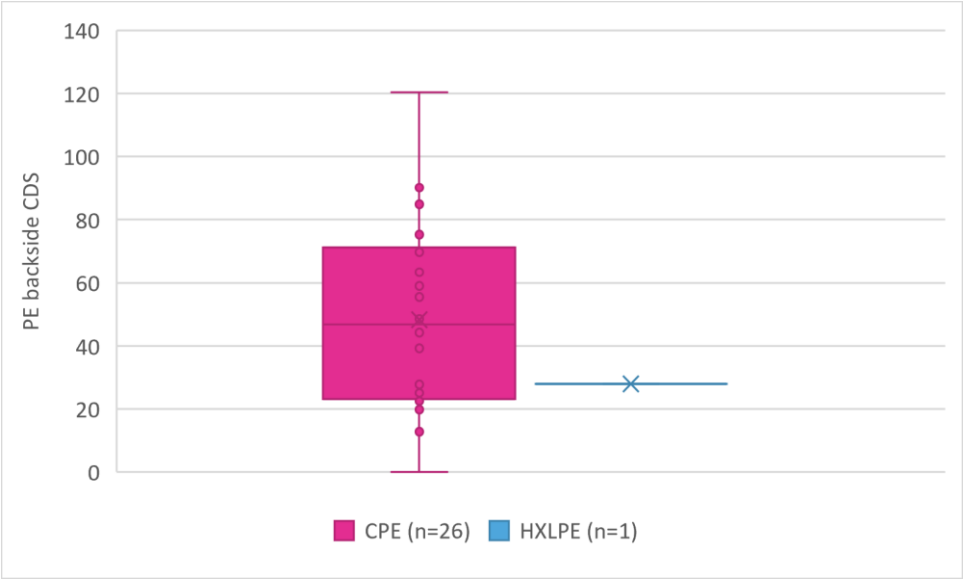

Figure 4.79. Box and whisker plot of PE backside surface CDS for conventional UHMWPE (CPE) inserts and highly cross-linked UHMWPE (HXLPE) inserts.

All of the PE inserts for which CMM analysis of the backside surface was achievable had a CoCr alloy corresponding tibial component, with the exception of one which had a TiN coated

corresponding tibial component. Therefore, no correlation analysis was performed for the variables of PE insert backside planicity and tibial component alloy.

The CDS of the backside surfaces of the PE inserts for different tibial component alloys are plotted in Figure 4.80. The average CDS for the PE insert backside surfaces corresponding to CoCr alloy tibial components was significantly higher than those corresponding to Ti alloy tibial components (50.95 ± 24.41 versus 18.72 ± 12.31, p = 0.021).

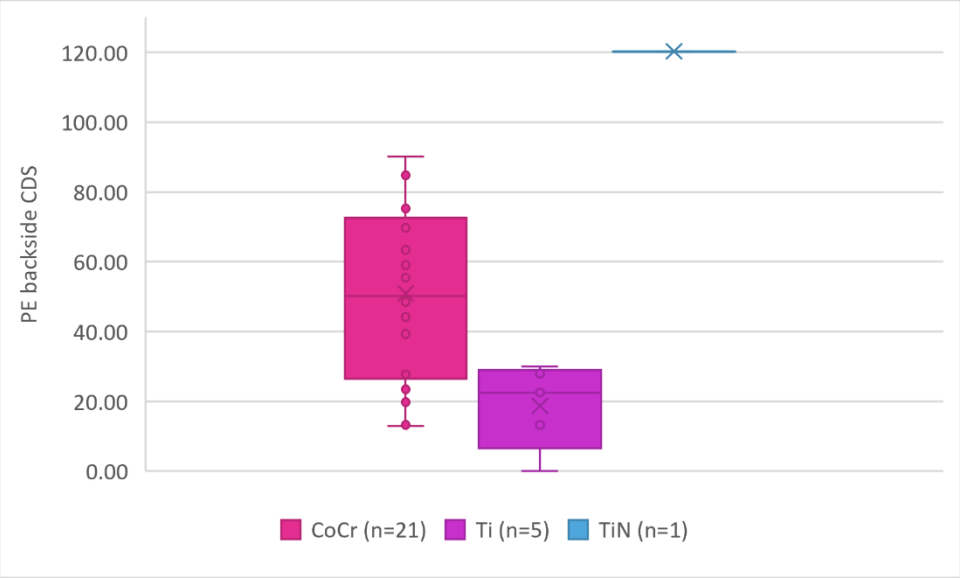

Figure 4.80. Box and whisker plot showing distribution of PE insert backside surface CDS for different tibial component alloys.

Figure 4.81 correlates the unworn S_a of the tibial component articulating surface with the CDS of the PE insert backside surface. A moderate negative relationship was identified between the two variables, indicating that as the average surface roughness of the tibial component increases, the damage identified on the PE insert backside surface decreases (Pearson correlation, r = -0.453).

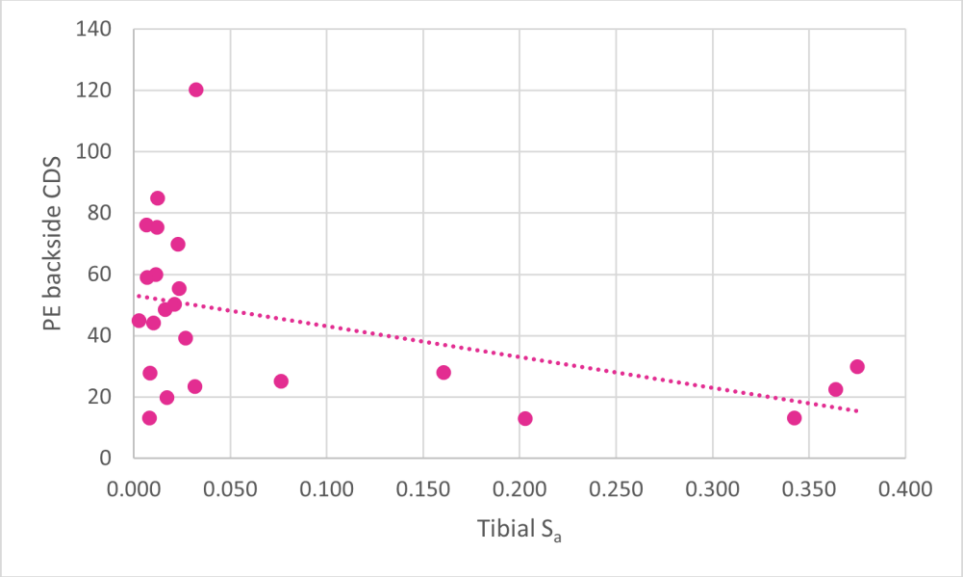

Figure 4.81. Scatter plot with linear trendline correlating mean unworn tibial component average surface roughness (S_a) with CDS of the PE insert backside surfaces.

The mean unworn talar component bearing surface average surface roughness (S_a) is plotted against the measured volumetric wear loss from the corresponding PE insert bearing surface in Figure 4.82. A weak positive correlation was seen between these two variables (Pearson correlation, r = 0.249).

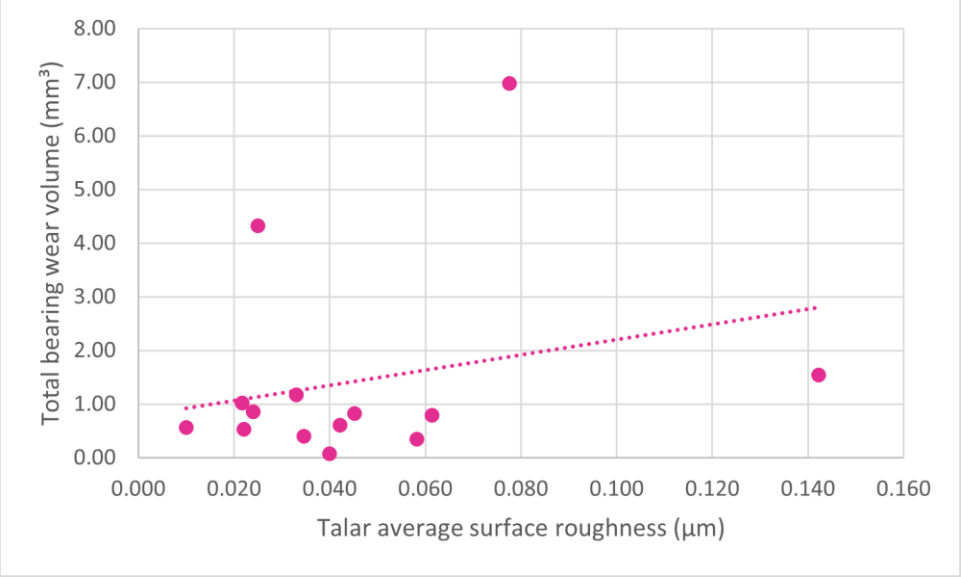

Figure 4.82. Scatter plot with linear trendline correlating mean unworn talar component average surface roughness (S_a) with the total PE insert bearing surface wear volume.

Figure 4.83 plots the mean unworn talar component bearing surface average surface roughness (S_a) against the CDS of the corresponding PE insert bearing surface. No correlation was found between these two variables (Pearson correlation, r = 0.152).

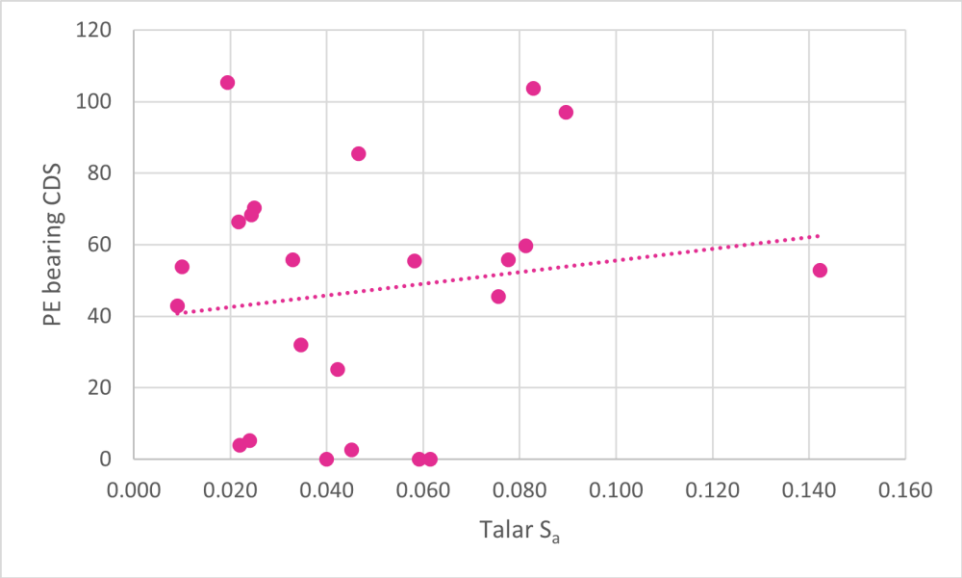

Figure 4.83. Scatter plot with linear trendline correlating mean unworn talar component average surface roughness (S_a) with the CDS of the PE insert bearing surfaces.

Figure 4.84 plots the thickness of the PE insert against the measured volumetric wear loss from the bearing surface of the PE insert. No correlation was found between these two variables (Pearson correlation, r = -0.054).

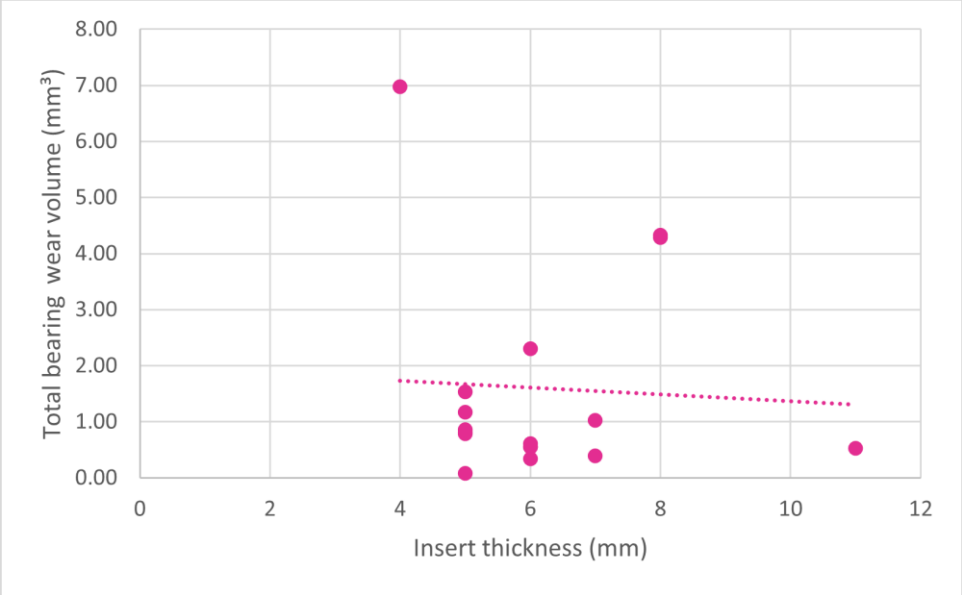

Figure 4.84. Scatter plot with linear trendline correlating the PE insert thickness with the corresponding PE insert bearing surface total wear volume.

The PE insert thickness is plotted against the corresponding CDS for the bearing surfaces of the PE inserts in Figure 4.85. No correlation was found between these two variables (Pearson correlation, r = 0.018).

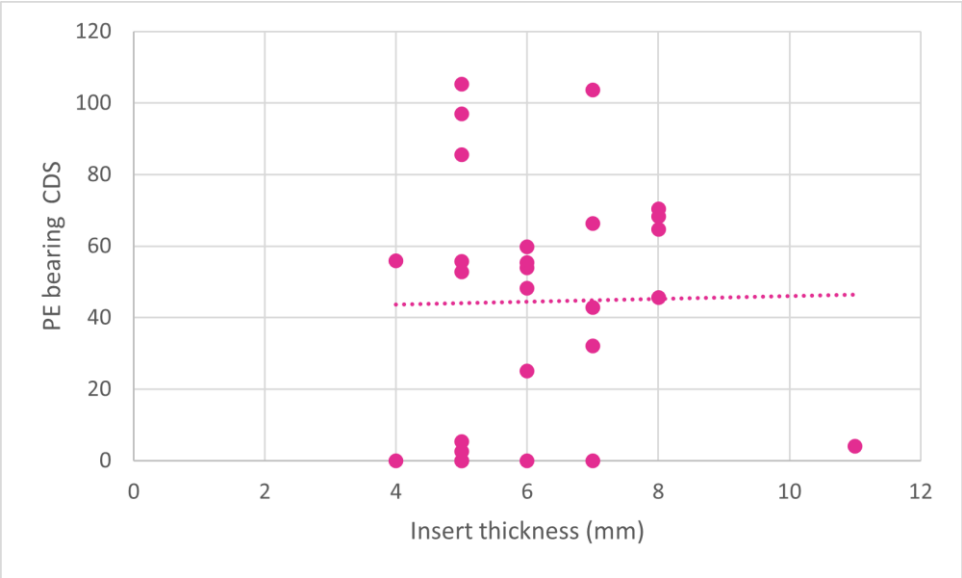

Figure 4.85. Scatter plot with linear trendline correlating the PE insert thickness with the corresponding CDS of the PE insert bearing surface.

Figure 4.86 plots the PE insert thickness against the corresponding planicity value of the PE insert backside surface. No correlation was found between these two variables (Pearson correlation, r = -0.086).

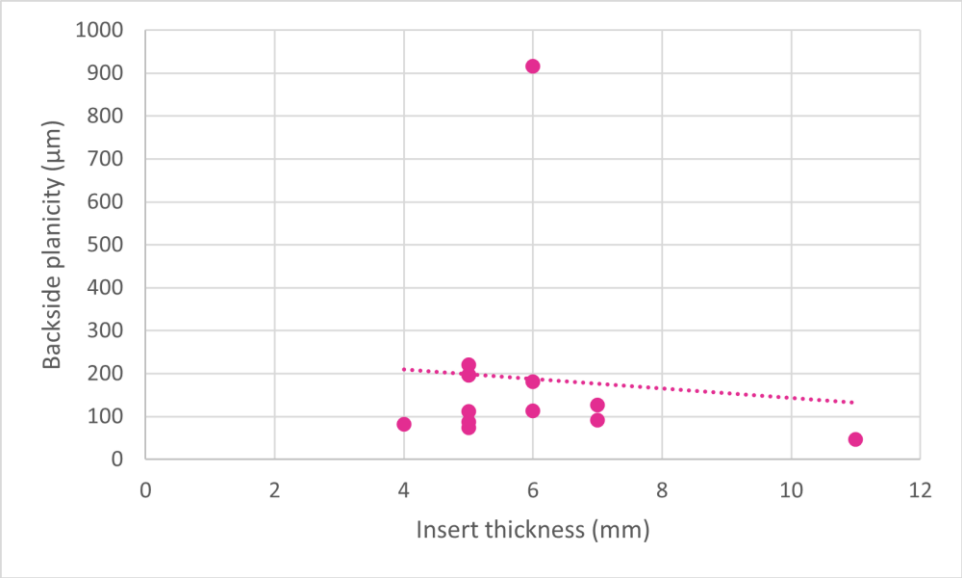

Figure 4.86. Scatter plot with linear trendline correlating the PE insert thickness with the corresponding planicity of the PE insert backside surface.

The thickness of the PE insert is plotted against the corresponding CDS for the backside surfaces of the PE inserts in Figure 4.87. Again, no correlation was found between these two variables (Pearson correlation, r = 0.106).

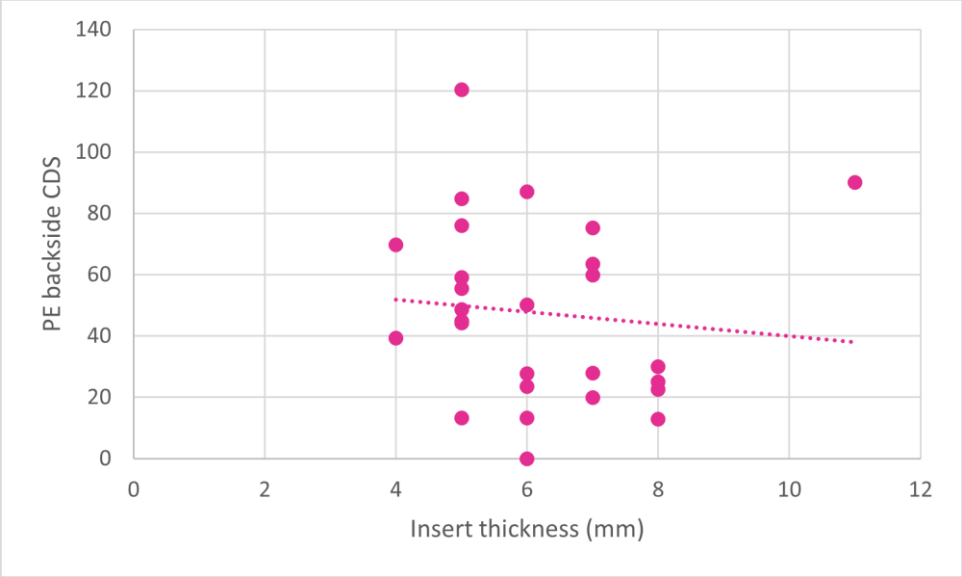

Figure 4.87. Scatter plot with linear trendline correlating the PE insert thickness with the corresponding CDS of the PE insert backside surface.

4.7. Summary

An overview of the damage mechanisms identified in each explanted TAR is given in Table 4.43. This summarises the main features relating to the high proportion of metallic pitting and talar sliding plane scratching damage identified.

Of the TARs with talar components exhibiting sliding plane scratching, indicative of the presence of hard third body particles at the bearing, all but two also exhibited coating loss from the corresponding tibial and/or talar components. For the two cases which didn't, one (Mobility) prosthesis had cement present on the talar component, with the tibial component not received. The other (Hintegra) had evidence of direct MoM contact occurring between the metal tibial and talar components, along with a PE insert which was broken into two pieces and which had high amounts of embedded debris, identified as containing CoCr. Similarly, for the TARs with metallic pitting of the tibial and/or talar component articulating surfaces, coating loss was also identified on one or more of the metal components for all except the same two prostheses.

Prosthesis	Tibial pitting	Talar pitting	Talar scratching	Cement present	Coating loss	Additional damage
INFINITY	Y	Y	Y		Y	
INFINITY		Y	Y		Y	Y*
INFINITY		Y	Y		Y	
INFINITY	-	-	-	-	-	
Cadence		Y			Y	
Salto Talaris	Y	-	-		Y	Y†
Salto Talaris	Y	Y			Y	Y§
Salto	Y	Y	Y		Y	
Mobility	Y	Y	Y		Y	
Mobility	-	Y	Y	Y		
Mobility	Y	Y	Y		Y	Y§
Mobility	Y	Y	Y		Y	
Mobility		Y	Y		Y	
Mobility	Y	Y	Y		Y	Y§
Mobility		Y	Y		Y	
Mobility		Y	Y		Y	
Mobility	-	-	-	-	-	
Mobility		Y	Y		Y	Y‡§
STAR	Y	Y			Y	
STAR	Y	Y			Y	Y‡
STAR	Y	Y	Y		Y	
Hintegra	-	-	-	-	-	Y*†
Hintegra		Y	Y			Y†‡§
Hintegra		Y	Y		Y	Y*
BOX		Y	Y		Y	
BOX			Y	Y	Y	
BOX	Y	Y			Y	Y‡§
Zenith		Y	Y		Y	

*Table 4.43. Overview of the damage mechanism identified in each of the explanted TARs. Notes: Y, damage identified; -, corresponding component not present; *, Ti embedded debris; †, Co and Cr embedded debris; ‡, metal-on-metal contact; §, severely damaged PE insert.*

Chapter 5. Discussion

The aim of this study was to investigate the failure mechanisms of retrieved contemporary TARs using an explant analysis approach. Thus, the specified objectives of the research were to characterise type, extent, and severity of damage modes present on the explanted components, to evaluate changes to the surface topography, to quantify volumetric wear loss, to correlate tribological changes with implant characteristics, and finally to determine likely failure mechanisms of TARs based on the analysed damage.

Several key limitations and debates, which the research contained within this thesis also sought to address, were identified within the existing literature in chapter 2.

In this chapter, the results of the study in relation to this aim are summarised and analysed for connections. These findings are then discussed in the context of the published literature. The limitations of the study are also considered.

5.1. Damage Mechanisms Identified

Damage to all of the components – PE insert, tibial component, and talar component – was observed in the cohort of TARs included in this explant analysis study. Whilst some degree of wear damage is to be expected – particularly to the PE bearing surface – from normal day-to-day use of a prosthesis, the metal damage identified was unexpected, both in terms of frequency and severity. Explant analysis studies of TARs are limited, and whilst metal damage has previously been reported, the majority of explant analysis studies within the existing literature have focused on surface damage to the PE component. The present study therefore sought to analyse explanted metal components also, both in terms of the damage identified and the surface topography. Another major finding of the study was that of coating loss occurring frequently on the non-articulating surfaces of the metal components. Combined, these findings form the basis of a proposal of a new failure mechanism of contemporary TARs.

5.1.1. Tribological changes

According to the calculated component damage scores, which took into account both the area covered and the severity of the different surface damage modes, as scored via semi-quantitative analysis, scratching of the talar components accounted for the greatest scoring damage,

followed by burnishing of the PE insert backside surfaces, pitting of the PE insert bearing surfaces, and scratching of the PE insert backside surfaces.

The component damage scores for the talar components were higher on average than those for the tibial components (considering the same three damage modes of pitting, scratching, and abrasion). However, a weak positive correlation between the component damage scores for these two components was also identified, meaning that as the damage on the talar component increased, the damage on the corresponding tibial component also increased. No patterns were found regarding the distribution of damage to any of the articulating surfaces of the components in terms of differences between anterior and posterior aspects and between medial and lateral aspects.

In well-functioning TARs, the PE insert separates the two metal components, thereby preventing any direct metal-on-metal contact from occurring. However, in situations where the PE insert fractures or migrates, this can mean that direct unintended contact between the metal tibial and talar components is able to occur. Evidence of this unintended direct metal-on-metal contact was seen in four cases within the cohort of explanted TARs from the present study. For one of these cases, the PE insert was not present with the explanted TAR; however, for the other three, the corresponding PE inserts all had severe damage, with one being broken into two pieces, and two having part broken off. These findings indicate that gross damage to the PE insert in the form of fracture or loss of part of the component may be cause the damage seen as a result of unintended direct metal-on-metal contact between the tibial and talar components.

As well as the three PE inserts which corresponded to TARs with evidence of direct metal-on-metal contact having occurred, an additional two PE inserts also had severe damage in the form of part of the component being broken off. Previously, the FDA has issued a safety communication regarding a *"higher than expected risk"* for fracture of the PE insert of the STAR prosthesis.[118] In particular, it was noted that thinner PE inserts (defined in this case as 6 mm) were more likely to fracture.[118] Of the PE inserts included in the present study, 63% had a thickness of 6 mm or less (Figure 5.1). Overall, the thicknesses of the PE inserts ranged from 4 to 11 mm (mean and median 6 mm). Of the 5 PE inserts which exhibited severe damage in the form of either fracture into two pieces or part broken off, 3 (60%) had a thickness of 6 mm or less (5, 5, and 6 mm) and 2 (40%) had a thickness of greater than 6 mm (7 and 7 mm). Overall, the proportion of PE inserts with a thickness of over 6 mm and those with a thickness of 6 mm or less which were intact (i.e., had not fractured or had part broken off) was similar

(80% versus 82%, respectively). This indicates that the thickness of the PE insert is probably not a primary factor influencing its likelihood of fracturing *in vivo*.

Of the 3 STAR TARs included in the present study, one did not have a PE insert present, and the other two had PE inserts with a thickness of 6 mm. Neither of these PE inserts were severely damaged in terms of PE insert fracture upon retrieval. However, it should be noted that clinical details such as implantation duration and reason for retrieval, as well as patient characteristics such as activity level and indication for primary TAR being unknown, as well as the small sample size of this design included in this study means that these results do not necessarily contradict those informing the previous safety notice.

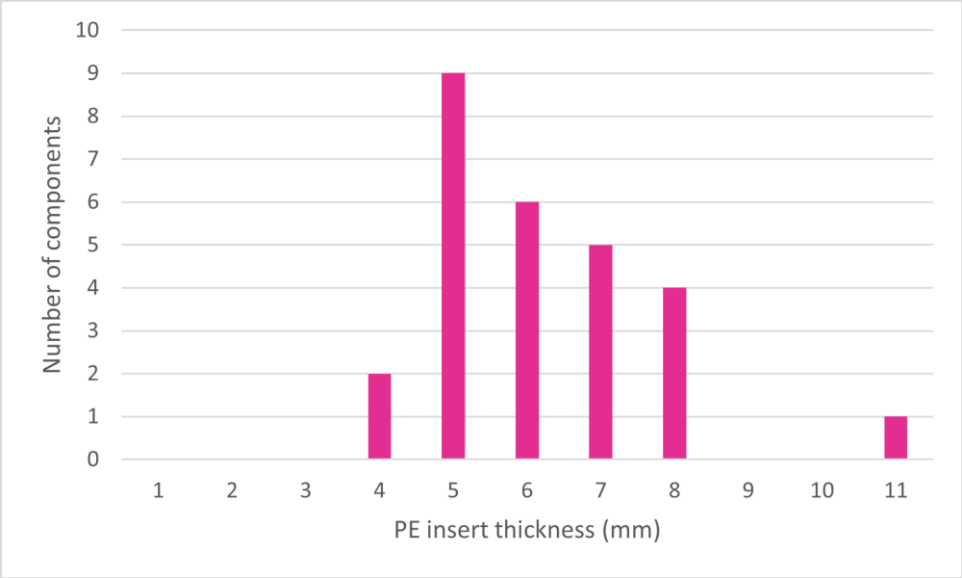

Figure 5.1. Graph showing the thicknesses of the PE inserts.

Historically, PE components have been considered to be the 'weak link' in MoP joints, with failures frequently being attributed to wear of this component. However, explant studies of MoP hip, knee, and ankle replacements have shown that metallic wear is also generated, to a not-insignificant extent.[16-18, 20] Analysis of all explanted components and consideration of all sources of wear debris is therefore important in order to try to understand the failure mechanisms at play.

In terms of the surface topography of the articulating surfaces of the metal components, in general, the measured surface roughness parameters of S_a, S_q, S_z, S_p, S_v, and S_{ku} all showed an

increase, and S_{sk} more negative, on worn areas compared to unwon areas of both tibial and talar components, with this difference being significant for the majority of the TAR designs. For the tibial components, exceptions to this were only seen with the Zenith prosthesis (recording a more negative S_{sk} and a lower S_{ku} on the worn surface area compared to the unworn), and the Cadence prosthesis (also recording a lower S_{ku} on the worn surface area compared to unworn). For both of these components, just one of the respective designs were analysed, meaning that these were perhaps outlier cases. Likewise, for the talar components, exceptions were only seen in cases where n = 1. The Zenith and Salto prostheses recorded a lower S_p on the worn surface areas compared to the unworn, and the Salto Talaris recorded a lower S_{ku} on the worn surface area compared to the unworn.

The frequency of which damage to the metallic components was identified in this cohort of explanted TARs was unexpected. Specifically, damage to the articulating surfaces of the metal components in terms of pitting and talar sliding plane scratching, as well as changes to the coatings present on the non-articulating surfaces was observed on a high proportion of these components. In particular, the damage to the articulating surfaces of the metal tibial and talar components was unexpected given that this would not be typical for a well-functioning MoP (hard-on-soft) bearing.

5.1.2. Metal debris release

The embedded debris identified in the bearing and backside surfaces of the PE inserts was confirmed as being metallic via SEM-EDX analysis. Specifically, Ti, Co, and Cr was identified in the embedded debris. All of the PE inserts for which embedded debris was identified had a coating on the non-articulating surfaces of the corresponding metal components containing Ti, and all had tibial and talar components composed of CoCr alloy with the exception of the INFINTY prosthesis, which had a Ti alloy tibial component. However, for the PE insert corresponding to this INFINITY TAR, embedded debris was identified on the bearing surface (in contact with the CoCr talar component) only. With this in mind, all of PE insert surfaces in which embedded debris was identified were in contact with CoCr alloy surfaces (PE insert bearing surfaces in contact with talar component bearing surfaces, and PE insert backside surfaces in contact with tibial component inferior surfaces). Therefore, the Ti embedded debris identified on the PE insert component surfaces was presumably from the Ti-containing porous coatings, and the CoCr embedded debris was presumably originating from the articulating

surfaces of the CoCr metal components. The findings of both loss of coatings and pitting of the metallic components frequently seen from this cohort of explanted TARs supports this theory.

Of the 5 PE inserts for which embedded debris was identified (5 bearing surfaces and 4 backside surfaces), Ti was identified in 2, CoCr(Mo) was identified in 2, and 1 had both Ti and CoCr. This therefore shows that both sources of metal particulate debris release – via loss of non-articulating surfaces coating and pitting of articulating surfaces – can act concurrently.

The TARs which had embedded debris in the PE inserts included two Hintegra prostheses. Despite being of the same design, different embedded debris was determined to be present in each, with CoCr identified in one and Ti in the other. The Hintegra prosthesis with the CoCr embedded debris displayed signs of unintended direct metal-on-metal contact having occurred *in vivo* between the articulating surfaces of the tibial and talar components, which likely caused the CoCr debris release and the resulting embedded debris. The Hintegra prosthesis with the Ti embedded debris, on the other hand, had evidence of coating loss; therefore, the Ti embedded debris most likely originated from the Ti-containing porous coating. The differences in the PE inserts and embedded debris of these two Hintegra prostheses is illustrated by Figure 5.2.

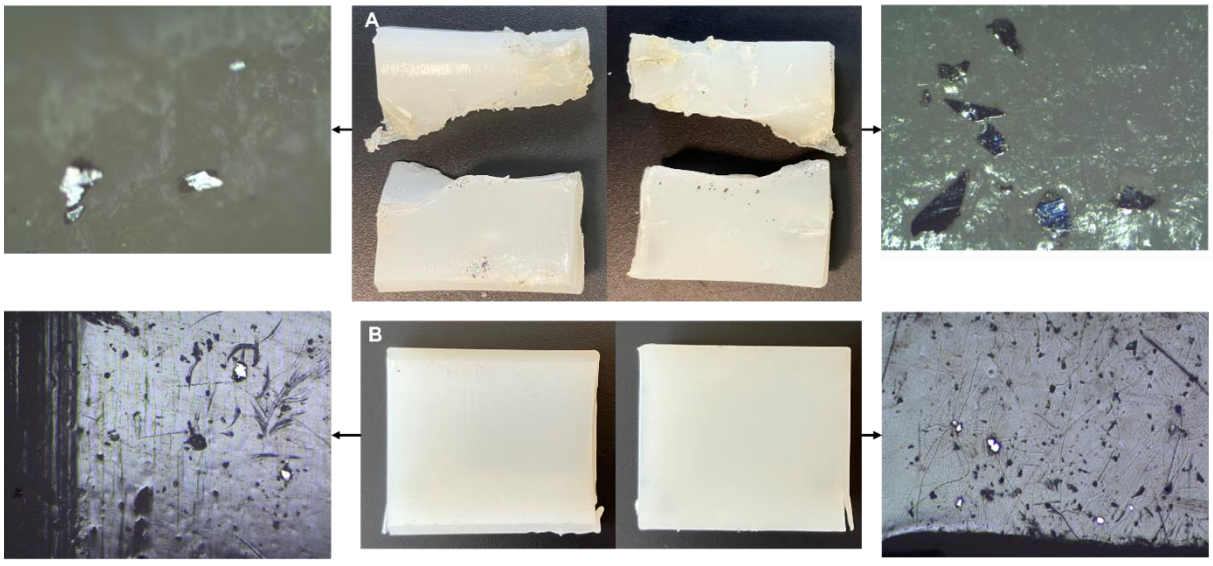

Figure 5.2. Comparison of the two Hintegra PE inserts with metallic embedded debris, showing macroscopic images of the PE insert bearing and backside surfaces and microscopic images of corresponding embedded metallic debris. (A) ANK6 with CoCr embedded debris. (B) ANK27 with Ti embedded debris.

Embedded metallic debris in the PE inserts of explanted TARs has also previously been reported by Vaupel et al.[145], in fixed bearing Agility prostheses, and a small amount in INFINITY and INBONE prostheses – both also fixed bearing designs – by Ho et al.[133] Stratton-Powell et al.[149] also reported CoCr and Ti wear particles, amongst others, surrounding failed AES TARs. These findings from the existing literature support those from the present study; together, the issue of various metal debris being released seems to be a widespread one, affecting different designs of TARs.

In addition to the metallic embedded debris identified in the PE inserts, Ti was also identified in 7 of the explanted metal components (all 3 BOX tibial and talar components, and 1 of the Mobility talar components). Given that the BOX prosthesis is the only TAR within this study to have a porous coating which does not contain Ti (being HA beads), the identified Ti was presumed to be part of the component composition in these cases. For the Mobility talar component, however, the presence of Ti suggests that metal particulate debris may have been released from the Ti beaded coating and become embedded into the component in this case.

Additionally, a large proportion (79%) of the talar components analysed were found to have macroscopically visible linear scratches on the sliding plane. For a normal MoP bearing, with a harder metal surface articulating against a softer PE surface, this kind of gross abrasive damage to the metal component would not be expected.[64] It is therefore indicative of the presence of hard third body particles at the bearing *in vivo* (Figure 5.3). Similar findings have previously been reported by Cottrino et al. on 6 AES CoCr talar component bearing surfaces, in which severe scratching was also observed on the sliding planes.[64] In this case, the authors attributed the damage as being due to hard foreign particles originating from removal of the Ti-HA coating of the metal components.[64] This was also determined to likely be the origin of hard third body particles causing scratching at the bearing in the present study, as almost all of the TARs for which talar sliding plane scratching was identified also exhibited coating loss from the non-articulating surfaces of the corresponding tibial and/or talar components. Whilst the analysis by Cottrino et al. consisted of one specific design of TAR only which did not feature in the present study, the similar findings shared extends the issue of coating removal and subsequent damage via third body debris to various designs of contemporary TARs.

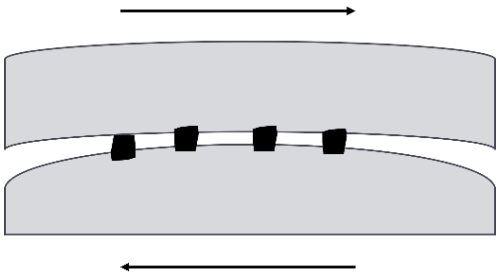

Figure 5.3. Schematic illustration of third body particles at the bearing. Third body particles (represented by the black shapes) present at the MoP bearing comprised of the PE insert (top) and talar component (bottom).

Pitting, indicative of localised material loss having occurred *in vivo* (Figure 5.4), was identified visually on the majority of the articulating surfaces of the metal components (54% of tibial components and 96% of talar components). The presence of these pits – which had dimensions of approximately 90 μm (length) x 40 μm (width) x 3 μm (depth) (Figure 5.5) – was confirmed via surface profilometry, which showed that for all models of tibial and talar components on which pitting had been identified prior, both the measured average surface roughness and maximum valley depth values were significantly higher on pitted areas compared to unpitted areas.

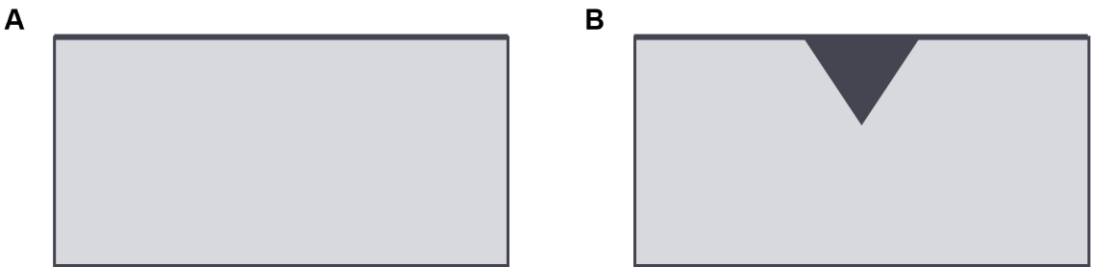

Figure 5.4. Schematic illustration of unpitted and pitted surfaces. (A) an unpitted surface. (B) a pit (i.e., localised removal of material) on a surface.

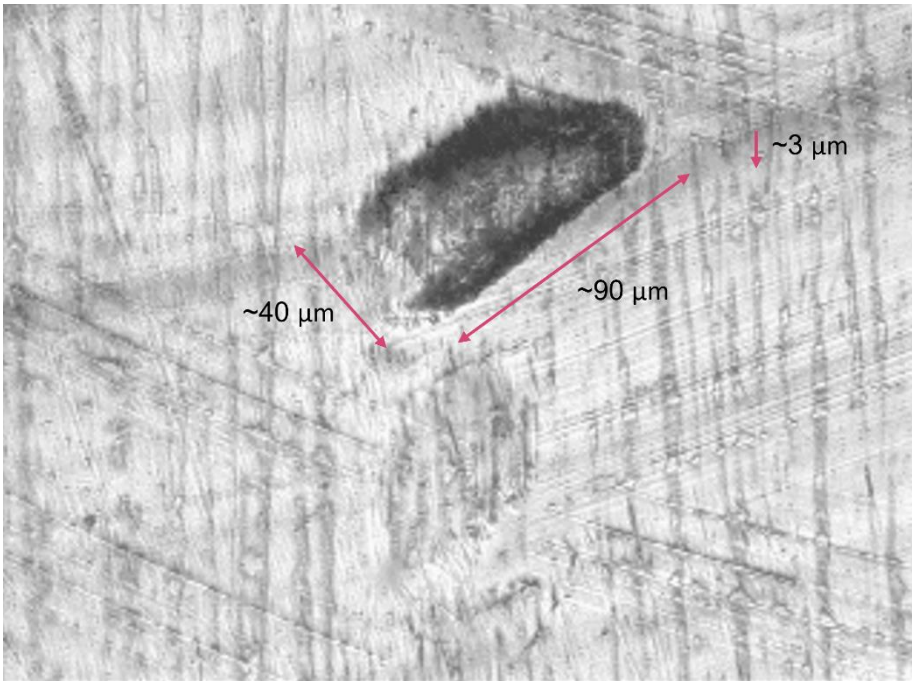

*Figure 5.5. Zygo intensity map of **BOX** talar component bearing surface showing the approximate dimensions of a typical identified pit. Length 90 µm, width 40 µm, depth 3 µm.*

The proportion of tibial and talar components with pitting was similar regardless of bearing type, fixed or mobile, suggesting that bearing constraint is not a factor affecting the likelihood of pitting of the metallic articulating surfaces occurring. The component alloy, on the other hand, may be an influencing factor. While the vast majority of talar components are manufactured from CoCr alloy, with all but one of those included in the present study being so, the tibial components are typically manufactured from either CoCr or Ti alloy. For the tibial components specifically, pitting was observed on those that were CoCr alloy only, with 63% of the CoCr alloy tibial components exhibiting pitting; none of the Ti alloy tibial components had pitting damage. It should be noted, however, that the group of CoCr alloy components analysed was substantially larger than the group of Ti alloy components (19 versus 4, excluding Ti coated with TiN (n = 1)).

Pitting of metallic TAR components has also previously been reported by Vaupel et al., though with a lower prevalence.[145] Of 9 Ti alloy tibial components analysed, scratching was observed on 7 (78%), and pitting on 1 (11%).[145] Of 10 CoCr alloy talar components analysed, scratching was observed on 6 (60%), and pitting on 6 (60%).[145] These findings are similar to those from the present study in that a greater proportion of talar components exhibited pitting compared to tibial components. Whilst overall, Vaupel et al. observed pitting of the metallic components

less frequently than the present study, there are possible explanations for these variations. Firstly, the different TAR models could play a role, as Vaupel et al. analysed one particular fixed bearing TAR design (Agility); a no longer used device which did not feature in the present study. Furthermore, it is possible that the lower proportion of tibial components with pitting specifically reported by Vaupel et al. may be explained by the composition of the components being Ti alloy, as the findings from the present study suggest that pitting may be more likely to occur on CoCr alloy tibial components compared to those of Ti alloy.

Whilst none of the Ti alloy tibial components exhibited pitting, abrasive changes were identified on the articulating surface of one, from an INFINITY TAR. These abrasive changes were indicative of micromotion occurring at this interface (i.e., between the backside of the PE insert and the inferior surface of the tibial component). In fixed bearing TKRs, micromotion between the PE insert and tibial tray components (both of which are similar in design to that of TARs), can cause backside wear of the PE insert, which may then go onto cause osteolysis.[163, 164] The surface roughness of the tibial component has been reported to influence the extent of the PE backside wear.[163] This is consistent with the findings from the present study, as the INFINITY tibial components had the highest measured average surface roughness of those analysed. Similarly, the changes in reflectivity observed on the majority of the porous coatings on the non-articulating surfaces of the metal tibial and talar components may also be indicative of micromotion, though in this case occurring between the bone-implant interface. The literature reports that bony ingrowth into a porous coating is highly dependent on achieving sufficient stability such that relative motion between the prosthesis and surrounding bone is eliminated.[15] The identified signs of micromotion occurring here therefore suggests that initial osteointegration may not have been achieved to a sufficient extent.

Changes to the non-articulating surfaces indicative of coating loss was identified for the vast majority of the metal tibial and talar components. As well as visual inspection of the non-articulating surfaces finding the removal of coating, the identification of Ti particles embedded in the PE inserts also suggests coating removal. This has also previously been shown with AES TARs. In a study of 6 AES mobile bearing TARs explanted during osteolysis, Cottrino et al. reported the presence of Ti particles embedded on the talar component bearing surfaces, as well as in retrieved periprosthetic tissue.[64] Since the implant metallic components were both composed of a CoCr alloy, these Ti particles were assumed to have originated from the coating (double coated Ti plasma spray and HA).[64]

The AES prosthesis previously had a HA coating, however in 2004 it was replaced with the porous coating of Ti along with HA, a change which resulted in increased incidence of osteolysis.[61] In a series of 130 AES TARs, Koivu et al. found the risk of osteolysis to be over 3 times higher for implants with the Ti-HA coating compared to the HA coating.[61] Furthermore, the osteolysis cases observed were more severe after the design change.[61] For AES implants with Ti-HA coating, SEM-EDX analysis by Koivu et al. revealed Ti and CoCr particles in periprosthetic tissue samples, with the amount of Ti high compared to that of the other metals present.[61] Although osteolysis following TAR is most commonly attributed to PE wear debris, studies have indicated that the inflammatory reaction may also be in response to other particles such as those which are metallic.[63] Therefore, the implant-derived Ti particles, reported previously with the AES prosthesis, may increase the risk of osteolysis occurring due to the associated inflammatory response to the particles, and therefore may in part explain the high prevalence of osteolysis following TAR which has been described.[18, 64]

In this cohort of explants, there was no substantial difference between those with a double coating of Ti and HA compared to those with a single layer HA coating only, in terms of changes in coating observed or the proportion of talar components with sliding plane scratching. However, the proportion of tibial and talar components exhibiting pitting was higher for devices double coated with Ti and HA (80% and 100%, respectively) compared to those with HA coating only (33% and 67%, respectively). When taking the layers of coating as a whole, by comparing double coatings of any type with single coatings of any type, no significant differences were seen between the proportion of each showing coating loss either.

Whilst the AES prosthesis was withdrawn in 2009 following complication rates higher than expected,[62] findings of embedded Ti debris from the present study extends the issue of coating removal, and therefore the potentially increased risk of implant failure due to periprosthetic bone resorption caused by the immune response to these particles, to various other contemporary TARs.

The metal components with a coating of Ti beads represented the highest proportion with changes to the coating, followed by those with a HA only coating, a double coating of Ti and HA, a Ti only coating, and finally those with a double coating of Ti and CaP represented the lowest proportion with half exhibiting coating changes. Ti is used in most of the porous coatings present on the non-bearing surfaces of the TAR metallic components. Apart from the BOX prosthesis, which has a HA plasma spray coating, all of the other TARs included in the

present study had a coating containing Ti, whether that be alone as a single coating or as one layer of a double coating. For the TARs in which embedded metallic debris was identified in the PE insert, the porous coatings all contained Ti. Like the AES, the Hintegra prosthesis, of which embedded debris was identified in two, had a double coated Ti plasma spray and HA coating, both the Salto Talaris and INFINITY implants had a Ti plasma spray coating, and the Mobility had a coating composed of Ti sintered beads. The different TAR models included with each of these coating types are given in Table 5.1, and examples pictured in Figure 5.6. For three of the coating types, only one model of TAR utilised them within this study.

Ti beads	**HA**	**Ti + HA**	**Ti**	**Ti + CaP**
Mobility	BOX	Hintegra, STAR	INFINITY, Cadence, Salto Talaris, Salto	Zenith

Table 5.1. The TAR models with each coating type.

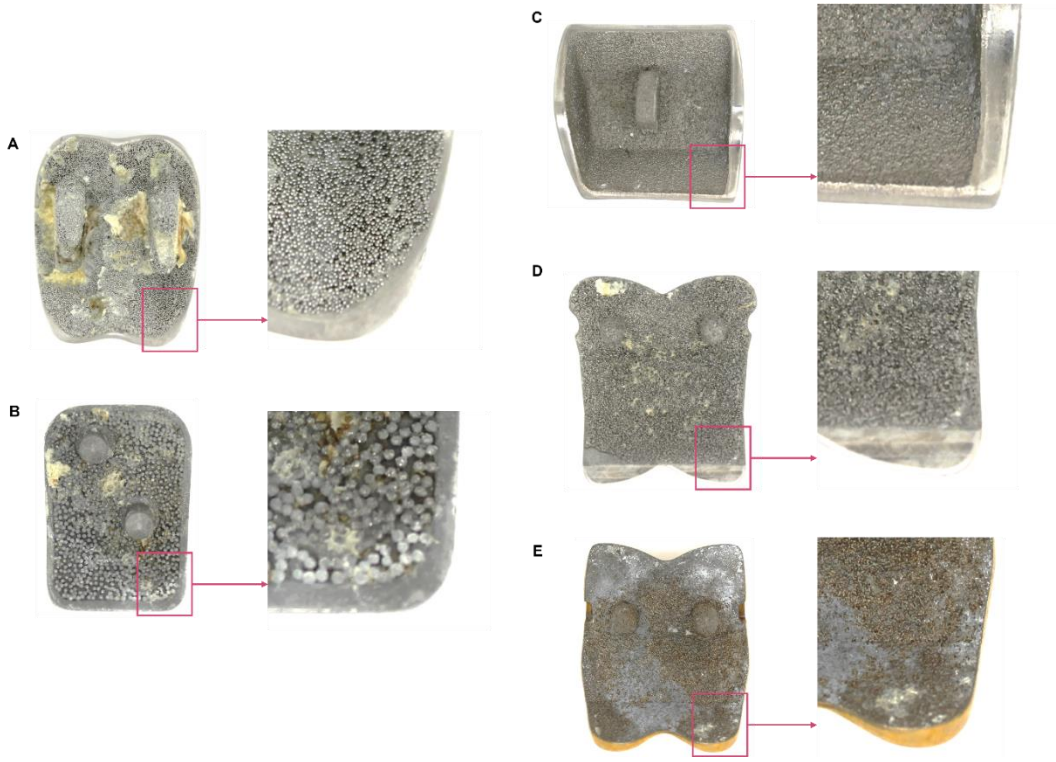

Figure 5.6. Examples of the different coating types on explanted talar components. (A) Ti beads (Mobility). (B) HA (BOX). (C) Ti + HA (STAR). (D) Ti (INFINITY). (E) Ti + CaP (Zenith). A-B are beaded coatings and C-E are non-beaded coatings.

The literature on the effect of different types of coatings for TARs is very limited. For hip replacements, however, beaded coatings have been reported to result in a better osseointegration and a reduced incidence of osteolysis.[61] Analysis of the cohort of explanted TARs within the present study is in agreement with this. When comparing beaded (Ti or HA) versus non-beaded coatings, a significant increase was seen in the proportion of metallic components with signs of coating loss for those with beaded coatings compared to those with non-beaded coatings.

Of the TARs with talar components exhibiting sliding plane scratching, indicative of the presence of hard third body particles at the bearing, all but two also exhibited coating loss from the non-articulating surfaces of the corresponding tibial and/or talar components. For the two cases which didn't, one (Hintegra) had evidence of severe direct MoM contact occurring between the metal tibial and talar components, along with a PE insert which was broken into two pieces and which had high amounts of embedded debris, identified as containing CoCr. For this case specifically, analysis suggests that failure was caused by PE insert fracture rather than the effect of coating loss leading to instability and third body debris damage. The other (Mobility) prosthesis had cement present on the talar component, with the tibial component not received and therefore the coating unable to be analysed. Similarly, for all TARs with metallic pitting of the articulating surfaces of the tibial and/or talar components, coating loss was also identified on one or more of the metal components except for the same two prostheses. These findings suggest that damage to the articulating surfaces of the metal components in the form of pitting and scratching may be caused by particles from the coatings of the non-articulating surfaces of these components acting as third body debris.

Since only two of the analysed TARs had used cement for fixation, cement particles were not likely to be a primary source of third body debris causing damage in this cohort of explanted prostheses. Rather, the findings suggest that particles from the porous coatings – the fixation method for the uncemented metal components – instead are more likely to be a primary cause of the observed damage to the articulating surfaces of the components by acting as third body debris at the articulations.

5.2. PE Form Analysis

PE wear at the bearing is inevitable from normal use of a MoP prosthesis, with this being the only 'intended' mode of wear in a well-functioning device.[165] Despite this, and the fact that PE wear has historically been associated with osteolysis-related failures, research into the amount of wear produced remains limited. To the best of the author's knowledge, no previously published studies have quantified volumetric wear from explanted TARs, with wear results instead coming from a limited number of simulator studies. Within the current study, volumetric wear was measured from the PE insert, therefore providing insights into the wear performance of TARs *in vivo* as well as enabling comparison with reported wear rates from *in vitro* studies.

5.2.1. CMM wear analysis

From the CMM analysis of PE insert bearing surfaces, the volumetric wear measured ranged from 0.08 mm^3 to 6.98 mm^3 (average 1.69 mm^3). The amount of material removed during the first round of the validation process (17.60 mm^3) in the first stage alone was therefore a gross overestimation of the amount of wear actually generated *in vivo*. Whilst the volumetric wear values generated from the CMM analysis and gravimetric analysis diverged at higher wear volumes (particularly beyond the second wear stage), with the corresponding percentage errors increasing with each wear stage, the margin of accuracy at lower wear volumes (1.29 mm^3 for the first wear stage) was comparable to the 1 mm^3 value which has previously been argued as being a clinically relevant margin of accuracy for MoP joints.[139] For the second round of validation, lower amounts of material were removed. Again, similar results were found in that differences between the CMM and gravimetrically measured wear volumes diverged as the amount of material removed increased. The first wear stage, where 4.62 mm^3 of removed (i.e., aligned to that which would be realistically expected from the explanted components), the absolute error from the CMM analysis was 1.64 mm^3; similar to that for the first wear stage of the first round of validation and also that which has been proposed as being an acceptable margin of accuracy.

For both rounds of validation, it was thought that the CMM analysis underestimated the amount of wear due to the probe being unable to fully trace the area of material removed, as the drill attachment created fairly sharp depressions, with this being particularly pronounced for the higher areas of wear. Since the values were comparable for amounts of wear which were

relevant to TAR PE inserts, this CMM method was deemed as being appropriate to use for quantification of PE volumetric wear from explanted TARs within the present study.

5.2.2. Bearing wear

CMM analysis was achievable for the bearing surfaces of 18 PE inserts. This represents the largest known cohort of TARs for which volumetric wear has been measured (with the published simulator studies described in the Literature Review (chapter 2) each including fewer samples). Relatively low levels of volumetric wear were measured from the bearing surfaces of the PE inserts (average 1.69 mm^3, range 0.08 mm^3 to 6.98 mm^3). The wear rates reported by the previously published TAR simulator studies ranged between 1.2 and 25.8 mm^3/million cycles, with the majority reporting figures between about 10 and 20 mm^3/million cycles. Taking 1 million cycles as equivalent to approximately 1 year *in vivo*, these values can also be thought of in terms of mm^3/year.

All except one of the TARs for which implantation side was known had greater volumetric wear measured on the lateral aspect compared to the medial aspect (Figure 5.7). This pattern could suggest that load is not distributed evenly across the PE insert. Asymmetric wear was also commonly seen across the analysed PE insert bearing surfaces, with one condyle having on average, over three times the amount of wear than the other, with this difference being up to over ten-fold for the most extreme case seen.

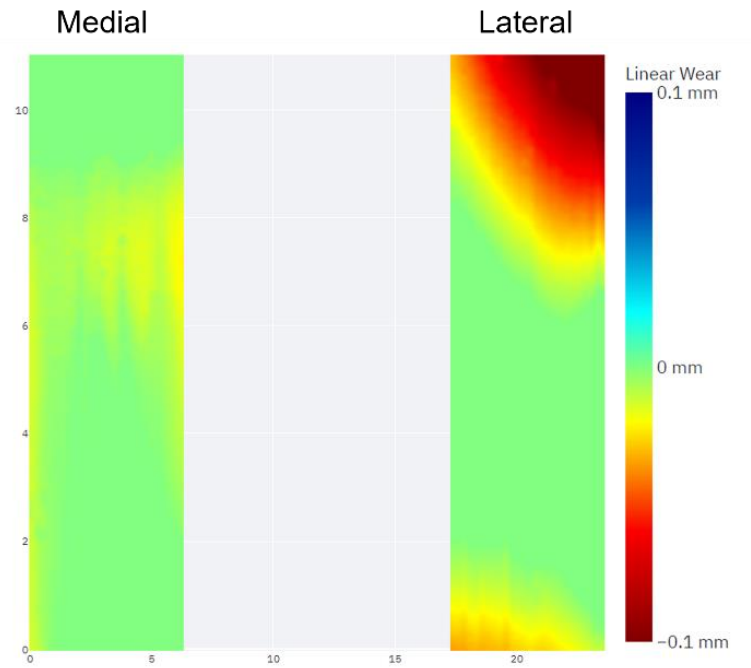

Figure 5.7. Linear wear map (scale -0.1 mm to 0.1 mm) from CMM analysis of a mobile bearing left Hintegra (ANK27) TAR PE insert bearing surface. Red indicates material removed and blue indicates material added.

It was also seen that fixed bearing PE inserts had a greater average wear volume on average than those of mobile bearing constraint. However, it should also be noted that mobile bearing TARs will most likely produce greater wear at the PE insert backside surface due to the articulation at this interface, as also shown by the increased wear-related damage scored on the backside surfaces of mobile bearing compared to fixed bearing PE inserts.

5.2.3. Backside planicity

CMM analysis was achievable for the backside surfaces of 13 of the PE inserts. Based on the backside geometry maps, no clear pattern could be identified visually in terms of locations of surface deviation. However, deviations extending superiorly in anatomical sense (represented by blue on the geometrical maps) were seen more frequently than areas of material removed (represented by red on the geometrical maps). These surface deviations are illustrated in Figure 5.8. This finding therefore suggests that it is deformation, rather than wear, that is occurring more frequently on the backside surfaces of the PE inserts.

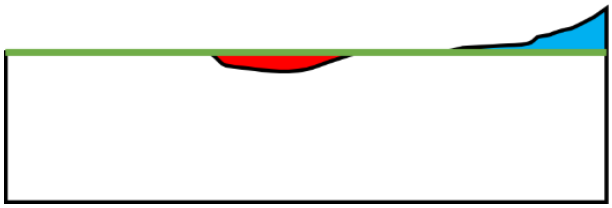

Figure 5.8. Schematic of a PE insert from a coronal plane view showing exaggerated backside surface deformation. Material removed (anatomically inferior deviations) in red, material added (anatomically superior deviations) in blue, and the flat surface in green.

The current literature is limited in terms of form analysis of TAR PE insert backside surfaces, and therefore there are no known published values specific to ankles with which to compare those found in the present study. The majority of the planicity values fell between 47.2 µm and 220.8 µm (with the exception of one Hintegra with a planicity of 916.2 µm). These values are not dissimilar from those which have previously been reported for the backside surfaces of PE components from knee replacements (averages of between 83 µm and 266 µm, depending on design).[158] The PE inserts on which surface deformation had previously been visually (macroscopically) identified recorded relatively high planicity values, as would be expected.

Normal ranges of planicity/deviations have not been established for TARs, and as such the implications of such surface changes are not currently understood.[166] The findings from the present study do however indicate that anatomically superior deviations of the surface are common on the backside surfaces of various mobile bearing TAR PE inserts.

5.3. Fixed versus Mobile Bearing

Despite fixed bearing TARs seeing a substantial increase in implantation rates compared to mobile bearing devices in the UK in recent years, there remains debate regarding the superiority of either option of bearing constraint within the literature. Theoretical advantages relating to the wear have been described within the literature for each,[167] although only one of the limited published TAR explant analysis studies has compared fixed and mobile bearing designs.[15] Said study, by Currier et al., did not compare the damage analysed from the fixed and mobile bearing TARs, but rather just the frequency of loosening leading to revision occurring. Within the current explant analysis study, the influence of bearing constraint on the damage observed was analysed throughout in terms of damage being more likely or more severe on the components from either fixed bearing or mobile bearing devices.

5.3.1. Damage modes

The proportion of metallic components on which changes to the non-articulating surfaces indicative of coating loss was identified was lower for components belonging to fixed bearing TARs than those belonging to mobile bearing TARs (73% versus 81%, respectively). This difference was attributed to the talar components; the proportion of fixed and mobile bearing tibial components with coating loss was the same (83%), whereas the proportion of talar components with coating loss was 60% for those corresponding to fixed bearing prostheses compared to 79% for those corresponding to mobile bearing prostheses. It should be noted that all of the tibial and talar components from fixed bearing TARs had a non-articulating surface coating of Ti, whereas the those from mobile bearing TARs had a range of different coating types (including Ti also). However, as the influence of coating type was investigated in the previous chapter (section 4.1.2), and the proportion of components with a Ti coating exhibiting changes (69%) was within the range of that for different coating types (50% to 94%), the difference in the proportion of metal components from fixed and mobile bearing TARs exhibiting coating loss is therefore not thought to be just down to the coating type.

In general, the proportion of explanted components on which various surface damage modes were identified was either similar for those from fixed bearing and mobile bearing TARs, or with the latter exhibiting damage more frequently and/or severely. This was the case for macroscopically visible sliding plane scratching of the talar component bearing surface, indicative of the presence of hard third body particles at the bearing; identified in 84% of components from mobile bearing TARs compared to 60% from fixed bearing TARs. This difference corresponds with that seen in the proportion of metallic components – specifically talar components – exhibiting signs of coating loss, with this being more prevalent in those from mobile bearing TARs. This agrees with other findings of the present study which suggest that third body particles from the porous coatings have caused damage *in vivo* by acting as third body particles.

Similar findings did not extend to the metallic pitting identified, however. Pitting was observed less frequently on the talar components but more frequently on the tibial components of mobile bearing TARs (95% and 56%, respectively) compared to those from fixed bearing TARs (100% and 50%, respectively). However, both of these differences are marginal, and so these findings

suggest that bearing constraint is not likely to be a factor influencing the likelihood of metallic pitting occurring.

Differences in the proportion of backside surfaces of fixed and mobile bearing PE inserts exhibiting damage in the form of burnishing was observed, with this identified on a higher proportion of those from mobile bearing TARs. This is as expected, since burnishing represents a polished effect indicative of repetitive articulation between surfaces, which is allowed to occur with mobile bearing devices whereas the constrained nature of fixed bearing devices prevents this. Perhaps surprisingly, the proportion of tibial component inferior surfaces on which pitting was identified was similar for those from both fixed and mobile bearing TARs. Given that the locking mechanism of fixed bearing TARs is designed to prevent motion occurring at the interface between the tibial component and the PE insert backside surface, it would follow that less damage would be expected to occur on these surfaces. Scratching on the bearing surface of talar components was also identified more frequently on those corresponding to mobile bearing compared to fixed bearing prostheses. On the other hand, a higher proportion of the bearing surface of PE inserts corresponding to fixed bearing TARs exhibited burnishing and striations compared to those from mobile bearing TARs. Although the bearing constraint of a TAR does not directly affect the bearing comprised of the talar component and PE insert bearing surfaces, these findings indicate that it may have some effect on the damage incurred at the bearing.

All of the PE inserts which were found to be not intact (i.e., had fractured into pieces or had part broken off) were of mobile bearing design. Correlating with this, all of the TARs for which evidence of unintended direct metal-on-metal contact was identified were also of mobile bearing design. The fact that these gross damage mechanisms were observed on mobile bearing TARs only is unsurprising given that the unconstrained nature of the designs would suggest that PE insert migration is more likely to occur than in those where this component is fixed in place.

The explanted mobile bearing PE inserts were also found to have greater surface damage on the backside, for which the component damage scores – which account for both the area covered and the severity of the damage to the component surface – were significantly higher on mobile compared to fixed bearing components, with this being the only statistically significant difference between the surface damage scores of components from fixed and mobile bearing TARs. This difference in the damage to the PE insert backside found was as expected,

since the nature of mobile bearing PE inserts means that they are unconstrained and so free to move against the articulating surface of the corresponding tibial component, whereas this level of movement is not permitted by fixed bearing devices.

The volumetric wear from the bearing surfaces of the PE inserts was higher on average on those from fixed than mobile bearing TARs, although volumetric wear rates could not be calculated due to unknown implantation durations.

5.3.2. Surface profilometry

The articulating surfaces of fixed bearing tibial components were rougher than those of mobile bearing components, for both unworn and worn areas. Specifically, the parameters of S_a, S_q, S_z, S_p, and S_v were all significantly greater on fixed bearing compared to mobile bearing tibial components. S_{ku}, on the other hand, was significantly higher on mobile bearing compared to fixed bearing tibial components, with this again being true for both unworn and worn areas. A high S_{ku} indicates the presence of exceptionally high peaks or deep valleys comprising the surface. In this case, it is most likely referring to valleys, as the skewness of pitted areas of tibial components was significantly more negative for mobile bearing components than for fixed bearing components. This negative skewness is indicative of a predominance of valleys, in terms of more severe valleys or a greater number of valleys, rather than peaks. In contrast, the skewness of unpitted areas of the same components was more negative for fixed bearing components compared to mobile bearing components. While this difference did not reach statistical significance, the change seen between the unpitted and pitted measurements suggests that mobile bearing tibial components may undergo more extreme changes to the surface topography than fixed bearing tibial components.

For the talar component bearing surfaces, differences between the surface roughness of those from fixed and mobile bearing TARs were not so clear. The measured values for S_a S_q, and S_p were all significantly higher on unworn areas of talar components corresponding to mobile bearing TARs compared to those corresponding to fixed bearing TARs, indicating a greater roughness for the former. On the other hand, the S_{ku} was significantly higher on unworn areas of talar components from fixed bearing than mobile bearing TARs, with the former also having a significantly more negative S_{sk}; together indicating a predominance of exceptionally deep valleys. More differences were seen for the worn areas too, as the S_v and S_{ku} was significantly higher on worn areas of talar components from fixed bearing than mobile bearing TARs, with

the former also having a significantly more negative S_{sk}. The S_p, on the other hand, was significantly higher on worn areas of talar components corresponding to mobile bearing than fixed bearing TARs. For the talar components with pitting (which was all except one), the pitted Sv was significantly higher on those from fixed bearing TARs compared to those from mobile bearing TARs, indicating that pitting may have been more severe (i.e., deeper) for these designs. No significant differences were identified in the S_a of worn areas of talar components from fixed and mobile bearing TARs.

It was expected that differences in the surface topography would be seen between tibial component of different bearing constraints, as mobile bearing devices are designed for articulation at this interface, whereas fixed bearing devices are not. Furthermore, the fixed bearing tibial components had more of a range of compositions (two-thirds being Ti alloy and one-third being CoCr alloy), whereas all but one of the mobile bearing tibial components were CoCr alloy. The talar components were almost exclusively CoCr alloy, regardless of the bearing constraint of the TAR. The fact that unworn areas of talar components from mobile bearing TARs than those from fixed bearing TARs would suggest that the metallic bearing surface roughness may not be directly correlated with PE bearing wear as previously thought, as the fixed bearing PE inserts within the present study were found to have higher bearing wear volumes than their mobile bearing counterparts (although, again, lack of implantation durations means than wear rates remain unknown).

5.3.3. Summary

As fixed bearing devices are implanted in much higher rates than mobile bearing devices in the UK (about a four-fold difference), it is important that any influence of bearing constraint on the performance of TARs is considered.

Overall, mobile bearing TARs were generally associated with greater damage than fixed bearing TARs in terms of porous coating loss, talar bearing surface sliding plane scratching, PE insert backside surface damage, and PE insert fracture. However, greater wear volumes were measured on the bearing surfaces of fixed bearing compared to mobile bearing PE inserts, although this was relatively low for both. Other damage modes, for example metallic pitting, was identified on similar proportions of components from both bearing types.

The only published TAR explant analysis studies identified in the Literature Review (chapter 2) to include both fixed and mobile bearing devices was that by Currier et al.[15] Loosening was

suggested to be more of an issue in fixed than mobile bearing prostheses in the analysed cohort, with it occurring more frequently and after a shorter time *in vivo*. For both bearing constraints, loosening was primarily attributed to lack of substantial bony ingrowth. This study did not include any other comparative analysis of damage of fixed versus mobile bearing components, however. The effect of bearing constraint on damage modes of explanted TARs is therefore a topic for which the existing literature is limited. The present study did identify some differences in the damage identified between explanted components of the two bearing types, warranting further research.

It should also be noted that two-thirds of the fixed bearing tibial components were Ti alloy, with the remaining one third being CoCr alloy, whereas all but one (94%) of the mobile bearing tibial components were CoCr alloy. Consideration should therefore be given as to whether observed differences between TARs of different bearing constraint are actually reflective of component alloy, or vice versa, or a combination of both factors.

In one of the fixed bearing devices, evidence of micromotion occurring at the interface between the PE insert backside surface and tibial component inferior surface was identified, indicated by abrasive changes to the tibial component inferior surface in an arc pattern. This finding suggests that rotational movement can occur at this interface in fixed bearing devices. However, substantially greater damage seen on the backside surfaces of PE inserts belonging to mobile bearing TARs compared to those from fixed bearing TARs indicates that the bearing constraint does impact the amount of damage incurred by the devices. Additionally, the evidence of direct contact between the metal tibial and talar components seen in some of the mobile bearing TARs suggests that the bearings of these designs are more mobile than those of fixed bearing constraint, in that the component can migrate such that it is no longer preventing the unintended MoM contact from occurring. Overall, these findings point towards mobile bearing TARs being more prone to suffering from gross damage to the PE insert.

5.4. Failure Mechanisms of TARs

Based on the discussion contained within the preceding sections of this chapter, the failure mechanisms of the contemporary TARs included in this explant analysis study may be proposed. The identified damage features are discussed in relation to wear modes as defined in the literature as well as the implications in terms of TAR failure. Various design factors may also contribute to the failure of TARs, such as material selection and bearing constraint,

amongst others. By considering these, suggestions for methods to potentially avoid or reduce the risk of TAR failure can be suggested.

5.4.1. Wear modes

McKellop defines four modes of wear relating to polyethylene components of joint replacements (Table 5.2), with these four modes referring to the surfaces which are in contact and so producing the wear.[165] Wear mode 1 is an inherent product of the intended use of the prosthesis from articulation of the two primary (bearing) surfaces. Wear modes 2, 3, and 4, on the other hand, are unintended and represent a prosthesis which is functioning outside of its intended use. The aim of the designer and surgeon of a prosthesis is always to minimise wear mode 1 and avoid completely wear modes 2, 3, and 4. Within the cohort of explanted TARs analysed in the current study, evidence of all four wear modes having occurred *in vivo* was identified.

Wear mode	Contacting surfaces	Description	Example
1	Primary-on-primary	Intended	MoP bearing (talar against PE bearing)
2	Primary-on-secondary	Unintended	Metal-on-metal (talar against tibial)
3	Primary-on-primary with third bodies	Unintended	Third body particles at bearing (e.g., from cement, coating etc.)
4	Secondary-on-secondary	Unintended	Backside wear (PE backside against tibial)

Table 5.2. Wear modes of a joint replacement as defined by McKellop.[165]

Wear mode 1 – the only intended of McKellop's defined wear modes – refers to wear from the bearing. In the case of TARs, this is the MoP bearing comprised of the bearing surfaces of the metal talar component and the PE insert. In the present study, volumetric wear loss of the PE insert bearing surfaces was quantified, and the damage modes of pitting, scratching, burnishing, and striations were also frequently identified on these PE insert bearing surfaces. PE pitting in

particular has previously been described as a form of fatigue damage[168] and is indicative of this bearing wear mode having occurred *in vivo*.

The second of the wear modes refers to contact between a primary (bearing) surface and a secondary (non-bearing) surface. This was evident in the TARs where it was determined that unintended direct metal-on-metal (MoM) contact between the tibial and talar components had occurred *in vivo*. In the cases of MoM contact identified in the present study, this phenomenon was associated with severe damage to the PE insert. It may also be caused by migration of the PE insert, however, such that this component is no longer preventing contact from occurring between the two metal surfaces. This effect has previously been described in TARs by Stratton-Powell et al., who reported that just over half of the PE inserts analysed exhibited edge loading – defined as *"a depressed area in the insert surface indicative of articulating with the edge of the tibial component"* – based on visual analysis.[166]

Evidence of wear mode 3 – primary-on-primary bearing surfaces with third bodies also present – having occurred was seen by the talar sliding plane scratching identified in the majority of the explanted TARs. This damage was indicative of the presence of hard third body particles at the bearing, determined to most likely have originated from the porous coatings of the metal components. Further evidence of this wear mode was seen with the embedded metallic debris which was identified on some PE insert bearing surfaces (as well as backside surfaces).

Finally, the fourth wear mode, referring to wear as a result of contact between two non-bearing surfaces, was seen at two points of contact: at the bone-implant interface, and at the articulation comprised of the PE insert backside surface and the tibial component inferior surface. Particulate coating loss was identified on the non-articulating surfaces of the metal components, indicative of micromotion at the bone-implant interface. Particulate debris from the coating may then also migrate to the bearing, therefore causing wear mode 3 to occur concurrently by acting as third bodies. The identified coating loss suggests instability of the implant due to insufficient fixation via bony ingrowth at the bone-implant interface, with the possibility then of device failure with the need for revision due to aseptic loosening. Evidence of micromotion was also identified at the interface between the tibial component inferior surface and PE insert backside surface in one (17%) of the fixed bearing TARs, with the identification of abrasive changes to the tibial component. Again, this may be indicative of instability of this interface. In mobile bearing TARs, where the PE insert is unconstrained and so free to articulate against the tibial component, planicity indicating deviation of the backside

of the PE inserts was quantified. Damage identified on the backside surfaces of PE inserts from mobile bearing compared to fixed bearing TARs was significantly greater, indicating that, as expected, wear is increased on this surface in mobile bearing designs.

5.4.2. Adverse response to implant-derived debris

Implant-derived particulate debris is known to cause adverse inflammatory responses *in vivo*, causing a reaction which can lead to failure of the implant via osteolysis and aseptic loosening. Whilst the literature reports osteolysis as having a high prevalence amongst TARs, the underlying mechanisms are not yet fully understood.[97] Multiple factors can contribute to the development of periprosthetic osteolysis, including body weight, activity level, age, fixation, and immune response.[97] However, osteolysis is known to occur as a result of an immune response to implant-derived wear debris, hence the term 'wear-induced osteolysis'.[63] Implant-derived debris may be attributed to a range of sources including the bulk material of the metal and polyethylene components, and the porous coatings (or cement particles in cemented devices), all of which may have the potential to cause adverse responses leading to implant loosening. Figure 5.9 illustrates these possible sources of particulate debris release.

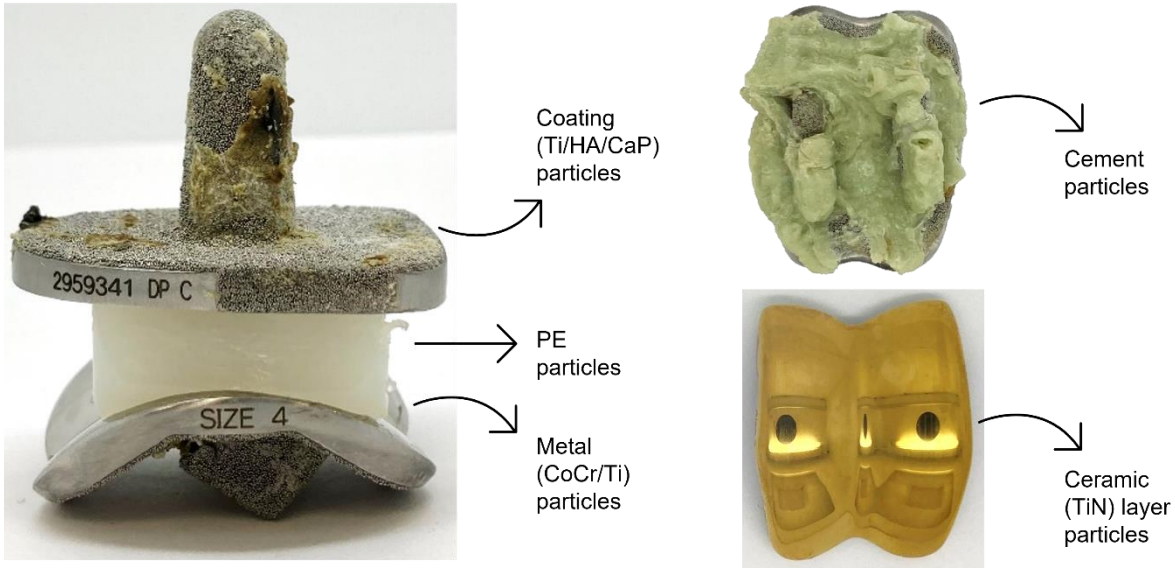

Figure 5.9. Potential sources of particulate debris release from TARs.

Of these potential sources, wear from the PE bearing surface is the only one which is intended, as bearing wear (i.e., wear mode 1 as defined by McKellop) is an inevitable product of normal day-to-day use of a prosthesis. It follows, therefore, that the majority of the published literature on TAR failure has focused on the PE wear. However, as discussed in the previous section, damage corresponding to all four wear mechanisms was frequently identified in this cohort of explanted TARs. It is therefore likely that implant-derived debris from a variety of sources may be surrounding the implant at a given time. Indeed, this has been shown to be the case, with a study of TAR periprosthetic wear debris by Stratton-Powell et al. reporting that 90% of the analysed samples contained at least 3 different types of particles from the 6 identified (UHMWPE, CaP, CoCr alloy, commercially pure Ti, Ti alloy, and SS).[149] It is therefore important to consider the potential responses to these different types of debris released *in vivo*; namely, from PE wear particles, metal from the tibial and talar components (CoCr and/or Ti), and coating particles.

Although wear-induced osteolysis has been more frequently attributed to that derived from the PE component, debris from other sources, for example metal particles, may also incite this adverse response.[63] The osteolytic potential of UHMWPE wear debris from MoP joint replacements is well documented in the literature; for TARs specifically, Schipper et al. found that osteolytic areas had an abundance of PE wear particles present.[18] However, in a different TAR study, Koivu et al. did not attribute osteolysis to PE wear particles only, instead concluding that it may also be caused by HA particles causing third body wear or directly incited by metal particles.[61] Furthermore, Ti particles were reported to enhance the osteolytic potential of macrophages by stimulating the release of pro-inflammatory mediators of these cells, even more so than that of PE particles.[61]

Metal hypersensitivity – an immune disorder – is also known to be a potential issue in hip and knee replacements containing CoCr, however the research of this in relation to TARs is relatively limited.[169] Metal hypersensitivity has been reported to be more prevalent in patients with total joint replacements than in the general population (10 to 15%).[170] Furthermore, this prevalence was even higher in patients with failed or poorly functioning prostheses (60%) compared to those with well-functioning prosthesis (25%).[170] These figures therefore indicate that metal hypersensitivity should be a factor for consideration regarding total joint replacement, whereas it is currently perhaps an under recognised issue.

For CoCr also, the associated complication of ALVAL may be caused by wear debris of this nature.[19, 120, 122, 171] Individual variation of HLA genotype has been shown to influence susceptibility to developing this metal hypersensitivity response, meaning that relatively low blood Co concentrations (< 2 μg/l) are sufficient to incite an adverse inflammatory response in some patients.[19] This is substantially lower than the MHRA recommended threshold of 7 μg/l as an indicator of an adverse reaction, and furthermore does not account for individual variance in tolerance.[19] It has also been reported that patient sex can influence the likelihood of developing a metal hypersensitivity response, with females at an apparently greater risk.[19]

Despite this, CoCr alloy components are used in most TARs, with almost all talar components in particular being of this composition. Of the TARs included within the present study, only the Zenith prosthesis did not have any CoCr components. Given that damage to the talar components in terms of sliding plane scratching as well as pitting indicative of material loss was identified in the majority of metal components, and that this was found to be more likely to occur on CoCr than Ti components, CoCr metal debris release is a potentially concerning issue for contemporary TARs.

Since the amount of metal debris released was not quantified in the present study, it cannot conclusively be stated whether there are sufficient amounts to trigger a response. However, given that relatively low blood Co concentrations have been shown to incite an adverse response in some patients who are predisposed to a metal hypersensitivity, combined with the metal debris release originating from multiple sources identified in the present study, it seems likely that an adverse response could be triggered by this. The high frequency of analysed TARs exhibiting metal debris release therefore provides a cause for concern.

Unexplained pain is known to be common following TKR, affecting between 5-30% of patients[126-128] and a direct association between the presence of ALVAL and patient reported pain levels has been shown.[123-125] Pain following TAR may also be a problem, with a reported up to two thirds of patients experiencing residual pain.[129] Whilst pain may be due to other causes such as malalignment of components or infection, in other cases the pain can be unexplained.[129] It is possible that the metal release demonstrated by the present study could be a potential cause of pain following TAR.

5.4.3. Influencing factors

Male sex has previously been linked with a greater PE insert backside damage score by Brandt et al. in TKRs.[172] The findings from the present study corroborated with those by Brandt et al., as greater damage was generally identified on components corresponding to male compared to female patients. Specifically, the average wear volume from the bearing surfaces of the PE inserts, as well as the component damage scores from both the bearing and backside surfaces of the PE inserts as well as the tibial component inferior surfaces were higher on average on those from male patients than those from female patients. The component damage scores for the talar component bearing surfaces, on the other hand, were higher on average on those from female patients than those from male patients. It should be noted however that none of these differences reached statistical significance. Brandt et al. explained the influence of patient sex by linking males with having a higher body mass and activity level than females, therefore resulting in increased PE wear.[172] As these patient characteristics were not known for the cohort included in the present study, this conclusion could not be investigated for explanted TARs.

A systematic review and meta-analysis by Arcângelo et al. identified a significant positive association between the presence of periprosthetic bone cysts (i.e., osteolysis) and TARs which were mobile bearing, HA coated, non-tibial stemmed, and non-atomically configured.[88] While the present study did not have access to reason for revision (i.e., whether osteolysis occurred or not), a potential influence of these design features can be discussed in terms of wear-related damage incurred (which potentially may have led to osteolysis). However, it is important to note that the implantation duration was not known for the majority of the TARs included in the present study, nor were patient characteristics such as activity level which would likely influence the degree of wear.[173]

As discussed in section 5.3 of this chapter, the explanted mobile bearing TARs analysed did, in general, exhibit certain damage modes more frequently than their fixed bearing counterparts. Specifically, this was the case for damage to the PE insert backside surfaces, as well as metallic components with porous coating loss, and, corresponding with this, talar components with bearing surface sliding plane scratching. These findings from the present study indicate that mobile bearing designs may be more susceptible to wear damage than fixed bearing designs, therefore agreeing with the conclusion by Arcângelo et al. et al. that bearing constraint may be a factor influencing the clinical performance of TARs.

Three of the TAR designs included in the present study had coatings which contained HA: the BOX prostheses with a HA coating and the Hintegra and STAR prostheses with a double coating of Ti and HA. Eighty-one percent of the coatings which did not contain HA showed signs of loss, compared to 75% of those containing HA (83% of HA only and 70% of double coated Ti and HA). These differences were not significant; rather, in the present study, the main difference in loss of different coatings was seen with beaded versus non-beaded types.

Within the present study, two of the designs of TARs included had tibial components which were stemmed: the Mobility and the Zenith (Figure 5.10). Overall, 9 of the analysed tibial components were stemmed designs, and 15 were non-stemmed designs. The proportion of either with coating changes was similar (89% and 80%, respectively), therefore stemmed tibial components were not found to provide superior performance in terms of coating retention in this cohort of explanted TARs.

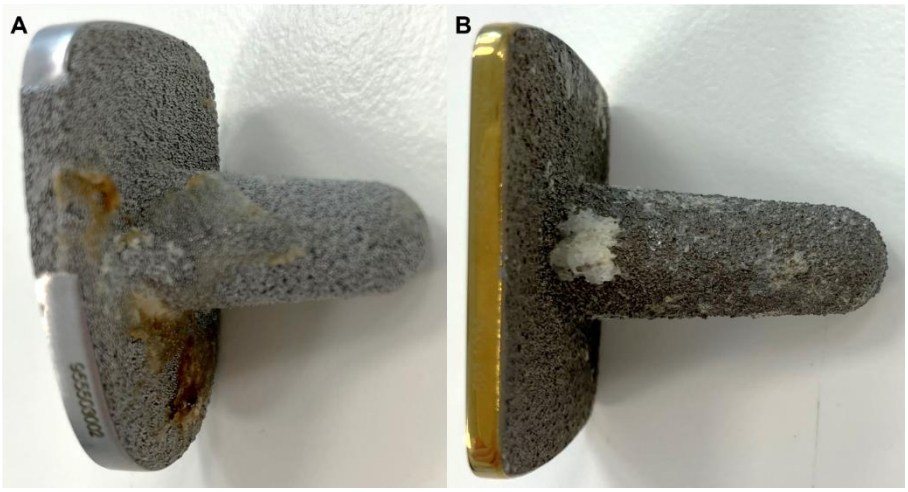

Figure 5.10. Macroscopic images of stemmed tibial components. (A) Mobility. (B) Zenith.

The anatomical nature of a TAR typically refers to the talar component; specifically, whether the geometry of it mimics that of the natural talus or not. Taking the classifications used by Arcângelo et al., 'spherical' talar components were classified as non-anatomical, and those with a 'two talar curve radii' were classified as anatomical (Figure 5.11). Therefore, just two of the TAR designs included in the present study were non-anatomically configured: the STAR and the Hintegra. In contrast to the conclusions by Arcângelo et al., the proportion of non-anatomical talar components with coating loss in the present study was lower than that for

anatomical components (70% versus 82%, respectively). However, it should be noted that both of the non-anatomically configured TARs analysed had a double coating on Ti and HA, while the other prostheses had a range of other different coatings. Therefore, it is not clear whether these findings are related to the non-anatomical configuration or the coating type, or some combination of both factors.

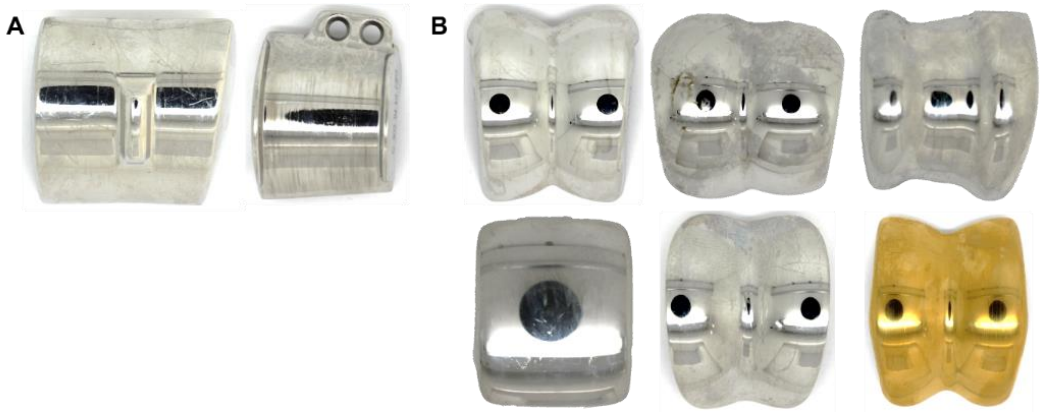

Figure 5.11. Talar components corresponding to non-anatomical and anatomical TARs. (A) non-anatomical (STAR, Hintegra). (B) anatomical (INFINITY, Cadence, Salto Talaris/Salto, BOX, Mobility, Zenith).

The effect of the PE insert thickness on the component performance in terms of volumetric wear loss and surface damage was investigated. However, no correlation between the PE insert thickness and measured bearing wear volume or between the insert thickness and the CDS for either the bearing or backside surfaces was found. The safety notice issued by the FDA regarding an increased risk of fracture of STAR PE inserts defined thinner (6 mm) inserts as being more likely to fracture. The present study included analysis of both thinner and thicker PE inserts, with 63% having a thickness of 6 mm or less (range 4 to 11 mm). The findings from the current study therefore suggest that thickness of the PE insert does not influence the damage incurred by the component in terms of wear and surface damage.

The tibial components included in this study were manufactured from alloys of either CoCr or Ti (with the Zenith prosthesis (n = 1) being Ti alloy coated with a TiN layer). Due to only one TiN coated prosthesis being in this cohort of explanted TARs, it was excluded from the statistical analyses performed to identify any potential influence of tibial component alloy on the performance of TARs. Generally, greater damage was associated with CoCr tibial

components compared those of Ti. The component damage scores of the backside of PE inserts in contact with CoCr tibial components was significantly higher on average than those in contact with Ti tibial components. Similarly, the component damage scores for the tibial components themselves were higher on average on CoCr than Ti components, although this difference was not statistically significant. Furthermore, the pitting damage identified on the tibial components occurred exclusively on those which were CoCr alloy.

The articulating surfaces of Ti tibial components were found to be rougher than those of CoCr alloy, with this being true for both unworn and worn areas of these components. A higher surface roughness of the metallic bearing surface has previously been correlated with increased PE wear.[23] This was also found to be the case in the present study; a positive correlation, albeit a weak one, was found between the unworn average surface roughness of the talar component bearing surface and the volumetric wear loss from the corresponding PE insert bearing surface. However, the common asymmetric wear seen on the PE insert bearing surfaces, as described in the previous chapter (section 4.5.2), suggests that metallic bearing surface roughness was not correlated with PE volumetric wear, as if this was the case then a lower degree of asymmetry between wear of the two condyles would be expected, as the corresponding surface roughness would be consistent for the two.

This correlation seen between the talar bearing average surface roughness and the PE insert bearing volumetric wear did not extend to the CDS of the PE insert bearing surface. However, the inverse was seen at the tibial-PE backside interface, with a moderate negative correlation found between the average surface roughness of the tibial component and the CDS of the PE insert backside surface (i.e., as the average surface roughness of the tibial component increased, the CDS of the corresponding PE insert backside surface decreased). This can perhaps be explained by the bearing constraint, as the average surface roughness of unworn areas of tibial component inferior surfaces was significantly higher on fixed bearing compared to mobile bearing components, with the latter also exhibiting greater PE insert backside surface wear damage due to the articulation permitted at this interface.

5.4.4. Methods to avoid failure

By considering the differences observed between pitting of the CoCr and Ti metal components, the cause of this metallic pitting may potentially be explained. CoCr is known to be a harder but less corrosion resistant material than Ti. It is therefore possible that along with third body

particles being present at the bearing, there could be corrosion pitting occurring on the articulating surfaces of the metal components, which may in part explain the difference in prevalence of pitting observed on CoCr and Ti components. It has also previously been demonstrated by Moharrami et al. that *in vivo* oxidation of Ti alloy can have a significant effect on its mechanical surface properties such that its hardness increases, whereas CoCr alloy was found to remain at a constant hardness.[80] It is therefore possible that an increase in Ti component hardness, thereby increasing their resistance to damage from third body particles, could also go some way to explaining why pitting was observed on tibial components of CoCr alloy only.

Based on the findings from the present study, Ti alloy rather than CoCr alloy seems to be a better material choice for tibial components in terms of avoiding pitting damage (and associated metal debris release).

For the talar components, which are made from CoCr alloy in the vast majority of cases, alternatives such as a TiN ceramic coating layer – at utilised by the metal components of the Zenith prosthesis (in this case on a Ti alloy base) – may offer a potential tribological solution for patients with CoCr hypersensitivity, however further investigation into the clinical effectiveness of these coatings is still required.[174] Since there was only one Zenith prosthesis included in the cohort of explanted TARs analysed in the present study, findings regarding tribological effects could not conclusively made within this thesis.

As all TAR models currently recorded by the NJR are CE marked as uncemented implants, and indeed the vast majority of TARs implanted are without the use of cement, the type of porous coating utilised for fixation should also be considered. Coating-derived Ti particles have also been shown to incite adverse inflammatory responses.[61] The identification of embedded Ti particles, along with the high prevalence of loss of coatings identified – the majority of which contain Ti – is therefore an issue of potential clinical concern. Coatings of HA only may be an alternative option. Although the rates of coating loss for those of HA only were comparable with other coating types in the present study, lower rates of osteolysis have previously been reported with this coating for TARs.[61]

Finally, in terms of the bearing constraint, the present study found that mobile bearing constraint was generally associated with greater damage in terms of porous coating loss, talar sliding plane scratching, PE insert backside surface damage, and PE insert fracture. However, the proportion of metallic components with pitting was similar for those from both fixed and

mobile bearing TARs, and a greater volumetric wear was measured from fixed bearing compared to mobile bearing PE insert bearing surfaces. Relatively low amounts of wear were measured from the PE insert bearing surfaces of both bearing constraints, however. The findings from the present study therefore indicate that TARs with a fixed bearing constraint may result in a reduction in some – but not all – of the damage mechanisms identified, although without associated clinical data, it is difficult to draw any definitive conclusions.

Aseptic loosening is commonly cited as the main reason for revision for TARs. This phenomenon can occur due to different reasons, including secondary to osteolysis resulting from an adverse response to particulate debris, or from micromotion between the bone-implant interface arising from issues with initial implantation or fixation. The present study found evidence of potential for both of these causes of aseptic loosening to occur. Particulate debris release from the PE bearing, the metal components, and the porous coatings were all common findings, the latter of which also indicating possible insufficient fixation. Based on the findings from the present study, several suggestions may be made. Clinicians should consider genetic testing of patients prior to TAR implantation as this could provide valuable information regarding a predisposition to developing a hypersensitivity response. This could then inform implant and/or procedure selection. For example, a patient with genes indicative of a low tolerance to Co release may be better off receiving an implant without a CoCr bearing surface, or even receiving an alternative treatment (e.g., arthrodesis). Manufacturers would also benefit from considering material selection based on the findings of the present study. Ti alloy tibial components were found to perform better than CoCr alloy tibial components in terms of resisting damage including pitting, and therefore may prove to be a better choice. Finally, current policies surrounding explant analysis should be considered in order to make it a routine process. The insights to be gained from it have the potential to provide further insights surrounding optimal implant design and selection, for the ultimate benefit of patients.

5.5. Limitations

A primary limitation of this explant analysis study was the lack of associated clinical data, for example reason for revision and implantation duration. The latter would have been particularly useful in allowing the calculation of volumetric wear rates (in terms of mm^3/year) to provide more context to the measured wear volumes.

It is also acknowledged that the numbers of different designs of TARs included were limited; this is a common constraint of TAR explant analysis studies. All available explanted TARs were analysed so as to maximise the cohort of the present study. This however meant that numbers of different groups varied, for example there were more mobile bearing than fixed bearing TARs included, and more CoCr alloy than Ti alloy tibial components included. Only one of the TARs had a HXLPE insert; likewise, only one had TiN coated metallic components. Therefore, analysis of the effect of these design features was limited.

Some of the prostheses included are no longer implanted (Mobility and BOX). However, the different available TARs do not vary greatly in design and therefore it was considered to be appropriate to include them on the basis that any findings would also be applicable to those currently on the market. Additionally, the time since the TARs which are no longer used were taken off the market is still within a duration such that they will have remained implanted in some patients (with use of the Mobility having ceased less than 10 years ago and BOX within the last 3 years).

The explant analysis performed within this study was limited to non-destructive techniques. Some of the analysis performed was observational, for example the semi-quantitative surface damage mode scoring; therefore, there was some degree of inherent uncertainty associated with it. Finally, the CMM technique for quantification of volumetric wear from the PE inserts was new (adapted from a previously validated method for knee replacement components), and CMM analysis was not achievable for some of the explants. This included some for which the PE insert surface was too damaged. Since these components may also be expected to have higher wear, it should be acknowledged that the exclusion of these may have skewed the results towards a lower overall average amount of volumetric wear measured. Additionally, for the backside surfaces, CMM analysis was only achievable for mobile bearing PE inserts. Whilst it would be expected that these would have substantially higher amounts of wear and/or damage compared to their fixed bearing counterparts, based on the visual damage mode analysis of these components, it is worth noting that this could not be corroborated via mapping of the surface geometry within the present study.

Chapter 6. Conclusions

The aim of this research was to investigate the wear-related damage modes and surface changes occurring *in vivo* of explanted contemporary TARs in order to better understand their failure mechanisms. To achieve this, a cohort of explanted contemporary TARs (n = 28) comprising a variety of different designs were analysed. The main explant analysis performed included visual (microscopic and macroscopic) analysis, material characterisation, surface profilometry, and form analysis (volumetric wear and planicity quantification). All explanted component surfaces (both articulating and non-articulating) were analysed, and the influence of design features including bearing constraint were assessed.

6.1. Summary

The initial research question posed was to determine what wear related damage and/or surface changes occur *in vivo* which may drive TAR failure. Five objectives were defined (chapter 1) in order to answer this question, thereby addressing the overall aim of the research. Key findings from the study relating to each will be considered in turn in the following sub-sections.

6.1.1. Characterisation of damage modes

The first objective was to characterise the modes of damage present on explanted TAR components in terms of type, extent and severity. Visual (microscopic and macroscopic) analysis was performed on the surfaces – both articulating and non-articulating – of the explanted TAR components. Initial analysis identified damage modes present, which then informed subsequent analysis. Key findings related to the identification of damage modes with a high prevalence in the cohort of analysed TARs; namely, metallic pitting, talar sliding plane scratching, and porous coating loss. In terms of characterising the extent and severity of the identified damage modes, a scoring system was used to perform a semi-quantitative analysis. This scoring showed that the greatest damage was accounted for by talar scratching, PE insert backside surface burnishing, PE insert bearing surface pitting, and PE insert backside surface scratching. A key finding scoring also found that significantly greater damage was present on the backside surfaces of mobile bearing PE inserts compared to those that were fixed bearing. An unexpectedly high frequency of damage to the articulating surfaces of the metal

components – specifically pitting and talar sliding plane scratching, along with porous coating loss – was observed for the analysed cohort of explanted TARs, suggesting that metal debris release may be an under-recognised issue. Additionally, gross damage to the PE insert was seen in a not-insubstantial number of the mobile bearing TARs, with this likely being linked to component migration and subsequent direct MoM contact of the tibial and talar components, indicative of unintended operation of the prosthesis. Overall, this study demonstrated that for the cohort of explanted TARs analysed, various modes of damage to all component surfaces were frequently identified; suggesting that multiple damage mechanisms may act concurrently *in vivo*, and that they likely also exacerbate each other. It is therefore important to consider these different mechanisms together, rather than in isolation, so as to account for potential knock-on effects.

6.1.2. Surface topography changes

The second objective was to evaluate the surface topography changes of explanted TAR components. The surface topography of the articulating surfaces of metal tibial and talar components was evaluated using non-contacting 3D profilometry. This was performed on both unworn and worn areas of the component surfaces in order to analyse any potential differences reflective of changes undergone *in vivo*. This analysis confirmed the presence of pitting indicative of localised material loss. A weak correlation between talar bearing surface roughness and PE insert bearing surface volumetric wear was also found.

6.1.3. Volumetric wear quantification

The following objective was to analyse the form changes of explanted TAR PE components. This encompassed two parts, both of which were achieved via CMM analysis. Firstly, the volumetric wear from PE insert bearing surfaces was quantified. Relatively low volumes of wear were measured, indicating that PE wear may not be the primary cause of failure in TARs. An asymmetric pattern of bearing surface volumetric wear was frequently observed, with this being higher for the lateral aspect than the medial aspect in most cases where the implantation side was known. A difference was also seen between the bearing surface wear volumes of fixed bearing and mobile bearing PE inserts, with the former being higher on average. However, due to a lack of known implantation durations, analysis of this was limited. Secondly, the planicity – the difference between the minimum and maximum linear deviations – was measured for the

PE insert backside surfaces. Deviations extending superiorly in an anatomical sense were frequently seen; more so than deviations indicative of material removed. Deformation, to varying degrees, of the backside surfaces was therefore found to be a common phenomenon for the mobile bearing PE inserts analysed. This work adds to the limited literature on explanted TARs, though further research is needed to fully understand the implications of these findings.

6.1.4. Influence of implant characteristics

The next objective was to correlate *in vivo* changes of explanted TAR components with implant characteristics. Several design features of TARs were analysed for a potential influence over observed *in vivo* changes to the components. The key findings related to the choice of bearing constraint (fixed or mobile) and tibial component alloy (CoCr or Ti). Specifically, mobile bearing TARs were generally associated with greater damage in terms of porous coating loss, talar bearing surface sliding plane scratching, PE insert backside surface damage, and PE insert fracture. However, bearing constraint was not found to be a factor affecting the likelihood of metallic pitting occurring. Rather, tibial component alloy was found to influence this, with metallic pitting identified on CoCr alloy components only. Furthermore, CoCr tibial components exhibited greater damage as well as on the corresponding PE insert backside surface also. These findings indicate that Ti alloy may be a better material choice than CoCr alloy for tibial components, and that there may also be a slight preference towards mobile over fixed bearing constraint in terms of reducing some of the damage modes seen in the present cohort of explanted TARs.

6.1.5. TAR failure mechanisms

The final objective was to determine damage mechanisms likely to cause TAR failure. Based on the findings of the explant analysis performed on the cohort of TARs in the present study, it was concluded that metal debris release may be an under recognised issue that likely contributes to TAR failure. There are various ways in which metal debris release as identified in the present study can result in TAR failure (i.e., revision surgery being required). An adverse response may be incited, either directly to the metal particulate debris, or to other implant-derived debris; the release of which may have been exacerbated by the metal particles. CoCr and Ti particles were both identified in the embedded debris of PE inserts, each of which has been shown to cause adverse inflammatory responses that can lead to aseptic loosening of the

device. It is therefore important to try to minimise the wear particles released from TARs; an aim which requires understanding of the sources of particulate debris, of which the present study has identified several.

Evidence of all four wear modes as described by McKellop et al. was seen in the present study, resulting from articulation of the following surfaces: primary-on-primary, primary-on-secondary, primary-on-primary with third bodies, and secondary-on-secondary.[165] Most of the analysed TARs displayed more than one wear mode; together with the variety of modes identified, this suggests that TARs are vulnerable to multiple mechanisms of wear occurring concurrently *in vivo*.

The commonly identified damage modes of metallic pitting and talar bearing surface sliding plane scratching were both frequently associated with porous coating loss of the metal components. Together with the identification of Ti from porous coatings in the PE inserts, it was concluded that coating particles were likely being released and migrating to the bearing, where they would cause further damage to both the PE and metal components through acting as third bodies.

In addition to the contribution of metal debris to TAR failure, other wear mechanisms may also cause failure, either alongside or independently of the metallic damage mechanisms discussed. The findings of coating loss also indicates that micromotion may be occurring at the bone-implant interface, which has the potential to cause osteolysis and subsequent aseptic loosening, a common reason for failure of TARs. Also, the potential impact of PE insert-generated wear debris and deformation should be considered. It is important that all of these potential mechanisms are taken into consideration when discussing TAR failure, and that actions taken to reduce the impact of one don't then neglect others which may be affected also.

6.2. Implications

Explants represent prostheses which have undergone the truest test through time *in vivo*; therefore, analysis of these explanted devices represents a valuable contribution to the body of knowledge.

To the best of the author's knowledge, no published studies to date have quantified volumetric wear from explanted TARs. The method and results described in the present study therefore

provide a useful starting point which may be used as a comparator against wear volumes given by simulator studies, as well as any future *ex-vivo* studies.

This is also, to the best of the author's knowledge, the first explant analysis study to compare damage of fixed and mobile bearing TARs. With the increase of fixed bearing devices and decrease of mobile bearing devices in the UK within the last decade leading to fixed bearing TARs being implanted at a far greater frequency, it is important to evaluate any differences. The literature on this topic currently contains mostly clinical follow-up studies; explant analysis comparing fixed and mobile bearing TARs can supplement this existing research in order to provide a more comprehensive picture of the effect of bearing constraint on the performance of TARs.

The findings from this explant analysis study provide conclusions that may inform future design and selection of TARs. In particular, material choice of the metal tibial component should be considered, as the present study found Ti alloy components to be more resistant to some forms of damage including pitting compared to those of CoCr alloy. With pitting being indicative of material loss, and CoCr known to have the potential to cause issues when released from implants, this is something that should be taken into account by manufacturers and surgeons, particularly in cases where the patient is known to be predisposed to metal hypersensitivity. Linked to this is the benefit that preoperative genetic tests could provide, by informing surgeons of which patients are likely to react adversely to relatively small amounts of metal debris release.

6.3. Suggestions for Further Work

The current research has provided a comprehensive analysis of wear-related surface damage modes of explanted TARs, as well as establishing a methodology for the quantification of PE volumetric wear. Since no published studies have quantified the volumetric wear from explanted TARs, there is scope for more studies analysing wear from *ex-vivo* TARs. It would also be useful to extend the quantification of volumetric wear to the backside surfaces of the PE inserts too. Although anatomically superior deviations were identified most frequently from the CMM analysis of the backside surfaces, the semi-quantitative analysis performed found damage modes indicative of wear, particularly on the mobile bearing PE insert backside surfaces. Volumetric wear analysis could therefore be useful in potentially supporting these findings. The CMM analysis of the backside surfaces could also be applied to PE inserts of

fixed bearing designs, in order to provide further insights into the effects of bearing constraint on TARs *in vivo*. Additionally, it would also be of interest to quantify the amount of volumetric wear accounted for by different materials, particularly metallic as metal debris release was commonly identified in the present study.

If the study were to be continued, then it is suggested that the primary focus would be on quantification of wear debris. Specifically, concentrating on measuring the amount of metal debris being released, as well as further work on the PE wear from both the bearing and backside surfaces of the PE insert. This could provide additional information on the main contributing sources of wear debris and therefore which of these the focus should primarily be on minimising in order to improve patient outcomes.

A primary limitation of the present study which was identified was the lack of correlated clinical information, specifically implantation durations and reasons for revision. If future wear studies of explanted TARs could take into account time *in vivo*, then wear rates could be reported, further increasing the applicability of the results to gain insights into the actual wear performance of contemporary TARs. The knowledge of reasons for revision and linking this information to damage analysis of explanted TARs would enable future studies to more conclusively link particular wear modes of TARs with failure mechanisms. For cases such as where the device was retrieved due to unexplained pain, such analysis may also have the potential to provide insights into explaining this phenomenon, and thus how to prevent it in the future.

In general, explant analysis studies of TARs are limited, and further studies would allow the research within the existing literature to be supported and expanded, especially if such studies included larger numbers of explanted TARs.

References

1 MacAusland WR, MacAusland AR. The mobilization of ankylosed joints by arthroplasty: Lea & Febiger 1929.

2 Ianuzzi A, Mkandawire C. Applications of UHMWPE in Total Ankle Replacements. *UHMWPE Biomaterials Handbook*: Elsevier 2016:197-216.

3 Cooke PH, Goldberg AJ. Total Ankle Replacement. In: Bentley G, ed. *European Surgical Orthopaedics and Traumatology: The EFORT Textbook*. Berlin, Heidelberg: Springer Berlin Heidelberg 2014:3705-23.

4 Brockett C. Biomechanics and Tribology of Total Ankle Replacement. Foot and Ankle Clinics. 2023.

5 Undén A, Jehpsson L, Kamrad I, Carlsson Å, Henricson A, Karlsson MK, Rosengren BE. Better implant survival with modern ankle prosthetic designs: 1,226 total ankle prostheses followed for up to 20 years in the Swedish Ankle Registry. Acta orthopaedica. 2020;91(2):191-6.

6 NJR. National Joint Registry 20th Annual Report 2023; 2023.

7 Saltzman CL, Salamon ML, Blanchard GM, Huff T, Hayes A, Buckwalter JA, Amendola A. Epidemiology of ankle arthritis: report of a consecutive series of 639 patients from a tertiary orthopaedic center. The Iowa orthopaedic journal. 2005;25:44.

8 World Health Organization. Osteoarthritis. 2023 13 July 2023 [cited; Available from: https://www.who.int/news-room/fact-sheets/detail/osteoarthritis#:~:text=With%20ageing%20populations%20and%20increasing,to%20continue%20to%20increase%20globally

9 AOANJRR. Australian Orthopaedic Association National Joint Replacement Registry 2023 Supplementary: Demographics and Outcome of Ankle Arthroplasty; 2023.

10 Henricson A, Carlsson A, Rydholm U. What is a revision of total ankle replacement? Foot and ankle surgery. 2011;17(3):99-102.

11 Abu-Amer Y, Darwech I, Clohisy JC. Aseptic loosening of total joint replacements: mechanisms underlying osteolysis and potential therapies. Arthritis research & therapy. 2007;9(1):1-7.

12 Regulation (EU) 2017/745 of the European Parliament and of the Council.

13 Reclassification. Lessons from a Notified Body: British Standards Institution; 2016.

14 Standardization IOf. ISO 22622:2019. *Implants for surgery — Wear of total ankle-joint prostheses — Loading and displacement parameters for wear-testing machines with load or displacement control and corresponding environmental conditions for test* 2019.

15 Currier BH, Hecht PJ, Nunley JA, Mayor MB, Currier JH, Van Citters DW. Analysis of failed ankle arthroplasty components. Foot & ankle international. 2019;40(2):131-8.

16 Matharu GS, Pandit HG, Murray DW, Judge A. Adverse reactions to metal debris occur with all types of hip replacement not just metal-on-metal hips: a retrospective observational study of 3340 revisions for adverse reactions to metal debris from the National Joint Registry for England, Wales, Northern Ireland and the Isle of Man. BMC musculoskeletal disorders. 2016;17(1):1-12.

17 Kretzer JP, Reinders J, Sonntag R, Hagmann S, Streit M, Jeager S, Moradi B. Wear in total knee arthroplasty—just a question of polyethylene? International orthopaedics. 2014;38(2):335-40.

18 Schipper ON, Haddad SL, Pytel P, Zhou Y. Histological analysis of early osteolysis in total ankle arthroplasty. Foot & Ankle International. 2017;38(4):351-9.

19 Langton DJ, Bhalekar RM, Joyce TJ, Rushton SP, Wainwright BJ, Nargol ME, et al. The influence of hla genotype on the development of metal hypersensitivity following joint replacement. Communications Medicine. 2022;2(1):1-12.
20 Reiner T, Sorbi R, Müller M, Nees T, Kretzer JP, Rickert M, Moradi B. Blood metal ion release after primary total knee arthroplasty: a prospective study. Orthopaedic Surgery. 2020;12(2):396-403.
21 Brockett CL, Chapman GJ. Biomechanics of the ankle. Orthopaedics and trauma. 2016;30(3):232-8.
22 Goldberg A. TARVA Randomised Clinical Trial. [cited 2023 08 March]; Available from: http://www.anklearthritis.co.uk/
23 Goldberg A, Cooke P. The Atlas of Ankle Replacements: World Scientific 2021.
24 Goldberg AJ, MacGregor A, Dawson J, Singh D, Cullen N, Sharp RJ, Cooke PH. The demand incidence of symptomatic ankle osteoarthritis presenting to foot & ankle surgeons in the United Kingdom. The Foot. 2012;22(3):163-6.
25 Glazebrook M, Daniels T, Younger A, Foote C, Penner M, Wing K, et al. Comparison of health-related quality of life between patients with end-stage ankle and hip arthrosis. JBJS. 2008;90(3):499-505.
26 Brockett C. Biomechanics and Tribology of Total Ankle Replacement. Foot and Ankle Clinics. 2023;28(1):1-12.
27 Goldberg AJ, Chowdhury K, Bordea E, Hauptmannova I, Blackstone J, Brooking D, et al. Total Ankle Replacement Versus Arthrodesis for End-Stage Ankle Osteoarthritis: A Randomized Controlled Trial. Annals of Internal Medicine. 2022;175(12):1648-57.
28 Valderrabano V, Horisberger M, Russell I, Dougall H, Hintermann B. Etiology of ankle osteoarthritis. Clinical Orthopaedics and Related Research®. 2009;467(7):1800-6.
29 Delco ML, Kennedy JG, Bonassar LJ, Fortier LA. Post-traumatic osteoarthritis of the ankle: a distinct clinical entity requiring new research approaches. Journal of Orthopaedic Research. 2017;35(3):440-53.
30 Arden N, Nevitt MC. Osteoarthritis: epidemiology. Best practice & research Clinical rheumatology. 2006;20(1):3-25.
31 Hutchings I, Shipway P. Tribology: friction and wear of engineering materials: Butterworth-Heinemann 2017.
32 Malekipour F, Whitton C, Oetomo D, Lee PVS. Shock absorbing ability of articular cartilage and subchondral bone under impact compression. Journal of the mechanical behavior of biomedical materials. 2013;26:127-35.
33 Malekipour F, Lee PV. Shock absorbing ability in healthy and damaged cartilage-bone under high-rate compression. Journal of the Mechanical Behavior of Biomedical Materials. 2019;90:388-94.
34 Ankle Arthritis. [cited 2022 28 December]; Available from: http://www.anklearthritis.co.uk/normal-structure-and-function
35 Hospital for Special Surgery. Ankle Replacement (Ankle Arthroplasty). 2022 [cited; Available from: https://www.hss.edu/condition-list_ankle-replacement-arthroplasty.asp
36 Herrera-Pérez M, Valderrabano V, Godoy-Santos AL, de César Netto C, González-Martín D, Tejero S. Ankle osteoarthritis: comprehensive review and treatment algorithm proposal. EFORT Open Reviews. 2022;7(7):448.
37 Kurtz S, Ong K, Lau E, Mowat F, Halpern M. Projections of primary and revision hip and knee arthroplasty in the United States from 2005 to 2030. Jbjs. 2007;89(4):780-5.
38 Nihal A, Gellman RE, Embil JM, Trepman E. Ankle arthrodesis. Foot and Ankle Surgery. 2008;14(1):1-10.

39 Cottino U, Collo G, Morino L, Cosentino A, Gallina V, Deregibus M, Tellini A. Arthroscopic ankle arthrodesis: a review. Current reviews in musculoskeletal medicine. 2012;5:151-5.
40 Yasui Y, Hannon CP, Seow D, Kennedy JG. Ankle arthrodesis: a systematic approach and review of the literature. World journal of orthopedics. 2016;7(11):700.
41 Roukis TS, Berlet GC, Bibbo C, Hyer CF, Penner MJ, Wünschel M, Prissel MA. Primary and revision total ankle replacement: evidence-based surgical management: Springer 2015.
42 Sundet M, Dybvik E, Furnes O, Eriksen ML, Hallan G. Poor survivorship of total ankle replacements. 1368 cases from the period 1994–2021 in the Norwegian arthroplasty register. Foot and Ankle Surgery. 2023.
43 National Joint Registry 19th Annual Report 2022: National Joint Registry; 2022.
44 New Zealand Joint Registry. The New Zealand Joint Registry Twenty-four Year Report; 2023.
45 Norwegian Arthroplasty Register. National quality and expertise network for joint prostheses and hip fractures; 2023.
46 van der Plaat LW, Hoornenborg D, Sierevelt IN, van Dijk CN, Haverkamp D. Ten-year revision rates of contemporary total ankle arthroplasties equal 22%. A meta-analysis. Foot and Ankle Surgery. 2021.
47 Total hip replacement and resurfacing arthroplasty for end-stage arthritis of the hip: NICE; 2014.
48 Onggo JR, Nambiar M, Phan K, Hickey B, Galvin M, Bedi H. Outcome after total ankle arthroplasty with a minimum of five years follow-up: A systematic review and meta-analysis. Foot and Ankle Surgery. 2020;26(5):556-63.
49 Agha M, Agha R. The rising prevalence of obesity: part A: impact on public health. International journal of surgery Oncology. 2017;2(7):e17.
50 Rutherford T, Socio A. Population ageing: statistics. House of Commons library (Standard not Retrieved Jan 2, 2013, from: www parliament uk/topics/PopulationArchive. 2012.
51 Kurtz SM, Lau E, Ong K, Zhao K, Kelly M, Bozic KJ. Future young patient demand for primary and revision joint replacement: national projections from 2010 to 2030. Clinical Orthopaedics and Related Research®. 2009;467(10):2606-12.
52 Stengel D, Bauwens K, Ekkernkamp A, Cramer J. Efficacy of total ankle replacement with meniscal-bearing devices: a systematic review and meta-analysis. Archives of orthopaedic and trauma surgery. 2005;125:109-19.
53 Gougoulias N, Khanna A, Maffulli N. How successful are current ankle replacements?: a systematic review of the literature. Clinical Orthopaedics and Related Research®. 2010;468:199-208.
54 Zaidi R, Cro S, Gurusamy K, Sivanadarajah N, Macgregor A, Henricson A, Goldberg A. The outcome of total ankle replacement: a systematic review and meta-analysis. The bone & joint journal. 2013;95(11):1500-7.
55 Curlewis K, Leung B, Sinclair L, Chan G, Bendall S, Ricketts D. Systemic medical complications following total ankle arthroplasty: A review of the evidence. Foot and Ankle Surgery. 2021.
56 Hermus J, van Kuijk S, Spekenbrink-Spooren A, Witlox M, Poeze M, van Rhijn L, Arts J. Risk factors for total ankle arthroplasty failure: A Dutch Arthroplasty Register study. Foot and Ankle Surgery. 2022;28(7):883-6.
57 Roukis TS, Bartel AF. Survivorship of first-, second-, and third-generation total ankle replacement systems. Primary and Revision Total Ankle Replacement: Evidence-Based Surgical Management. 2016:15-23.

58 Gougoulias N, Maffulli N. History of total ankle replacement in North America. *Primary and Revision Total Ankle Replacement*: Springer 2016:3-13.
59 Malik SS, Malik SS. Orthopaedic biomechanics made easy: Cambridge University Press 2015.
60 Hintermann B, Zwicky L, Knupp M, Henninger HB, Barg A. HINTEGRA revision arthroplasty for failed total ankle prostheses. JBJS. 2013;95(13):1166-74.
61 Koivu H, Kohonen I, Sipola E, Alanen K, Vahlberg T, Tiusanen H. Severe periprosthetic osteolytic lesions after the Ankle Evolutive System total ankle replacement. The Journal of Bone and Joint Surgery British volume. 2009;91(7):907-14.
62 Di Iorio A, Viste A, Fessy MH, Besse JL. The AES total ankle arthroplasty analysis of failures and survivorship at ten years. International Orthopaedics. 2017;41(12):2525-33.
63 Mehta N, Serino J, Hur ES, Smith S, Hamid KS, Lee S, Bohl DD. Pathogenesis, evaluation, and management of osteolysis following total ankle arthroplasty. Foot & Ankle International. 2021;42(2):230-42.
64 Cottrino S, Fabrègue D, Cowie A, Besse J-L, Tadier S, Gremillard L, Hartmann D. Wear study of total ankle replacement explants by microstructural analysis. Journal of the mechanical behavior of biomedical materials. 2016;61:1-11.
65 INVISION Total Ankle Revision System. 2020 [cited 2023 7 May]; Available from: https://www.wright.com/footandankleproducts/invision-total-ankle-revision-system
66 Lai WC, Arshi A, Ghorbanifarajzadeh A, Williams JR, Soohoo NF. Incidence and predictors of early complications following primary and revision total ankle arthroplasty. Foot and Ankle Surgery. 2019;25(6):785-9.
67 Kamrad I, Henricsson A, Karlsson MK, Magnusson H, Nilsson J-Å, Carlsson Å, Rosengren BE. Poor prosthesis survival and function after component exchange of total ankle prostheses: An analysis of 69 cases in the Swedish Ankle Registry. Acta Orthopaedica. 2015;86(4):407-11.
68 Williams JR, Wegner NJ, Sangeorzan BJ, Brage ME. Intraoperative and perioperative complications during revision arthroplasty for salvage of a failed total ankle arthroplasty. Foot & Ankle International. 2015;36(2):135-42.
69 Cifaldi AJ, Barton EC, Roukis TS, Prissel MA. Total ankle replacement based on worldwide registry data trends. *Primary and Revision Total Ankle Replacement: Evidence-Based Surgical Management*: Springer 2021:13-27.
70 Kooner S, Marsh A, Wilson IR, Fu J, Lau JTC. History of total ankle replacement in North America. *Primary and Revision Total Ankle Replacement: Evidence-Based Surgical Management*: Springer 2021:3-12.
71 Mulcahy H, Chew FS. Current concepts in total ankle replacement for radiologists: features and imaging assessment. American Journal of Roentgenology. 2015;205(5):1038-47.
72 Assal M, Kutaish H, Acker A, Hattendorf J, Lübbeke A, Crevoisier X. Three-Year Rates of Reoperation and Revision Following Mobile Versus Fixed-Bearing Total Ankle Arthroplasty: A Cohort of 302 Patients with 2 Implants of Similar Design. JBJS. 2021;103(22):2080-8.
73 Roukis TS, Elliott AD. Incidence of revision after primary implantation of the Salto® mobile version and Salto Talaris™ total ankle prostheses: a systematic review. The Journal of Foot and Ankle Surgery. 2015;54(3):311-9.
74 McKenna BJ, Cook J, Cook EA, Crafton J, Knabel M, Swenson E, et al. Total ankle arthroplasty survivorship: a meta-analysis. The Journal of Foot and Ankle Surgery. 2020;59(5):1040-8.

75 Nunley JA, Adams SB, Easley ME, DeOrio JK. Prospective randomized trial comparing mobile-bearing and fixed-bearing total ankle replacement. Foot & ankle international. 2019;40(11):1239-48.
76 Queen RM, Sparling TL, Butler RJ, Adams Jr SB, DeOrio JK, Easley ME, Nunley JA. Patient-reported outcomes, function, and gait mechanics after fixed and mobile-bearing total ankle replacement. JBJS. 2014;96(12):987-93.
77 Gaudot F, Colombier J-A, Bonnin M, Judet T. A controlled, comparative study of a fixed-bearing versus mobile-bearing ankle arthroplasty. Foot & ankle international. 2014;35(2):131-40.
78 Valderrabano V, Pagenstert GI, Müller AM, Paul J, Henninger HB, Barg A. Mobile- and fixed-bearing total ankle prostheses: is there really a difference? Foot and ankle clinics. 2012;17(4):565-85.
79 Patel B, Favaro G, Inam F, Reece MJ, Angadji A, Bonfield W, et al. Cobalt-based orthopaedic alloys: Relationship between forming route, microstructure and tribological performance. Materials Science and Engineering: C. 2012;32(5):1222-9.
80 Moharrami N, Langton D, Sayginer O, Bull S. Why does titanium alloy wear cobalt chrome alloy despite lower bulk hardness: A nanoindentation study? Thin Solid Films. 2013;549:79-86.
81 Shen F. Ultrahigh-molecular-weight polyethylene (UHMWPE) in joint replacement. *Biomedical polymers*: Elsevier 2007:141-73.
82 Kurtz SM. UHMWPE biomaterials handbook: ultra high molecular weight polyethylene in total joint replacement and medical devices: Academic Press 2009.
83 Bischoff JE, Fryman JC, Parcell J, Orozco Villaseñor DA. Influence of crosslinking on the wear performance of polyethylene within total ankle arthroplasty. Foot & ankle international. 2015;36(4):369-76.
84 Schipper ON, Haddad SL, Fullam S, Pourzal R, Wimmer MA. Wear characteristics of conventional ultrahigh-molecular-weight polyethylene versus highly cross-linked polyethylene in total ankle arthroplasty. Foot & Ankle International. 2018;39(11):1335-44.
85 Gougoulias NE, Khanna A, Maffulli N. History and evolution in total ankle arthroplasty. British medical bulletin. 2009;89(1):111-51.
86 Røkkum M, Reigstad A, Johansson CB. HA particles can be released from well-fixed HA-coated stems. Acta Orthopaedica Scandinavica. 2002;73(3):298-306.
87 Gandhi R, Davey JR, Mahomed NN. Hydroxyapatite coated femoral stems in primary total hip arthroplasty: a meta-analysis. The Journal of arthroplasty. 2009;24(1):38-42.
88 Arcângelo J, Guerra-Pinto F, Pinto A, Grenho A, Navarro A, Oliva XM. Peri-prosthetic bone cysts after total ankle replacement. A systematic review and meta-analysis. Foot and Ankle Surgery. 2019;25(2):96-105.
89 Jin Z, Stone M, Ingham E, Fisher J. (v) Biotribology. Current Orthopaedics. 2006;20(1):32-40.
90 Rabinowicz E, Tanner R. Friction and wear of materials. Journal of Applied Mechanics. 1966;33(2):479.
91 Goodman SB, Gibon E, Yao Z. The basic science of periprosthetic osteolysis. Instructional course lectures. 2013;62:201.
92 Ingham E, Fisher J. The role of macrophages in osteolysis of total joint replacement. Biomaterials. 2005;26(11):1271-86.
93 Patil N, Goodman SB. Wear particles and osteolysis. In: Deb S, ed. *Orthopaedic Bone Cements*. Woodhead Publishing Series in Biomaterials: Woodhead Publishing 2008:140-63.

94 Hench LL. Joint replacement. In: Hench LL, Jones JR, eds. *Biomaterials, Artificial Organs and Tissue Engineering*. Woodhead Publishing Series in Biomaterials: Woodhead Publishing 2005:129-41.
95 ISO. ISO 22622:2019. *Implants for surgery — Wear of total ankle-joint prostheses — Loading and displacement parameters for wear-testing machines with load or displacement control and corresponding environmental conditions for test*.
96 ISO. ISO 14242-1:2014. *Implants for surgery — Wear of total hip-joint prostheses — Part 1: Loading and displacement parameters for wear-testing machines and corresponding environmental conditions for test*.
97 Espinosa N, Klammer G, Wirth SH. Osteolysis in total ankle replacement: how does it work? Foot and ankle clinics. 2017;22(2):267-75.
98 Stribeck Curves. [cited 2023 6 June]; Available from: https://ingramtribology.com/stribeck-curves/
99 Glazebrook MA, Arsenault K, Dunbar M. Evidence-based classification of complications in total ankle arthroplasty. Foot & ankle international. 2009;30(10):945-9.
100 Ebaugh MP, Alford T, Kutzarov K, Davis E, Greaser M, McGarvey WC. Patient-Reported Outcomes of Primary Total Ankle Arthroplasty in Patients Aged< 50 Years. Foot & ankle orthopaedics. 2022;7(1).
101 Fletcher AN, Mody KS, Adams Jr SB, DeOrio JK, Easley ME, Nunley JA. Effect of gender differences on patient-reported outcomes and complications in total ankle replacement. Foot & Ankle International. 2021;42(6):776-87.
102 Gross CE, Lampley A, Green CL, DeOrio JK, Easley M, Adams S, Nunley JA. The effect of obesity on functional outcomes and complications in total ankle arthroplasty. Foot & Ankle International. 2016;37(2):137-41.
103 Gross CE, Green CL, DeOrio JK, Easley M, Adams S, Nunley JA. Impact of diabetes on outcome of total ankle replacement. Foot & ankle international. 2015;36(10):1144-9.
104 Nam H, Martinazzi BJ, Kirchner G, Bonaddio V, Koroneos Z, Manto K, et al. The Effects of Anxiety and Depression in Outcomes of Patients with Total Ankle Replacement. Foot & Ankle Orthopaedics. 2022;7(4):2473011421S00838.
105 McPhee C, Aninye IO, Horan L, Group SfWsHRBHW. Recommendations for Improving Women's Bone Health Throughout the Lifespan. Journal of Women's Health. 2022;31(12):1671-6.
106 Cody EA, Lachman JR, Gausden EB, Nunley JA, Easley ME. Lower bone density on preoperative computed tomography predicts periprosthetic fracture risk in total ankle arthroplasty. Foot & ankle international. 2019;40(1):1-8.
107 Simonson DC, Roukis TS. Incidence of complications during the surgeon learning curve period for primary total ankle replacement: a systematic review. Clinics in Podiatric Medicine and Surgery. 2015;32(4):473-82.
108 Sopher RS, Amis AA, Calder JD, Jeffers JR. Total ankle replacement design and positioning affect implant-bone micromotion and bone strains. Medical engineering & physics. 2017;42:80-90.
109 Thermann H. Total Ankle Arthroplasty: Why does it fail? The Journal of Foot and Ankle Surgery (Asia-Pacific). 2014;1(2):41-7.
110 Le V, Escudero M, Symes M, Salat P, Wing K, Younger A, et al. Impact of sagittal talar inclination on total ankle replacement failure. Foot & Ankle International. 2019;40(8):900-4.
111 Deorio JK, Easley ME. Total ankle arthroplasty. Instructional course lectures. 2008;57:383-413.

112 Kihara S, Kanzaki N, Yamashita T, Yamamoto T, Nishida K, Nagai K, et al. Talar component subsidence correlates with periprosthetic osteolysis after total ankle arthroplasty. European Journal of Orthopaedic Surgery & Traumatology. 2023:1-7.
113 Kim D-R, Choi YS, Potter HG, Li AE, Chun K-Y, Jung YY, et al. Total Ankle Arthroplasty: An Imaging Overview. kjr. 2016 04;17(3):413-23.
114 Karachalios T. Bone-implant interface in orthopedic surgery: basic science to clinical applications: Springer Science & Business Media 2013.
115 Togher CJ, Perkins JM, Thompson JM, Hyer CF, Berlet GC. Stress Shielding and Aseptic Loosening in Fully Porous-Coated vs Smooth Stemmed Tibial Implants in Total Ankle Arthroplasty. Foot & Ankle Orthopaedics. 2022;7(4):2473011421S00973.
116 Raffa ML, Nguyen VH, Hernigou P, Flouzat-Lachaniette CH, Haiat G. Stress shielding at the bone-implant interface: influence of surface roughness and of the bone-implant contact ratio. Journal of Orthopaedic Research®. 2021;39(6):1174-83.
117 Sivananthan S, Goodman S, Burke M. Failure mechanisms in joint replacement. *Joint Replacement Technology*: Elsevier 2021:373-402.
118 Risk of Device Component Breaking in Patients with Stryker's STAR Ankle: FDA Safety Communication. 2021 15 March 2021 [cited 2021 17 March]; Available from: https://www.fda.gov/medical-devices/safety-communications/risk-device-component-breaking-patients-strykers-star-ankle-fda-safety-communication
119 Ali A, Forrester R, O'Connor P, Harris N. Revision of failed total ankle arthroplasty to a hindfoot fusion: 23 consecutive cases using the Phoenix nail. Bone Joint J. 2018;100(4):475-9.
120 Natu S, Sidaginamale RP, Gandhi J, Langton DJ, Nargol AV. Adverse reactions to metal debris: histopathological features of periprosthetic soft tissue reactions seen in association with failed metal on metal hip arthroplasties. Journal of clinical pathology. 2012;65(5):409-18.
121 Rajpura A, Porter ML, Gambhir AK, Freemont AJ, Board TN. Clinical experience of revision of metal on metal hip arthroplasty for aseptic lymphocyte dominated vasculitis associated lesions (ALVAL). Hip International. 2011;21(1):043-51.
122 Willert H-G, Buchhorn GH, Fayyazi A, Flury R, Windler M, Köster G, Lohmann CH. Metal-on-metal bearings and hypersensitivity in patients with artificial hip joints: a clinical and histomorphological study. JBJS. 2005;87(1):28-36.
123 Ng VY, Lombardi AV, Berend KR, Skeels MD, Adams JB. Perivascular lymphocytic infiltration is not limited to metal-on-metal bearings. Clinical Orthopaedics and Related Research®. 2011;469(2):523-9.
124 Kurmis AP, Herman A, McIntyre AR, Masri BA, Garbuz DS. Pseudotumors and high-grade aseptic Lymphocyte-Dominated vasculitis-associated lesions around total knee replacements identified at aseptic revision surgery: findings of a large-scale histologic review. The Journal of Arthroplasty. 2019;34(10):2434-8.
125 Crawford DA, Passias BJ, Adams JB, Berend KR, Lombardi AV. Impact of perivascular lymphocytic infiltration in aseptic total knee revision. The Bone & Joint Journal. 2021;103(6 Supple A):145-9.
126 Baker P, Van der Meulen J, Lewsey J, Gregg P. The role of pain and function in determining patient satisfaction after total knee replacement: data from the National Joint Registry for England and Wales. The Journal of bone and joint surgery British volume. 2007;89(7):893-900.
127 Planckaert C, Larose G, Ranger P, Lacelle M, Fuentes A, Hagemeister N. Total knee arthroplasty with unexplained pain: new insights from kinematics. Archives of Orthopaedic and Trauma Surgery. 2018;138(4):553-61.

128 Momoli A, Giaretta S, Modena M, Micheloni GM. The painful knee after total knee arthroplasty: evaluation and management. Acta Bio Medica: Atenei Parmensis. 2017;88(Suppl 2):60.
129 Vulcano E, Myerson M. The painful total ankle arthroplasty: a diagnostic and treatment algorithm. The Bone & Joint Journal. 2017;99(1):5-11.
130 Hood RW, Wright TM, Burstein AH. Retrieval analysis of total knee prostheses: a method and its application to 48 total condylar prostheses. Journal of biomedical materials research. 1983;17(5):829-42.
131 Wasielewski RC, Galante JO, Leighty RM, Natarajan RN, Rosenberg AG. Wear patterns on retrieved polyethylene tibial inserts and their relationship to technical considerations during total knee arthroplasty. Clinical orthopaedics and related research. 1994(299):31-43.
132 Brandt J-M, Haydon C, Harvey E, McCalden R, Medley J. Semi-quantitative assessment methods for backside polyethylene damage in modular total knee replacements. Tribology international. 2012;49:96-102.
133 Ho NC, Park S-H, Campbell P, Van Citters DW, Ebramzadeh E, Sangiorgio S. Damage patterns in polyethylene fixed bearings of retrieved total ankle replacements. Foot and Ankle Surgery. 2020.
134 Bhushan B. Surface roughness analysis and measurement techniques. *Modern tribology handbook, two volume set*: CRC press 2000:79-150.
135 Zygo. NewView 7200 & 7300 Operating Manual; 2011.
136 Sağbaş B, Durakbasa M. Measurement of wear in orthopedic prosthesis. Acta Physica Polonica A. 2012;121.
137 Engh Jr CA, Zimmerman RL, Hopper Jr RH, Engh GA. Can microcomputed tomography measure retrieved polyethylene wear? Comparing fixed-bearing and rotating-platform knees. Clinical Orthopaedics and Related Research®. 2013;471(1):86-93.
138 Lord J, Langton D, Nargol A, Joyce T. Volumetric wear assessment of failed metal-on-metal hip resurfacing prostheses. Wear. 2011;272(1):79-87.
139 Langton D, Sidaginamale R, Holland J, Deehan D, Joyce T, Nargol A, et al. Practical considerations for volumetric wear analysis of explanted hip arthroplasties. Bone & joint research. 2014;3(3):60-8.
140 Bhalekar RM, Nargol ME, Shyam N, Nargol AV, Wells SR, Collier R, et al. Tibial tray debonding from the cement mantle is associated with deformation of the backside of polyethylene tibial inserts. The Bone & Joint Journal. 2021:1-11.
141 Affatato S, Leardini A, Leardini W, Giannini S, Viceconti M. Meniscal wear at a three-component total ankle prosthesis by a knee joint simulator. Journal of biomechanics. 2007;40(8):1871-6.
142 Bell CJ, Fisher J. Simulation of polyethylene wear in ankle joint prostheses. Journal of Biomedical Materials Research Part B: Applied Biomaterials: An Official Journal of The Society for Biomaterials, The Japanese Society for Biomaterials, and The Australian Society for Biomaterials and the Korean Society for Biomaterials. 2007;81(1):162-7.
143 Smyth A, Fisher J, Suñer S, Brockett C. Influence of kinematics on the wear of a total ankle replacement. Journal of biomechanics. 2017;53:105-10.
144 Affatato S, Taddei P, Leardini A, Giannini S, Spinelli M, Viceconti M. Wear behaviour in total ankle replacement: a comparison between an in vitro simulation and retrieved prostheses. Clinical Biomechanics. 2009;24(8):661-9.

145 Vaupel Z, Baker EA, Baker KC, Kurdziel MD, Fortin PT. Analysis of retrieved Agility™ total ankle arthroplasty systems. Foot & ankle international. 2009;30(9):815-23.
146 Greenwald AS. EVALUATION OF A MOBILE BEARING TOTAL ANKLE REPLACEMENT IN SIMULATION AND CLINICAL RETRIEVAL.
147 Dalat F, Barnoud R, Fessy M-H, Besse J-L, Surgery FAoF. Histologic study of periprosthetic osteolytic lesions after AES total ankle replacement. A 22 case series. Orthopaedics & Traumatology: Surgery & Research. 2013;99(6):S285-S95.
148 van Wijngaarden R, van der Plaat L, Weme RAN, Doets HC, Westerga J, Haverkamp D. Etiopathogenesis of osteolytic cysts associated with total ankle arthroplasty, a histological study. Foot and Ankle Surgery. 2015;21(2):132-6.
149 Stratton-Powell AA, Williams S, Tipper JL, Redmond AC, Brockett CL. Isolation and characterisation of wear debris surrounding failed total ankle replacements. Acta Biomaterialia. 2023;159:410-22.
150 Kobayashi A, Minoda Y, Kadoya Y, Ohashi H, Takaoka K, Saltzman CL. Ankle arthroplasties generate wear particles similar to knee arthroplasties. Clinical Orthopaedics and Related Research (1976-2007). 2004;424:69-72.
151 Wilson J. A changing landscape: explant analysis. Clinical Services Journal. 2022 29 Nov 2022.
152 Jennison T, Ukoumunne O, Lamb S, Sharpe I, Goldberg AJ. How long do ankle arthroplasties last? Bone Joint J. 2023;105(3):301-6.
153 Harman M, Affatato S, Spinelli M, Zavalloni M, Stea S, Toni A. Polyethylene insert damage in unicondylar knee replacement: a comparison of in vivo function and in vitro simulation. Proceedings of the Institution of Mechanical Engineers, Part H: Journal of Engineering in Medicine. 2010;224(7):823-30.
154 Harman M, Cristofolini L, Erani P, Stea S, Viceconti M. A pictographic atlas for classifying damage modes on polyethylene bearings. Journal of Materials Science: Materials in Medicine. 2011;22(5):1137-46.
155 Zygo. NewView 5000. 2002 [cited 2022 11 August]; Available from: https://www.equipx.net/uploads/ZygoNuview5000.pdf
156 Weaver A. Enhancing the Capability of White Light Interferometry on Complex Surfaces; 2005.
157 Zygo. Mx Surface Texture Parameters; 2018.
158 Bhalekar RM, Nargol ME, Shyam N, Nargol AV, Wells SR, Collier R, et al. Tibial tray debonding from the cement mantle is associated with deformation of the backside of polyethylene tibial inserts. The Bone & Joint Journal. 2021;103(12):1791-801.
159 Clarke I. Ultra-High Molecular Weight Polyethylene - UHMWPE. 2001 [cited 2022 2 August]; Available from: https://www.azom.com/article.aspx?ArticleID=854
160 BSI. Implants for surgery - Wear of total hip prostheses. *Part 2: Methods of measurement* 2016.
161 Bhalekar RM, Wells SR, Nargol ME, Shariatpanahi S, Nargol AV, Waller S, et al. Aseptic loosening of the option stemmed tibial tray in the Zimmer NexGen LPS total knee arthroplasty system. The Knee. 2024;47:1-12.
162 Muir D, Aoina J, Hong T, Mason R. The outcome of the Mobility total ankle replacement at a mean of four years: can poor outcomes be predicted from pre-and post-operative analysis? The Bone & Joint Journal. 2013;95(10):1366-71.
163 Łapaj Ł, Mróz A, Kokoszka P, Markuszewski J, Wendland J, Helak-Łapaj C, Kruczyński J. Peripheral snap-fit locking mechanisms and smooth surface finish of tibial trays reduce backside wear in fixed-bearing total knee arthroplasty: A retrieval analysis of 102 inlays. Acta orthopaedica. 2017;88(1):62-9.

164 Levine RA, Lewicki KA, Currier JH, Mayor MB, Van Citters DW. Contribution of micro-motion to backside wear in a fixed bearing total knee arthroplasty. Journal of Orthopaedic Research. 2016;34(11):1933-40.
165 McKellop HA. The lexicon of polyethylene wear in artificial joints. Biomaterials. 2007;28(34):5049-57.
166 Stratton-Powell A, Tipper J, Williams S, Redmond A, Brockett C. Edge loading in explanted total ankle replacements: a polyethylene insert form and volume analysis. Orthopaedic Proceedings; 2017: Bone & Joint; 2017. p. 18-.
167 Easley ME, Vertullo CJ, Urban CW, Nunley JA. Total ankle arthroplasty. JAAOS-Journal of the American Academy of Orthopaedic Surgeons. 2002;10(3):157-67.
168 Chakrabarty G, Vashishtha M, Leeder D. Polyethylene in knee arthroplasty: A review. journal of clinical orthopaedics and trauma. 2015;6(2):108-12.
169 Akil S, Newman JM, Shah NV, Ahmed N, Deshmukh AJ, Maheshwari AV. Metal hypersensitivity in total hip and knee arthroplasty: current concepts. Journal of Clinical Orthopaedics and Trauma. 2018;9(1):3-6.
170 King SW, Royeca JM, Cunningham CM, Madegowda R, Sha S, Pandit H. Metal Hypersensitivity in Total Knee Arthroplasty. Journal of Arthroscopy and Joint Surgery. 2020.
171 Watters TS, Cardona DM, Menon KS, Vinson EN, Bolognesi MP, Dodd LG. Aseptic lymphocyte-dominated vasculitis-associated lesion: a clinicopathologic review of an underrecognized cause of prosthetic failure. American journal of clinical pathology. 2010;134(6):886-93.
172 Brandt J-M, MacDonald SJ, Bourne RB, Medley JB. Retrieval analysis of modular total knee replacements: factors influencing backside surface damage. The Knee. 2012;19(4):306-15.
173 Schmalzried TP, Shepherd EF, Dorey FJ, Jackson WO, dela Rosa M, McKellop HA, et al. Wear is a function of use, not time. Clinical Orthopaedics and Related Research (1976-2007). 2000;381:36-46.
174 Titanium nitride ceramic film against polyethylene. A 48 million cycle wear test. Clinical Orthopaedics and Related Research. 1995(317):64-70.

Appendix A. Published Paper

Haston S, Langton D, Townshend D, Bhalekar R, Joyce T. Metal debris release is commonly seen from explanted total ankle replacements. Journal of the Mechanical Behavior of Biomedical Materials. 2023;144:105932.

Abstract

This study aimed to characterise the damage mechanisms present on the metal components used in various contemporary total ankle replacements. Twenty-seven explanted total ankle replacements comprising 8 different designs (3 fixed bearing and 5 mobile bearing) were analysed using various explant analysis techniques. Pitting and scratching were the most commonly observed wear features. Microscopic analysis revealed metallic pitting on 52% of tibial components and 95% of talar components. Pitting was identified on more cobalt-chromium than titanium alloy tibial components (63% versus 0%). Non-contact profilometry confirmed the presence of pitting, with significant ($p < 0.05$) differences in the measured average surface roughness values of pitted and unpitted areas for tibial and talar components. There was macroscopically visible sliding plane scratching, indicating the presence of hard third body particles, on 78% of talar components. Changes to the non-articulating surfaces coatings in terms of coating loss and/or changes in reflectivity was identified visually on 80% of metal components. Scanning electron microscopy with energy dispersive X-ray spectroscopy identified metallic embedded debris in 19% of polyethylene inserts. This explant study demonstrates the release of metal debris from both the metallic tibial and talar component articulating surfaces and non-articulating surface coatings of various contemporary total ankle replacements. Metal particulate debris release from total ankle replacements may be more common than previously recognised. Metal debris should be considered in further study into the aetiology of failed total ankle arthroplasty.

1. Introduction

Total ankle replacement (TAR) has become an increasingly popular alternative to ankle fusion in the surgical management of severe ankle arthritis. The benefits of TAR are perceived to be better gait mechanics and protection of adjacent joints which are put under additional load by

ankle fusion (Gougoulias et al., 2016). The outcomes of TAR have improved significantly over the last decade (Undén et al., 2020) but revision rates remain high (Perry et al., 2022) compared to those for primary total hip replacement and total knee replacement, with considerably higher long-term revision rates for ankles (9.01% at 10 years, compared with 4.05% and 4.01% for hips and knees respectively according to data from the National Joint Registry for England, Wales, Northern Ireland, the Isle of Man and the States of Guernsey (NJR) 2022 Annual Report) (Reed et al., 2022).

Contemporary TARs are metal-on-polyethylene (MoP) implants, consisting of metal tibial and talar components, with a polyethylene (PE) (typically ultra-high molecular weight polyethylene (UHMWPE)) insert in between. The PE insert may be either fixed to the tibial component (fixed bearing), or unconstrained (mobile bearing).

The metal talar component is usually manufactured from cobalt-chromium (CoCr) alloy via either cast or wrought forming (ASTM F75 or ASTM F1537, respectively), and the metal tibial component may be either CoCr alloy also or titanium (Ti) alloy, again formed by either cast or wrought methods (ASTM F1108 or ASTM F136, respectively). Both F75 and F1537 CoCr alloys have previously been shown to have similar microstructures and microhardness (Patel et al., 2012).

The metal components typically have a porous coating (usually Ti and/or hydroxyapatite (HA)) on the non-bearing surface to promote osseointegration at the bone-implant interface rather than using cement for fixation as previous designs did (Gougoulias et al., 2016; Malik and Malik, 2015). However, whilst the NJR states that all brands of TAR recorded by them are (CE marked as) uncemented implants, cement is used by surgeons in some instances (4.3% of primary procedures), for example where the bone stock is poor (Reed et al., 2022).

The number of TARs performed is increasing, with 710 primary procedures recorded by the NJR in 2021 (though the actual number is likely higher due to underreporting), and this increase has largely been with fixed bearing designs (Reed et al., 2022). This change may be linked with the introduction of the fixed bearing INFINITY prosthesis (Wright Medical) in 2014; the same year that the market leader at the time, the mobile bearing Mobility prosthesis (DePuy), was voluntarily recalled (Reed et al., 2022). The INFINITY prosthesis is now the most commonly implanted TAR in the UK, used in 65.4% of procedures in 2021, as well as in Australia, New

Zealand and Norway (Reed et al., 2022; Australian Orthopaedic Association National Joint Replacement Registry (AOANJRR), 2021; McKie et al., 2022; Furnes et al., 2021).

In vivo, the bearing surface of the PE insert articulates against the bearing surface of the metal talar component, while the backside surface of the PE insert is in contact with the inferior surface of the metal tibial component, meaning there is no direct metal-on-metal contact (Fig. 1).

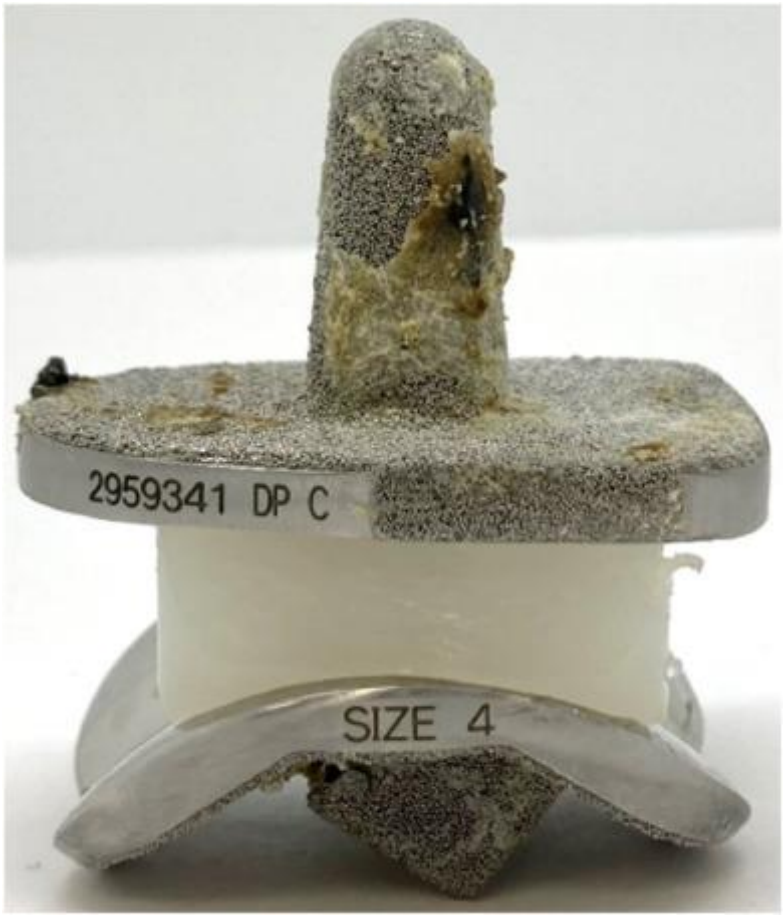

Fig. 1. Sagittal plane view of an explanted Mobility total ankle replacement. Top: metal tibial component. Middle: PE insert. Bottom: metal talar component.

Explant analysis of TARs is limited, and previous studies have mostly focused on the analysis of the damage identified on PE inserts (Greenwald and Postal, 2010; Ho et al., 2020; Currier et al., 2019; Affatao et al., 2009). Retrieval studies by Vaupel et al. (2009), on 10 Agility (DePuy) second-generation fixed bearing TARs, and by Cottrino et al. (2016), on 6 Ankle

Evolutive System (AES) (Biomet) third-generation mobile bearing TARs, both of which are no longer in use, have included analysis of the metal tibial and talar components using light microscopy and scanning electron microscopy (SEM). Histological studies, again primarily of the Agility and AES implants, have reported the presence of metal particles, along with PE particles, in the periprosthetic tissue of between 60% and 90% of osteolytic samples (Schipper et al., 2017; Koivu et al., 2009; Dalat et al., 2013; van Wijngaarden et al., 2015; Stratton-Powell et al., 2023).

This study aimed to characterise the damage mechanisms present in a cohort of contemporary TARs to test the hypothesis that appreciable metal debris is produced from these devices.

2. Materials and methods

2.1. Samples

Third and fourth generation TARs which had been revised for any reason were included. The samples were retrieved by multiple surgeons at various hospitals. Twenty-seven TARs were included, comprised of 8 different models (Fig. 2). Three of the prosthesis designs were fixed bearing, and 5 were mobile bearing. The majority of the components were manufactured from CoCr alloy (Co28Cr6Mo) as per ASTM F75, referring to forming by casting method, with Ti alloy (Ti6Al4V) formed by wrought method as per ASTM F136 also known to be used (Table 1).

Fig. 2. Macroscopic images of explanted TAR components, showing the different surfaces analysed from the prosthesis models included.

Table 1. Details of the total ankle replacement designs included.

Prosthesis (manufacturer)	**No. samples**	**Bearing type**	**Tibial component alloy**	**Talar component alloy**	**Non-articulating surfaces coating**
INFINITY (Wright Medical)	4	Fixed	Ti	CoCr	Ti plasma spray
Cadence (Integra)	1	Fixed	Ti ASTM F136	CoCr ASTM F75	Ti plasma spray
Salto Talaris (Integra)	2	Fixed	CoCr ASTM F75	CoCr ASTM F75	Ti plasma spray

Prosthesis (manufacturer)	No. samples	Bearing type	Tibial component alloy	Talar component alloy	Non-articulating surfaces coating
Salto (Integra)	1	Mobile	CoCr ASTM F75	CoCr ASTM F75	Ti plasma spray
Mobility (DePuy)	10	Mobile	CoCr	CoCr	Ti sintered beads (Porocoat; DePuy)
STAR (Stryker)	3	Mobile	CoCr ASTM F75	CoCr ASTM F75	Double coated Ti plasma spray and HA
Hintegra (Integra; Newdeal)	2	Mobile	CoCr ASTM F75	CoCr ASTM F75	Double coated Ti plasma spray and HA
BOX (MatOrtho)	3	Mobile	CoCr ASTM F75	CoCr ASTM F75	HA plasma sprayed beads

Analysis was performed by one author to ensure consistency throughout. Prior to analysis, all explants were disinfected using a surgical grade washer (IQ4, KEN Hygiene Systems, Broby, Denmark) and then cleaned with acetone and lint-free cloth to ensure any debris was removed.

Two of the TARs had been affixed using cement, with one BOX prosthesis having cement visible on the non-articulating surfaces of both the tibial and talar components, and one Mobility having cement visible on the talar component, with the tibial component not received. The remaining 22 tibial and 23 talar components were uncemented, meaning fixation was achieved using bony ingrowth only.

2.2. Damage mode analysis

Twenty-three tibial component inferior surfaces and 23 talar component bearing surfaces, along with 26 PE insert bearing and backside surfaces, were visually inspected using a measuring microscope (Mitutoyo, Kanagawa, Japan) with 30× magnification as well as macroscopically for the following common damage modes: pitting, scratching, embedded debris, burnishing, abrasion, delamination, striations, and surface deformation (Vaupel et al., 2009; Harman et al., 2010). Surgical retrieval damage, determined as being deep grooves not correlating with worn areas, was excluded.

The non-articulating surfaces of the metal tibial and talar components were also macro- and microscopically visually inspected for signs of loss of their porous coatings.

2.3. Surface roughness measurement

For the 13 tibial components and 22 talar components on which pitting was identified, surface roughness measurements were taken using a non-contact 3D profilometer (NewView 5000, Zygo Corporation, Connecticut, USA). The parameters of average surface roughness (Sa) and maximum valley depth (Sv) were measured. For both unpitted and pitted areas, identified prior via light microscopy, 5 measurements were taken.

2.4. SEM-EDX analysis

A SEM with energy dispersive X-ray spectroscopy (EDX) (TM3030, Hitachi High-Technologies Corporation, Tokyo, Japan) was used to determine the composition of the embedded debris identified in 5 PE inserts (5 bearing surfaces and 4 backside surfaces).

2.5. Statistical analysis

Statistical analysis was carried out using statistical software (Minitab, Pennsylvania State University, USA). A 2-proportion test was performed on the proportions of tibial and talar components with pitting, analysing bearing type and alloy. For measured average surface roughness (Sa) and maximum valley depth (Sv) values of the tibial and talar components, a Ryan-Joiner test was performed to test the data for normality. The data was nonparametric, therefore a Mann-Whitney *U* test with a 95% confidence level was performed with reported p-values adjusted for ties. Statistical significance was defined as $p < 0.05$.

3. Results

3.1. Damage modes identified

An overview of the damage mechanisms identified in each explant is given in Table 2.

Table 2. Overview of the damage mechanism identified in each of the explanted TARs. Notes: Y, damage identified; -, corresponding component not present; *, Ti embedded debris; †, Co and Cr embedded debris; ‡, metal-on-metal contact; §, damaged PE insert.

Prosthesis	**Tibial pitting**	**Talar pitting**	**Talar scratching**	**Cement present**	**Coating loss**	**Additional damage**
INFINITY	Y	Y	Y		Y	
INFINITY		Y	Y		Y	Y*
INFINITY		Y	Y		Y	
INFINITY	–	–	–	–	–	
Cadence		Y			Y	
Salto Talaris	Y	–	–		Y	Y†
Salto Talaris	Y	Y			Y	Y§

Prosthesis	Tibial pitting	Talar pitting	Talar scratching	Cement present	Coating loss	Additional damage
Salto	Y	Y	Y		Y	
Mobility	Y	Y	Y		Y	
Mobility	–	Y	Y	Y		
Mobility	Y	Y	Y		Y	Y§
Mobility	Y	Y	Y		Y	
Mobility		Y	Y		Y	
Mobility	Y	Y	Y		Y	Y§
Mobility		Y	Y		Y	
Mobility		Y	Y		Y	
Mobility	–	–	–	–	–	
Mobility		Y	Y		Y	Y‡§
STAR	Y	Y			Y	
STAR	Y	Y			Y	Y‡
STAR	Y	Y	Y		Y	
Hintegra	–	–	–	–	–	Y*†
Hintegra		Y	Y			Y†‡§
Hintegra		Y	Y		Y	Y*

Prosthesis	Tibial pitting	Talar pitting	Talar scratching	Cement present	Coating loss	Additional damage
BOX		Y	Y		Y	
BOX			Y	Y	Y	
BOX	Y	Y			Y	Y‡§

The most commonly observed wear features from the microscopic damage mode analysis, across all surfaces, metallic and polymeric, were pitting and scratching (Fig. 3).

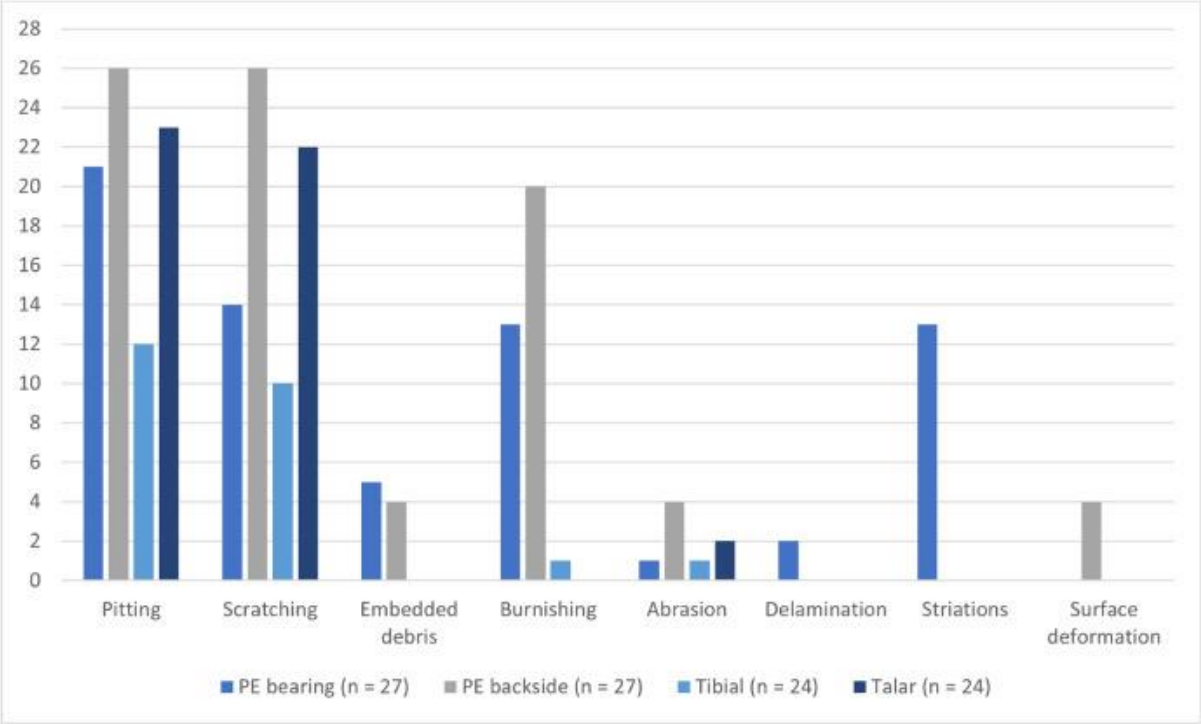

Fig. 3. Results of surface damage mode analysis. showing number of each component surfaces on which each damage mode was present.

3.2. Non-articulating surfaces

Visual inspection – both macro-and microscopic – revealed changes to non-articulating surfaces in terms of coating loss or changes in reflectivity indicative of this in 20 (87%) of the 23 tibial components and 17 (74%) of the 23 talar components analysed (Fig. 4). For the designs

which utilise beads on the non-articulating surfaces (Mobility and BOX), bead loss was not identified. Fig. 5 illustrates the percentage of tibial and talar components with each coating type which exhibited changes (coating loss/changes in reflectivity), with this ranging from 69% to 94% (mean 80%).

Fig. 4. Changes in the coating of a STAR tibial component non-articulating surface.

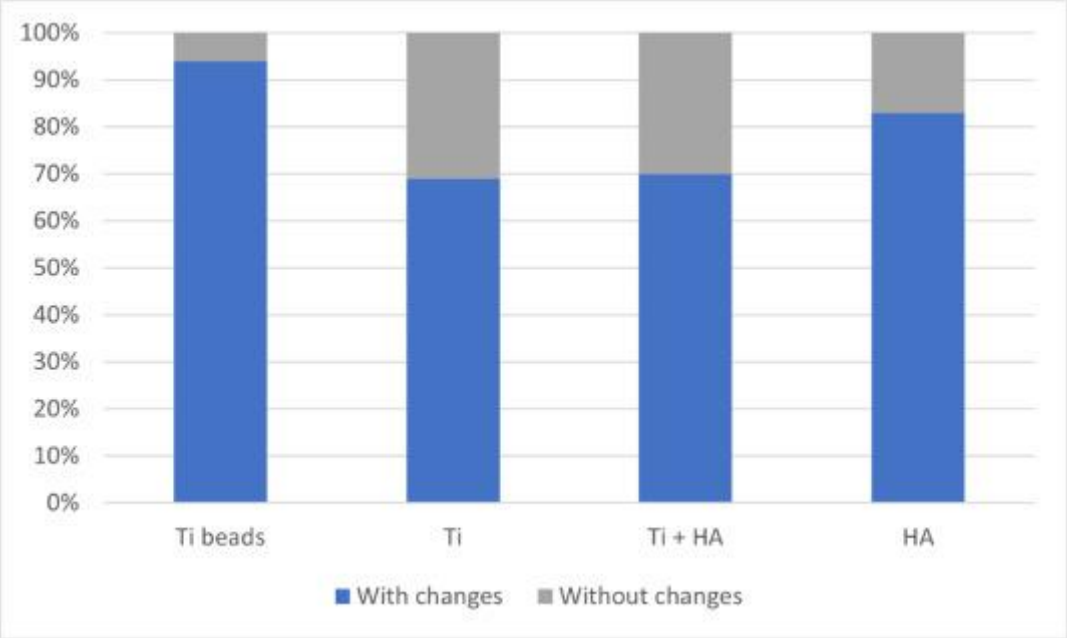

Fig. 5. Percentage of tibial and talar components with each coating type which exhibited changes.

Coating loss/changes in reflectivity was identified on the non-articulating surfaces of the metal components of all of the TARs which had tibial pitting and on all except 2 of those which had talar pitting and/or talar sliding plane scratching. In these 2 cases, the tibial component of one was not present and so the porous coating was not able to be analysed, and the other exhibited evidence of direct metal-on-metal contact occurring, along with a severely damaged PE insert. These findings therefore suggest that loss of coating may be a major cause of the metal component damage observed by acting as third body debris at the articulations.

3.3. Talar sliding plane scratching

Scratching on the sliding plane (i.e., linear scratches in the direction of the antero-posterior movement allowed at the ankle during plantarflexion and dorsiflexion), as shown in Fig. 6, was observed macroscopically on 18 (78%) of the 23 metal talar components analysed.

Fig. 6. Macroscopic image showing severe talar component scratching of a Hintegra talar component bearing surface.

3.4. Pitting and abrasive changes

Light microscopy revealed the presence of pitting on the articulating surfaces of 12 (52%) of the 23 tibial components and on 22 (95%) of the 23 CoCr alloy talar components (Fig. 7A and B, respectively). Pitting was defined as small indentations indicative of material loss, most likely to have occurred *in vivo*. The pits had dimensions of approximately 90 μm (length) x 40 μm (width) x 3 μm (depth). The pitted tibial components were all manufactured from CoCr alloy, with 63% exhibiting this pitting. None of the Ti alloy components exhibited pitting, however abrasive changes were identified on one (Fig. 7C).

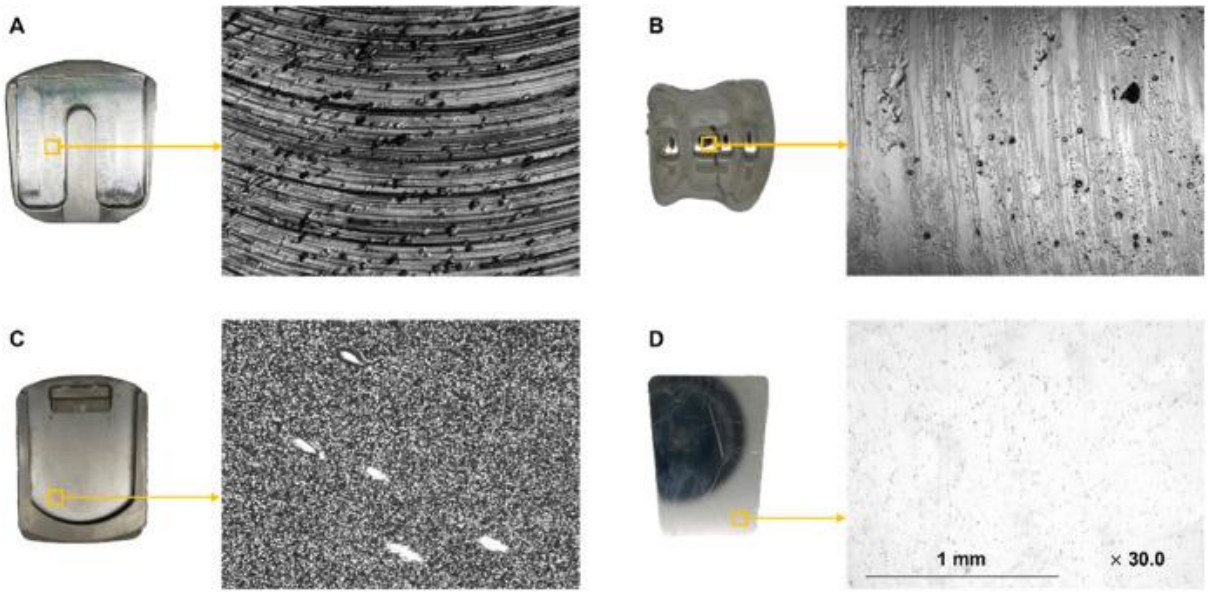

Fig. 7. Microscopic images of (A) pitting on a CoCr alloy tibial component, (B) pitting on a CoCr alloy talar component, (C) abrasive changes on a Ti alloy tibial component, and (D) as manufactured surface of a CoCr alloy tibial component. (A) Salto Talaris. (B) Salto Talaris. (C) INFINITY. (D) STAR.

3.5. Surface roughness

The results of the surface roughness measurements of the tibial and talar components showing pitting are given by Table 3 and Table 4. All tibial component models and all talar component models except Hintegra showed a significant increase between the measured Sa of unpitted and pitted areas, and all showed a significant increase between the Sv values ($p < 0.05$).

Table 3. Surface profilometry and p-values for different tibial components showing pitting. Notes: Sa, average surface roughness; Sv, maximum valley depth; SD, standard deviation.

Tibial component	No. samples with pitting	Unpitted Sa (µm) (mean ± SD)	Pitted Sa (µm) (mean ± SD)	P-value	Unpitted Sv (µm) (mean ± SD)	Pitted Sv (µm) (mean ± SD)	P-value
Salto Talaris	2	0.133 ± 0.002	0.252 ± 0.015	<0.001	−0.786 ± 0.387	−5.399 ± 0.403	<0.001
Salto	1	0.023 ± 0.002	0.152 ± 0.001	0.012	−0.359 ± 0.017	−2.262 ± 0.010	0.012
Mobility	4	0.012 ± 0.007	0.125 ± 0.093	<0.001	−0.423 ± 0.133	−3.068 ± 1.222	<0.001
STAR	3	0.022 ± 0.012	0.166 ± 0.099	<0.001	−0.312 ± 0.082	−2.677 ± 0.286	<0.001
Hintegra	1	0.010 ± 0.001	0.095 ± 0.002	0.011	−0.473 ± 0.037	−2.384 ± 0.020	0.012
BOX	1	0.034 ± 0.001	0.147 ± 0.003	0.012	−0.538 ± 0.030	−2.938 ± 0.010	0.012

Table 4. Surface profilometry and p-values for different tibial components showing pitting.
Notes: Sa, average surface roughness; Sv, maximum valley depth; SD, standard deviation.

Talar component	No. samples with pitting	Unpitted Sa (µm) (mean ± SD)	Pitted Sa (µm) (mean ± SD)	P-value	Unpitted Sv (µm) (mean ± SD)	Pitted Sv (µm) (mean ± SD)	P-value
INFINITY	3	0.021 ± 0.007	0.071 ± 0.027	<0.001	−0.362 ± 0.036	−2.822 ± 0.593	<0.001
Cadence	1	0.027 ± 0.027	0.194 ± 0.004	0.011	−.0336 ± 0.011	−2.850 ± 0.040	0.012
Salto Talaris	1	0.022 ± 0.005	0.079 ± 0.003	0.012	−1.146 ± 0.024	−4.123 ± 0.382	0.012
Salto	1	0.058 ± 0.002	0.075 ± 0.004	0.012	−0.676 ± 0.027	−2.459 ± 0.419	0.012

Talar component	No. samples with pitting	Unpitted Sa (µm) (mean ± SD)	Pitted Sa (µm) (mean ± SD)	P-value	Unpitted Sv (µm) (mean ± SD)	Pitted Sv (µm) (mean ± SD)	P-value
Mobility	9	0.036 ± 0.021	0.124 ± 0.082	<0.001	−0.385 ± 0.252	−2.262 ± 0.784	<0.001
STAR	3	0.033 ± 0.018	0.084 ± 0.035	<0.001	−0.386 ± 0.105	−2.654 ± 0.288	<0.001
Hintegra	2	0.110 ± 0.096	0.362 ± 0.254	0.062	−0.427 ± 0.179	−2.239 ± 0.522	<0.001
BOX	2	0.029 ± 0.012	0.061 ± 0.025	0.004	−5.09 ± 0.120	−4.201 ± 0.775	<0.001

Representative surface topography images for the tibial and talar components are shown in Fig. 8, Fig. 9, respectively.

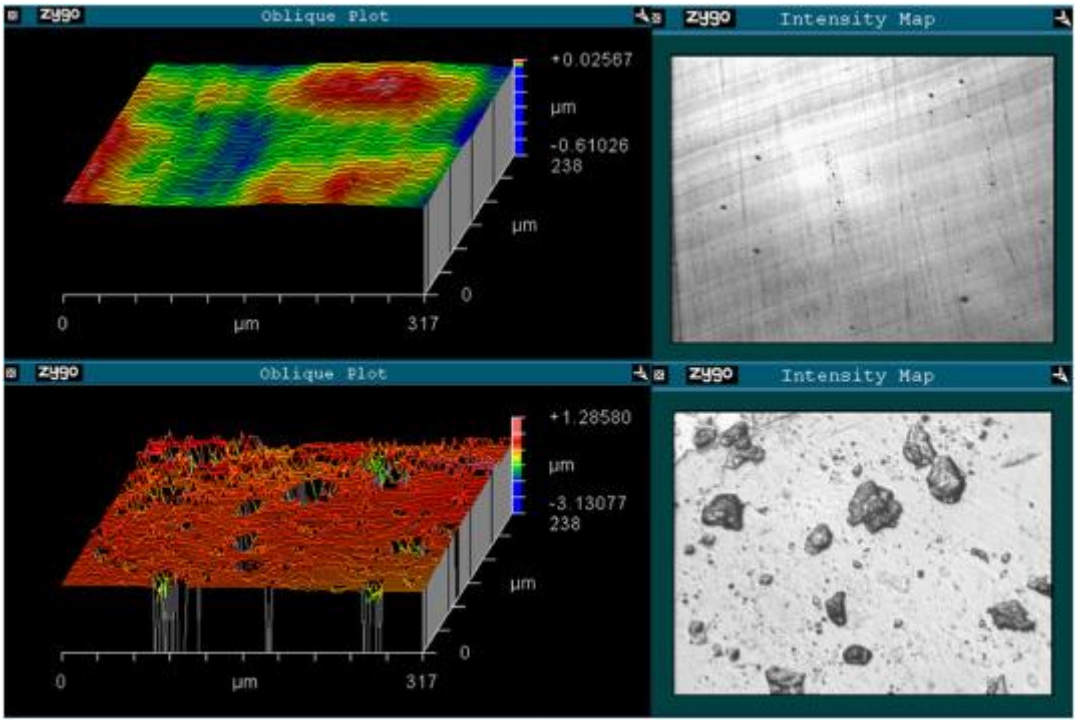

Fig. 8. Surface profilometry images of unpitted and pitted areas of a tibial component. (A) Unpitted and (B) pitted areas of a Mobility tibial component inferior surface.

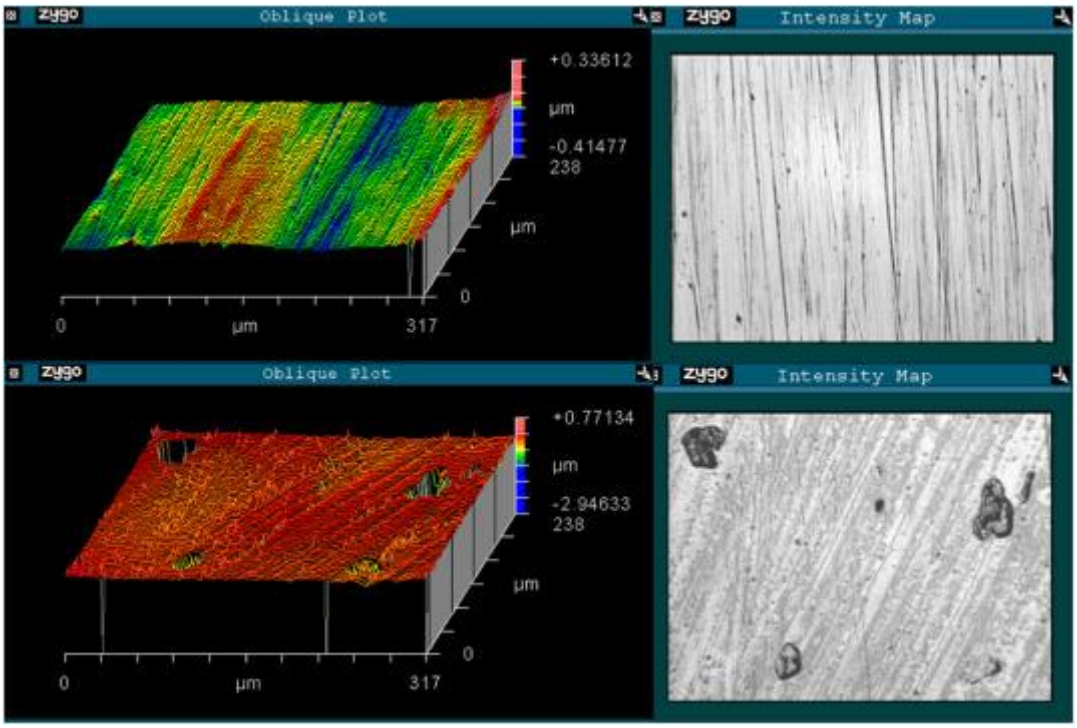

Fig. 9. Surface profilometry images of unpitted and pitted areas of a talar component. (A) Unpitted and (B) pitted areas of a Mobility talar component bearing surface.

3.6. Embedded debris

Embedded debris was identified via light microscopy in the PE inserts of 5 TARs (19%), 4 of which had embedded debris on both the bearing and backside surfaces, and 1 of which had embedded debris on the bearing surface only (Fig. 10).

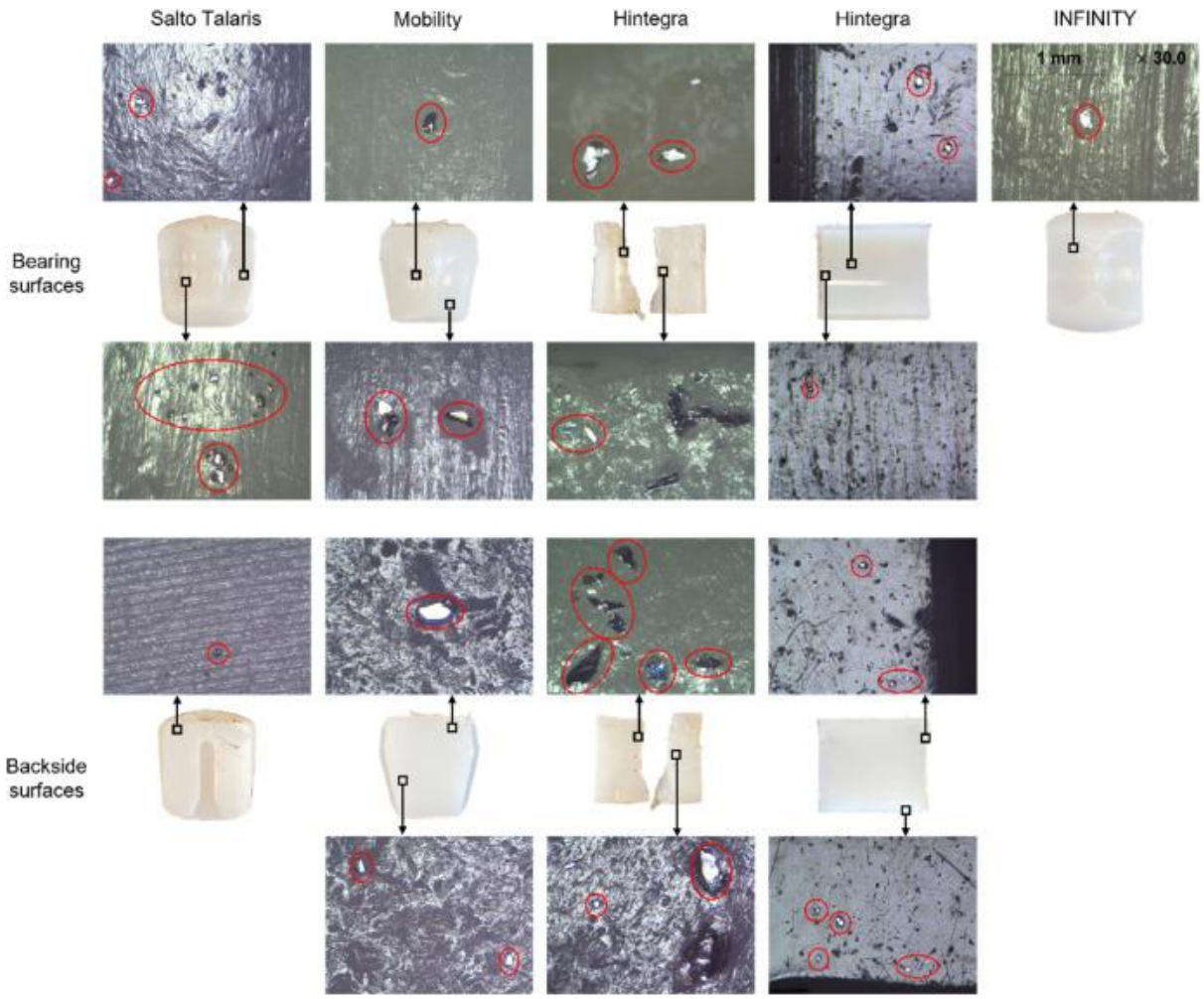

Fig. 10. Microscopic images of polyethylene insert embedded debris. The embedded debris (indicated by red ellipses) on the bearing and/or backside surfaces of 5 PE inserts.

Embedded debris was observed on 5 PE inserts. SEM-EDX analysis confirmed that the embedded debris identified on these PE inserts was metallic; specifically, the presence of Co and Cr or Ti was confirmed for each surface (Table 5).

Table 5. The elements identified in the embedded debris of the polyethylene inserts.

PE insert	**Bearing surface embedded debris**	**Backside surface embedded debris**
Salto Talaris	Ti, Co, Cr	Ti

PE insert	Bearing surface embedded debris	Backside surface embedded debris
Mobility	Co, Cr	Co, Cr, Mo
Hintegra (in pieces)	Co, Cr, Mo	Co, Cr
Hintegra	Ti	Ti
INFINITY	Ti	–

The non-articulating surfaces coating for all of the devices which had embedded debris identified on the PE inserts contained Ti, and all corresponding tibial and talar components were manufactured from CoCr alloy, with the exception of the Ti alloy INFINITY tibial component (which was not in contact with the PE insert bearing surface on which Ti debris was identified in this case). It is therefore likely that the Ti embedded debris identified originated from the porous coatings of these prostheses.

3.7. Special cases

Macroscopic analysis of the PE inserts revealed severe damage in 6 of the 26 PE inserts analysed (1 insert had broken in half, 1 had a crack in the bearing surface, and 4 had part broken off) (Fig. 11). However, it is not known whether the damage of these components occurred *in vivo* or during surgical retrieval of the device.

Fig. 11. Macroscopic images of severely damaged PE inserts. (A) with part broken off), (B) in pieces, and (C) with a crack in the bearing surface.

Evidence of direct metal-on-metal contact occurring was identified in 4 of the TARs (Fig. 12). Of these 4 devices, one did not have a PE insert present. The corresponding PE inserts for the other 3 devices all had signs of severe damage, with the PE insert either being broken into 2 pieces (in one case) or have part broken off (in 2 cases).

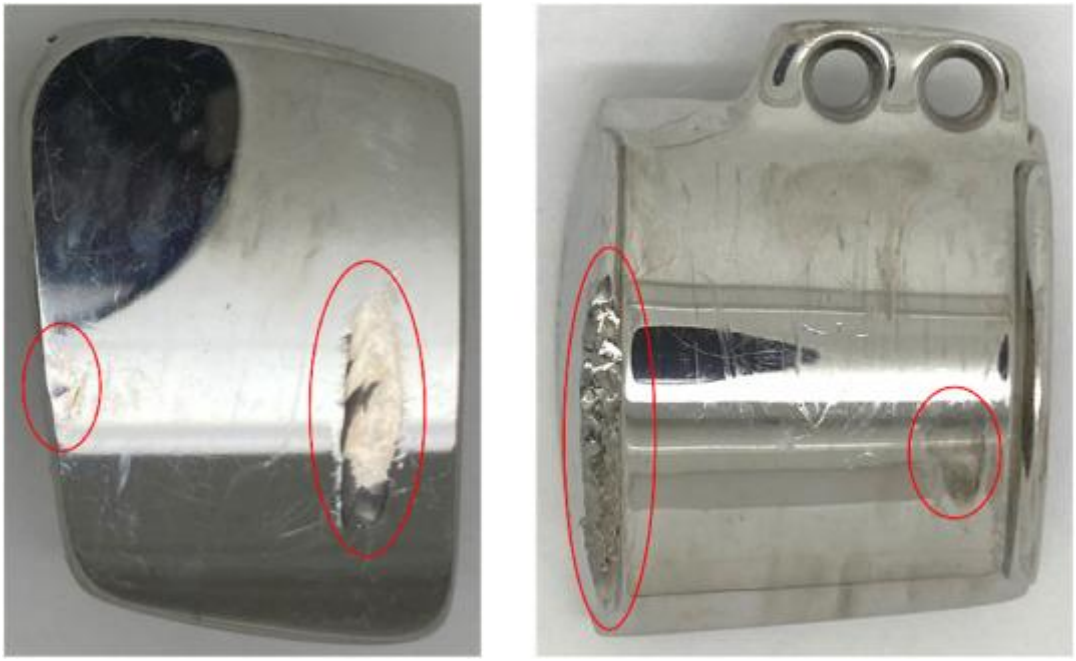

Fig. 12. Hintegra tibial and talar components. The corresponding polyethylene insert was broken into 2 pieces. Red ellipses indicate areas of material removal most likely due to direct metal-on-metal contact occurring as a result of fracture of the PE insert.

4. Discussion

4.1. Damage mechanisms identified

Damage to the articulating surfaces of the metal tibial and talar components in the form of pitting and scratching was commonly seen in this cohort of explanted TARs. Damage to the talar component was identified particularly frequently, with pitting in 95% and sliding plane scratching in 78% of the samples analysed. Of those talar components on which sliding plane scratching, the corresponding PE inserts for all but 4 had pitting on the bearing surface also. These findings indicate the presence of hard third body particles at the bearing interface, as the abrasive changes seen with the talar component scratching would not be typical from the normal articulation between the hard talar component and the PE insert (Cottrino et al., 2016). Similar findings have previously been reported by Cottrino et al. on 6 AES CoCr talar component bearing surfaces, in which severe scratching was also observed on the sliding plane, most likely due to removal of the Ti-HA coating of the metal components, meaning hard foreign particles were present (Cottrino et al., 2016).

As the PE insert prevents direct metal-on-metal contact in well-functioning TARs, the proportion of metallic components on which pitting and scratching was observed was unexpected. The proportion of tibial and talar components exhibiting pitting was similar regardless of bearing type, fixed or mobile, suggesting that bearing constraint is not a factor affecting the likelihood of tibial or talar pitting occurring. The component alloy, on the other hand, may be an influencing factor, as pitting was observed more frequently on CoCr alloy (63%) than Ti alloy (0%) tibial components. It should be noted, however, that the group of CoCr alloy components was substantially larger than the group of Ti alloy components (19 versus 4).

On all components on which pitting was identified, there were statistically significant ($p < 0.05$) differences between the measured Sv values of unpitted and pitted areas, therefore confirming that material loss occurred.

Pitting of metallic TAR components has also previously been reported by Vaupel et al., though with a lower prevalence. Of 9 Ti alloy tibial components analysed, scratching was observed on 7, pitting on 1, and burnishing on 1 (Vaupel et al., 2009). Of 10 CoCr alloy talar components analysed, scratching was observed on 6, and pitting on 6 (Vaupel et al., 2009). Whilst Vaupel et al. observed less frequent metallic pitting, there are possible explanations for these variations. The difference in TAR models could play a role, as Vaupel et al. analysed one particular fixed bearing TAR design (Agility) which did not feature in the present study. Furthermore, it is possible that the lower proportion of tibial components with pitting reported by Vaupel et al. may be explained by the Ti alloy composition, as the findings from the present study suggest that pitting may be more likely to occur on CoCr than Ti alloy tibial components.

Ti, Co and Cr were identified in the embedded debris of the PE inserts. All had a coating on the non-bearing surfaces of the metallic components containing Ti, and all had tibial and talar components composed of CoCr alloy except for the INFINITY TAR, which had a Ti alloy tibial component. However, embedded debris was only identified on the bearing surface (in contact with the CoCr talar component) of this INFINITY PE insert. Therefore, since all the surfaces in which embedded debris was identified were in contact with CoCr alloy surfaces, the identified Ti embedded debris on the PE insert bearing surfaces was presumably from the coatings, and the CoCr debris was presumed to originate from the articulating surfaces of the metallic components. The finding of tibial and talar pitting is in agreement with this idea and indicates the release of metal debris from the component surfaces.

The TARs which had embedded debris in the PE inserts included 2 Hintegra prostheses. Despite being the same design, different embedded debris was identified for each prosthesis, with Co and Cr identified in one, and Ti in the other. The former of these devices displayed signs of direct metal-on-metal contact occurring *in vivo*, which likely resulted in the CoCr debris release, whereas the latter exhibited evidence of coating loss, likely being responsible for the Ti debris. Furthermore, Co and Cr along with Ti were identified in the embedded debris in the Salto Talaris PE insert bearing surface. Embedded metallic debris in TAR PE inserts has also previously been reported by Vaupel et al., in fixed bearing Agility TARs, and a small amount in fixed bearing INFINITY and INBONE (Wright Medical) TARs by Ho et al. (Ho et al., 2020; Vaupel et al., 2009) Stratton-Powell et al. also reported CoCr and Ti wear particles surrounding failed AES TARs (Stratton-Powell et al., 2023). These findings indicate that both sources of metal debris release (pitting of the metallic components and loss of coating) may occur concurrently *in vivo*.

4.2. Causes of damage

The identification of Ti particles embedded in the PE insert bearing surfaces suggests the removal of coating, allowing the particles to act as third body debris. This has previously been shown with AES TARs. In a study of 6 AES mobile bearing TARs explanted due to osteolysis, Cottrino et al. reported the presence of Ti particles embedded on the talar component bearing surfaces, as well as in retrieved periprosthetic tissue (Cottrino et al., 2016). Since the implant metallic components were both composed of a CoCr alloy, these Ti particles were assumed to have originated from the coating (double coated Ti plasma spray and HA) (Cottrino et al., 2016).

The AES prosthesis previously had a HA coating, however in 2004 it was replaced with the coating of Ti along with HA, a change which resulted in increased incidence of osteolysis (Koivu et al., 2009). In a series of 130 AES TARs, Koivu et al. found the risk of osteolysis to be over 3 times higher for implants with the Ti-HA coating compared to the HA coating (Koivu et al., 2009). Furthermore, the osteolysis cases observed were more severe after the design change (Koivu et al., 2009). For AES implants with Ti-HA coating, SEM-EDX analysis by Koivu et al. revealed Ti and CoCr particles in periprosthetic tissue samples, with the amount of Ti high compared to that of the other metals present (Koivu et al., 2009). Although osteolysis following TAR is most commonly attributed to PE wear debris, studies have indicated that the

inflammatory reaction may also be in response to necrotic autologous tissues or metal particles (Mehta et al., 2021). Therefore, the implant-derived Ti particles, reported previously with the AES prothesis, may increase the risk of osteolysis occurring due to the associated inflammatory response to the particles, and therefore may in part explain the high prevalence of osteolysis following TAR which has been described (Cottrino et al., 2016; Schipper et al., 2017).

In this cohort of explants, there was no substantial differences between those with a double coating of Ti and HA compared to those with a single layer HA coating only in terms of changes in coating observed or the proportion of talar components with sliding plane scratching, however the proportion of tibial and talar components exhibiting pitting was higher for devices double coated with Ti and HA (80% and 100%, respectively) compared to those with HA coating only (33% and 67%, respectively).

Whilst the AES was withdrawn in 2009 following complication rates higher than expected (Di Iorio et al., 2017), findings of embedded Ti debris from the present study extends the issue of coating removal, and therefore the potentially increased risk of implant failure due to periprosthetic bone resorption caused by the immune response to these particles, to various other contemporary TARs.

Ti is used in most of the porous coatings for TAR metallic component non-bearing surfaces. Apart from the BOX prosthesis, which has a HA plasma spray coating, all of the other TARs included in the present study had a coating containing Ti. For the TARs in which embedded metallic debris was identified in the PE insert, the porous coatings all contained Ti. Like the AES, the Hintegra prosthesis, of which embedded debris was identified in 2, had a double coated Ti plasma spray and HA coating, both the Salto Talaris and INFINITY implants had a Ti plasma spray coating, and the Mobility had a coating made from Ti sintered beads.

The vast majority of the components were uncemented, therefore, while cement particles are a possible source of third body debris with the potential to cause surface damage, this was not found to be a primary cause in this cohort of explants. Rather, metal particulate debris from the porous coatings on the non-articulating surfaces of the metal components is more likely to be responsible for the metal damage seen by acting as third body particles.

The abrasive changes identified on the inferior surface of one of the fixed bearing INFINITY tibial trays is indicative of micromotion occurring at this interface. The observed changes in reflectivity on the majority of the non-articulating surfaces of the metal components may also be a result of micromotion, though in this case between the bone-implant interface.

4.3. Methods to avoid damage

Implant-derived metal debris has the potential to cause adverse inflammatory responses, with relatively low blood cobalt concentrations being sufficient to incite this in some patients (Langton et al., 2022). Despite this, CoCr alloy components are used in most TARs. In this cohort of explanted TARs, pitting indicative of material loss was found to occur more frequently in CoCr than Ti components.

CoCr is known to be a harder but less corrosion resistant material than Ti. It is therefore possible that along with third body particles being present in the bearing, there could potentially be corrosion pitting occurring on the articulating surfaces of the metal components, which may in part explain the higher prevalence of pitting observed on CoCr alloy compared to Ti alloy tibial components.

It has also previously been demonstrated by Moharrami et al. that *in vivo* oxidation of Ti alloy can have a significant effect on its mechanical surface properties such that its hardness increases, whereas CoCr alloy was found to remain at a constant hardness (Moharrami et al., 2013). It is therefore possible that an increase in Ti alloy tibial component hardness could also go some way to explaining why pitting was observed on fewer of these components compared to those made of CoCr alloy, by increasing their resistance to damage from third body particles.

These findings suggest that Ti alloy rather than CoCr alloy tibial components may be a better choice in terms of avoiding pitting damage. For the talar components, alternatives such as titanium nitride (TiN) ceramic coatings may offer a potentially tribological solution for patients with CoCr sensitivity, however further investigation into the clinical effectiveness of these coatings is still required (Pappas et al., 1995).

Coating-derived Ti particles have also been shown to incite adverse inflammatory responses (Koivu et al., 2009). The identification of embedded Ti particles along with the loss of coatings identified is therefore another potential issue. Coatings of HA only may be an alternative option associated with lower rates of osteolysis as previously reported (Koivu et al., 2009).

4.4. Limitations

The primary limitation of this study was the lack of clinical data available, as the findings of the explant analysis could not be linked to data such as reason for revision and implantation duration, which could provide further insights into the clinical performance of TARs related to metal release.

5. Conclusions

This explant study identified common damage to metal tibial and talar TAR components in the form of pitting and scratching, along with the presence of third body debris at the bearing, most likely accounted for by coating particles from the non-articulating surfaces of the metallic components. These findings demonstrate metal release from contemporary TARs; a phenomenon which warrants quantification through further research.

Funding

British Orthopaedic Foot and Ankle Society provided a grant through which the microscope was funded. Shona Haston's PhD studentship was provided by the Intensive Industrial Innovation Programme.

CRediT authorship contribution statement

Shona Haston: Writing – original draft, Methodology, Investigation, Formal analysis, Data curation, Conceptualization. David Langton: Writing – review & editing, Supervision, Resources. David Townshend: Writing – review & editing, Resources. Rohan Bhalekar: Writing – review & editing, Methodology. Thomas Joyce: Writing – review & editing, Supervision.

Declaration of competing interest

The authors declare the following financial interests/personal relationships which may be considered as potential competing interests: David Langton is an expert witness for plaintiffs in ongoing metal-onmetal hip litigation. David Townshend reports institutional support and personal consultancy fees, both for Stryker.

Data availability

Data will be made available on request.

References

Affatao, S., Taddei, P., Leardini, A., et al., 2009. Wear behaviour in total ankle replacement: a comparison between an in vitro simulation and retrieved prostheses. Clin. Biomech. 24 (8), 661–669. https://doi.org/10.1016/j. clinbiomech.2009.06.006.

Australian Orthopaedic Association National Joint Replacement Registry (AOANJRR), 2021. Demographics and outcome of ankle arthroplasty: supplementary report. In: Hip, Knee & Shoulder Arthroplasty: 2021 Annual Report.

Cottrino, S., Fabr`egue, D., Cowie, A., et al., 2016. Wear study of total ankle replacement explants by microstructural analysis. J. Mech. Behav. Biomed. Mater. 61, 1–11. https://doi.org/10.1016/j.jmbbm.2015.12.035.

Currier, B.H., Hecht, P.J., Nunley, J.A., et al., 2019. Analysis of failed ankle arthroplasty components. Foot Ankle Int. 40 (2), 131–138. https://doi.org/10.1177/ 1071100718802589.

Dalat, F., Barnoud, R., Fessy, M.-H., et al., 2013. Histologic study of periprosthetic osteolytic lesions after AES total ankle replacement. A 22 case series. Orthop. Traumatol. Surg. Res. 99 (6), S285–S295. https://doi.org/10.1016/j. otsr.2013.07.009.

Di Iorio, A., Viste, A., Fessy, M.H., Besse, J.L., 2017. The AES total ankle arthroplasty analysis of failures and survivorship at ten years. Int. Orthop. 41 (12), 2525–2533. https://doi.org/10.1007/s00264-017-3605-0.

Furnes, O., Gjertsen, J.E., Hallan, G., et al., 2021. Report 2021. Norwegian National Advisory Unit on Arthroplasty and Hip Factures.

Gougoulias, N., Maffulli, N., 2016. History of total ankle replacement in north America. In: Roukis, T.S., Berlet, G.C., Bibbo, C., et al. (Eds.), Primary and Revision Total Ankle Replacement: Evidence-Based Surgical Management. Springer Nature, pp. p3–p14. https://doi.org/10.1007/978-3-319-24415-0_1.

Greenwald, A.S., Postal, P.D., 2010. Evaluation of a mobile bearing total ankle replacement in simulation and clinical retrieval. Available from: https://orl-inc. com/wp-content/uploads/2016/03/STAR-Simulator-Retrieval-2010.pdf.

Harman, M., Affatato, S., Spinelli, M., et al., 2010. Polyethylene insert damage in unicondylar knee replacement: a comparison of in vivo function and in vitro simulation. Proc. Inst. Mech. Eng. H 224 (7), 823–830. https://doi.org/10.1243/09544119JEIM699.

Ho, N.C., Park, S.H., Campbell, P., et al., 2020. Damage patterns in polyethylene fixed bearings of retrieved total ankle replacements. Foot Ankle Surg. 27 (3), 316–320. https://doi.org/10.1016/j.fas.2020.06.012.

Koivu, H., Kohonen, I., Sipola, E., et al., 2009. Severe periprosthetic osteolytic lesions after the Ankle Evolutive System total ankle replacement. J. Bone Joint Surg. Br. 91 (7), 907–914. https://doi.org/10.1302/0301-620X.91B7.22434.

Langton, D.J., Bhalekar, R.M., Joyce, T.J., et al., 2022. The influence of hla genotype on the development of metal hypersensitivity following joint replacement. Commun. Med. 2 (1), 1–12. https://doi.org/10.1038/s43856-022-00158-9.

Malik, S.S., Malik, S.S., 2015. Biomechanics of the ankle and foot. In: Orthopaedic Biomechanics Made Easy. Cambridge University Press, pp. p150–p157.

McKie, J., Hobbs, T., Frampton, C., et al., 2022. The New Zealand Joint Registry Twenty-Two Year Report. The New Zealand Joint Registry.

Mehta, N., Serino, J., Hur, E.S., et al., 2021. Pathogenesis, evaluation, and management of osteolysis following total ankle arthroplasty. Foot Ankle Int. 42 (2), 230–242. https://doi.org/10.1177/1071100720978426.

Moharrami, N., Langton, D., Sayginer, O., et al., 2013. Why does titanium alloy wear cobalt chrome alloy despite lower bulk hardness: a nanoindentation study? Thin Solid Films 549, 79–86. https://doi.org/10.1016/j.tsf.2013.06.020.

Pappas, M.J., Makris, G., Buechel, F.F., 1995. Titanium nitride ceramic film against polyethylene. A 48 million cycle wear test. Clin. Orthop. Relat. Res. 317, 64–70.

Patel, B., Favaro, G., Inam, F., et al., 2012. Cobalt-based orthopaedic alloys: relationship between forming route, microstructure and tribological performance. Mater. Sci. Eng. C Mater. Biol. Appl. 32 (5), 1222–1229. https://doi.org/10.1016/j.msec.2012.03.012.

Perry, T.A., Silman, A., Culliford, D., et al., 2022. Survival of primary ankle replacements: data from global joint registries. J. Foot Ankle Res. 15 (1), 1–7. https://doi.org/10.1186/s13047-022-00539-2.

Reed, M., Brittain, R., Howard, P., et al., 2022. National Joint Registry 19th Annual Report 2022. National Joint Registry.

Schipper, O.N., Haddad, S.L., Pytel, P., Zhou, Y., 2017. Histological analysis of early osteolysis in total ankle arthroplasty. Foot Ankle Int. 38 (4), 351–359. https://doi.org/10.1177/1071100716682333.

Stratton-Powell, A.A., Williams, S., Tipper, J.L., et al., 2023. Isolation and characterisation of wear debris surrounding failed total ankle replacements. Acta Biomater. 159, 410–422. https://doi.org/10.1016/j.actbio.2023.01.051.

Und´en, A., Jehpsson, L., Kamrad, I., et al., 2020. Better implant survival with modern ankle prosthetic designs: 1,226 total ankle prostheses followed for up to 20 years in the Swedish Ankle Registry. Acta Orthop. 91 (2), 191–196. https://doi.org/10.1080/17453674.2019.1709312.

van Wijngaarden, R., van der Plaat, L., Weme, R.A.N., et al., 2015. Etiopathogenesis of osteolytic cysts associated with total ankle arthroplasty, a histological study. J. Foot Ankle Surg. 21 (2), 132–136. https://doi.org/10.1016/j.fas.2015.02.004.

Vaupel, Z., Baker, E.A., Baker, K.C., et al., 2009. Analysis of retrieved Aglity™ total ankle arthroplasty systems. Foot Ankle Int. 30 (9), 815–823. https://doi.org/10.3113/FAI.2009.0815.

Appendix B. TAR Component Surfaces

Supplementary images showing enlarged versions of the macroscopic images included in Figure 3.2 are included here.

Hintegra

BOX

Zenith

Appendix C. CMM Bearing Protocol

To scan the bearing surfaces of the TAR PE inserts, the ‘Ankle Front End’ MCOSMOS programme was used, for which the protocol was as follows:

Step 1: Mount the PE insert onto the CMM platform and ensure the exposed surface is clean

Step 2: Input file name as e.g. ANK1BearingSH

Step 3: Input point pitch variable (distance between points) as 0.1

Step 4: Input contour spacing variable (distance between contour scans) as 0.25

Step 5: Select ‘manual position of datum’

Step 6: Follow prompt to ‘place probe in centre of component’ and lower speed

Appendix D. CMM Backside Protocol

To scan the backside surfaces of the TAR PE inserts, the ‘UNI DSHAPE ULTIMATE” MCOSMOS programme was used, for which the protocol was as follows:

Step 1: Mount the PE insert onto the CMM platform and ensure the exposed surface is clean

Step 2: Input file name as e.g. ANK1BacksideSH

Step 3: Input contour spacing variable (distance between contour scans) as 0.5

Step 4: Input point pitch variable (distance between points) as 0.1

Step 5: Input depth of perimeter scan variable as -1

If probe collides then reduce in -0.5 increments

Step 6: Follow prompt to position probe above the right edge of the component in the middle